

THE INFRARED TELESCOPE FACILITY (IRTF) SPECTRAL LIBRARY: COOL STARS

JOHN T. RAYNER¹, MICHAEL C. CUSHING^{1,3}, AND WILLIAM D. VACCA²

¹ Institute for Astronomy, University of Hawai‘i, 2680 Woodlawn Drive, Honolulu, HI 96822, USA; rayner@ifa.hawaii.edu, michael.cushing@gmail.com

² SOFIA-USRA, NASA Ames Research Center MS N211-3, Moffett Field, CA 94035, USA; wvacca@sofia.usra.edu

Received 2009 March 5; accepted 2009 September 3; published 2009 November 17

ABSTRACT

We present a 0.8–5 μm spectral library of 210 cool stars observed at a resolving power of $R \equiv \lambda/\Delta\lambda \sim 2000$ with the medium-resolution infrared spectrograph, SpeX, at the 3.0 m NASA Infrared Telescope Facility (IRTF) on Mauna Kea, Hawaii. The stars have well-established MK spectral classifications and are mostly restricted to near-solar metallicities. The sample not only contains the F, G, K, and M spectral types with luminosity classes between I and V, but also includes some AGB, carbon, and S stars. In contrast to some other spectral libraries, the continuum shape of the spectra is measured and preserved in the data reduction process. The spectra are absolutely flux calibrated using the Two Micron All Sky Survey photometry. Potential uses of the library include studying the physics of cool stars, classifying and studying embedded young clusters and optically obscured regions of the Galaxy, evolutionary population synthesis to study unresolved stellar populations in optically obscured regions of galaxies and synthetic photometry. The library is available in digital form from the IRTF Web site.

Key words: atlases – infrared: stars – stars: AGB and post-AGB – stars: carbon – stars: fundamental parameters – stars: late-type – techniques: spectroscopic

1. INTRODUCTION

Spectral libraries play an important role in attempts to understand and classify individual stellar sources as well as to decompose the integrated spectrum of an aggregate system, such as a galaxy, into its various stellar populations. For example, the most widely used stellar classification process, as originally developed by Morgan et al. (1943), consists of comparing the spectrum of a star against a set of reference stellar spectra (for a review see Garrison 1994). Infrared spectral libraries are particularly useful for studying the physics of cool stars (e.g., Joyce et al. 1998; Gautschy-Loidl et al. 2004), classifying and studying stars in nearby embedded young clusters (e.g., Greene & Meyer 1995; Peterson et al. 2008) and optically obscured regions of the Galaxy (e.g., Figer et al. 1995; Frogel et al. 2001; Kurtev et al. 2007, for evolved, globular, and young clusters, respectively), and studying the unresolved stellar populations of optically obscured extragalactic regions using evolutionary population synthesis (EPS; e.g., Lançon et al. 2007; Riffel et al. 2008). EPS techniques attempt to simulate observed galaxy spectra by combining individual stellar spectra from a library and thereby derive the chemical and evolutionary properties of the unresolved stellar populations (e.g., Fioc & Rocca-Volmerange 1997; Leitherer et al. 1999; Bruzual & Charlot 2003; Maraston 2005; Bruzual 2007; Ramos Almeida et al. 2009).

The niche of near-infrared (NIR ~ 1 –5 μm) spectral classification is clear. While stars earlier than roughly M0 (~ 3800 K) are brighter at optical wavelengths, unobscured stars later than about M0 are brighter in the NIR and are thus better characterized at these wavelengths. Furthermore, it makes sense to use infrared diagnostics only when optical extinction compromises optical diagnostics. The optimum infrared wavelengths for observation depend on the amount of extinction. For some objects, such as young stellar objects or evolved stars, the presence of

circumstellar dust can result in significant excess continuum emission longward of 2 μm . For this reason the J and H bands are perhaps best to characterize embedded young stars since they avoid the veiling due to warm dust in the K band, while at the same time taking advantage of the reduced extinction relative to the optical (e.g., Meyer et al. 1998). On the other hand, heavily obscured objects without veiling are better characterized in the K band, or even the L' band in extreme cases. Consequently, the ideal infrared spectral library should contain spectra covering a wide range of wavelengths to satisfy a variety of possible applications.

With the maturing of NIR spectrographs and detector arrays, it has become possible to generate increasingly sophisticated NIR libraries of stellar spectra. Ivanov et al. (2004) presented a compilation of NIR spectral libraries available at that time. In Table 1 we revise and update this list. (The list does not include spectral libraries covering mostly L and T dwarfs. For our purposes a “library” is assumed to contain more than ten objects.) All of these libraries have shortcomings since none of them contains a large sample of stars, with a range of metallicities, covering all spectral types and luminosity classes, with spectra spanning a large wavelength range. In light of this, we have undertaken a project to construct an improved spectral library using the facility NIR spectrograph, SpeX, at the 3.0 m NASA Infrared Telescope Facility (IRTF) on Mauna Kea, Hawaii. The result of this work is the IRTF Spectral Library, which we are presenting in a series of papers. In the first paper of this series, Cushing et al. (2005) presented the spectra of M, L, and T dwarfs. The current paper presents 210 spectra of F, G, K, and M stars with luminosity classes between I and V (with mostly near-solar metallicities), and includes some asymptotic giant branch (AGB) stars, carbon stars, and S stars. The spectra of all of these stars, including the 13 L dwarfs and two T dwarfs from Cushing et al. (2005), and the gas giant planets (spectra summed along the central meridian) are available in digital form on the IRTF Web site.⁴ Additional papers on hot stars are currently in preparation.

³ Visiting Astronomer at the Infrared Telescope Facility, which is operated by the University of Hawai‘i under cooperative agreement No. NCC 5-538 with the National Aeronautics and Space Administration, Office of Space Science, Planetary Astronomy Program.

⁴ http://irtfweb.ifa.hawaii.edu/~spex/IRTF_Spectral_Library

Table 1
Near-IR Spectral Libraries

Spectral Library Reference	λ (μm)	Spectral Type	Luminosity Class	Number of Stars	Resolving Power
Johnson & Méndez (1970)	1.2–2.5	A–M	I–V	32	550
Kleinmann & Hall (1986)	2.0–2.5	F–M	I–V	26	2500–3100
Lambert et al. (1986)	1.5–2.5	C		30	75,000
McGregor et al. (1988)	1.0–2.5	Be, Ae	I	13	500
Tanaka et al. (1990)	1.5–2.5	C		33	2000
Terndrup et al. (1991)	0.45–2.45	M	III	32	1000
Lançon & Rocca-Volmerange (1992)	1.4–2.5	O–M	I–V	56	550
Origlia et al. (1993)	1.5–1.7	G–M	I–V	40	1500
Lazaro et al. (1994)	1.1–4.2	C		15	500
Ali et al. (1995)	2.0–2.4	F–M	V	33	1380
Oudmaijer et al. (1995)	2.1–2.4	post-AGB		18	400–700, ~1500
Dallier et al. (1996)	1.57–1.64	O–M	I–V	37	1500–2000
Hanson et al. (1996)	2.0–2.4	O–B	I–V	180	800–3000
Jones et al. (1996)	1.16–1.22	M	V	13	1085
Morris et al. (1996)	1.45–2.4	WR, O, B, LBV	I	26	570–1600
Wallace & Hinkle (1996)	2.02–2.41	G–M	I–V	12	45000
Blum et al. (1997)	1.5–1.8	O–B	I–V	11	575
Figer et al. (1997)	2.0–2.4	WR		38	525
Ramírez et al. (1997)	2.19–2.34	K–M	III	43	1380, 4830
Wallace & Hinkle (1997)	2.0–2.4	O–M	I–V	115	3000
Joyce (1998)	1.0–4.1	C		29	~500
Joyce et al. (1998)	1.0–1.3	M, S, C AGB	III	103	1100
Meyer et al. (1998)	1.5–1.7	O–M	I–V	85	3000
Pickles (1998) (compilation)	0.15–2.5	O–M	I–V	131	50–6000
Förster Schreiber (2000)	1.95–2.45	G–M	I–III	31	830, 3000
Lançon & Wood (2000)	0.5–2.5	K–M, AGB	I–III	77	1100
Wallace et al. (2000)	1.05–1.34	O–M	I–V	88	3000
Frogel et al. (2001)	2.17–2.34	RGB		129	1500
Lenorzer et al. (2002)	2.36–4.05	O–B	I–V	75	1500–2000
Malkan et al. (2002)	1.08–1.35	O–M	I–V	105	650
Vandenbussche et al. (2002)	2.36–4.05	O–M	I–V	293	1500–2000
Wallace & Hinkle (2002)	3.3–4.2	G–M, AGB	I–V	42	3000
Ivanov et al. (2004)	1.48–2.45	G–M	I–V	218	2000–3000
Ranade et al. (2004)	1.5–1.8	O5–M3	I–V	135	1000
Cushing et al. (2005)	0.8–4.2	M, L, T	V	30	940–2000
Lodieu et al. (2005)	0.6–1.0, 1.0–2.5	M6–L2	V	71	600
Hanson et al. (2005)	1.6–2.2	O–B	I–V	37	8000–12000
Ranade et al. (2007)	2.0–2.2	O7–M7	I–V	114	1000
van Loon et al. (2008)	2.9–4.1	C, AGB, RSG		50	200–400
Ranade et al. (2007)	1.1–1.3	O5–M8	I–V	125	1000
Venkata Raman & Anandarao (2008)	1.5–1.8, 2.0–2.4	AGB		78	1000
Mármol-Queraltó et al. (2008)	2.1–2.4	O–M	I–V	220	2500
Rayner et al. (this work)	0.8–5	F–M, S, C, AGB	I–V	212	2000, 2500

There are several important features of the IRTF Spectral Library. The wide wavelength range of ~ 0.8 – $5 \mu\text{m}$ (with a larger subset at 0.8 – $2.4 \mu\text{m}$) is covered in only two cross-dispersed instrument settings. For each setting, several spectral orders are simultaneously recorded during a single exposure. In addition, most of the spectral orders in each setting have significant wavelength overlap with the adjacent spectral orders. These instrumental aspects minimize potential calibration problems posed by stitching together multiple nonoverlapping wavelength ranges observed at different times (e.g., sequentially), a situation typically encountered with observations obtained with non-cross-dispersed (single-order) spectrographs. The signal-to-noise ratio (S/N) is better than ~ 100 across most of this range (except for the regions of poor atmospheric transmission and for $\lambda > 4 \mu\text{m}$) and the resolving powers of $R \equiv \lambda/\Delta\lambda \approx 2000$ at 0.8 – $2.4 \mu\text{m}$, and $R \approx 2500$ at 2.4 – $5 \mu\text{m}$, enable the accurate measurement of spectral type and luminosity class using established equivalent width (EW) and line ratio criteria

(see Section 3.1). In contrast to some other NIR spectral libraries, the continuum shape is preserved during data reduction (for details see Section 2.3), which is particularly useful for characterizing cool stars with strong molecular absorption bands that have been observed at low resolution $R \sim 100$. Preserving the continuum shape also allows for absolute flux calibration by scaling the spectra to published Two Micron All Sky Survey photometry (2MASS; Skrutskie et al. 2006) and for the computation of synthetic colors (e.g., $Y - J$, $J - H$, $H - K$, and $K - L'$).

2. OBSERVATIONS AND DATA REDUCTION

2.1. Sample Selection

As described by Morgan & Keenan (1973), the MK spectral classification system “is a phenomenology of spectral lines, blends, and bands, based on a general progression of color index (abscissa) and luminosity (ordinate). It is defined by an array of

standard stars located on a two-dimensional spectral type versus luminosity-class diagram. These standard reference points do not depend on specific line intensities or ratios of intensities; they have come to be defined by the *totality* of lines, blends, and bands in the ordinary *photographic region*” (emphasis added). In the MK system, the classification gives the spectral subtype and luminosity class (e.g., K0 III); this is the observational analogue to the projection on the luminosity-temperature plane (H–R diagram) for stars of a particular composition. Abundance adds a third dimension to the two-dimensional MK diagram and is represented by additional symbols determined by the relative intensities of lines or bands that reveal compositional differences from the Sun. For example, as a means of distinguishing a solar metallicity Population I giant K0 III star from one with a lower metal/hydrogen abundance, the classification of the latter becomes K0 III CN-1 or K0 III CN-2 (e.g., Morgan & Keenan 1973). With better quality spectra, increased precision in spectral classification is possible. For example, giants can often be subdivided into luminosity subclasses IIIa, IIIab, and IIIb. A fundamental characteristic of the MK system is that a finite array of discrete cells (spectral types) represents a continuum; i.e., spectra of stars of a given spectral subtype (e.g., K5 V) are not all identical. The precision attainable with MK classification has been estimated to be ± 0.6 spectral subtypes for B and A dwarfs by Jaschek & Jaschek (1973) and ± 0.65 spectral subtypes for G and K dwarfs by Gliese (1971). This precision depends upon observational dispersion (heterogeneous group of observers and instruments) and cosmic dispersion (e.g., chemical composition effects and rotation effects).

We attempted to construct a sample of stars with undisputed spectral types, traceable to the original developers of the MK classification system. The original MK standard stars (Johnson & Morgan 1953; Morgan & Keenan 1973) are generally too bright for us to observe. To that end, for the majority of the sample, we chose stars with classifications given by Morgan & Abt (1973), Morgan & Keenan (1973), Morgan et al. (1978), Keenan & McNeil (1989), Keenan & Newsom (2000),⁵ which in several cases were supplemented by stars taken from compilations of MK standard stars by Garcia (1989) and Jaschek (1978). Whenever references gave conflicting classifications, we chose the most recent revision. For F stars, we supplemented the lists generated from the aforementioned references with stars whose spectral types are given by Gray & Garrison (1989), Gray et al. (2001), and Abt & Morrell (1995). Additionally, for M stars, we included objects with classifications given by Kirkpatrick et al. (1991), Henry et al. (1994), and Kirkpatrick et al. (1997), again deferring to the latest revised classifications whenever conflicting or multiple spectral types were found in the various sources. In a few instances, stars with less certain classifications were observed in order to fill gaps in our coverage of spectral types due to observing limitations.

Despite their known variability in spectral type and relative rarity, we included AGB stars in our sample because their high luminosity makes them important in EPS studies of galaxies. Population synthesis and star counts in clusters indicate that AGB stars contribute more than 50% of the *K*-band light of stellar populations at 0.1–1 Gyr after an instantaneous burst of star formation (Lançon et al. 1999; Lançon 1999). The AGB phase is also important in providing feedback in the chemical evolution of galaxies. AGB stars are intermediate mass stars ($\sim 0.8\text{--}8 M_{\odot}$), which ascend the AGB in the H–R diagram

when helium and hydrogen ignite in shells surrounding their cores (this phase lasts about 2×10^5 yr). Shell burning in young AGB stars is stable but becomes increasingly unstable as the stars become more luminous, which leads to thermal pulsations. These stars are known as thermally pulsating AGB (TPAGB) stars. TPAGB stars are recognizable by a variety of observational criteria by which they are variously named: characteristic spectra (late-M, S, and C stars), pulsating variability (Mira variables, long-period variables), mass loss and maser emission (OH/IR stars). In our sample TPAGB stars are identified by their variability types (L: irregular, SR: semiregular, and M: Mira) given in the General Catalog of Variable Stars (GCVS; Kholopov et al. 1998).⁶ About 40 TPAGB stars are included in our sample.

Mass loss eventually removes the hydrogen-rich stellar envelope, effectively terminating the TPAGB phase. The central star subsequently evolves to higher temperatures while the circumstellar envelope expands and cools, exposing the star. Ionizing wind and radiation from the star quickly form a planetary nebula (PN). The transition from TPAGB to PN is known as the post-AGB (PAGB) or protoplanetary nebula phase and lasts a few thousand years. Although PAGB stars were not targeted in our sample, several supergiants that were observed have some of the characteristics of PAGB stars (see Section 4.3). (For a comprehensive review of AGB stars see Habing & Olofsson 2003).

In order to obtain a high S/N out into the thermal infrared ($\sim 2.3\text{--}5 \mu\text{m}$), we selected relatively bright stars. Consequently, they tend to be local and therefore of mostly solar composition. Figure 1(a) shows the distribution of metallicities for stars in our sample with spectroscopic measurements of [Fe/H] (Cayrel de Strobel et al. 1997). The distribution is typical for stars in the solar neighborhood (Nordström et al. 2004).

The object name, spectral classification and associated reference, GCVS variable type, *V*, $B - V$, and 2MASS (*J*, *H*, and *K_S*) magnitudes for each star in the sample are given in Table 2. All objects in the sample have declinations $-30 \deg > \delta > +70 \deg$, a range set by the latitude and declination limit of IRTF, and an airmass < 2 for good telluric correction. The stars have *K*-band magnitudes of $\sim 11 > K > 0$; the faint limit was set by the desire to obtain high S/N spectra in less than about 30 minutes of integration time, and the bright limit corresponds to detector saturation in the minimum exposure time of 0.1 s (although several brighter targets were observed using ad hoc methods). The total number of stars in the sample is 210. Table 3 gives the composition of the sample by spectral type and luminosity class. Due to practical limitations of observing time, there is no multiepoch coverage of variable stars or large numbers of stars with nonsolar metallicity. However, we anticipate future observing campaigns with SpeX at IRTF will add to the sample.

2.2. Observations

The observations were carried out over a period of eight years using SpeX at the IRTF. A detailed description of SpeX is given by Rayner et al. (2003). Briefly, SpeX is a 0.8–5.4 μm , medium-resolution, cross-dispersed spectrograph equipped with a 1024×1024 Aladdin 3 InSb array. The entire 0.8–5.4 μm wavelength range can be covered with two cross-dispersed modes: the short-wavelength cross-dispersed mode (SXD) and the long-wavelength cross-dispersed mode (LXD).

⁵ <http://www.astronomy.ohio-state.edu/MKcool>

⁶ <http://www.sai.msu.su/groups/cluster/gcvs/gcvs>

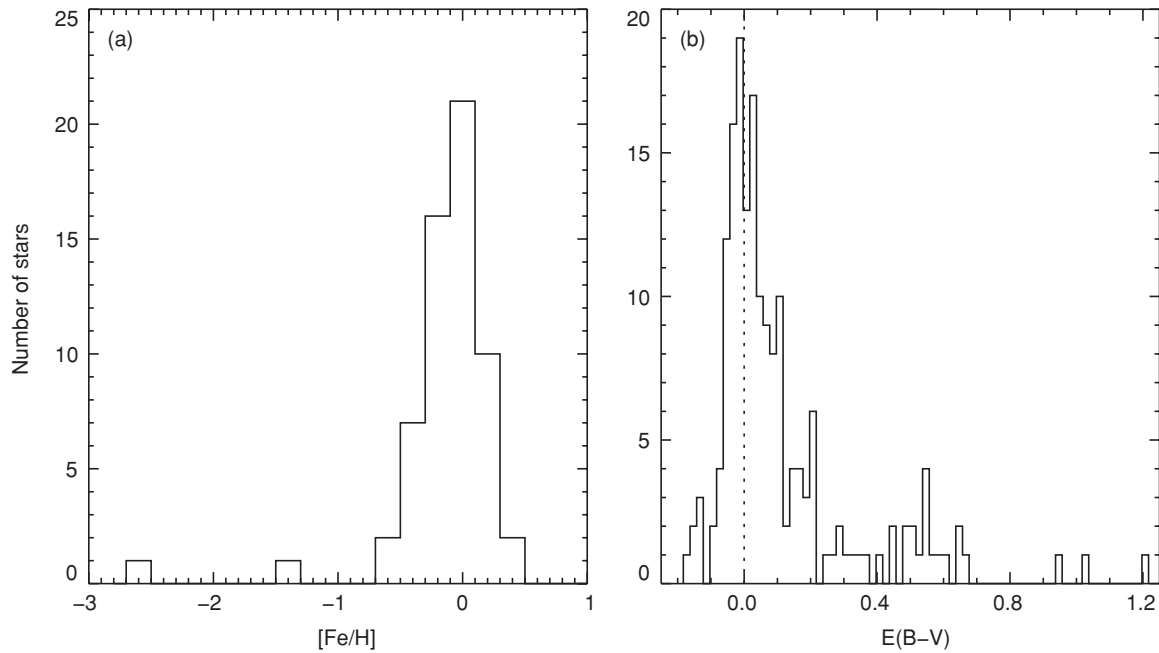


Figure 1. (a) Distribution of metallicities for stars in our sample with spectroscopic measurements of [Fe/H] (61 out of 210, mostly F, G, and K stars) from Cayrel de Strobel et al. (1997). The mean is -0.1 and the dispersion 0.2 dex, which is typical for stars in the solar neighborhood (within 40 pc; Nordström et al. 2004). (b) Distribution of $E(B-V)$ color excesses for the stars in our sample. The width of the peak at negative values indicates that the uncertainty in the color excesses is 0.036 mag.

The SXD mode provides simultaneous coverage of the 0.8–2.42 μm wavelength range, except for a 0.06 μm gap between the H and K bands, while the LXD1.9, LXD2.1, and LXD2.3 modes cover the 1.9–4.2, 2.20–5.0, and 2.38–5.4 μm wavelength ranges, respectively. For nearly all stars, the $0''.3$ (2 pixel) slit was used for both the SXD and LXD modes, providing resolving powers of 2000 and 2500, respectively. Measurements of arc lines obtained with the internal calibration unit indicate that the FWHM is 2 pixels at all wavelengths for the $0''.3$ slit. (The resolving power R varies by $\sim 20\%$ across a spectral order since it depends on the changing grating diffraction angle.) The length of the slit for these modes is $15''.0$ and the spatial scale is $0''.15 \text{ pixel}^{-1}$. The spectrograph also includes a high-throughput low-resolution $R \sim 200$ prism mode and a single-order $60''$ long-slit $R \sim 2000$ mode. An autonomous infrared slit viewer employing a 512×512 Aladdin 2 InSb array is used for object acquisition, guiding, and imaging photometry. The slit viewer covers a $60'' \times 60''$ field of view at a spatial scale of $0''.12 \text{ pixel}^{-1}$. An internal K-mirror image rotator enables the field to be rotated on the slit. Calibration observations are obtained using the internal calibration unit consisting of flat field and arc lamps, integrating sphere, and illumination optics that reproduce the beam from the telescope. A log of the observations including the object name, spectral type, UT date of observation, spectroscopic mode, resolving power, exposure time, associated telluric standard star, and sky conditions is presented in Table 4.

To facilitate subtraction of the additive components of the total signal (electronic bias level, dark current, sky and background emission) during the reduction process, the observations were obtained in a series of exposures in which the target was nodded along the slit between two positions separated by $7''.5$, and a sequence of nodded pairs was taken to build up S/N. A minimum of three pairs were taken (six spectra) to allow noisy pixels (mainly due to cosmic ray hits) to be rejected by a sigma-clipping algorithm. Guiding was done on spill-over from the science target in the slit using the infrared slit-viewing camera.

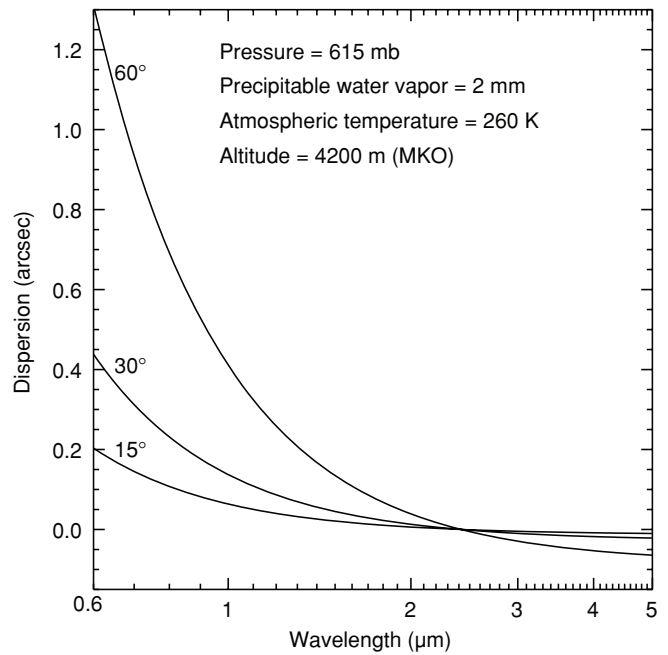


Figure 2. Atmospheric dispersion for the summit of Mauna Kea and the conditions indicated, as a function of wavelength (relative to $2.4 \mu\text{m}$) and zenith angle. Since the magnitude of atmospheric dispersion in the NIR is significant compared to the slit width used ($0''.3$), observations were made at the parallactic angle to minimize slit losses and measure the spectral shape more accurately.

In the SXD mode, where atmospheric dispersion is significant compared to the slit width of $0''.3$ (see Figure 2), the image rotator was set to the parallactic angle prior to each observation. As discussed in Section 2.3, observing at the parallactic angle minimized spectral slope variations. This is not as important in the LXD mode where atmospheric dispersion is an order a magnitude smaller.

Table 2
The Sample

Object (1)	HR Number (2)	Other Name (3)	Spectral Type (4)	Ref. (5)	Variability ^a Type (6)	<i>V</i> ^b (mag) (7)	<i>B</i> – <i>V</i> ^b (mag) (8)	<i>J</i> (mag) (9)	<i>H</i> (mag) (10)	<i>K_s</i> (mag) (11)
HD 7927	HR 382	ϕ Cas	F0 Ia	1	var	4.987	0.680	3.751 ± 0.296	3.537 ± 0.248	3.186 ± 0.268
HD 135153	HR 5660	i Lup	F0 Ib–II	1		4.904	0.376	4.258 ± 0.252	4.007 ± 0.194	3.991 ± 0.276
HD 6130	HR 292		F0 II	1		5.919	0.491	4.991 ± 0.274	4.690 ± 0.254	4.406 ± 0.020
HD 89025	HR 4013	ζ Leo	F0 IIIa	1	var	3.435	0.307	2.700 ± 0.232	2.628 ± 0.208	2.631 ± 0.280
HD 13174	HR 623	14 Ari	F0 III–IVn	2		4.989	0.335	4.441 ± 0.308	4.357 ± 0.240	4.062 ± 0.036
HD 27397	HR 1351	h Tau	F0 IV	1	DSCTC	5.593	0.283	5.002 ± 0.037	4.927 ± 0.047	4.853 ± 0.015
HD 108519			F0 V(n)	1		7.705	0.273	7.093 ± 0.021	6.998 ± 0.031	6.965 ± 0.040
HD 173638	HR 7055		F1 II	1	*I	5.710	0.595	4.213 ± 0.262	3.908 ± 0.228	3.840 ± 0.298
HD 213135	HR 8563		F1 V	2	var	5.942	0.343	5.276 ± 0.020	5.122 ± 0.027	5.031 ± 0.020
BD +38 2803	UU Her		F2–F5 Ib	3	SRd	8.190	0.090	7.635 ± 0.020	7.347 ± 0.053	7.253 ± 0.018
HD 182835	HR 7387	ν Aql	F2 Ib	1	var	4.660	0.593	3.109 ± 0.250	2.866 ± 0.214	2.728 ± 0.224
HD 40535	HR 2107	1 Mon	F2 III–IV	2	DSCT	6.128	0.297	5.489 ± 0.020	5.354 ± 0.029	5.281 ± 0.024
HD 164136	HR 6707	ν Her	kA9hF2mF2 (IV)	2	SRd:	4.411	0.383	2.967 ± 0.172	2.823 ± 0.168	2.771 ± 0.214
HD 113139	HR 4931	78 UMa	F2 V	1	var	4.929	0.365	4.323 ± 0.282	4.166 ± 0.274	3.953 ± 0.020
HD 26015	HR 1279		F3 V	1	var	6.026	0.395	5.244 ± 8.888	5.055 ± 0.031	5.030 ± 0.026
HD 21770	HR 1069	36 Per	F4 III	4	var	5.312	0.401	4.696 ± 0.240	4.442 ± 0.194	4.241 ± 0.036
HD 87822	HR 3979		F4 V	5		6.240	0.445	5.372 ± 0.018	5.251 ± 0.033	5.131 ± 0.021
HD 16232	HR 764	30 Ari B	F4 V	6		7.394	0.510	6.080 ± 0.020	5.908 ± 0.029	5.822 ± 0.021
HD 213306	HR 8571	δ Cep	F5 Ib–G1 Ib	7	DCEP	3.562	0.480	2.865 ± 0.200	2.608 ± 0.190	2.354 ± 0.216
HD 186155	HR 7495		F5 II–III	1	var	5.066	0.386	4.419 ± 0.254	4.219 ± 0.218	4.142 ± 0.278
HD 17918	HR 856		F5 III	8		6.295	0.471	5.430 ± 0.032	5.288 ± 0.044	5.176 ± 0.021
HD 218804	HR 8825	6 And	F5 V	1		5.923	0.436	5.147 ± 0.236	4.738 ± 0.031	4.674 ± 0.018
HD 27524			F5 V	1		6.800	0.436	5.970 ± 0.020	5.786 ± 0.016	5.762 ± 0.020
HD 75555			F5.5 III–IV	1		8.095	0.484	7.214 ± 0.018	7.035 ± 0.016	6.992 ± 0.018
HD 160365	HR 6577		F6 III–IV	1		6.116	0.556	5.005 ± 0.037	4.769 ± 0.020	4.697 ± 0.016
HD 11443	HR 544	α Tri	F6 IV	1	ELL	3.416	0.488	2.406 ± 0.236	2.182 ± 0.206	2.274 ± 0.266
HD 215648	HR 8665	ξ Peg	F6 V	1	var:	4.197	0.502	3.358 ± 0.254	3.078 ± 0.214	2.961 ± 0.286
HD 201078	HR 8084		F7 II–	1	DCEPS	5.769	0.532	4.638 ± 0.256	4.390 ± 0.222	4.374 ± 0.016
HD 124850	HR 5338	iota Vir	F7 III	1	*	4.079	0.514	3.140 ± 0.266	2.909 ± 0.236	2.801 ± 0.266
HD 126660	HR 5404	23 Boo	F7 V	1	*	4.052	0.497	3.179 ± 0.244	2.980 ± 0.216	2.739 ± 0.332
HD 190323			F8 Ia	1	var:	6.834	0.874	5.269 ± 0.024	4.992 ± 0.038	4.888 ± 0.018
HD 51956			F8 Ib	9		7.507	0.803	6.063 ± 0.024	5.756 ± 0.033	5.612 ± 0.031
HD 220657	HR 8905	68 Peg	F8 III	1		4.407	0.610	3.527 ± 0.266	3.230 ± 0.208	3.033 ± 0.256
HD 111844			F8 IV	1		7.870	0.560	6.796 ± 0.018	6.569 ± 0.017	6.524 ± 0.018
HD 219623	HR 8853		F8 V	1		5.577	0.524	4.871 ± 0.250	4.599 ± 0.190	4.306 ± 0.036
HD 27383		55 Tau	F8 V	1	BY:	6.886	0.560	5.820 ± 0.018	5.588 ± 0.021	5.542 ± 0.020
HD 102870	HR 4540	β Vir	F8.5 IV–V	1		3.608	0.442	2.597 ± 0.252	2.363 ± 0.230	2.269 ± 0.254
HD 6903	HR 339	ψ^3 Psc	F9 IIIa	10		5.550	0.689	4.565 ± 0.270	4.189 ± 0.228	4.183 ± 0.348
HD 176051	HR 7162		F9 V	1		5.224	0.588	3.847 ± 0.254	3.611 ± 0.252	3.655 ± 0.042
HD 165908	HR 6775	b Her	F9 V metal weak	1		5.046	0.519	3.459 ± 0.198	3.242 ± 0.190	3.107 ± 0.230
HD 114710	HR 4983	β Com	F9.5 V	10	BY:	4.257	0.571	3.232 ± 0.234	2.992 ± 0.192	2.923 ± 0.274
HD 185018	HR 7456		G0 Ib–II	11		5.978	0.881	4.364 ± 0.242	3.925 ± 0.216	3.953 ± 0.036
HD 109358	HR 4785	β CVn	G0 V	10	var	4.260	0.585	3.213 ± 0.218	2.905 ± 0.198	2.848 ± 0.310
HD 74395	HR 3459	F Hya	G1 Ib	11		4.628	0.840	3.194 ± 0.278	2.786 ± 0.262	2.710 ± 0.300
HD 216219			G1 II–III: Fe–1	11	CH0.5	7.450	0.640	6.265 ± 0.020	6.034 ± 0.021	5.935 ± 0.017
HD 21018	HR 1023		G1 III: CH–1:	10		6.383	0.862	4.864 ± 0.026	4.568 ± 8.888	4.357 ± 0.018
HD 10307	HR 483		G1 V	10		4.958	0.618	4.000 ± 0.262	3.703 ± 0.226	3.577 ± 0.314
HD 95128	HR 4277	47 UMa	G1–V Fe–0.5	10		5.049	0.606	3.960 ± 0.296	3.736 ± 0.224	3.750 ± 0.340
HD 20619			G1.5 V	10		7.049	0.656	5.876 ± 0.019	5.552 ± 0.040	5.469 ± 0.021
HD 42454			G2 Ib	12		7.361	1.232	5.121 ± 0.037	4.693 ± 0.036	4.598 ± 0.055
HD 39949			G2 Ib	12		7.225	1.090	5.279 ± 0.035	4.814 ± 0.036	4.664 ± 0.016
HD 3421	HR 157		G2 Ib–II	10		5.422	0.884	3.708 ± 0.208	3.320 ± 0.216	3.212 ± 0.276
HD 219477	HR 8842	61 Peg	G2 II–III	11		6.490	0.850	5.351 ± 0.248	4.771 ± 0.204	4.537 ± 8.888
HD 126868	HR 5409	ϕ Vir	G2 IV	11	var	4.810	0.698	3.541 ± 0.264	3.116 ± 0.426	3.067 ± 0.306
HD 76151	HR 3538		G2 V	10	var:	5.999	0.666	4.871 ± 0.037	4.625 ± 0.276	4.456 ± 0.023
HD 192713	HR 7741	22 Vul	G3 Ib–II Wk H&K comp?	11	EA/GS	5.167	1.046	3.532 ± 0.244	3.130 ± 0.202	2.938 ± 0.242
HD 176123	HR 7164		G3 II	11		6.37	0.990	4.651 ± 0.037	4.120 ± 0.202	4.067 ± 0.322
HD 88639	HR 4006		G3 IIIb Fe–1	10	var	6.046	0.844	4.726 ± 0.250	4.226 ± 0.204	4.018 ± 0.036
HD 10697	HR 508	109 Psc	G3 Va	10		6.260	0.725	5.386 ± 0.268	4.678 ± 0.031	4.601 ± 0.021
HD 179821			G4 O–Ia	11	SRd (post-AGB)	8.145	1.555	5.371 ± 0.023	4.998 ± 0.023	4.728 ± 0.020
HD 6474			G4 Ia	10	SRd	7.611	1.617	4.808 ± 0.354	4.199 ± 0.290	3.919 ± 0.458
HD 94481	HR 4255		G4 III–IIIb	10		5.653	0.830	4.235 ± 0.234	3.756 ± 0.224	3.745 ± 0.246
HD 108477	HR 4742		G4 III	10		6.313	0.865	4.838 ± 0.037	4.497 ± 0.232	4.271 ± 0.036
HD 214850	HR 8631		G4 V	11		5.726	0.714	4.619 ± 0.196	4.212 ± 0.180	3.937 ± 0.036

Table 2
(Continued)

Object (1)	HR Number (2)	Other Name (3)	Spectral Type (4)	Ref. (5)	Variability ^a Type (6)	V ^b (mag) (7)	B – V ^b (mag) (8)	J (mag) (9)	H (mag) (10)	K _s (mag) (11)
HD 190113			G5 Ib	11		7.870	1.500	5.301 ± 0.029	4.777 ± 0.036	4.557 ± 0.018
HD 18474	HR 885		G5: III: CN–3 CH–2 H _δ –1	10		5.470	0.890	3.616 ± 0.196	3.185 ± 0.158	2.975 ± 0.232
HD 193896	HR 7788		G5 IIIa	11		6.290	0.910	4.393 ± 0.278	3.938 ± 0.270	4.139 ± 0.036
HD 165185	HR 6748		G5 V	12	var	5.944	0.618	4.835 ± 0.037	4.614 ± 0.016	4.469 ± 0.016
HD 161664	HR 6617		G6 Ib H _δ 1	11	*	6.180	1.490	3.520 ± 0.282	2.850 ± 0.240	2.636 ± 0.280
HD 202314	HR 8126		G6 Ib–IIa Ca1 Ba0.5	11		6.169	1.102	4.701 ± 0.222	4.098 ± 0.250	4.020 ± 0.270
HD 58367	HR 2828	ε CMi	G6 IIb	10		4.988	1.007	3.457 ± 0.282	2.964 ± 0.224	2.826 ± 0.242
HD 27277			G6 III	10		8.090	0.990	6.278 ± 0.030	5.785 ± 0.029	5.680 ± 0.018
HD 115617	HR 5019	61 Vir	G6.5 V	10		4.739	0.709	3.334 ± 0.200	2.974 ± 0.176	2.956 ± 0.236
HD 333385	BD +29 3865		G7 Ia	11	L	8.705	2.187	4.766 ± 0.037	4.305 ± 0.214	3.793 ± 0.036
HD 25877	HR 1270		G7 II	10		6.316	1.161	4.444 ± 0.280	3.973 ± 0.172	3.819 ± 0.220
HD 182694	HR 7382		G7 IIIa	11		5.862	0.924	4.437 ± 0.264	3.994 ± 0.206	3.835 ± 0.286
HD 20618	HR 995	59 Ari	G7 IV	10		5.900	0.860	4.446 ± 0.266	4.050 ± 0.220	4.106 ± 0.286
HD 114946	HR 4995	55 Vir	G7 IV	10		5.318	0.878	3.742 ± 0.238	3.169 ± 0.192	3.114 ± 0.256
HD 16139			G7.5 IIIa	10		8.058	1.052	6.180 ± 0.026	5.707 ± 0.026	5.587 ± 0.021
HD 208606	HR 8374		G8 Ib	13		6.157	1.600	3.751 ± 0.246	3.124 ± 0.188	2.811 ± 0.280
HD 122563	HR 5270		G8: III: Fe–5	10	*	6.198	0.907	4.786 ± 0.298	4.030 ± 0.234	3.731 ± 0.036
HD 104979	HR 4608	ø Vir	G8 III Ba1 CN0.5 CH1	10		4.117	0.982	2.543 ± 0.328	2.126 ± 0.270	2.014 ± 0.270
HD 135722	HR 5681	δ Boo	G8 III Fe–1	11	*	3.482	0.951	1.659 ± 0.238	0.985 ± 0.192	1.223 ± 0.196
HD 101501	HR 4496	61 UMa	G8 V	10	var	5.323	0.723	3.988 ± 0.242	3.648 ± 0.228	3.588 ± 0.036
HD 75732	HR 3522	ρ ¹ Cnc	G8 V	14		5.944	0.860	4.768 ± 0.244	4.265 ± 0.234	4.015 ± 0.036
HD 170820			G9 II CN1 H _δ 1	11		7.371	1.575	4.469 ± 0.264	3.666 ± 0.200	3.543 ± 0.232
HD 222093	HR 8958		G9 III	11		5.652	1.023	4.205 ± 0.268	3.556 ± 0.222	3.520 ± 0.214
HD 165782		AX Sgr	K0 Ia	11	SRd	7.680	2.140	3.791 ± 0.258	3.098 ± 0.222	2.798 ± 0.254
HD 44391			K0 Ib	12		7.740	1.400	5.301 ± 0.019	4.759 ± 0.036	4.548 ± 0.017
HD 179870			K0 II	11		7.063	1.245	4.887 ± 0.034	4.048 ± 0.226	4.191 ± 0.036
HD 100006	HR 4433	86 Leo	K0 III	15		5.525	1.059	3.970 ± 0.266	3.379 ± 0.216	3.122 ± 0.330
HD 145675		14 Her	K0 V	11		6.652	0.877	5.158 ± 0.029	4.803 ± 0.016	4.714 ± 0.016
HD 164349	HR 6713	93 Her	K0.5 IIb	11		4.669	1.257	2.574 ± 0.282	2.033 ± 0.208	1.937 ± 0.202
HD 9852			K0.5 III CN1	10		7.930	1.460	5.339 ± 0.041	4.775 ± 0.023	4.576 ± 0.015
HD 63302	HR 3026	QY Pup	K1 Ia–Iab	10	SRd	6.347	1.752	3.746 ± 0.248	2.958 ± 0.224	2.702 ± 0.266
HD 36134	HR 1830		K1–III Fe–0.5	10	var	5.778	1.156	3.903 ± 0.280	3.207 ± 0.266	3.124 ± 0.276
HD 91810			K1–IIIb CN1.5 Ca1	10		6.550	1.170	4.998 ± 0.280	4.297 ± 0.015	4.182 ± 0.344
HD 25975	HR 1277	49 Per	K1 III	4		6.089	0.944	4.599 ± 0.304	4.057 ± 0.246	4.022 ± 0.366
HD 165438	HR 6756		K1 IV	11		5.766	0.967	4.376 ± 0.322	3.788 ± 0.254	3.749 ± 0.228
HD 142091	HR 5901	11 CrB	K1 IVa	11		4.812	0.996	3.035 ± 0.184	2.575 ± 0.180	2.423 ± 0.242
HD 10476	HR 493	107 Psc	K1 V	10	var	5.242	0.836	3.855 ± 0.240	3.391 ± 0.226	3.285 ± 0.266
HD 124897	HR 5340	Arcturus	K1.5 III Fe–0.5	11	var	-0.050	1.231	-2.252 ± 0.157	-2.810 ± 0.996	-2.911 ± 0.170
HD 212466		RW Cep	K2 O–Ia	11	SRd	6.626	2.275	3.090 ± 0.212	2.462 ± 0.192	2.027 ± 0.238
HD 2901			K2 III Fe–1	10		6.917	1.232	5.130 ± 0.300	4.250 ± 0.282	4.116 ± 0.338
HD 132935			K2 III	11		6.697	1.364	4.598 ± 0.200	3.654 ± 0.208	3.590 ± 0.240
HD 137759	HR 5744	12 Dra	K2 III	11	*	3.291	1.166	1.293 ± 0.220	0.724 ± 0.146	0.671 ± 0.200
HD 3765			K2 V	10	E:	7.363	0.942	5.694 ± 0.024	5.272 ± 0.051	5.164 ± 0.016
HD 23082			K2.5 II	10		7.520	1.850	3.874 ± 0.190	3.116 ± 0.202	2.786 ± 0.224
HD 187238			K3 Iab–Ib	12		7.100	2.040	3.625 ± 0.268	2.749 ± 0.204	2.418 ± 0.268
HD 16068			K3 II–III	10		7.380	1.790	4.773 ± 0.264	3.868 ± 0.296	3.676 ± 0.352
HD 221246	HR 8925		K3 III	11		6.170	1.460	3.989 ± 0.280	3.177 ± 0.244	2.949 ± 0.330
HD 178208	HR 7252		K3 III	11		6.441	1.393	4.514 ± 0.262	3.820 ± 0.222	3.571 ± 0.278
HD 35620	HR 1805	φ Aur	K3 III Fe1	10		5.079	1.403	2.905 ± 0.256	2.167 ± 0.192	2.104 ± 0.262
HD 99998	HR 4432	e Leo	K3+ III Fe–0.5	10		4.675	1.531	2.160 ± 0.266	1.390 ± 0.244	1.247 ± 0.264
HD 114960			K3.5 IIIb CN0.5 CH0.5	10		6.565	1.412	4.207 ± 0.254	3.358 ± 0.242	3.339 ± 0.268
HD 219134	HR 8832		K3 V	11	*	5.567	0.994	3.981 ± 0.258	3.469 ± 0.226	3.261 ± 0.304
HD 185622	HR 7475		K4 Ib	11	Lc:	6.376	2.026	2.138 ± 0.214	1.312 ± 0.140	0.986 ± 0.166
HD 201065			K4 Ib–II	11		7.584	1.793	4.868 ± 0.256	3.939 ± 0.260	3.669 ± 0.260
HD 207991			K4– III	11		6.870	1.600	4.039 ± 0.226	3.222 ± 0.210	2.923 ± 0.270
HD 45977			K4 V	16		9.140	1.120	7.079 ± 0.024	6.601 ± 0.034	6.406 ± 0.018
HD 216946	HR 8726		K5 Ib	11	Lc	4.969	1.773	1.792 ± 0.264	0.958 ± 0.150	0.724 ± 0.178
HD 181596			K5 III	11		7.510	1.600	4.923 ± 0.216	4.026 ± 0.190	3.817 ± 0.206
HD 36003			K5 V	10		7.640	1.113	5.615 ± 0.019	5.111 ± 0.071	4.880 ± 0.024
HD 120477	HR 5200	υ Boo	K5.5 III	10	var	4.046	1.520	1.218 ± 0.264	0.438 ± 0.180	0.435 ± 0.182
HD 3346	HR 152		K6 IIIa	10	SRs	5.101	1.582	2.257 ± 0.282	1.375 ± 0.182	1.263 ± 0.182
HD 181475			K7 IIa	11	SRb:	6.960	2.070	2.978 ± 0.298	2.121 ± 0.252	1.816 ± 0.282
HD 194193	HR 7800		K7 III	11	var	5.926	1.612	3.129 ± 0.226	2.240 ± 0.180	1.966 ± 0.264
HD 237903		36 UMa B	K7 V	13		8.691	1.352	6.119 ± 0.020	5.499 ± 0.034	5.361 ± 0.016

Table 2
(Continued)

Object (1)	HR Number (2)	Other Name (3)	Spectral Type (4)	Ref. (5)	Variability ^a Type (6)	V^b (mag) (7)	$B - V^b$ (mag) (8)	J (mag) (9)	H (mag) (10)	K_s (mag) (11)
HD 201092	HR 8086	61 Cyg B	K7 V	11	IS	6.055	1.354	3.546 ± 0.278	2.895 ± 0.218	2.544 ± 0.328
HD 213893			M0 IIIb	11		6.691	1.534	4.009 ± 0.330	3.092 ± 0.248	2.869 ± 0.274
HD 19305			M0 V	10		9.072	1.360	6.492 ± 0.021	5.843 ± 0.034	5.646 ± 0.021
HD 236697			M0.5 Ib	10	Lc	8.630	2.157	4.860 ± 0.316	3.878 ± 0.176	3.434 ± 0.358
HD 209290		Gl 846	M0.5 V	11		9.167	1.457	6.196 ± 0.023	5.562 ± 0.051	5.322 ± 0.023
HD 339034		NR Vul	M1 Ia	13	Lc	9.302	3.036	3.253 ± 0.266	2.141 ± 0.222	1.691 ± 0.224
HD 14404		PR Per	M1–Iab–Ib	10	Lc	7.904	2.303	3.556 ± 0.312	2.682 ± 0.192	2.247 ± 0.298
HD 39801	HR 2061	Betelgeuse	M1–M2 Ia–Iab	10	SRc	0.481	1.861	-2.989 ± 0.103	-4.007 ± 0.162	-4.378 ± 0.186
HD 204724	HR 8225	2 Peg	M1+ III	11	var	4.554	1.618	1.701 ± 0.292	0.784 ± 0.166	0.666 ± 0.182
HD 42581		Gl 229 A	M1 V	17	UV	8.152	1.491	5.104 ± 0.037	4.393 ± 0.254	4.166 ± 0.232
HD 35601			M1.5 Iab–Ib	11	Lc	7.350	2.200	2.930 ± 0.248	1.942 ± 0.222	1.662 ± 0.234
BD +60 265			M1.5 Ib	10		8.493	2.345	4.002 ± 0.208	3.147 ± 0.162	2.625 ± 0.242
HD 36395		Gl 205	M1.5 V	17	BY:	7.966	1.474	4.999 ± 0.300	4.149 ± 0.212	4.039 ± 0.260
HD 206936	HR 8316	μ Cep	M2–Ia	11	SRc	4.104	2.327	-0.326 ± 0.204	-1.264 ± 0.180	-1.620 ± 0.160
HD 10465			M2 Ib	10	Lc	6.816	1.860	2.658 ± 0.218	1.862 ± 0.168	1.507 ± 0.194
HD 23475	HR 1155	BE Cam	M2 II	10	Lc	4.462	1.877	0.567 ± 0.194	-0.422 ± 0.158	-0.650 ± 0.166
HD 120052	HR 5181	87 Vir	M2 III	11	var	5.436	1.619	1.884 ± 0.252	1.018 ± 0.216	0.730 ± 0.256
HD 95735		Gl 411	M2 V	17	BY:	7.498	1.508	4.203 ± 0.242	3.640 ± 0.202	3.254 ± 0.306
Gl 806			M2 V	17	var	10.730	1.570	7.329 ± 0.018	6.769 ± 0.023	6.533 ± 0.016
HD 219734	HR 8860	8 And	M2.5 III Ba0.5	11	var	4.830	1.655	1.615 ± 0.198	0.539 ± 0.168	0.506 ± 0.182
Gl 381			M2.5 V	17	var	10.640	1.573	7.021 ± 0.023	6.471 ± 0.049	6.193 ± 0.026
Gl 581		HO Lib	M2.5 V	18	BY	10.572	1.601	6.706 ± 0.026	6.095 ± 0.033	5.837 ± 0.023
RW Cyg			M3 to M4 Ia–Iab	11	SRc	8.361	2.881	2.117 ± 0.294	0.964 ± 0.152	0.640 ± 0.210
CD –31 4916			M3 Iab–Ia	13	Lc	8.878	2.238	4.612 ± 0.208	3.486 ± 0.234	3.139 ± 0.246
HD 14469		SU Per	M3–M4 Iab	10	SRc	7.697	2.175	2.824 ± 0.254	1.928 ± 0.184	1.455 ± 0.222
HD 40239	HR 2091	π Aur	M3 IIb	10	Lc	4.290	1.698	0.245 ± 0.220	-0.602 ± 0.174	-0.813 ± 0.168
HD 39045	HR 2018		M3 III	10	Lb:	6.249	1.752	2.655 ± 0.300	1.698 ± 0.196	1.407 ± 0.178
Gl 388		AD Leo	M3 V	18	UV	9.421	1.544	5.449 ± 0.027	4.843 ± 0.020	4.593 ± 0.017
HD 14488		RS Per	M3.5 Iab Fe–1 var?	10	SRc	8.490	2.256	3.054 ± 0.218	2.108 ± 0.192	1.562 ± 0.210
HD 28487			M3.5 III Ca–0.5	10	SRc:	6.800	1.740	2.684 ± 0.304	1.784 ± 0.268	1.457 ± 0.302
Gl 273		Luyten's Star	M3.5 V	17		9.832	1.554	5.714 ± 0.032	5.219 ± 0.063	4.857 ± 0.023
HD 19058	HR 921	ρ Per	M4+ IIIa	10	SRb	3.390	1.646	-0.779 ± 0.182	-1.675 ± 0.158	-1.904 ± 0.152
HD 214665	HR 8621		M4+ III	11	Lb	5.090	1.580	1.087 ± 0.246	0.131 ± 0.168	-0.159 ± 0.174
HD 4408	HR 211	57 Psc	M4 III	10	SRs	5.341	1.616	1.441 ± 0.246	0.504 ± 0.156	0.254 ± 0.168
HD 27598		DG Eri	M4– III	11	SRb	7.017	1.671	2.987 ± 0.270	2.106 ± 0.230	1.847 ± 0.264
Gl 213			M4 V	18	BY	11.597	1.655	7.124 ± 0.021	6.627 ± 0.018	6.389 ± 0.016
Gl 299			M4 V	18	BY:	12.834	1.768	8.424 ± 0.023	7.927 ± 0.042	7.660 ± 0.026
HD 204585	HR 8223	NV Peg	M4.5 IIIa	11	SRb	5.856	1.500	1.262 ± 0.280	0.260 ± 0.162	-0.051 ± 0.186
Gl 268AB		QY Aur	M4.5 V	18	UV	11.49	1.70	6.731 ± 0.026	6.152 ± 0.047	5.846 ± 0.018
HD 156014	HR 6406	α^1 Her A	M5 Ib–II	11	SRc	3.057	1.447	-2.302 ± 0.166	-3.224 ± 0.174	-3.511 ± 0.150
HD 175865	HR 7157	13 R Lyr	M5 III	13	SRb	4.026	1.588	-0.738 ± 0.222	-1.575 ± 0.230	-1.837 ± 0.208
Gl 51			M5 V	17	UV	13.78	1.68	8.611 ± 0.027	8.014 ± 0.023	7.718 ± 0.020
Gl 866ABC		EZ Aqr	M5 V	18	UV+BY	12.33	1.96	6.553 ± 0.019	5.954 ± 0.031	5.537 ± 0.020
HD 94705	HR 4267	VY Leo	M5.5 III:	10	Lb:	5.786	1.453	0.434 ± 0.204	-0.449 ± 0.248	-0.762 ± 0.296
HD 196610	HR 7886	EU Del	M6 III	11	SRb	6.058	1.482	0.345 ± 0.206	-0.774 ± 0.210	-1.009 ± 0.204
HD 18191	HR 867	ρ^2 Ari	M6– III:	10	SRb	5.815	1.452	0.230 ± 0.208	-0.652 ± 0.200	-0.868 ± 0.222
Gl 406		CN Leo	M6 V	17	UV	13.529	2.013	7.085 ± 0.024	6.482 ± 0.042	6.084 ± 0.017
GJ 1111		DX Cnc	M6.5 V	18	UV	14.824	2.066	8.235 ± 0.021	7.617 ± 0.018	7.260 ± 0.024
HD 14386		Mira	M5e–M9e III	19	M	4.954	1.549	-0.732 ± 0.149	-1.574 ± 0.192	-2.213 ± 0.216
HD 108849		BK Vir	M7– III:	10	SRb	7.460	1.540	0.544 ± 0.186	-0.376 ± 0.186	-0.730 ± 0.214
HD 207076		EP Aqr	M7– III:	11	SRb	6.686	1.491	-0.296 ± 0.202	-1.373 ± 0.274	-1.708 ± 0.376
Gl 644C		vB 8	M7 V	17	UV	16.80	2.20	9.776 ± 0.029	9.201 ± 0.024	8.816 ± 0.023
MY Cep			M7–M7.5 I	19	SRc	14.520	1.86	4.583 ± 0.280	2.980 ± 0.242	2.138 ± 0.278
HD 69243	HR 3248	R Cnc	M6e–M9e III	19	M	7.752	1.516	0.770 ± 0.198	-0.327 ± 0.156	-0.705 ± 0.168
BRI B2339–0447			M7–8 III	20		9.143 ± 0.023	8.174 ± 0.031	7.653 ± 0.021
IRAS 01037+1219		WX Psc	M8 III	19	M (OH/IR)	7.437 ± 0.026	4.641 ± 0.200	2.217 ± 0.298
Gl 752B		vB 10	M8 V	17	UV:	17.50	2.13	9.908 ± 0.025	9.226 ± 0.026	8.765 ± 0.022
LP 412–31			M8 V	21		11.759 ± 0.021	11.066 ± 0.022	10.639 ± 0.018
IRAS 21284–0747		HY Aqr	M8–9 III	20	M	6.173 ± 0.026	5.316 ± 0.026	4.757 ± 0.023
IRAS 14436–0703		AQ Vir	M8–9 III	20	M	5.654 ± 0.021	4.980 ± 0.016	4.497 ± 0.316
IRAS 14303–1042			M8–9 III	20	M	6.502 ± 0.019	5.643 ± 0.040	4.959 ± 0.021
IRAS 15060+0947		FV Boo	M9 III	20	M	5.450 ± 0.020	4.520 ± 0.232	3.836 ± 0.272
BRI B1219–1336		VX Crv	M9 III	20	M	8.659 ± 0.026	7.892 ± 0.031	7.344 ± 0.021
DENIS–P J104814.7 –395606.1			M9 V	22		9.538 ± 0.022	8.905 ± 0.044	8.447 ± 0.023

Table 2
(Continued)

Object (1)	HR Number (2)	Other Name (3)	Spectral Type (4)	Ref. (5)	Variability ^a Type (6)	V ^b (mag) (7)	B – V ^b (mag) (8)	J (mag) (9)	H (mag) (10)	K _s (mag) (11)
LP 944–20			M9 V	23	10.725 ± 0.021	10.017 ± 0.021	9.548 ± 0.023	
LHS 2065			M9 V	17	UV	18.85	...	11.212 ± 0.026	10.469 ± 0.026	9.942 ± 0.024
LHS 2924			M9 V	17	UV	19.58	...	11.990 ± 0.021	11.225 ± 0.029	10.744 ± 0.024
BRI B0021–0214			M9.5 V	23	BY	...	11.992 ± 0.035	11.084 ± 0.022	10.539 ± 0.023	
IRAS 14086–0703		IO Vir	M10+ III	20	6.645 ± 0.019	4.861 ± 0.286	3.587 ± 0.356	
HD 142143		V* ST Her	M6.5S to M7S III:	11	SRb	...	0.743 ± 0.242	–0.137 ± 0.210	–0.542 ± 0.206	
BD +44 2267		AV CVn	S2.5 Zr 2	24	Lb	9.801	1.886	6.278 ± 0.035	5.431 ± 0.061	5.157 ± 0.018
HD 64332		NQ Pup	S4.5 Zr 2 Ti 4	10	Lb	7.550	1.730	3.542 ± 0.292	2.587 ± 0.212	2.306 ± 0.274
HD 44544		FU Mon	SC5.5 Zr 0.5	24	SR	8.945	3.085	3.395 ± 0.236	2.101 ± 0.204	1.675 ± 0.226
HD 62164		SU Mon	S5–S6 Zr 3 to 4 Ti 0	10	SRb	8.250	2.600	2.805 ± 0.258	1.705 ± 0.242	1.257 ± 0.298
HD 76846			C–R2+ IIIa: C2 2.5	10		9.350	1.390	7.354 ± 0.020	6.812 ± 0.023	6.636 ± 0.016
HD 31996	HR 1607	R Lep	C7, 6e(N4)	19	M	8.081	5.699	2.160 ± 0.268	0.884 ± 0.224	0.137 ± 0.244
HD 44984	HR 2308	BL Ori	C–N4 C2 3.5	10	Lb	6.215	2.341	2.192 ± 0.324	1.006 ± 0.190	0.770 ± 0.196
HD 76221	HR 3541	X Cnc	C–N 4.5 C2 5.5 MS 3	10	SRb	6.647	3.365	1.569 ± 0.236	0.489 ± 0.186	0.063 ± 0.194
HD 92055	HR 4163	U Hya	C–N4.5 C2 4.5	10	SRb	4.955	2.662	0.803 ± 0.248	–0.254 ± 0.322	–0.716 ± 0.362
HD 70138			C–J4.5 IIIa: C2 6 j 6	10	Lb:	9.420	1.667	5.809 ± 0.023	4.899 ± 0.021	4.382 ± 0.018
HD 48664		CZ Mon	C–N5 C2 6	10	Lb	9.450	3.190	4.327 ± 0.260	3.039 ± 0.202	2.434 ± 0.234
HD 57160		BM Gem	C–J5– C2 5– j 4	10	SRb	4.398 ± 0.232	3.304 ± 0.210	2.728 ± 0.254

Notes. ^a Variability type from the General Catalog of Variable Stars (Kholopov et al. 1998). The variability type is described in <http://www.sai.msu.su/groups/cluster/gcvs/gcvs/iii/vartype.txt>.

^b V and B – V values are primarily from Mermilliod (2006) and are augmented with values from Kharchenko (2001), Beauchamp et al. (1994), and Leggett (1992).

References. (1) Gray et al. 2001; (2) Gray & Garrison 1989; (3) Rosino 1951; (4) Roman 1955; (5) Abt 1981; (6) Cowley 1976; (7) Kraft 1960; (8) Morgan & Keenan 1973; (9) MacConnell & Bidelman 1976; (10) Keenan & Newsom 2000; (11) Keenan & McNeil 1989; (12) Jaschek 1978; (13) Garcia 1989; (14) Cowley et al. 1967; (15) Kharchenko 2001; (16) Upgren et al. 1972; (17) Kirkpatrick et al. 1991; (18) Henry et al. 1994; (19) Kholopov et al. 1998; (20) Kirkpatrick et al. 1997; (21) Kirkpatrick et al. 1995; (22) Delfosse et al. 2001; (23) Kirkpatrick et al. 1999; (24) Ake 1979.

An A0 V star was observed before or after each science object to correct for absorption due to the Earth's atmosphere (see Figure 3) and to flux calibrate the science object spectra. The airmass difference between the object and “telluric standard” was almost always less than 0.1 and usually less than 0.05. However, in a few cases where there was a paucity of nearby A0 V stars, the airmass difference was as large as 0.15. Standard stars were also chosen to be located within 10 deg of the science object whenever possible, to minimize the effects of any differential flexure in the instrument between the observations of the object and standard. This limit on the angular distance provides a good compromise between the requirements to match airmass, minimize flexure, and find suitably bright standard stars. On those few occasions when it was necessary to observe a telluric standard more than 10 deg away from the object due to a lack of A0 V stars in certain parts of the sky, we found that telluric CO₂ (predominantly at 2.01 μm) features were sometimes not adequately removed by the standard star despite a good airmass match and good correction of telluric H₂O. (See, for example, Figure 54, where the F7 III and F8 III stars were corrected with telluric standard stars at separations and airmass differences of 14 deg and 0.09, and 21 deg and 0.05, respectively.) We attribute this to the possibility that telluric H₂O and CO₂ are not well mixed and to patchy CO₂ distribution. Finally, a set of internal flat field exposures and argon arc lamp exposures was taken after each object/standard pair for flat fielding and wavelength calibration purposes.

2.3. Data Reduction

We reduced the data using Spextool (Cushing et al. 2004), the facility IDL-based data reduction package for SpeX. The initial image processing consisted of correcting each science

Table 3
Spectral Composition of Library

Spectral Type	Luminosity Class					
	0	I	II	III	IV	V
F	0	7	4	10	5	15
G	1	12	6	13	3	11
K	1	7	5	19	2	8
M	0	14	2	27	0	25
S	5
C	8

frame for nonlinearity, subtracting the pairs of images taken at the two different slit positions, and dividing the pair-subtracted images by a normalized flat field. In each frame, the spectra in the individual orders were then optimally extracted (e.g., Horne 1986) and wavelength calibrated. (All wavelengths are given in vacuum.) The extracted spectra in each order from the set of frames for a given object were then combined using the median. This resulted in a single spectrum in each order for a given object.

The spectra in the individual orders were then corrected for telluric absorption and flux calibrated using the extracted A0 V spectra and the technique described by Vacca et al. (2003). In addition to correcting for the absorption due to the atmosphere, this process also removes the signature of the instrumental throughput and restores the intrinsic (i.e., above the atmosphere) spectrum of each science object in each spectral order. Briefly, this technique scales a theoretical model spectrum of Vega to the observed visual magnitude of the observed standard star, convolves it to the observed resolution, and adjusts the H₁ line strengths to match the observed strengths of the standard star. The ratio

Table 4
Log of SpeX Observations

Object (1)	Spectral Type (2)	UT Date (3)	Spectroscopy Mode (4)	R (5)	Exp. Time (sec) (6)	A0 V Standard (7)	Sky Conditions (8)
HD 7927	F0 Ia	2005 Oct 6	SXD	2000	120	HD 12365	Clear
		2005 Oct 6	LXD1.9	2500	150	HD 12365	Clear
HD 135153	F0 Ib-II	2007 Jun 24	SXD	2000	96	HD 146624	Clear
		2007 Jun 24	LXD2.1	2500	300	HD 146624	Clear
HD 6130	F0 II	2001 Sep 1	SXD	2000	100	HD 12365	Thin Cirrus
		2001 Sep 1	LXD1.9	2500	200	HD 12365	Thin Cirrus
HD 89025	F0 IIIa	2007 Apr 25	SXD	2000	100	HD 88960	Clear
		2007 Apr 25	LXD1.9	2500	200	HD 88960	Clear
HD 13174	F0 III-IVn	2003 Oct 16	SXD	2000	150	HD 16811	Thin Cirrus
		2003 Oct 16	LXD2.1	2500	300	HD 16811	Thin Cirrus
HD 27397	F0 IV	2005 Oct 6	SXD	2000	120	HD 31295	Clear
		2005 Oct 6	LXD2.1	2500	300	HD 31295	Clear
HD 108519	F0 V(n)	2007 Jun 24	SXD	2000	480	HD 107655	Clear
		2007 Jun 24	LXD1.9	2500	600	HD 107655	Thin Cirrus
HD 173638	F1 II	2008 Oct 8	SXD	2000	120	HD 171149	Thin Cirrus
		2008 Oct 12	LXD2.1	2500	300	HD 171149	Thin Cirrus
HD 213135	F1 V	2008 Oct 8	SXD	2000	180	HD 212643	Thin Cirrus
		2008 Oct 12	LXD1.9	2500	450	HD 212643	Thin Cirrus
BD +38 2803	F2-F5 Ib	2003 Aug 10	SXD	2000	720	HD 157778	Clear
		2003 Aug 10	LXD2.1	2500	600	HD 157778	Clear
HD 182835	F2 Ib	2003 Oct 16	SXD	2000	200	HD 177724	Thin Cirrus
HD 40535	F2 III-IV	2006 Dec 21	SXD	2000	150	HD 45380	Clear
		2006 Dec 21	LXD2.1	2500	300	HD 45380	Clear
HD 164136	kA9hF2mF2 (IV)	2005 Oct 6	SXD	2000	120	HD 165029	Clear
		2001 Sep 1	LXD1.9	2500	100	HD 174567	Thin Cirrus
HD 113139	F2 V	2002 May 29	SXD	2000	210	HD 118214	Clear
		2002 May 29	LXD2.1	2500	250	HD 118214	Clear
HD 26015	F3 V	2000 Oct 24	SXD	2000	200	HD 23258	Clear
		2005 Oct 7	LXD2.1	2500	300	HD 21686	Clear
HD 21770	F4 III	2006 Dec 21	SXD	2000	150	HD 21038	Clear
		2006 Dec 21	LXD2.1	2500	300	HD 21038	Clear
HD 87822	F4 V	2001 Mar 10	SXD	2000	300	HD 88960	Thin Cirrus
		2001 Mar 10	LXD2.3	2500	500	HD 88960	Thin Cirrus
HD 16232	F4 V	2001 Aug 6	SXD	2000	60	HD 13869	Clear
		2003 Oct 6	LXD2.1	2500	250	HD 16811	Thin Cirrus
HD 213306	F5 Ib - G1 Ib	2003 Oct 16	SXD	2000	140	HD 223386	Thin Cirrus
		2003 Oct 16	LXD2.1	2500	60	HD 223386	Thin Cirrus
HD 186155	F5 II-III	2001 Aug 31	SXD	2000	90	HD 192538	Thin Cirrus
		2001 Aug 31	LXD1.9	2500	250	HD 192538	Thin Cirrus
HD 17918	F5 III	2000 Oct 24	SXD	2000	200	HD 16811	Clear
		2000 Oct 25	LXD2.3	2500	300	HD 16811	Clear
HD 218804	F5 V	2001 Oct 20	SXD	2000	225	HD 219290	Thin Cirrus
		2001 Oct 20	LXD1.9	2500	200	HD 219290	Thin Cirrus
HD 27524	F5 V	2003 Jan 14	SXD	2000	120	HD 25175	Clear
		2003 Sep 21	LXD2.1	2500	300	HD 25175	Clear
HD 75555	F5.5 III-IV	2007 Apr 25	SXD	2000	600	HD 71906	Clear
HD 160365	F6 III-IV	2003 Jul 7	SXD	2000	100	HD 165029	Thin Cirrus
		2003 Jul 7	LXD2.1	2500	300	HD 165029	Thin Cirrus
HD 11443	F6 IV	2005 Oct 7	SXD	2000	61	HD 13869	Clear
		2005 Oct 7	LXD2.1	2500	150	HD 13869	Clear
HD 215648	F6 V	2008 Oct 8	SXD	2000	180	HD 210501	Thin Cirrus
HD 201078	F7 II-	2008 Oct 11	SXD	2000	360	HD 196724	Thick Cirrus
HD 124850	F7 III	2007 Apr 25	SXD	2000	120	HD 126129	Clear
HD 126660	F7 V	2007 Jun 22	SXD	2000	120	HD 121409	Clear
		2007 Jun 22	LXD2.1	2500	400	HD 121409	Clear
HD 190323	F8 Ia	2008 Oct 8	SXD	2000	160	HD 196724	Thin Cirrus
		2008 Oct 8	LXD2.1	2500	300	HD 196724	Thin Cirrus
HD 51956	F8 Ib	2003 Oct 16	SXD	2000	200	HD 53205	Thin Cirrus
		2006 Dec 21	LXD2.1	2500	300	HD 60357	Clear
HD 220657	F8 III	2006 Dec 21	SXD	2000	90	HD 222749	Clear
		2008 Oct 12	LXD1.9	2500	150	HD 210501	Thin Cirrus
HD 111844	F8 IV	2007 Apr 25	SXD	2000	360	HD 107655	Clear
HD 219623	F8 V	2001 Oct 20	SXD	2000	105	HD 219290	Thin Cirrus
		2001 Oct 20	LXD1.9	2500	200	HD 219290	Thin Cirrus

Table 4
(Continued)

Object (1)	Spectral Type (2)	UT Date (3)	Spectroscopy Mode (4)	R (5)	Exp. Time (sec) (6)	A0 V Standard (7)	Sky Conditions (8)
HD 27383	F8 V	2000 Oct 24	SXD	2000	150	HD 23258	Clear
		2000 Oct 25	LXD2.3	2500	300	HD 23258	Clear
HD 102870	F8.5 IV–V	2007 Apr 25	SXD	2000	120	HD 97585	Clear
		2007 Apr 25	LXD1.9	2500	180	HD 97585	Clear
HD 6903	F9 IIIa	2001 Aug 29	SXD	2000	120	HD 6457	Clear
		2001 Aug 31	LXD1.9	2500	200	HD 13869	Thin Cirrus
HD 176051	F9 V	2001 Oct 11	SXD	2000	180	HD 174567	Clear
		2004 Jul 6	LXD1.9	2500	150	HD 174567	Clear
HD 165908	F9 V metal weak	2003 Aug 10	SXD	2000	40	HD 171623	Clear
		2003 Aug 10	LXD2.1	2500	300	HD 171623	Clear
HD 114710	F9.5 V	2004 Apr 30	SXD	2000	100	HD 121996	Clear
		2004 Apr 30	LXD2.1	2500	150	HD 121996	Clear
HD 185018	G0 Ib–II	2001 Oct 11	SXD	2000	72	HD 182919	Clear
		2003 Oct 7	LXD2.1	2500	250	HD 182919	Clear
HD 109358	G0 V	2007 Jun 24	SXD	2000	120	HD 109615	Clear
		2007 Jun 24	LXD2.1	2500	200	HD 109615	Clear
HD 74395	G1 Ib	2003 Jan 14	SXD	2000	126	HD 71155	Clear
		2003 Nov 20	LXD1.9	2500	150	HD 71155	Clear
HD 216219	G1 II–III: Fe–1 CH0.5	2005 Oct 6	SXD	2000	300	HD 210501	Clear
		2005 Oct 7	LXD2.1	2500	300	HD 208108	Clear
HD 21018	G1 III: CH–1:	2005 Oct 6	SXD	2000	135	HD 21686	Clear
		2005 Oct 6	LXD2.1	2500	300	HD 21686	Clear
HD 10307	G1 V	2006 Dec 21	SXD	2000	120	HD 13869	Clear
		2006 Dec 21	LXD2.1	2500	300	HD 13689	Clear
HD 95128	G1–V Fe–0.5	2001 Mar 10	SXD	2000	150	HD 88960	Thin Cirrus
		2003 May 7	LXD1.9	2500	300	HD 88960	Thin Cirrus
HD 20619	G1.5 V	2001 Jan 25	SXD	2000	300	HD 21686	Thin Cirrus
		2001 Jan 25	LXD2.3	2500	300	HD 21686	Thin Cirrus
HD 42454	G2 Ib	2001 Oct 12	SXD	2000	180	HD 46553	Clear
HD 39949	G2 Ib	2001 Oct 12	SXD	2000	180	HD 46553	Clear
HD 3421	G2 Ib–II	2005 Oct 7	SXD	2000	150	HD 7215	Clear
		2005 Oct 7	LXD2.1	2500	300	HD 7215	Clear
HD 219477	G2 II–III	2008 Oct 12	SXD	2000	180	HD 210501	Thin Cirrus
HD 126868	G2 IV	2007 Jun 24	SXD	2000	150	HD 126129	Clear
		2007 Jun 24	LXD2.1	2500	150	HD 126129	Clear
HD 76151	G2 V	2000 Dec 11	SXD	2000	180	HD 71155	Clear
		2000 Dec 11	LXD2.3	1500	250	HD 71155	Clear
HD 192713	G3 Ib–II Wk H&K comp?	2005 Oct 6	SXD	2000	225	HD 196724	Clear
		2005 Oct 7	LXD2.1	2500	300	HD 196724	Clear
HD 176123	G3 II	2005 Jun 22	SXD	2000	140	HD 182110	Thin Cirrus
		2004 Jul 4	LXD1.9	2500	150	HD 182678	Clear
HD 88639	G3 IIIb Fe–1	2003 Feb 25	SXD	2000	84	HD 88960	Clear
		2003 May 7	LXD1.9	2500	300	HD 88960	Thin Cirrus
HD 10697	G3 Va	2000 Oct 24	SXD	2000	100	HD 6457	Clear
		2000 Oct 25	LXD2.3	2500	300	HD 6457	Clear
HD 179821	G4 O–Ia	2001 Oct 11	SXD	2000	180	HD 171149	Clear
		2005 Aug 26	LXD2.1	2500	300	HD 177724	Clear
HD 6474	G4 Ia	2003 Aug 10	SXD	2000	135	HD 11946	Clear
		2003 Aug 10	LXD2.1	2500	300	HD 11946	Clear
HD 94481	G4 III–IIIb	2003 Feb 25	SXD	2000	120	HD 92245	Clear
HD 108477	G4 III	2003 Feb 25	SXD	2000	144	HD 105764	Clear
		2003 May 8	LXD2.1	2500	300	HD 112304	Clear
HD 214850	G4 V	2004 Jul 5	SXD	2000	160	HD 210501	Clear
		2001 Aug 6	LXD2.1	2500	400	HD 208108	Clear
HD 190113	G5 Ib	2001 Oct 11	SXD	2000	120	HD 192538	Clear
		2001 Oct 19	LXD1.9	2500	240	HD 192538	Thin Cirrus
HD 18474	G5: III: CN–3 CH–2 H _δ –1	2006 Dec 21	SXD	2000	125	HD 21038	Clear
		2006 Dec 21	LXD2.1	2500	300	HD 21038	Clear
HD 193896	G5 IIIa	2003 Oct 16	SXD	2000	200	HD 190454	Thin Cirrus
HD 165185	G5 V	2003 Jul 7	SXD	2000	150	HD 157486	Thin Cirrus
		2003 Jul 7	LXD2.1	2500	300	HD 157486	Thin Cirrus
HD 161664	G6 Ib H _δ 1	2003 Aug 5	SXD	2000	125	HD 170364	Thin Cirrus
		2004 Jul 5	LXD1.9	2500	300	HD 155379	Clear
HD 202314	G6 Ib–IIa Ca1 Ba0.5	2005 Oct 6	SXD	2000	300	HD 208108	Clear
		2005 Oct 7	LXD2.1	2500	300	HD 196724	Clear

Table 4
(Continued)

Object (1)	Spectral Type (2)	UT Date (3)	Spectroscopy Mode (4)	R (5)	Exp. Time (sec) (6)	A0 V Standard (7)	Sky Conditions (8)
HD 58367	G6 IIb	2003 Jan 14	SXD	2000	150	HD 50931	Clear
		2004 Mar 9	LXD2.3	2500	300	HD 64648	Clear
HD 27277	G6 III	2005 Oct 7	SXD	2000	160	HD 29526	Clear
		2005 Oct 7	LXD2.1	2500	300	HD 29526	Clear
HD 115617	G6.5 V	2002 May 29	SXD	2000	120	HD 112304	Clear
		2002 May 29	LXD2.1	2500	250	HD 112304	Clear
HD 333385	G7 Ia	2002 Jul 13	SXD	2000	200	HD 192538	Clear
		2004 Jul 5	LXD1.9	2500	300	HD 196724	Clear
HD 25877	G7 II	2005 Oct 6	SXD	2000	120	HD 34787	Clear
		2005 Oct 6	LXD2.1	2500	300	HD 34787	Clear
HD 182694	G7 IIIa	2001 Aug 31	SXD	2000	90	HD 192538	Clear
		2001 Aug 31	LXD1.9	2500	200	HD 192538	Clear
HD 20618	G7 IV	2003 Oct 15	SXD	2000	140	HD 20995	Thin Cirrus
		2003 Oct 15	LXD2.1	2500	200	HD 20995	Thin Cirrus
HD 114946	G7 IV	2007 Jun 24	SXD	2000	90	HD 112304	Clear
		2007 Jun 24	LXD2.1	2500	240	HD 112304	Clear
HD 16139	G7.5 IIIa	2000 Oct 24	SXD	2000	200	HD 13869	Clear
		2000 Oct 25	LXD2.3	2500	300	HD 13869	Clear
HD 208606	G8 Ib	2001 Sep 1	SXD	2000	100	HD 223386	Thin Cirrus
		2001 Aug 31	LXD1.9	2500	200	HD 223386	Thin Cirrus
HD 122563	G8: III: Fe-5	2002 May 31	SXD	2000	200	HD 131951	Clear
		2003 May 8	LXD2.1	2500	300	HD 126129	Clear
HD 104979	G8 III BaI CN0.5 CH1	2002 May 31	SXD	2000	100	HD 111744	Clear
		2003 May 7	LXD1.9	2500	200	HD 110411	Thin Cirrus
HD 135722	G8 III Fe-1	2004 Jul 6	SXD	2000	153	HD 127304	Clear
		2004 Jul 6	LXD2.1	2500	100	HD 127304	Clear
HD 101501	G8 V	2003 Feb 25	SXD	2000	120	HD 105388	Clear
		2003 Jan 16	LXD2.1	2500	210	HD 107655	Clear
HD 75732	G8 V	2001 Mar 11	SXD	2000	60	HD 71906	Clear
		2001 Mar 11	LXD2.3	2500	250	HD 71906	Clear
HD 170820	G9 II CN1 H _δ 1	2005 Oct 7	SXD	2000	120	HD 163336	Clear
		2005 Oct 7	LXD2.1	2500	300	HD 163336	Clear
HD 222093	G9 III	2001 Aug 29	SXD	2000	360	HD 218639	Clear
		2001 Sep 1	LXD1.9	2500	100	HD 218639	Thin Cirrus
HD 165782	K0 Ia	2005 Jun 22	SXD	2000	250	HD 163336	Thin Cirrus
HD 44391	K0 Ib	2003 Jan 14	SXD	2000	120	HD 46553	Clear
		2003 Nov 20	LXD1.9	2500	300	HD 46553	Clear
HD 179870	K0 II	2003 Oct 7	LXD2.1	2500	250	HD 182919	Clear
		2005 Jun 22	SXD	2000	140	HD 177724	Thin Cirrus
HD 100006	K0 III	2003 Feb 25	SXD	2000	105	HD 101060	Clear
		2003 May 7	LXD1.9	2500	300	HD 107655	Thin Cirrus
HD 145675	K0 V	2003 Jul 6	SXD	2000	140	HD 157778	Thin Cirrus
		2003 Jul 6	LXD2.1	2500	300	HD 157778	Thin Cirrus
HD 164349	K0.5 IIb	2003 Aug 5	SXD	2000	60	HD 165029	Thin Cirrus
HD 9852	K0.5 III CN1	2003 Aug 10	SXD	2000	120	HD 12365	Clear
		2003 Sep 21	LXD2.1	2500	300	HD 11946	Clear
HD 63302	K1 Ia-Iab	2005 Oct 6	SXD	2000	120	HD 67725	Clear
		2005 Oct 7	LXD2.1	2500	125	HD 67725	Clear
HD 36134	K1- III Fe-0.5	2003 Jan 14	SXD	2000	120	HD 34317	Clear
		2003 Nov 20	LXD1.9	2500	200	HD 34317	Clear
HD 91810	K1- IIIb CN1.5 Ca1	2003 Feb 25	SXD	2000	120	HD 92728	Clear
		2003 May 7	LXD1.9	2500	300	HD 92728	Thin Cirrus
HD 25975	K1 III	2003 Jan 14	SXD	2000	144	HD 25152	Clear
		2003 Nov 20	LXD1.9	2500	300	HD 25152	Clear
HD 165438	K1 IV	2002 May 29	SXD	2000	150	HD 171149	Clear
HD 142091	K1 IVa	2003 Feb 24	SXD	2000	180	HD 140729	Clear
HD 10476	K1 V	2002 Nov 11	SXD	2000	120	HD 13869	Thin Cirrus
		2003 Sep 21	LXD2.1	2500	300	HD 6457	Clear
HD 124897	K1.5 III Fe-0.5	2003 May 28	SXD	2000	120	HD 121996	Clear
		2003 May 28	LXD2.1	2500	150	HD 121996	Clear
HD 212466	K2 O-Ia	2005 Aug 26	SXD	2000	100	HD 205314	Clear
		2005 Aug 26	LXD2.1	2500	200	HD 205314	Clear
HD 2901	K2 III Fe-1	2003 Aug 10	SXD	2000	90	HD 1561	Clear
		2003 Aug 10	LXD2.1	2500	300	HD 1561	Clear

Table 4
(Continued)

Object (1)	Spectral Type (2)	UT Date (3)	Spectroscopy Mode (4)	R (5)	Exp. Time (sec) (6)	A0 V Standard (7)	Sky Conditions (8)
HD 132935	K2 III	2002 May 31	LXD2.1	2500	500	HD 141513	Clear
		2004 Jul 5	SXD	2000	200	HD 133772	Clear
HD 137759	K2 III	2003 Feb 23	SXD	2000	72	HD 143187	Clear
		2000 Oct 20	SXD	2000	300	HD 1561	Thin Cirrus
HD 3765	K2 V	2003 Oct 7	LXD2.1	2500	250	HD 6457	Clear
		2003 Oct 7	LXD2.1	2500	150	HD 21038	Clear
HD 23082	K2.5 II	2003 Oct 3	SXD	2000	180	HD 21038	Clear
		2003 Oct 3	LXD2.1	2500	200	HD 182919	Clear
HD 187238	K3 Iab—Ib	2003 Aug 10	SXD	2000	50	HD 182919	Clear
		2005 Aug 26	LXD2.1	2500	200	HD 23452	Clear
HD 16068	K3 II—III	2003 Aug 10	SXD	2000	75	HD 23594	Clear
		2005 Oct 7	LXD2.1	2500	300	HD 219290	Thin Cirrus
HD 221246	K3 III	2002 Nov 11	SXD	2000	200	HD 219290	Thin Cirrus
		2008 Oct 8	LXD2.1	2500	150	HD 31069	Clear
HD 178208	K3 III	2005 Jun 22	SXD	2000	200	HD 31592	Clear
		2003 Jan 16	SXD	2000	120	HD 178207	Thin Cirrus
HD 35620	K3 III Fe1	2003 Nov 20	LXD1.9	2500	150	HD 97585	Thin Cirrus
		2003 May 29	SXD	2000	120	HD 97585	Thin Cirrus
HD 99998	K3+ III Fe—0.5	2003 May 29	LXD1.9	2500	200	HD 116960	Clear
		2003 Feb 25	SXD	2000	150	HD 110411	Thin Cirrus
HD 219134	K3 V	2003 May 7	LXD1.9	2500	300	HD 223386	Clear
		2001 Aug 6	SXD	2000	45	HD 223386	Clear
HD 185622	K4 Ib	2003 Aug 10	LXD2.1	2500	200	HD 182919	Clear
		2001 Oct 11	SXD	2000	150	HD 205314	Clear
HD 201065	K4 Ib—II	2001 Oct 11	LXD1.9	2500	300	HD 205314	Clear
		2002 Jul 13	SXD	2000	150	HD 205314	Clear
HD 207991	K4— III	2003 Oct 7	LXD2.1	2500	200	HD 178207	Thin Cirrus
		2003 Oct 16	SXD	2000	150	HD 178207	Thin Cirrus
HD 45977	K4 V	2003 Oct 16	SXD	2000	300	HD 48481	Thin Cirrus
		2003 Oct 16	SXD	2000	110	HD 219290	Thin Cirrus
HD 216946	K5 Ib	2003 Oct 16	LXD2.1	2500	125	HD 219290	Thin Cirrus
		2005 Jun 24	SXD	2000	250	HD 178207	Thin Cirrus
HD 36003	K5 V	2000 Dec 11	SXD	2000	300	HD 36058	Clear
		2000 Dec 11	LXD2.3	1500	250	HD 36058	Clear
HD 120477	K5.5 III	2003 May 29	SXD	2000	78	HD 121996	Thin Cirrus
		2003 May 29	LXD1.9	2500	15	HD 121996	Thin Cirrus
HD 3346	K6 IIIa	2003 Oct 16	SXD	2000	100	HD 1561	Thin Cirrus
		2003 Oct 16	SXD	2000	200	HD 171149	Thin Cirrus
HD 181475	K7 IIa	2003 Oct 16	SXD	2000	150	HD 199312	Thin Cirrus
		2005 Aug 26	LXD2.1	2500	300	HD 192538	Clear
HD 237903	K7 V	2002 Jan 10	SXD	2000	300	HD 92728	Clear
		2002 Jan 11	LXD2.1	1500	500	HD 92728	Thin Cirrus
HD 201092	K7 V	2001 Oct 20	SXD	2000	125	HD 192538	Thin Cirrus
		2005 Oct 7	SXD	2000	150	HD 212061	Clear
HD 213893	M0 IIIb	2005 Oct 7	LXD2.1	2500	300	HD 212061	Clear
		2001 Oct 12	SXD	2000	600	HD 21379	Clear
HD 19305	M0 V	2000 Oct 25	LXD2.3	2500	300	HD 23258	Clear
		2001 Oct 11	SXD	2000	180	HD 1561	Clear
HD 236697	M0.5 Ib	2001 Oct 19	LXD1.9	2500	300	HD 1561	Clear
		2000 Oct 24	SXD	2000	200	GJ 9779	Thin Cirrus
HD 209290	M0.5 V	2000 Oct 25	LXD2.3	2500	300	GJ 9779	Clear
		2003 Jul 6	SXD	2000	150	HD 182919	Thin Cirrus
HD 339034	M1 Ia	2003 Jul 6	LXD2.1	2500	200	HD 182919	Thin Cirrus
		2003 Nov 6	SXD	2000	150	HD 121996	Thin Cirrus
HD 14404	M1— Iab—Ib	2003 Nov 20	LXD1.9	2500	250	HD 19844	Thin Cirrus
		2003 Jan 16	SXD	2000	120	HD 15090	Clear
HD 39801	M1—M2 Ia—Iab	2003 Nov 6	SXD	2000	200	HD 41076	Clear
		2003 Nov 6	LXD2.1	2500	200	HD 41076	Clear
HD 204724	M1+ III	2005 Oct 6	SXD	2000	153	HD 208108	Clear
		2005 Oct 6	LXD2.1	2500	184	HD 208108	Clear
HD 42581	M1 V	2002 Jan 10	SXD	2000	200	HD 42301	Clear
		2002 Jan 11	LXD2.1	2500	250	HD 42301	Thin Cirrus
HD 35601	M1.5 Iab—Ib	2003 Nov 20	SXD	2000	180	HD 31069	Clear
		2001 Oct 12	LXD1.9	2500	150	HD 31592	Clear
BD +60 265	M1.5 Ib	2005 Aug 26	SXD	2000	300	HD 11946	Clear
		2005 Aug 26	LXD2.1	2500	200	HD 11946	Clear

Table 4
(Continued)

Object (1)	Spectral Type (2)	UT Date (3)	Spectroscopy Mode (4)	R (5)	Exp. Time (sec) (6)	A0 V Standard (7)	Sky Conditions (8)
HD 36395	M1.5 V	2000 Oct 24	SXD	2000	100	HD 40210	Clear
		2000 Oct 25	LXD2.3	2500	300	HD 34317	Clear
HD 206936	M2– Ia	2005 Aug 26	SXD	2000	100	HD 219290	Clear
		2005 Aug 26	LXD2.3	2500	100	HD 194354	Clear
HD 10465	M2 Ib	2003 Jan 16	SXD	2000	180	HD 1561	Clear
		2003 Oct 7	LXD2.1	2500	200	HD 21038	Clear
HD 23475	M2 II	2003 Jan 16	SXD	2000	60	HD 14632	Clear
HD 120052	M2 III	2002 May 28	SXD	2000	90	HD 124683	Clear
		2002 May 28	LXD2.1	2500	150	HD 124683	Clear
HD 95735	M2 V	2000 Dec 10	SXD	2000	60	HD 88960	Clear
		2000 Dec 10	LXD2.3	1500	500	HD 88960	Clear
Gl 806	M2 V	2003 Jul 7	SXD	2000	300	HD 199312	Thin Cirrus
HD 219734	M2.5 III Ba0.5	2002 Nov 11	SXD	2000	150	HD 219290	Thin Cirrus
		2003 Oct 7	LXD2.1	2500	100	HD 219290	Clear
Gl 381	M2.5 V	2002 Jan 10	SXD	2000	300	HD 85504	Clear
		2002 Jan 11	LXD2.1	1500	500	HD 85504	Thin Cirrus
Gl 581	M2.5 V	2000 Jun 24	SXD	2000	200	HD 141513	Clear
		2000 Jun 24	LXD2.1	2500	150	HD 141513	Clear
RW Cyg	M3 to M4 Ia–Iab	2003 Jul 7	SXD	2000	82	HD 199312	Thin Cirrus
		2003 Jul 7	LXD1.9	2500	70	HD 199312	Thin Cirrus
CD –31 4916	M3 Iab–Ia	2002 Jan 11	SXD	2000	250	HD 68027	Thin Cirrus
		2003 Nov 20	LXD1.9	2500	200	HD 70963	Clear
HD 14469	M3–M4 Iab	2003 Jan 16	SXD	2000	120	HD 15090	Clear
		2003 Oct 6	LXD2.1	2500	100	HD 23594	Thin Cirrus
HD 40239	M3 IIb	2002 Jan 10	SXD	2000	50	HD 45105	Clear
		2001 Jan 11	LXD2.1	2500	100	HD 45105	Thin Cirrus
HD 39045	M3 III	2002 Jan 10	SXD	2000	150	HD 46533	Clear
		2002 Jan 11	LXD2.1	2500	125	HD 46533	Thin Cirrus
Gl 388	M3 V	2000 Dec 10	SXD	2000	180	HD 88960	Clear
		2000 Dec 10	LXD2.3	1500	250	HD 88960	Clear
HD 14488	M3.5 Iab Fe–1 var?	2005 Aug 26	SXD	2000	150	HD 23452	Clear
		2005 Aug 26	LXD2.1	2500	150	HD 23594	Clear
HD 28487	M3.5 III Ca–0.5	2003 Jan 16	SXD	2000	126	HD 31411	Clear
		2003 Oct 8	LXD2.1	2500	125	HD 31295	Clear
Gl 273	M3.5 V	2002 Jan 11	SXD	2000	300	HD 50931	Thin Cirrus
		2002 Feb 28	LXD2.1	2500	600	HD 50931	Clear
HD 19058	M4+ IIIa	2003 Jan 16	SXD	2000	108	HD 20995	Clear
		2003 Nov 20	LXD1.9	2500	100	HD 21038	Clear
HD 214665	M4+ III	2001 Oct 21	SXD	2000	100	HD 223386	Thin Cirrus
		2001 Oct 21	LXD1.9	2500	100	HD 223386	Thin Cirrus
HD 4408	M4 III	2003 Jan 3	SXD	2000	50	HD 6457	Clear
		2003 Oct 7	LXD2.1	2500	102	HD 6457	Clear
HD 27598	M4– III	2003 Jan 16	SXD	2000	180	HD 29575	Clear
		2003 Oct 8	LXD2.1	2500	300	HD 29573	Clear
Gl 213	M4 V	2000 Dec 9	SXD	2000	720	HD 34203	Clear
		2000 Dec 9	LXD2.3	1500	500	HD 41076	Clear
Gl 299	M4 V	2000 Dec 11	SXD	2000	1200	HD 75137	Clear
		2000 Dec 11	LXD2.3	1500	5000	HD 75137	Clear
HD 204585	M4.5 IIIa	2002 Jul 14	SXD	2000	110	HD 208108	Clear
Gl 268AB	M4.5 V	2000 Dec 10	SXD	2000	600	HD 56386	Clear
		2000 Dec 10	LXD2.3	1500	500	HD 56386	Clear
HD 156014	M5 Ib–II	2005 Aug 26	SXD	2000	100	HD 165029	Clear
		2005 Aug 26	LXD1.9	2500	100	HD 165029	Clear
HD 175865	M5 III	2003 May 7	SXD	2000	60	HD 174567	Thin Cirrus
Gl 51	M5 V	2000 Nov 6	SXD	2000	600	HD 11946	Clear
		2000 Nov 6	LXD2.3	1500	250	HD 11946	Clear
Gl 866ABC	M5 V	2001 Oct 11	SXD	2000	600	HD 218639	Clear
		2001 Oct 19	LXD1.9	2500	300	HD 218639	Clear
HD 94705	M5.5 III:	2003 May 8	SXD	2000	60	HD 97595	Clear
		2003 May 8	LXD2.1	2500	60	HD 97595	Thin Cirrus
HD 196610	M6 III	2002 Jul 14	SXD	2000	100	HD 196724	Clear
HD 18191	M6– III:	2003 Oct 7	LXD2.1	2500	100	HD 196724	Clear
		2003 Jan 16	SXD	2000	120	HD 16811	Clear
Gl 406	M6 V	2003 Sep 20	LXD2.1	2500	31	HD 16811	Clear
		2001 Jan 25	SXD	2000	360	HD 97585	Clear

Table 4
(Continued)

Object (1)	Spectral Type (2)	UT Date (3)	Spectroscopy Mode (4)	R (5)	Exp. Time (sec) (6)	A0 V Standard (7)	Sky Conditions (8)
GJ 1111	M6.5 V	2001 Jan 24	LXD2.3	2500	500	HD 97585	Clear
		2000 Dec 9	SXD	2000	960	HD 64648	Clear
		2000 Dec 9	LXD2.3	2000	1000	HD 64648	Clear
HD 14386	M5e–M9e III	2003 Nov 6	SXD	2000	100	HD 15130	Clear
		2003 Sep 20	LXD2.1	2500	153	HD 13936	Clear
HD 108849	M7– III:	2003 May 8	SXD	2000	100	HD 110411	Clear
		2003 May 8	LXD2.1	2500	54	HD 110411	Clear
HD 207076	M7– III:	2003 Oct 16	SXD	2000	100	HD 212061	Thin Cirrus
		2003 Oct 16	LXD2.1	2500	100	HD 212061	Thin Cirrus
Gl 644C	M7 V	2001 Jul 12	SXD	2000	1440	HD 148968	Thin Cirrus
		2001 Jul 12	LXD1.9	940	660	HD 148968	Thin Cirrus
MY Cep	M7–M7.5 I	2003 Aug 10	SXD	2000	450	HD 223386	Clear
		2003 Aug 10	LXD2.1	2500	200	HD 223386	Clear
HD 69243	M6e–M9e III	2007 Jan 18	SXD	2000	100	HD 64648	Clear
		2007 Jan 18	LXD2.1	2500	100	HD 64648	Clear
BRI B2339–0447	M7–8 III	2006 Nov 29	SXD	2000	1200	HD 215143	Thin Cirrus
		2006 Nov 29	LXD1.9	2500	300	HD 215143	Thick Cirrus
IRAS 01037+1219	M8 III	2007 Jan 18	SXD	2000	450	HD 6457	Clear
		2007 Jan 18	LXD2.1	2500	100	HD 6457	Clear
Gl 752B	M8 V	2001 Jul 13	SXD	2000	600	HD 183324	Clear
		2001 Jul 13	LXD1.9	940	600	HD 183324	Clear
LP 412–31	M8 V	2003 Sep 20	SXD	2000	1800	HD 21686	Clear
		2003 Sep 21	LXD1.9	1500	600	HD 21686	Clear
IRAS 21284–0747	M8–9 III	2006 Nov 29	SXD	2000	300	HD 198070	Thin Cirrus
		2006 Nov 29	LXD2.1	2500	300	HD 212061	Clear
IRAS 14436–0703	M8–9 III	2006 Jun 24	SXD	2000	200	HD 132072	Thin Cirrus
		2006 Jun 24	SXD	2000	600	HD 132072	Thin Cirrus
IRAS 14303–1042	M8–9 III	2006 Jun 24	SXD	2000	150	HD 131951	Thin Cirrus
		2006 Jun 24	SXD	2000	300	HD 110902	Thin Cirrus
DENIS–P J104814.7–395606.1	M9 V	2000 Dec 9	SXD	2000	1440	HD 99627	Clear
		2000 Dec 11	LXD1.9	940	1260	HD 99627	Clear
LP 944–20	M9 V	2001 Jan 24	SXD	2000	2400	HD 18735	Clear
		2002 Jan 11	LXD2.1	940	3600	HD 18735	Thin Cirrus
LHS 2065	M9 V	2000 Dec 10	SXD	1200	1920	HD 71155	Clear
LHS 2924	M9 V	2003 Feb 23	SXD	2000	1200	HD 127304	Clear
BRI B0021–0214	M9.5 V	2001 Oct 12	SXD	2000	1440	HD 9485	Thin Cirrus
		2000 Nov 6	LXD1.9	940	600	HD 1663	Thin Cirrus
IRAS 14086–0703	M10+ III	2006 Jun 24	SXD	2000	300	HD 132072	Thin Cirrus
		2006 Jul 10	SXD	2000	75	HD 121409	Clear
BD +44 2267	S2.5 Zr 2	2008 Apr 2	SXD	2000	90	HD 99966	Clear
		2008 Apr 2	LXD1.9	2500	90	HD 99966	Clear
HD 64332	S4.5 Zr 2 Ti 4	2007 Mar 16	SXD	2000	150	HD 67725	Clear
		2007 Mar 16	LXD2.1	2500	300	HD 67725	Clear
HD 44544	SC5.5 Zr 0.5	2008 Apr 2	SXD	2000	90	HD 45137	Clear
		2008 Apr 2	LXD1.9	2500	90	HD 45137	Clear
HD 62164	S5–S6 Zr 3 to 4 Ti 0	2007 Mar 15	SXD	2000	135	HD 67725	Clear
		2007 Mar 15	LXD2.1	2500	150	HD 67725	Clear
HD 76846	C–R2+ IIIa: C2 2.5	2007 Mar 15	SXD	2000	360	HD 71906	Clear
		2007 Mar 16	LXD1.9	2500	300	HD 71906	Clear
HD 31996	C7, 6e(N4)	2007 Jan 18	SXD	2000	140	HD 29573	Clear
		2007 Jan 18	LXD2.1	2500	150	HD 29573	Clear
HD 44984	C–N4 C2 3.5	2007 Mar 15	SXD	2000	306	HD 42477	Clear
		2007 Mar 15	LXD2.1	2500	255	HD 42477	Clear
HD 76221	C–N 4.5 C2 5.5 MS 3	2007 Mar 15	SXD	2000	92	HD 64648	Clear
		2007 Mar 16	LXD2.1	2500	102	HD 64648	Clear
HD 92055	C–N4.5 C2 4.5	2007 Apr 25	SXD	2000	180	HD 92245	Clear
		2007 Apr 25	LXD1.9	2500	255	HD 92245	Clear
HD 70138	C–J4.5 IIIa: C2 6 j 6	2007 Mar 17	SXD	2000	180	HD 69589	Clear
		2007 Mar 17	LXD2.1	2500	300	HD 69589	Clear
HD 48664	C–N5 C2 6	2007 Mar 16	SXD	2000	180	HD 45137	Clear
		2007 Mar 16	LXD2.1	2500	300	HD 45137	Clear
HD 57160	C–J5– C2 5– j 4	2007 Mar 17	SXD	2000	150	HD 64648	Clear
		2007 Mar 17	LXD2.1	2500	300	HD 64648	Clear

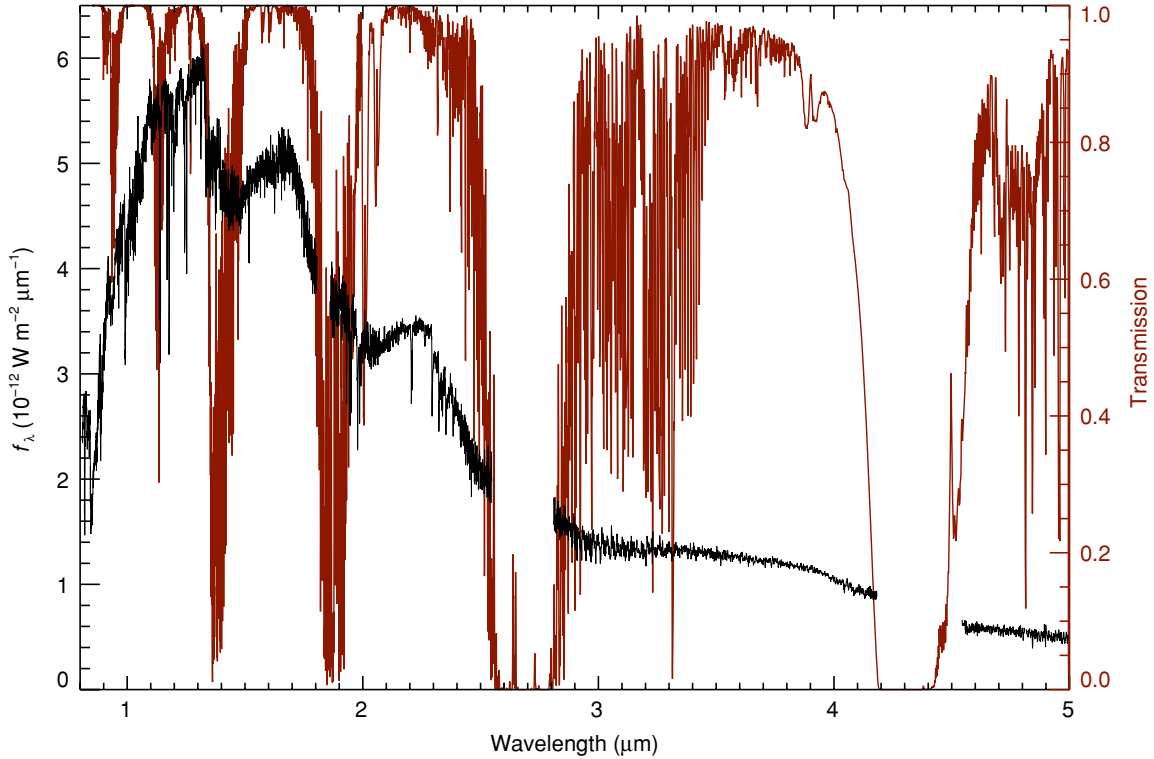


Figure 3. Atmospheric transmission for Mauna Kea (4200 m, airmass 1.15, precipitable water vapor 2 mm) overplotted with the spectrum of Gl 406 (M6 V).

of the adjusted model spectrum to the observed spectrum of the A0V star gives the telluric correction spectrum (which also includes correction for the instrument throughput) in each order. The science object spectrum is then divided by the telluric spectrum. The resulting flux calibration is accurate to about 10%. The sharp and deep telluric absorption features are marginally sampled with a 2 pixel-wide slit so that when the object and telluric correction spectra are ratioed, residuals remain at the wavelengths of these features due to a small amount of instrumental flexure between the object and standard star positions. In order to minimize these systematic errors, the telluric correction spectrum is first shifted relative to the object spectrum until the noise in these regions is minimized. Typically, these shifts are $\sim 0.1\text{--}0.2$ pixel for telescope movements of 10 deg.

In principle, the flux density levels of the telluric-corrected spectra in two adjacent orders should match exactly in the wavelength region where they overlap; in practice we find offsets of usually less than 1%, although occasionally as large as 3%. The level mismatch was removed by scaling one spectrum to the level of the other. The scale factor was determined from a section of the overlap region where both spectra were judged to have sufficient S/N to allow an accurate determination. The telluric-corrected and scaled spectra in the individual orders were then merged together to form a single, continuous spectrum for the science object. Regions of strong telluric absorption were then removed. The precise wavelength intervals removed depended on the transparency of the atmosphere at the time of observation but always included the $\sim 2.5\text{--}2.8 \mu\text{m}$ and $\sim 4.2\text{--}4.6 \mu\text{m}$ regions. For each object, the SXD and LXD spectra were combined in a manner similar to that used to combine the individual orders. A scale factor was determined from the overlapping wavelength region and then used to adjust the SXD and LXD spectra to a common level.

The next step in the reduction process was to absolutely flux calibrate the spectra using the 2MASS photometry listed in

Table 2. For each spectrum, we computed correction factors based on the JHK_S photometry given by

$$C_X = \frac{F_X^{\text{Vega}} \times 10^{-0.4(m_X + ZP_X)}}{\int f_{\lambda}^{\text{obs}}(\lambda) S_X(\lambda) d\lambda}, \quad (1)$$

where F_X^{Vega} is the Vega flux, m_X is the magnitude of the object, ZP_X is the passband zero point, $S_X(\lambda)$ is the system response function in bandpass X , and f_{λ}^{obs} is the flux density of the object. We used the Vega fluxes (5.082×10^{-10} , 2.843×10^{-10} , $1.122 \times 10^{-10} \text{ W m}^{-2}$), zero points (+0.001, -0.019, +0.017), and the system response functions given by Cohen et al. (2003). Each spectrum was then multiplied by a single scale factor $\langle C \rangle$ given by the weighted average of the J -, H -, and K_S -band correction factors ($f_{\lambda} = f_{\lambda}^{\text{obs}} \times \langle C \rangle$). The weights were given by the errors in the scale factors, which in turn were derived from the photometric uncertainties. This scaling has the effect of shifting the entire spectrum up or down so that the overall absolute flux level is correct, while simultaneously preserving the relative flux calibration of each spectral order derived from the observations and telluric correction procedures. For variable stars in the sample (mostly TPAGB stars), the absolute flux calibration is only approximate since the 2MASS photometry was obtained at an earlier epoch than the SpeX spectroscopy. Furthermore, not all the SXD and LXD spectra of individual stars were obtained at the same epoch.

The spectrum of each object is then shifted to zero radial velocity. To do this, we first selected two stars, HD 219623 (F8 V) and HD 201092 (K7 V), as representatives of F–G, and K–M stars, respectively, and measured their apparent radial velocities using the observed wavelengths of strong, isolated atomic lines. For HD 219623 we measured the positions of the Pa ϵ ($0.9548590 \mu\text{m}$), Pa γ ($1.0052128 \mu\text{m}$), Pa β ($1.282159 \mu\text{m}$), Mg I ($1.4881683 \mu\text{m}$), Mg I ($1.7113304 \mu\text{m}$), and Br γ

(2.166120 μm) lines and for HD 201092 we used the Si I (1.0588042 μm), Mg I (1.1831408 μm), Mg I (1.4881683 μm), and Mg I (1.7113304 μm) lines. The observed radial velocities for these two stars were determined by averaging the radial velocity measurements obtained from these lines. The standard error on the mean radial velocity was $\sim 3 \text{ km s}^{-1}$ for both stars. We then shifted the spectra of these two stars in wavelength to correspond to zero radial velocity. To determine the radial velocities of the remaining stars in the library, we cross-correlated the 1.05–1.10 μm spectra of the F–G stars (which contain isolated lines of Si, C, Mg, and Fe) against that of HD 219623 and the 2.285–2.33 μm spectra of the K and M stars (which contain the $\Delta\nu = +2$ CO overtone bands) against that of HD 201092. The peak of each cross-correlation function was fitted with a second-order polynomial to determine the radial velocity. Based on our implementation of the cross-correlation technique described by Tonry & Davis (1979) as well as a comparison of the radial velocities derived from different wavelength regions in each spectrum, we estimate the uncertainty in our radial velocity values to be generally less than 30 km s^{-1} . The spectrum of each object was then shifted to zero radial velocity using the radial velocity derived from the cross-correlation. It should be noted that, in order to preserve the accuracy of our data, we did not resample or rebin the final spectra to a common wavelength scale after shifting them, and therefore each spectrum has a unique wavelength array. In most cases, the velocity shifts are small: the average shift was found to be $4.5 \pm 37 \text{ km s}^{-1}$ with a maximum of about 131 km s^{-1} . Both values are smaller than our velocity resolution (150 km s^{-1} per resolution element).

Although the stars in our sample are generally bright and nearby, some stars show evidence of interstellar reddening. For those applications requiring true spectral energy distributions (e.g., EPS studies) reddening needs to be corrected. Consequently, as a final step in the data reduction, we corrected the spectra for reddening. We determined the $E(B - V) \equiv (B - V) - (B - V)_0$ color excess from the observed $(B - V)$ color and an intrinsic $(B - V)_0$ color appropriate for its spectral type. The observed colors were taken from the Mermilliod (2006) catalog and are on the Johnson photometric system. For the few stars that were not included in this catalog, we adopted the $(B - V)$ color given by Kharchenko (2001), Leggett (1992), and Beauchamp et al. (1994). We adopted the calibration of intrinsic colors as a function of spectral type by Fitzgerald (1970). For the M dwarfs, we found that the Fitzgerald (1970) values gave unreasonably large color excess values for stars that are very nearby (less than 20 pc). Furthermore, while other calibrations of intrinsic colors (e.g., Schmidt-Kaler 1982) agree well with that of Fitzgerald (1970) at earlier spectral types, they differ markedly for M stars, with the later calibrations becoming progressively redder. For these reasons, we adopted the intrinsic colors given by Leggett (1992) for the M dwarfs, which generally yield very small (or even negative) values for $E(B - V)$ for these stars. To derive intrinsic colors for stars with intermediate spectral types and luminosity classes not tabulated in the combined Fitzgerald/Leggett calibration, we performed a two-dimensional surface interpolation over the intrinsic color values as a function of spectral subtype and luminosity class. The distribution of $E(B - V)$ values for the stars in our sample is shown in Figure 1(b). As expected for the bright (and generally nearby) stars in our sample, the distribution is peaked near zero. Fitting a Gaussian to the values of $E(B - V) < 0$ indicates that the uncertainty on the color excesses is about $\sigma = 0.036$ mag. All color excesses determined to be less than zero were

set to zero in the dereddening process. Furthermore, based on our findings for the standard deviation of the distribution, we chose not to correct any spectra with $E(B - V) < 0.108$. The 66 dereddened stars along with their $(B - V)$, $(B - V)_0$, $E(B - V)$, and A_V values are given in Table 5.

The reddening-corrected spectrum $f_{\lambda}^{\text{cor}}(\lambda)$ is given by

$$f_{\lambda}^{\text{cor}}(\lambda) = f_{\lambda}(\lambda) \times 10^{(0.4 \times A_{\lambda})}, \quad (2)$$

where $f_{\lambda}(\lambda)$ is the absolute flux calibrated spectrum and A_{λ} is the extinction law as a function of wavelength. We adopted the NIR law given by Fitzpatrick & Massa (2007) with $R_V = 3.0$. For this law,

$$A_{\lambda} = 1.057 \times E(B - V) \lambda^{-1.84}. \quad (3)$$

We note that these dereddened spectra should be used with care because the dereddening process assumes an intrinsic stellar color and a mean Galactic extinction law that may not be accurate or appropriate in all cases. For example, we find $E(B - V) = 0.06$ (or $A_V = 0.18$) for the M6 dwarf Gl 406, which resides at a distance of only 2.4 pc (van Altena et al. 1995). No significant extinction is expected at this distance. In addition, M giant stars and PAGB and TPAGB stars may have local extinction due to dust formation in their cool outer atmospheres, which is difficult to separate for any interstellar extinction that may be present. Variable stars are also problematic due to changes in the intrinsic color. Therefore, unless otherwise noted, we will continue to use the uncorrected spectra in the remainder of the analysis, including the figures. Nevertheless, the dereddened spectra are available on the IRTF Web site (see footnote 4).

We have found that the observed spectral slope from any given object varies slightly between individual observations. An example of this small effect is illustrated in Figure 4. In order to quantify this effect, we have computed the differences ($\Delta_{X-Y} = (X - Y)_{\text{obs}} - (X - Y)_{\text{synth}}$) between the colors derived from the 2MASS photometry and those derived from synthetic photometry on our observed spectra. The synthetic color for any two of the 2MASS bandpasses is given by

$$X - Y = -2.5 \times \log \left[\frac{\int f_{\lambda} S_X(\lambda) d\lambda}{F_X^{\text{Vega}}} \right] + 2.5 \times \log \left[\frac{\int f_{\lambda} S_Y(\lambda) d\lambda}{F_Y^{\text{Vega}}} \right] + (z_{PY} - z_{PX}), \quad (4)$$

where the symbols have the same meaning as in Equation (1). The results for the 53 stars with relatively good (5%) 2MASS photometry (from Table 2) are plotted in Figure 5. The average differences are $\langle \Delta_{J-H} \rangle = 0.00 \pm 0.04$ (RMS), $\langle \Delta_{H-K_S} \rangle = 0.02 \pm 0.04$, and $\langle \Delta_{J-K_S} \rangle = 0.01 \pm 0.05$. Although the colors derived from the 2MASS photometry are not as precise as those measured from the spectra via synthetic photometry (better than 1%), the photometric residuals on the sample of 53 cool stars indicate that our measurements of spectral slope are accurate to within a few percent for F, G, K, and M spectral types. Similar (but larger) effects have been observed by Goto et al. (2003) while using adaptive optics with medium resolution spectroscopy. Their simulations demonstrate that spectral slope variations result from changes in the fraction of light from the object transmitted by a finite width slit as a function of

Table 5
Stars with $E(B - V) > 0.108$

Object (1)	Spectral Type (2)	$(B - V)$ (mag) (3)	$(B - V)_0$ (mag) (4)	$E(B - V)$ (mag) (5)	A_V (mag) (6)
HD 6130	F0 II	0.491	0.200	0.291	0.9
HD 7927	F0 Ia	0.680	0.150	0.530	1.6
HD 135153	F0 Ib-II	0.376	0.180	0.196	0.6
HD 173638	F1 II	0.595	0.220	0.375	1.1
HD 182835	F2 Ib	0.593	0.180	0.413	1.2
HD 213306	F5 Ib – G1 Ib	0.480	0.260	0.220	0.7
HD 190323	F8 Ia	0.874	0.550	0.324	1.0
HD 51956	F8 Ib	0.803	0.550	0.253	0.8
HD 6903	F9 IIIa	0.689	0.580	0.109	0.3
HD 185018	G0 Ib-II	0.881	0.770	0.111	0.3
HD 21018	G1 III: CH-1:	0.862	0.690	0.172	0.5
HD 39949	G2 Ib	1.090	0.880	0.210	0.6
HD 42454	G2 Ib	1.232	0.880	0.352	1.1
HD 192713	G3 Ib-II Wk H&K comp?	1.046	0.890	0.156	0.5
HD 176123	G3 II	0.990	0.870	0.120	0.4
HD 179821	G4 O-Ia	1.555	0.960	0.595	1.8
HD 6474	G4 Ia	1.617	0.960	0.657	2.0
HD 190113	G5 Ib	1.500	1.000	0.500	1.5
HD 202314	G6 Ib-IIa Ca1 Ba0.5	1.102	0.980	0.122	0.4
HD 161664	G6 Ib H_δ 1	1.490	1.040	0.450	1.4
HD 16139	G7.5 IIIa	1.052	0.940	0.112	0.3
HD 333385	G7 Ia	2.187	1.100	1.087	3.3
HD 25877	G7 II	1.161	0.950	0.211	0.6
HD 208606	G8 Ib	1.600	1.140	0.460	1.4
HD 75732	G8 V	0.860	0.740	0.120	0.4
HD 170820	G9 II CN1 H_δ 1	1.575	1.020	0.555	1.7
HD 165782	K0 Ia	2.140	1.180	0.960	2.9
HD 44391	K0 Ib	1.400	1.180	0.220	0.7
HD 9852	K0.5 III CN1	1.460	1.050	0.410	1.2
HD 164349	K0.5 IIb	1.257	1.100	0.157	0.5
HD 179870	K0 II	1.245	1.060	0.185	0.6
HD 124897	K1.5 III Fe-0.5	1.231	1.120	0.111	0.3
HD 63302	K1 Ia-Iab	1.752	1.200	0.552	1.7
HD 124897	K1.5 III Fe-0.5	1.231	1.120	0.111	0.3
HD 23082	K2.5 II	1.850	1.350	0.500	1.5
HD 132935	K2 III	1.364	1.160	0.204	0.6
HD 212466	K2 O-Ia	2.275	1.230	1.045	3.1
HD 221246	K3 III	1.460	1.260	0.200	0.6
HD 187238	K3 Iab-Ib	2.040	1.420	0.620	1.9
HD 16068	K3 II-III	1.790	1.260	0.530	1.6
HD 35620	K3 III Fe1	1.403	1.260	0.143	0.4
HD 178208	K3 III	1.393	1.260	0.133	0.4
HD 99998	K3+III Fe-0.5	1.531	1.260	0.271	0.8
HD 185622	K4 Ib	2.026	1.500	0.526	1.6
HD 201065	K4 Ib-II	1.793	1.460	0.333	1.0
HD 207991	K4- III	1.600	1.430	0.170	0.5
HD 45977	K4 V	1.120	1.000	0.120	0.4
HD 216946	K5 Ib	1.773	1.600	0.173	0.5
HD 181475	K7 IIa	2.070	1.520	0.550	1.6
HD 236697	M0.5 Ib	2.157	1.650	0.507	1.5
HD 35601	M1.5 Iab-Ib	2.200	1.650	0.550	1.7
HD 39801	M1-M2 Ia-Iab	1.861	1.650	0.211	0.6
HD 14404	M1- Iab-Ib	2.303	1.650	0.653	2.0
HD 339034	M1 Ia	3.036	1.650	1.386	4.2
BD+60 265	M1.5 Ib	2.345	1.650	0.695	2.1
HD 10465	M2 Ib	1.860	1.650	0.210	0.6
HD 206936	M2- Ia	2.327	1.650	0.677	2.0
HD 23475	M2 II	1.877	1.590	0.287	0.9
CD -31 4916	M3 Iab-Ia	2.238	1.670	0.568	1.7
HD 14469	M3-M4 Iab	2.175	1.670	0.505	1.5
HD 28487	M3.5 III Ca-0.5	1.740	1.620	0.120	0.4
HD 14488	M3.5 Iab Fe-1 var?	2.256	1.710	0.546	1.6

Table 5
(Continued)

Object (1)	Spectral Type (2)	$(B - V)$ (mag) (3)	$(B - V)_0$ (mag) (4)	$E(B - V)$ (mag) (5)	A_V (mag) (6)
HD 39045	M3 III	1.752	1.600	0.152	0.5
RW Cyg	M3 to M4 Ia–Iab	2.881	1.670	1.211	3.6
Gl 299	M4 V	1.768	1.650	0.118	0.4
Gl 866ABC	M5 V	1.960	1.800	0.160	0.5

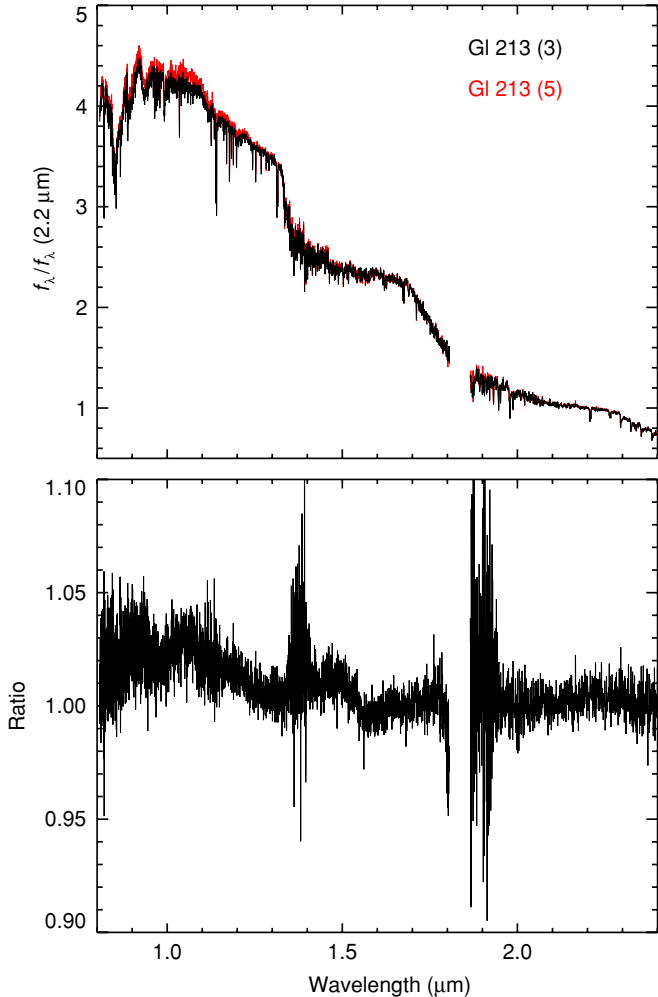


Figure 4. Top: the third (black) and fifth (red) spectra in a sequence of ten consecutive spectra of Gl 213 (M4 V). These two spectra show the largest slope difference in the sequence. The difference is equivalent to $J - K_S = 0.015$. Bottom: the flux ratio of the two spectra showing that the difference in slope is small across the range 0.8–2.4 μm . As described in Section 2.3 we can measure spectral slopes (i.e., photometric colors) accurate to a few percent.

wavelength. Therefore, temporal changes in seeing, guiding, and differential atmospheric refraction are probably the cause of the small variations we observe. Although SpeX does not have an atmospheric dispersion corrector, we minimized the effects of differential refraction (and therefore the wavelength-dependent light loss through the slit) by moving the internal image rotator to observe at the parallactic angle (see Figure 6 of Rayner et al. 2004) and by combining multiple spectra together.

As a further test of the accuracy of the spectral slopes, we have computed the synthetic $Z - Y$, $Y - J$, $J - H$, $H - K$, and $K - L'$ colors of eight A0 V stars observed with the same

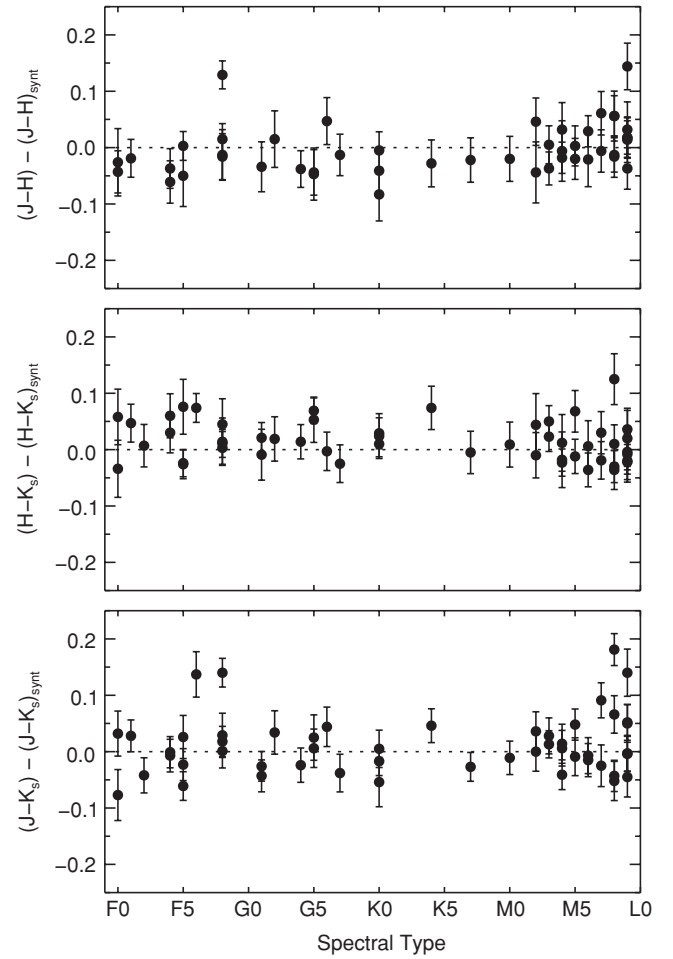


Figure 5. Computed residuals (observed–synthetic) between the observed and synthesized 2MASS $J - H$, $H - K_S$, and $J - K_S$ colors of 53 library stars with relatively good (5%) 2MASS photometry. The average residuals are $\langle \Delta_{J-H} \rangle = 0.00 \pm 0.04$ (rms), $\langle \Delta_{H-K_S} \rangle = 0.02 \pm 0.04$ (rms), and $\langle \Delta_{J-K_S} \rangle = 0.01 \pm 0.05$ (rms). The plotted error bars show the 2MASS error in magnitudes. The error on the synthetic color is insignificant by comparison. The residuals imply that the measured spectral slope of these cool stars is accurate to within a few percent.

instrumental setup. The synthetic color for any two bandpasses X and Y is given by

$$X - Y = -2.5 \times \log \left[\frac{\int \lambda f_\lambda(\lambda) S_X(\lambda) d\lambda}{\int \lambda f_\lambda^{\text{Vega}}(\lambda) S_X(\lambda) d\lambda} \right] + 2.5 \times \log \left[\frac{\int \lambda f_\lambda(\lambda) S_Y(\lambda) d\lambda}{\int \lambda f_\lambda^{\text{Vega}}(\lambda) S_Y(\lambda) d\lambda} \right], \quad (5)$$

where $f_\lambda(\lambda)$ is the flux density of the object, $f_\lambda^{\text{Vega}}(\lambda)$ is the flux density of Vega, and $S(\lambda)$ is the system response

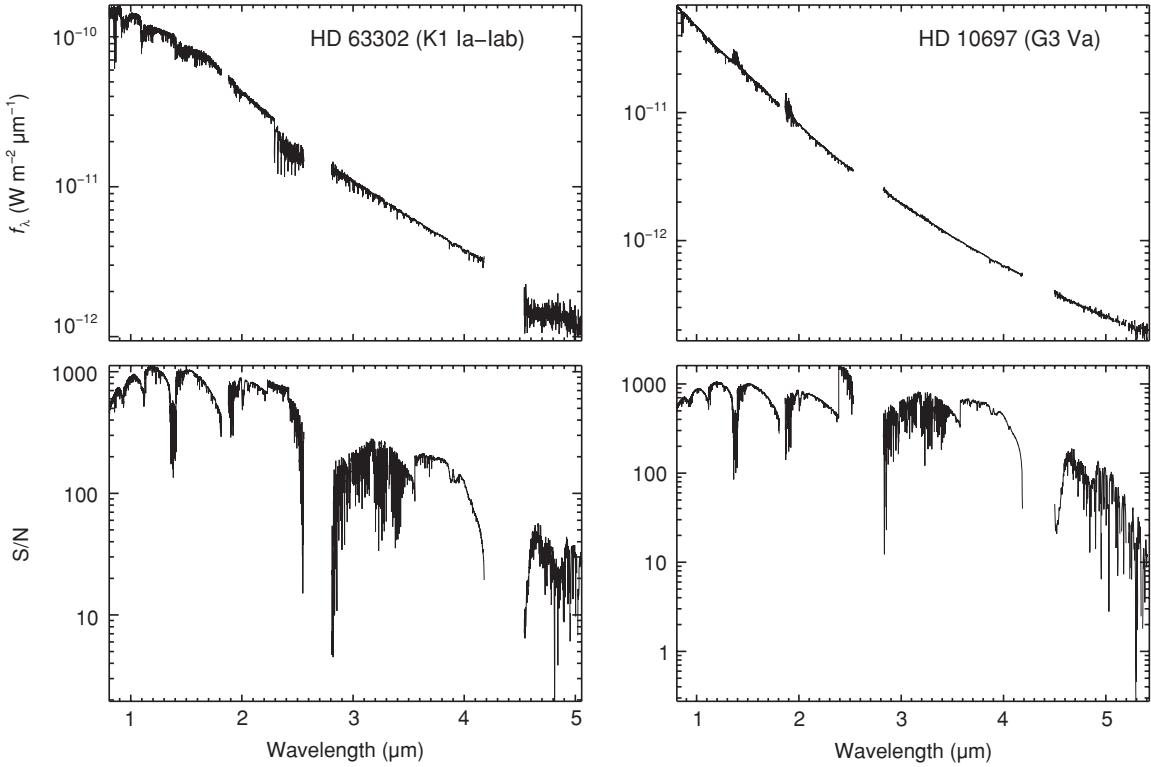


Figure 6. Left: the flux and S/N spectra of HD 63302 (K1 Ia–Iab). Telluric correction is excellent. Right: the flux and S/N spectra of HD 10697 (G3 Va). Note the flux error in the spectrum at $\sim 1.9 \mu\text{m}$ and $\sim 1.4 \mu\text{m}$ despite the fact that the S/N > 100. This is due to relatively poor telluric correction in these regions for this particular observation. Therefore, care must be taken in interpreting features in regions of high telluric contamination even if the S/N is high.

function for each bandpass that we assume to be given by the product of the filter transmission and the atmospheric transmission. Equation (5) assumes that Vega has zero color in all passband combinations. We used the Wide Field Camera (WFCAM; Casali et al. 2007) ZYJHK filter profiles that include the atmospheric transmission at an airmass of 1.3 with a precipitable water vapor content of 1.0 mm (Hewett et al. 2006). The Z and Y bands are custom filters designed for the UKIRT Infrared Deep Sky Survey (UKIDSS; Lawrence et al. 2007) centered at ~ 0.88 and $\sim 1.03 \mu\text{m}$, while the JHK bands were constructed to the specifications of the Mauna Kea Observatories Near-Infrared (MKO-NIR) filter set (Tokunaga et al. 2002). We constructed an L' system response function using the MKO-NIR L' -band filter profile and ATRAN (Lord 1992) to calculate the atmospheric transmission under the same atmospheric conditions. For $f_\lambda^{\text{Vega}}(\lambda)$ we used a Kurucz model of Vega ($T_{\text{eff}} = 9550 \text{ K}$, $\log g = 3.950$, $v_{\text{rot}} = 25 \text{ km s}^{-1}$, and $v_{\text{turb}} = 2 \text{ km s}^{-1}$), scaled to the flux density at $\lambda = 5556 \text{ \AA}$ given by Mégezzi (1995). The factors of λ inside the integrals convert the energy flux densities f_λ to photon flux densities, which ensures that the integrated fluxes are proportional to the observed photon count rate (e.g., Koornneef et al. 1986; Buser & Kurucz 1992).

The mean colors of the eight A0 V stars are $\langle Z - Y \rangle = -0.015 \pm 0.007$ (rms), $\langle Y - J \rangle = 0.007 \pm 0.006$ (rms), $\langle J - H \rangle = 0.019 \pm 0.005$ (rms), $\langle H - K \rangle = -0.005 \pm 0.004$, and $\langle K - L' \rangle = -0.001 \pm 0.010$. Given that we expect the mean colors to be zero, the mean colors of the A0V stars represent the precision in our ability to measure spectral slope. Taken together, the 2MASS and A0V star photometry indicates that we can measure spectral slope to within a few percent. Finally, slope variations introduced due to uncertainties in the spectral types of the A0 V standard stars are small since an uncertainty of a 0.5

subtype at A0 is equivalent to $\delta_{J-H} = 0.003$, $\delta_{H-K} = 0.005$, and $\delta_{J-L'} = 0.010$ (Cox 2000).

3. DATA AND ANALYSIS

3.1. The Spectra

Digital versions of the spectra are available at the IRTF Web site, which contains a full description of the data products. The data are available in text or Spextool FITS format and files can be downloaded individually or bundled together in a tar file. The files contain wavelength, flux, and error. The errors include the photon Poisson noise and read noise (Vacca et al. 2004) for both the object and the associated telluric standard, which are then propagated through each step of the reduction process. The file headers contain more information (including object name, epoch, spectral type, observing modes, 2MASS JHK magnitudes, measured radial velocity, flux, and wavelength units). As an example, the flux and S/N spectra of HD 63302 (K1 Ia–Iab) and HD 10696 (G3 V) are shown in Figure 6. We estimate that the actual S/N in our fully reduced stellar spectra is limited to less than 1000 by systematic errors in the flat field measurement even though the formal S/N can be greater than 1000. Also, systematic errors in telluric correction (e.g., if the airmasses of an object and standard star are not ideally matched), systematic errors in the slope, as well as any errors in the spectral type of the A0 V telluric standard are not accounted for in the formal S/N estimate (see Figure 6).

Representative spectra, covering 0.8–5.0 μm , of dwarfs, giants, and supergiants in our sample are shown in Figures 7–9. Given the large wavelength range and the change in flux wavelength and spectral type, it is difficult to display the spectra at a scale that allows close examination of all of the interesting spectral features in one plot. For display pur-

poses, we therefore use λf_λ (normalized at the given wavelength) as a function of $\log \lambda$. The plots show the general trend of spectral features with MK spectral type. Feature identifications and changes with spectral type are described in more detail in Sections 3.2–3.4.

It should be noted that MK spectral classification is based on comparing an *optical* spectrum with a set of stars (anchor points) that define certain spectral types. Therefore it is not necessarily the case that the trends in NIR spectral features will follow the optical types. Also, the exact numbers for the effective temperature, surface gravity, and composition (i.e., metallicity) are model dependent (i.e., not directly observable) and will change as models improve. Although there are no formal MK classification criteria for the NIR, much work has been conducted on NIR spectral classification. The pioneering study on cool stars was done by Kleinmann & Hall (1986), who identified a number of temperature and luminosity sensitive atomic (Na I , Ca I , $\text{Br} \gamma$) and molecular (CO , H_2O) features in the K band. Subsequent studies developed a variety of spectral type versus EW indices for cool stars. Notable examples among these are the studies by Origlia et al. (1993), Dallier et al. (1996), Meyer et al. (1998), Ramírez et al. (1997), Förster Schreiber (2000), Gorlova et al. (2003), Davies et al. (2007), Ivanov et al. (2004), and Mármol-Queraltó et al. (2008). We do not propose to add to these and other NIR classification schemes but present the IRTF Spectral Library as a resource for further investigation. The examples of EWs of several prominent features in data as a function of spectral type and luminosity are, however, presented in Section 4.1.

As an example of the mismatches in the trends of the NIR spectral features with MK type, Figure 10 shows a spectral sequence of K giant stars from 0.8 to 2.45 μm based on their MK types. From the trend in the overall spectral shape and depth of the first overtone vibration–rotation bands of CO in the K band (~ 2.29 – $2.5 \mu\text{m}$), two of the stars appear out of sequence (they are bluer and with shallower CO absorption than expected) and should appear earlier in the sequence by about one spectral subtype. When the stars are corrected for reddening (see Figure 11 and Table 5), the sequence of spectral shapes behaves as expected but the CO band depths still appear to be out of sequence. A possible explanation is that these stars are slightly metal poor (see, for example, Mármol-Queraltó et al. 2008). However, this explanation is inconsistent with the assigned MK spectral types: one star being of approximately solar metallicity (HD 137759, K2 III) and the other star being slightly metal rich (HD 114960, K3.5 IIIb CN0.5 CH0.5), although neither star has a formal [Fe/H] measurement. Another possibility is the uncertainty in assigning the MK spectral type as discussed in Section 2.1. Given these uncertainties, spectral classification using the IRTF Spectral Library is probably best done by comparing a given stellar spectrum of an unknown type with an ensemble of spectra for a sequence of MK types, rather than trying to find the closest individual spectral match. The effect of reddening should also be considered.

Plots of the dwarf sequences F3, F5, F9, G2, G8, K1, K7, M3, and M7 for the I , Y , J , H , K , and L bands, respectively, are shown in Figures 12–17. Luminosity effects at spectral types F, G, K, and M, across the 0.8–5 μm range, are shown in Figures 18–21. Plots showing luminosity effects at spectral types F5 and G6 for the I , Y , J , H , K , and L bands, respectively, are shown in Figures 22–27; likewise luminosity effects at spectral types K5 and M5 are shown in Figures 28–33. A 0.8–5 μm sequence of M, S, and C giants is plotted in Figure 34. All these

spectra are discussed in more detail in the subsequent sections. More complete spectral sequences are given in the Appendix.

3.2. Atomic Line Identifications

The S/N of the spectra is high enough that almost all of the absorption features seen in the spectra are real and not noise. However given that the resolving power of the spectra is $R \sim 2000$, the carriers of only the strongest and most isolated lines can be unambiguously identified. We therefore use the line identifications presented in the high-resolution ($R \sim 100000$) spectral atlases of the solar photosphere (Wallace et al. 1993; Wallace & Livingston 2003) and Arcturus (K1.5 III; Hinkle et al. 1995, 2000). We selected only those absorption lines in the atlases with depths less than 0.8 (where the continuum has been normalized to unity) because weaker lines are only marginally detectable in our spectra.

Tables 6 and 7 list all atomic metal lines with depths less than 0.8 in the solar and Arcturus atlases, respectively. The wavelengths of the lines are in vacuum and were taken primarily from the atlases themselves. The revised solar atlas (Wallace & Livingston 2003) does not present the wavelengths of the lines, so we obtained them from an earlier version of the atlas (Livingston & Wallace 1991). A few of the lines in the revised atlas either lack identifications in the original atlas or have since been identified as being carried by two lines. We determined the wavelengths of these lines using the National Institute of Standards and Technology Atomic Spectra Database,⁷ the Atomic Line List,⁸ and the Fe I line list compiled by Nave et al. (1994). For several interesting atomic absorption lines we have calculated EW values for our sample of stars. Table 8 gives the EW definitions and Table 9 gives the EW values (see Section 4.1 for a discussion and Figure 35 for plots of prominent EWs).

3.3. Molecular Band Identifications

Molecular absorption bands are prominent in the spectra of late-type stars. Identifications for many of these features can be found in Spinrad & Wing (1969), Brett (1990), Brett (1989), and Lançon & Wood (2000). Table 10 lists the vacuum wavelengths and identifications for each of the band heads identified in the spectra. Below, we describe some of the absorption bands in detail.

3.3.1. TiO

Absorption bands of TiO that arise from the γ ($A^3\Phi - X^3\Delta$), ϵ ($E^3\Pi - X^3\Delta$), δ ($b^1\Pi - a^1\Delta$), and ϕ ($b^1\Pi - d^1\Sigma$) systems are conspicuous in the spectra of late-type stars over the 0.8–1.5 μm wavelength range (see Figures 7–9, 12, 28–30). The γ and ϵ systems involve triplet electronic states and thus exhibit triple-headed bands, while the δ and ϕ systems involve singlet electronic states and thus exhibit only single-headed bands.

The $\Delta\nu = -2$ bands of the γ system (0.82–0.86 μm) are often identified in both low and high resolution spectra of late-type stars (e.g., Kirkpatrick et al. 1991; Tinney & Reid 1998; Reiners et al. 2007). In particular, four TiO band heads (R_2 , Q_2 , R_1 , Q_1) are identified between 0.849 and 0.860 μm (see Figures 12 and 36). However, as can be seen in both our data and the high-resolution spectra of late-type M and early-type L dwarfs, (Tinney & Reid 1998; Reiners et al. 2007), two

⁷ <http://physics.nist.gov/PhysRefData/ASD/index.html>

⁸ <http://www.pa.uky.edu/~peter/atomic/>

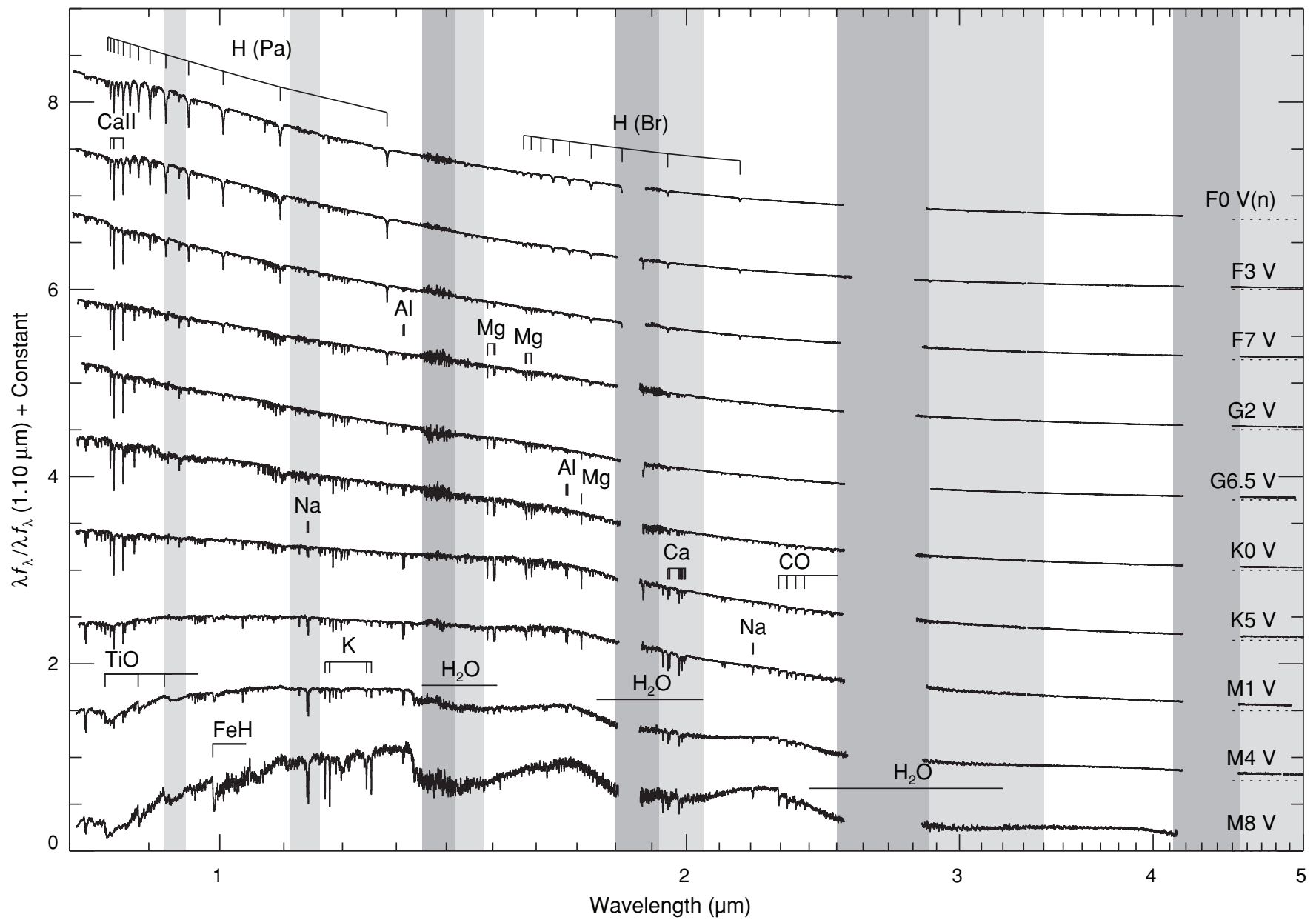


Figure 7. Dwarf sequence from 0.8–5 μm . The spectra are of HD 108159 (F0 V(n)), HD 26015 (F3 V), HD 126660 (F7 V), HD 76151 (G2 V), HD 115617 (G6.5 V), HD 145675 (K0 V), HD 36003 (K5 V), HD 42581 (M1 V), Gl 213 (M4 V), and Gl 752B (M8 V). The spectra have been normalized to unity at 1.10 μm and offset by constants (dotted lines). Regions of strong (transmission <20%) telluric absorption are shown in dark gray, while regions of moderate (transmission <80%) telluric absorption are shown in light gray.

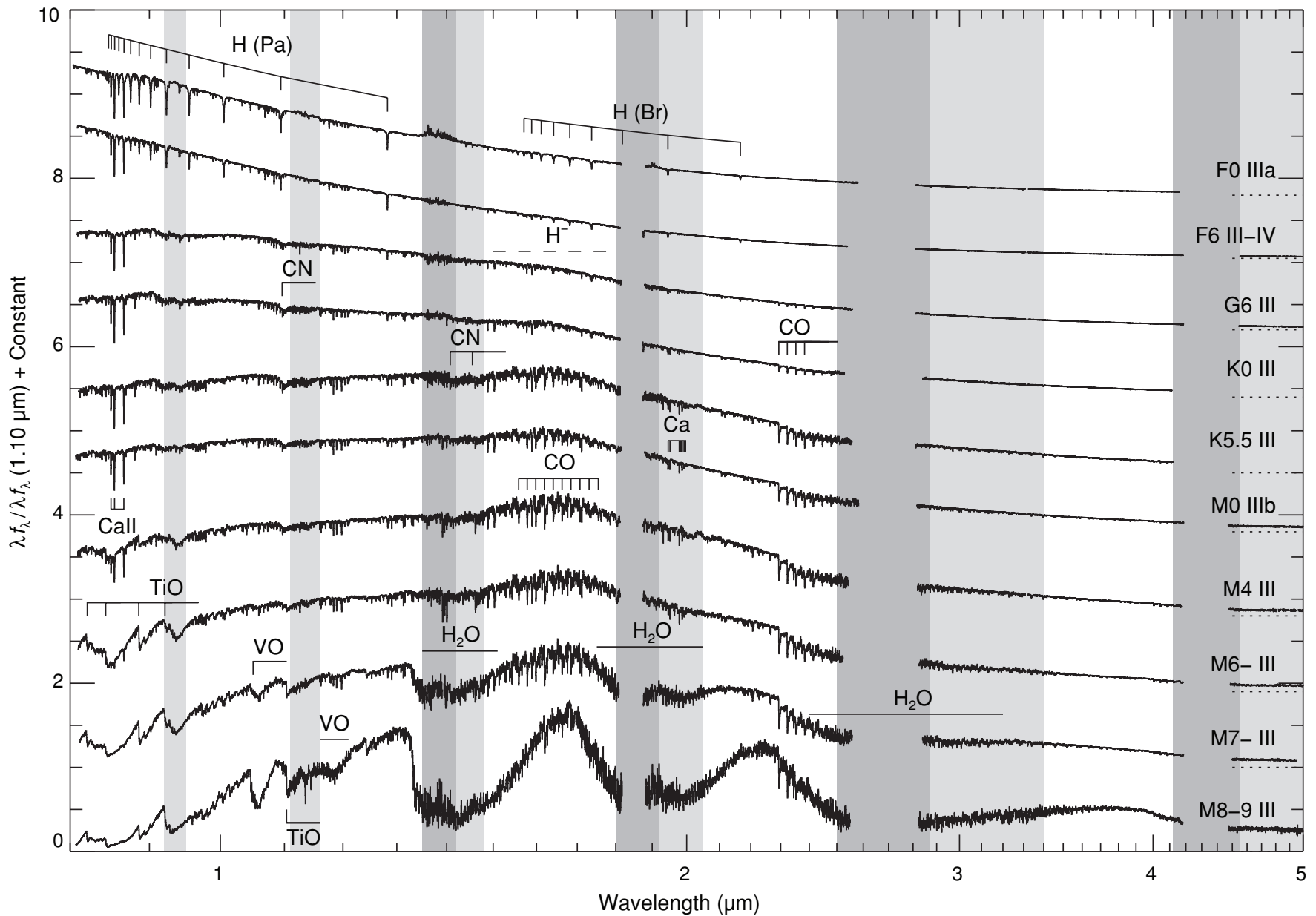


Figure 8. Giant sequence from 0.8–5 μm . The spectra are of HD 89025 (F0 IIIa), HD 160365 (F6 III-IV), HD 27277 (G6 III), HD 100006 (K0 III), HD 120477 (K5.5 III), HD 213893 (M0 IIIb), HD 4408 (M4 III), HD 18191 (M6- III), HD 108849 (M7- III), and IRAS 21284-0747 (M8-9 III). The spectra have been normalized to unity at 1.10 μm and offset by constants (dotted lines). Regions of strong (transmission $<20\%$) telluric absorption are shown in dark gray, while regions of moderate (transmission $<80\%$) telluric absorption are shown in light gray.

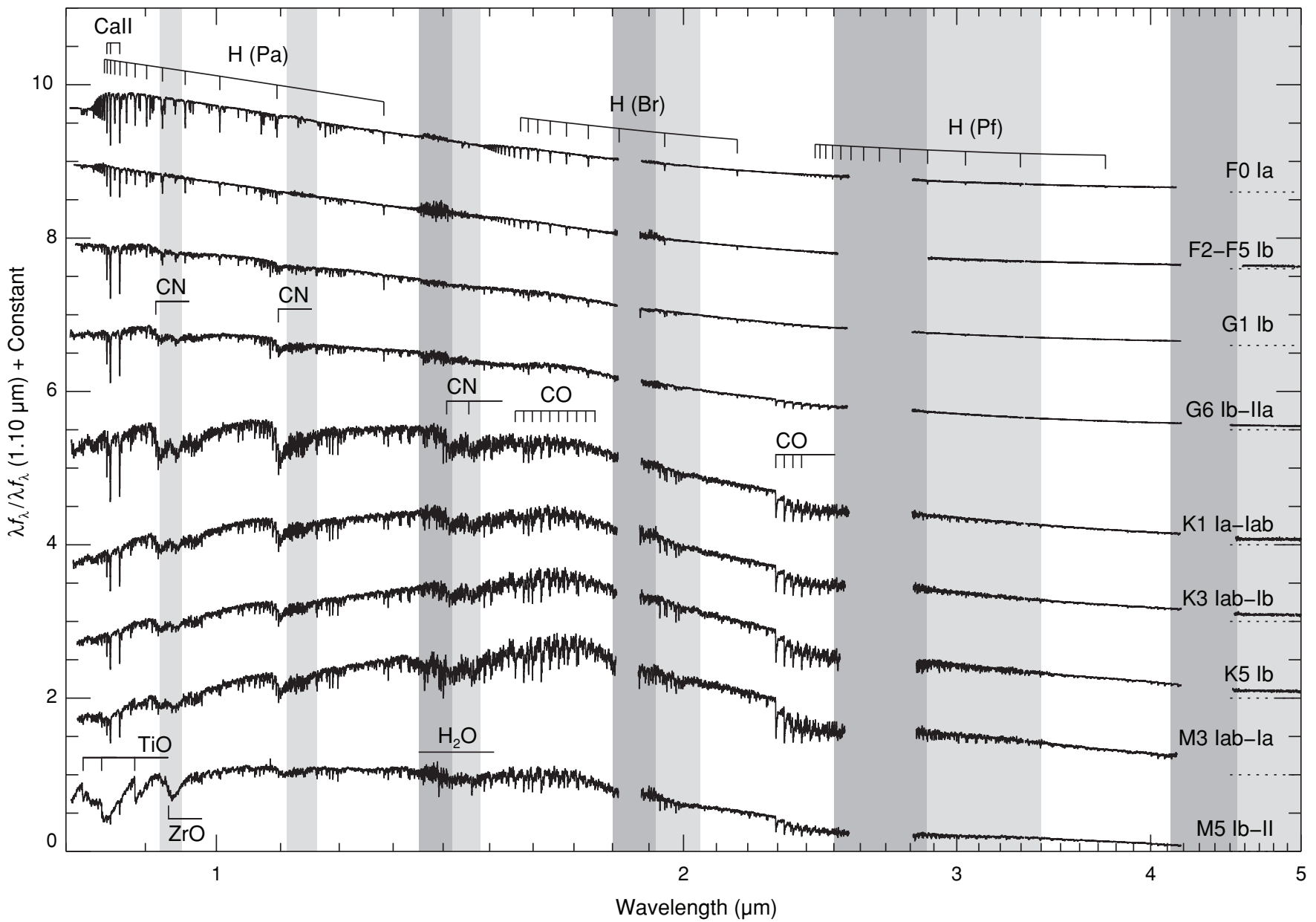


Figure 9. Supergiant sequence from 0.8–5.0 μm . The spectra are of HD 7927 (F0 Ia), BD +38 2803 (F2–F5 Ib), HD 74395 (G1 Ib), HD 202314 (G6 Ib–IIa Ca1 Ba0.5), HD 63302 (K1 Ia–Iab), HD 187238 (K3 Iab–Ib), HD 216946 (K5 Ib Ca1 Ba0.5), CD –31 4916 (M3 Iab–Ia), and HD 156014 (M5 Ib–II). The spectra have been normalized to unity at 1.10 μm and offset by constants (dotted lines). Regions of strong (transmission <20%) telluric absorption are shown in dark gray, while regions of moderate (transmission <80%) telluric absorption are shown in light gray.

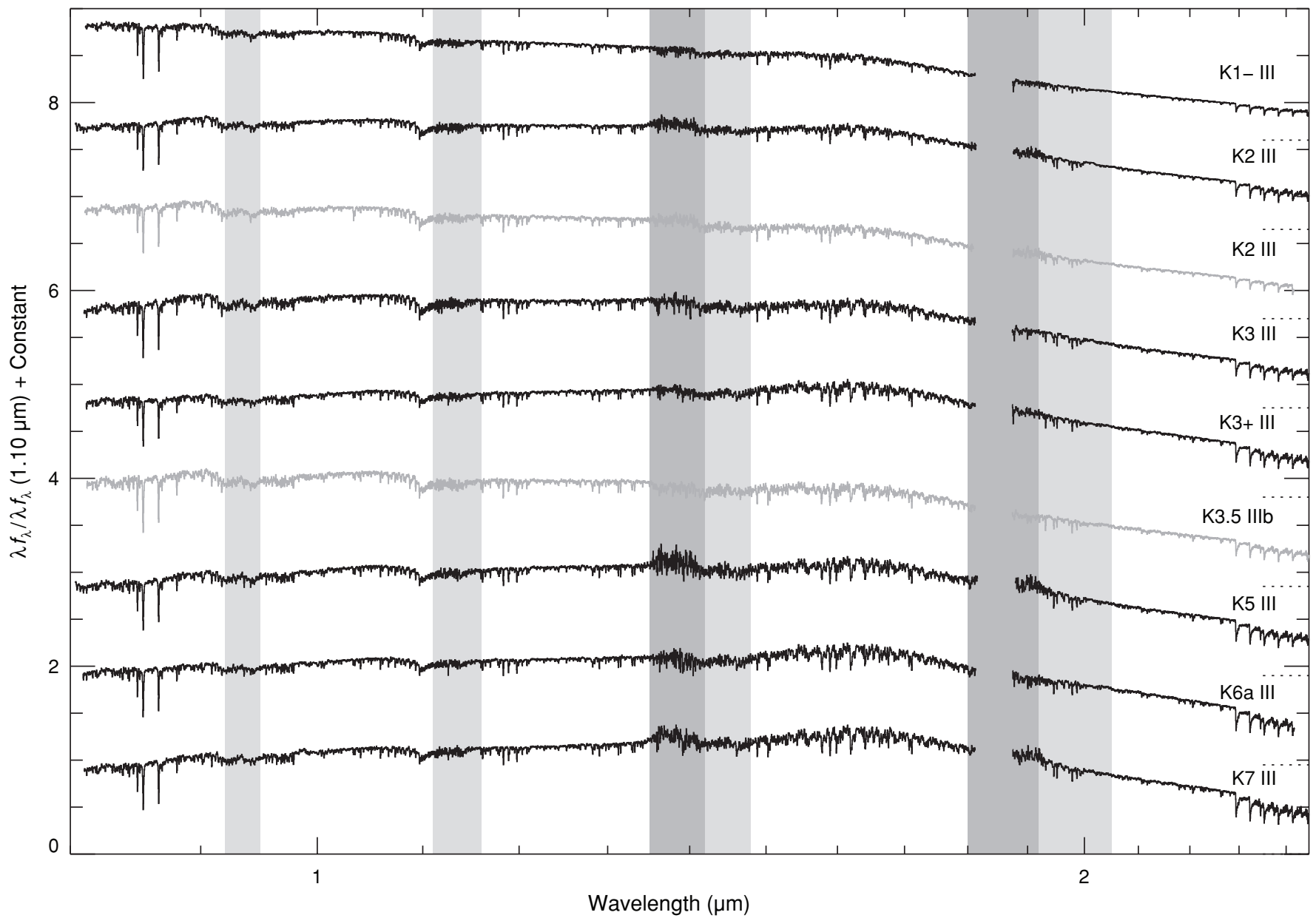


Figure 10. K giant sequence from 0.8–2.45 μm . The stars are HD 36124 (K1 – III Fe-0.5), HD 132935 (K2 III), HD 137759 (K2 III), HD 221246 (K3 III), HD 99998 (K3+ III Fe-0.5), HD 114960 (K3.5 IIIb CN0.5 CH0.5), HD 181596 (K5 III), HD 3346 (K6 IIIa), and HD 194193 (K7 III). Stars forming a smooth spectral sequence are plotted in black, while the two stars (HD 137759 and HD 114960), which appear slightly out of sequence (see Section 3.1), are plotted in gray.

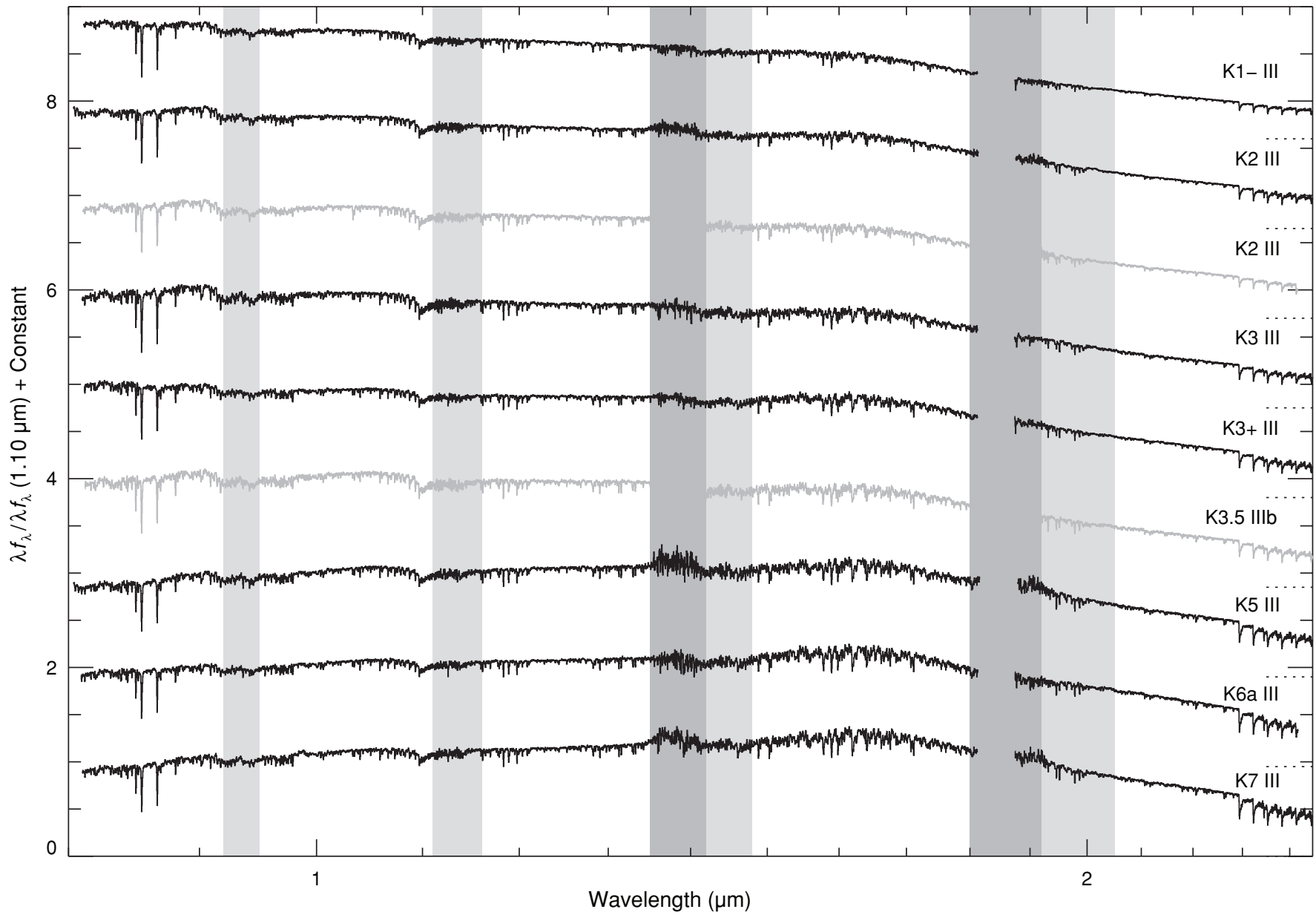


Figure 11. Same as Figure 11 except that the dereddened spectra are plotted. The spectral continuum shapes now behave as expected but the CO band depths (wavelengths $\geq 2.29 \mu\text{m}$) of the two stars HD 137759 and HD 114960 (plotted in gray) still appear slightly out of sequence (see Section 3.1).

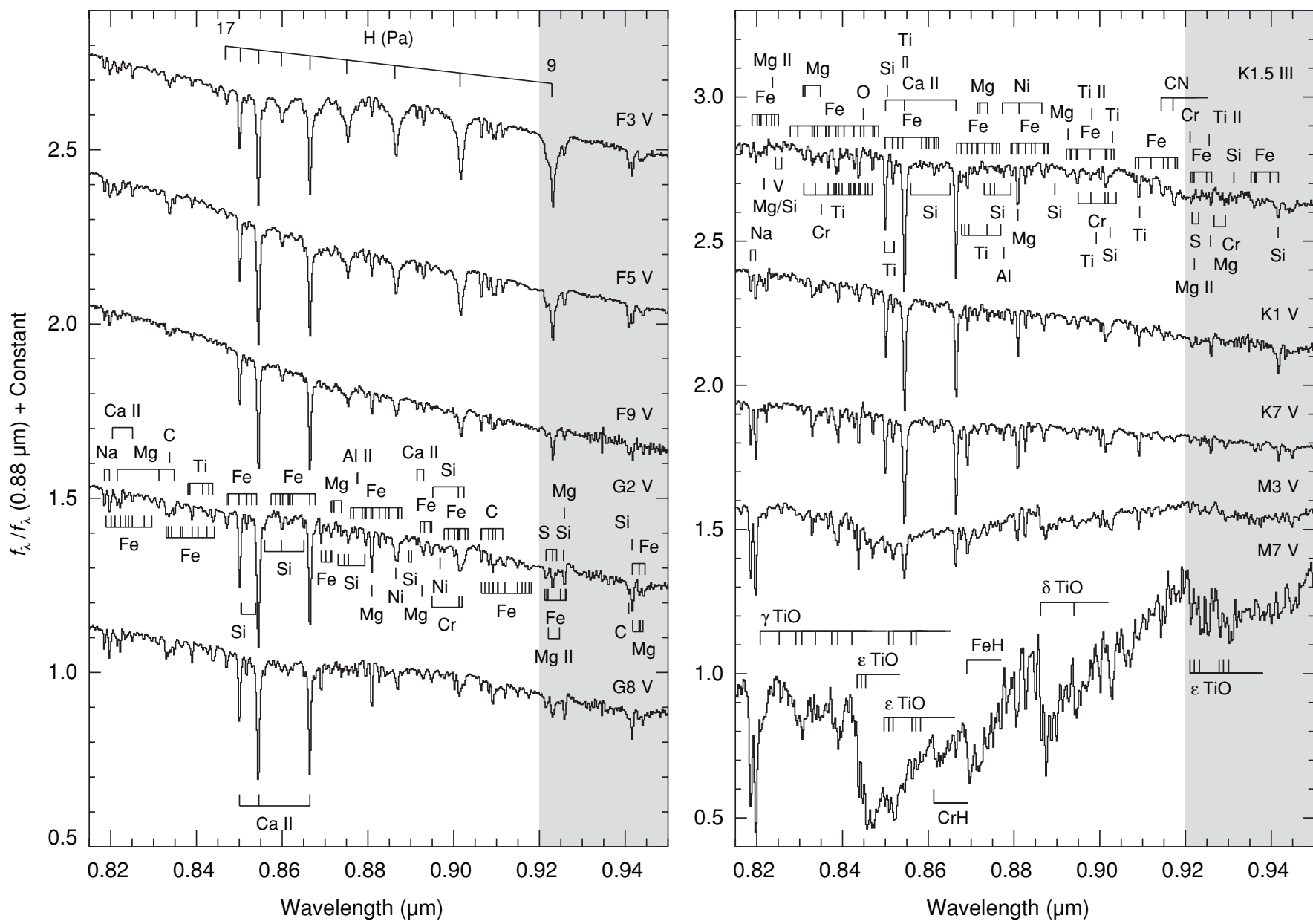


Figure 12. Sequence of F, G, K, and M dwarf stars plotted over the I band (0.82 – $0.95 \mu\text{m}$). The spectra are of HD 26015 (F3 V), HD 27524 (F5 V), HD 165908 (F9 V metal weak), HD 76151 (G2 V), HD 101501 (G8 V), HD 10476 (K1 V), HD 237903 (K7 V), Gl 388 (M3 V), and Gl 644C (vB 8) (M7 V). The K1.5 III comparison star is Arcturus (HD 124897). The spectra have been normalized to unity at $0.88 \mu\text{m}$ and offset by constants.

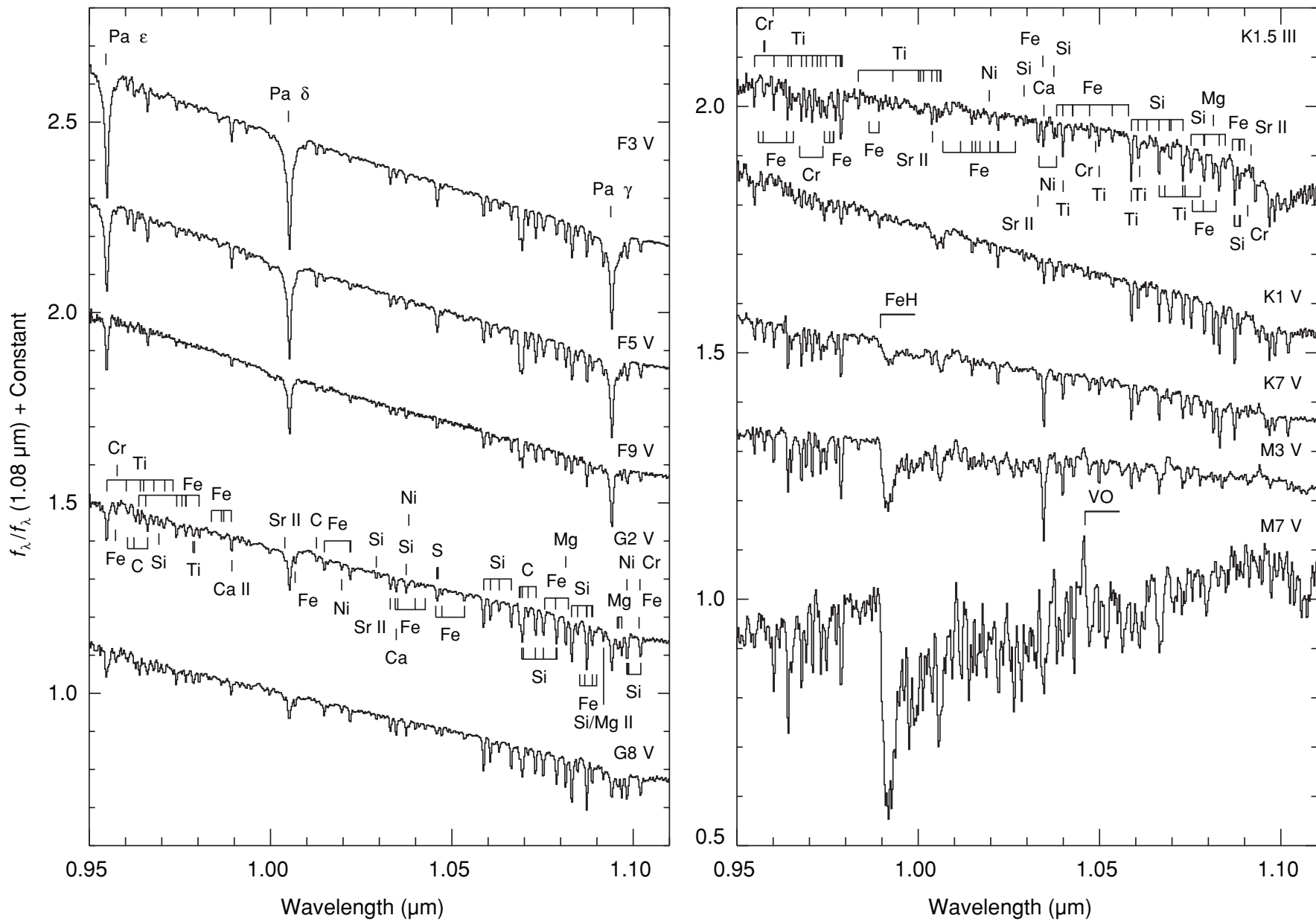


Figure 13. Same as Figure 12 except over the Y band (0.95–1.10 μm). The spectra have been normalized to unity at 1.08 μm and offset by constants.

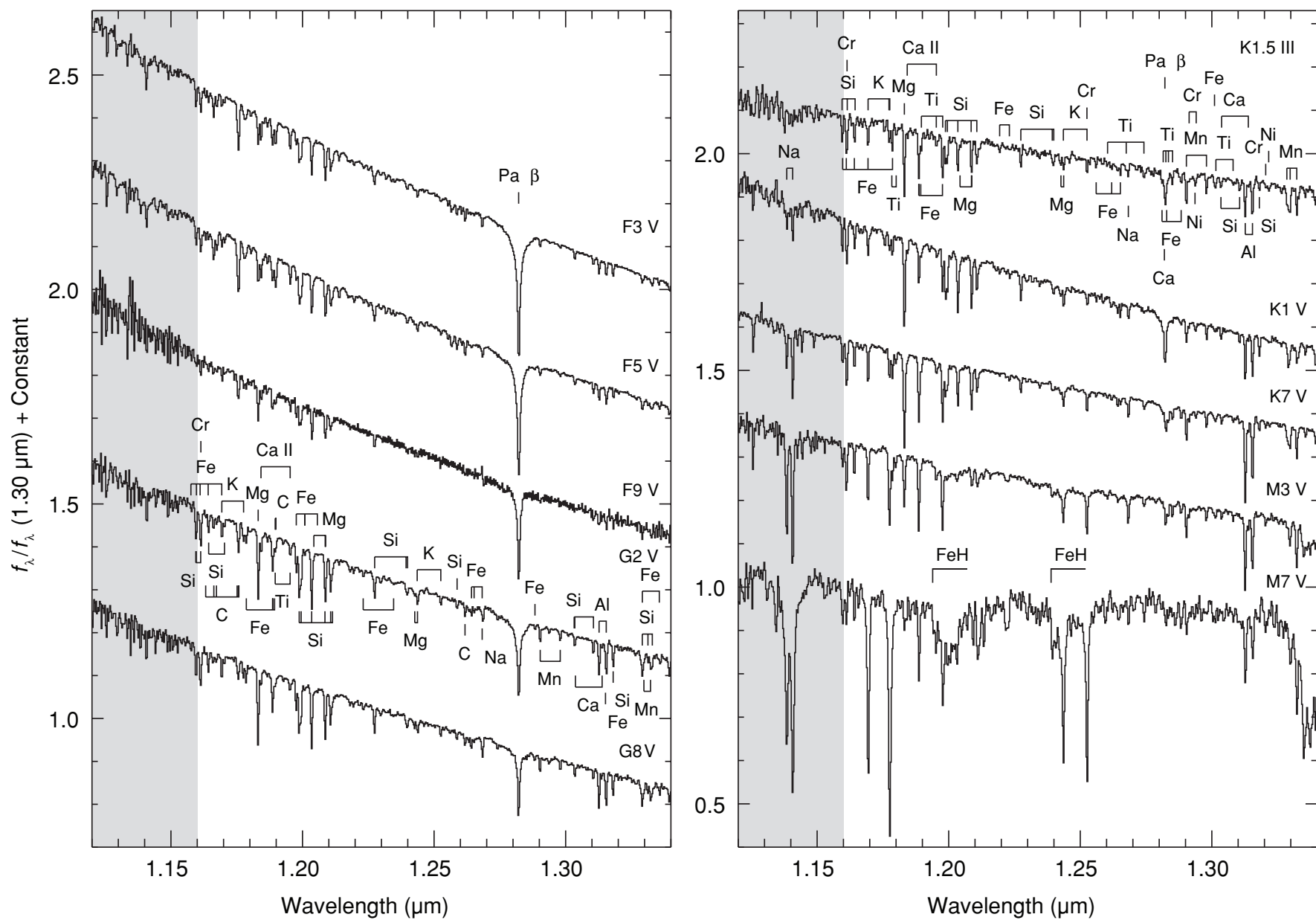


Figure 14. Same as Figure 12 except over the *J* band (1.12–1.34 μm). The spectra have been normalized to unity at 1.30 μm and offset by constants.

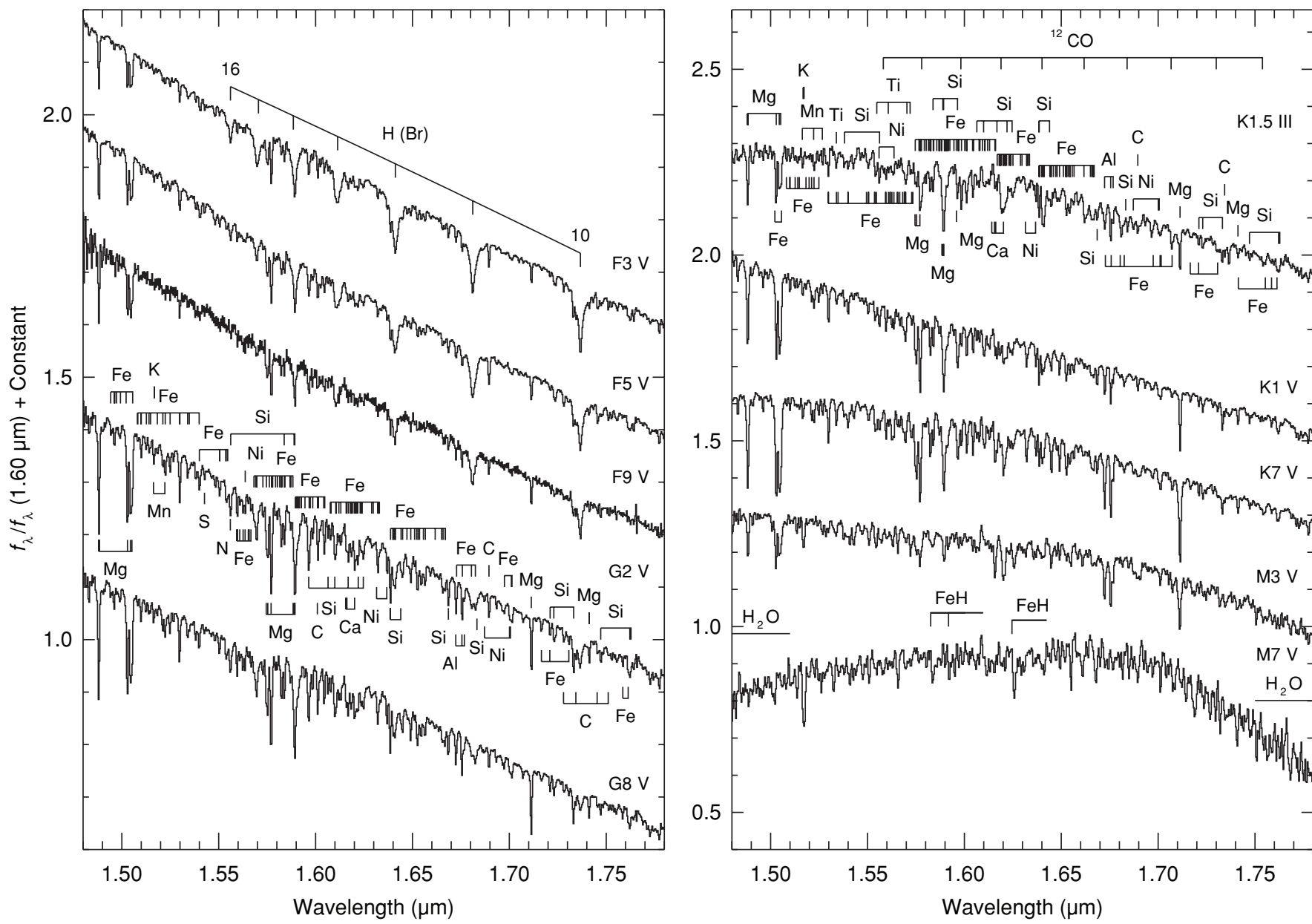


Figure 15. Same as Figure 12 except over the H band ($1.48\text{--}1.78\ \mu\text{m}$). The spectra have been normalized to unity at $1.60\ \mu\text{m}$ and offset by constants.

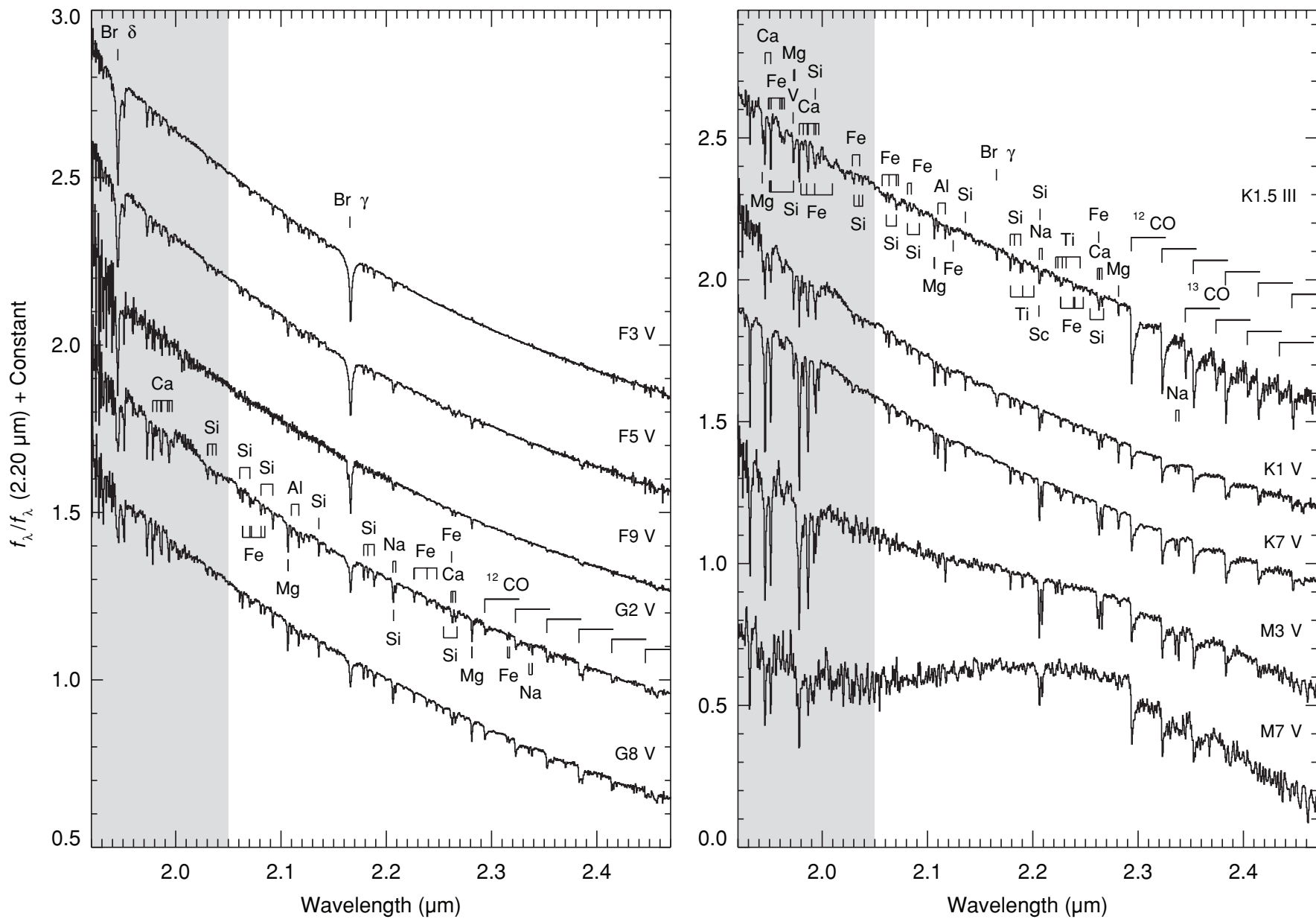


Figure 16. Same as Figure 12 except over the *K* band (1.92–2.5 μm). The spectra have been normalized to unity at 2.20 μm and offset by constants.

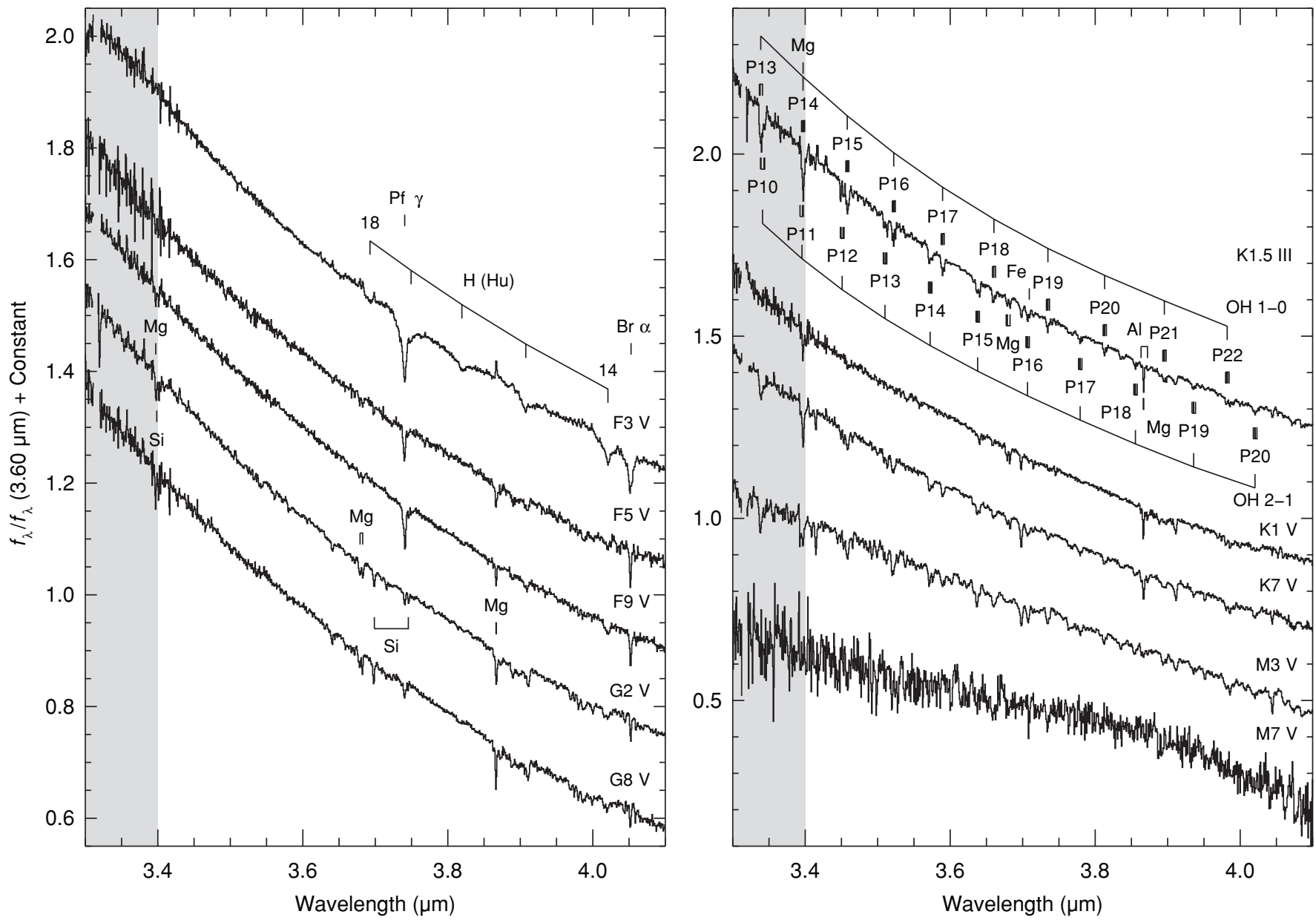


Figure 17. Same as Figure 12 except over the *L* band (3.3–4.2 μm). The spectra have been normalized to unity at 3.60 μm and offset by constants.

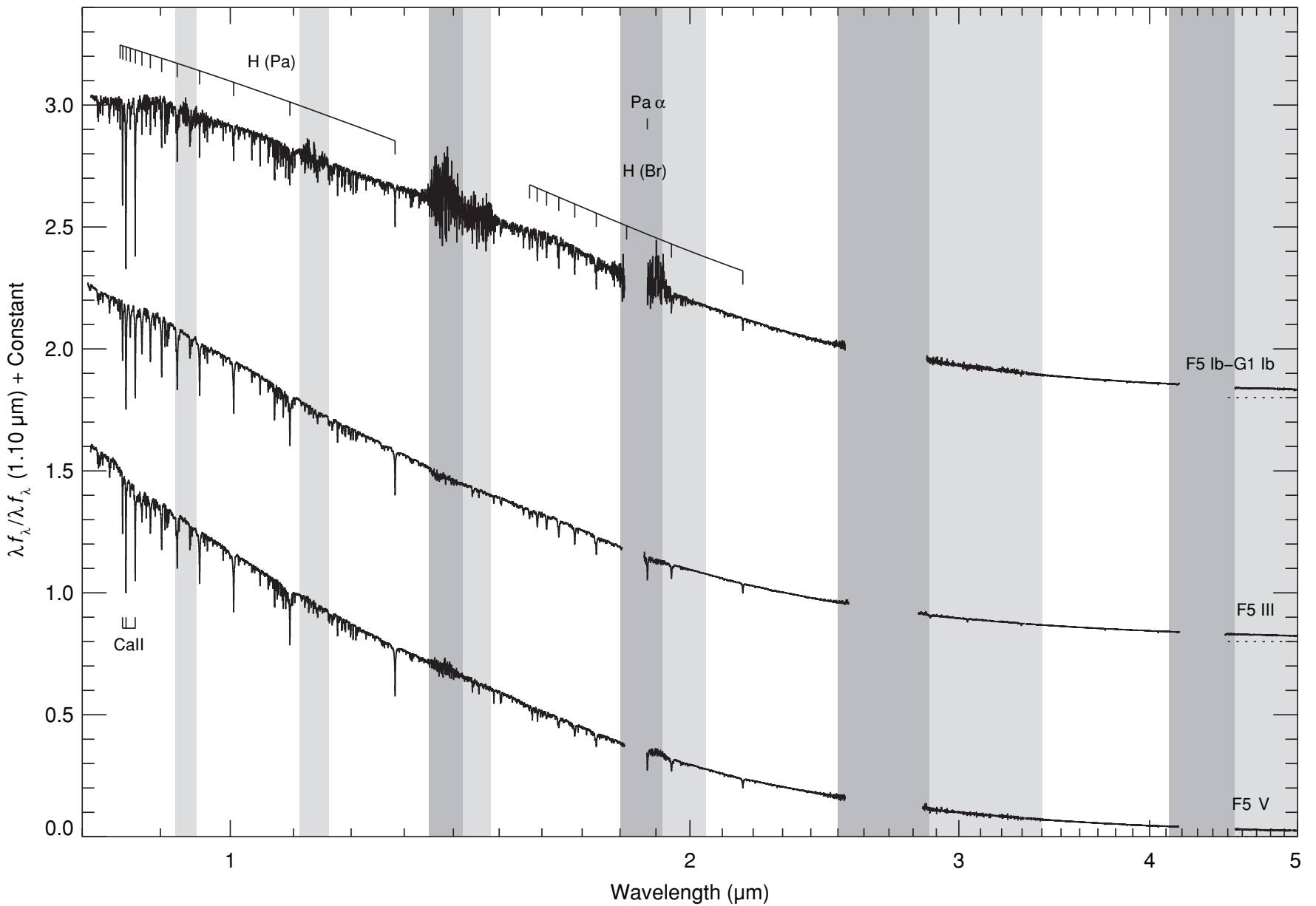


Figure 18. Luminosity effects at spectral type F. The spectra are of HD 27524 (F5 V), HD 17918 (F5 III), and HD 213306 (F5 Ib–G1 Ib) and have been normalized to unity at $1.10 \mu\text{m}$ and offset by constants (dotted lines). Regions of strong (transmission $<20\%$) telluric absorption are shown in dark gray, while regions of moderate (transmission $<80\%$) telluric absorption are shown in light gray.

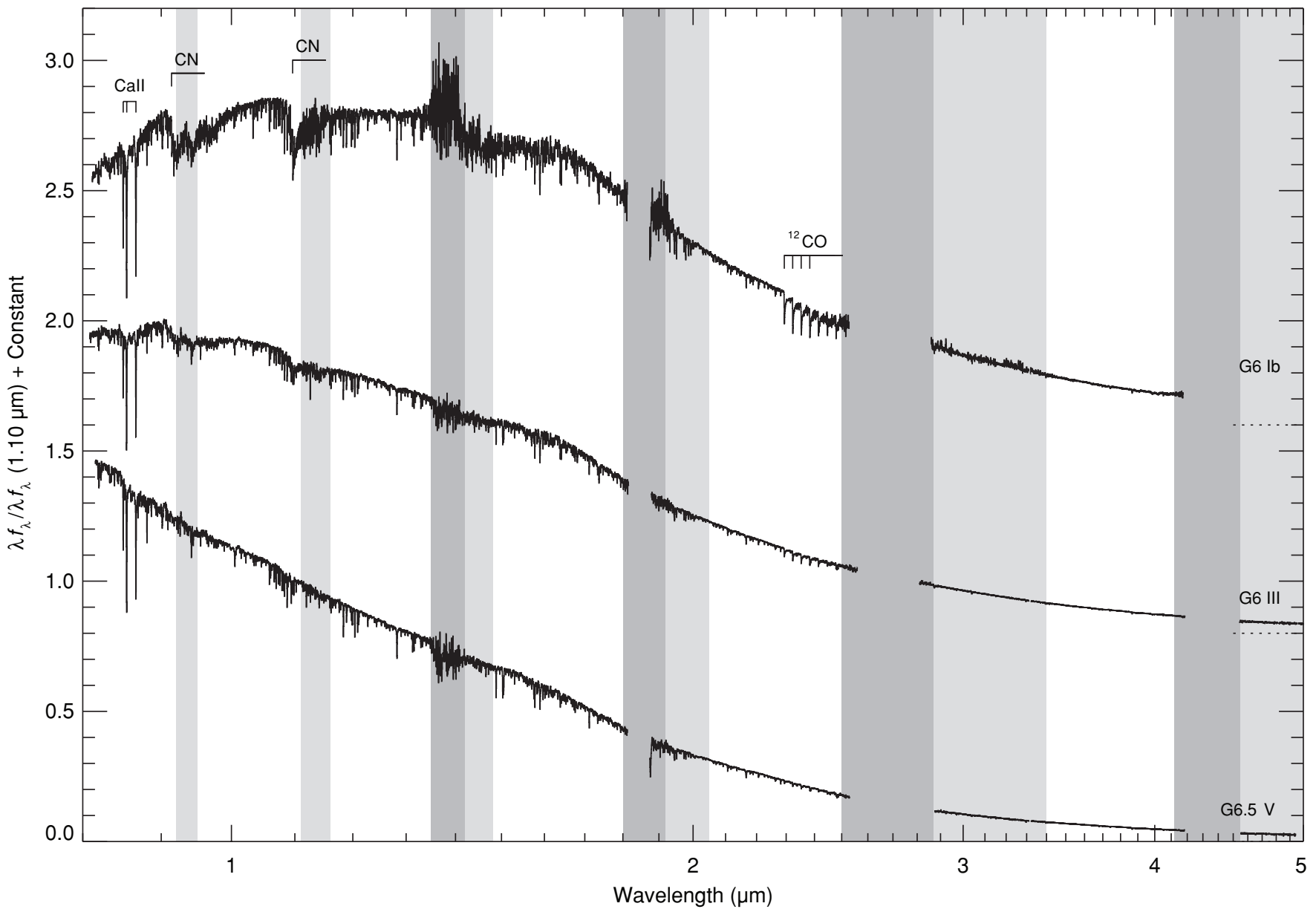


Figure 19. Luminosity effects at spectral type G. The spectra are of HD 115617 (G6.5 V), HD 27277 (G6 III), and HD 161664 (G6 Ib H δ 1) and have been normalized to unity at 1.10 μm and offset by constants (dotted lines). Regions of strong (transmission <20%) telluric absorption are shown in dark gray, while regions of moderate (transmission <80%) telluric absorption are shown in light gray.

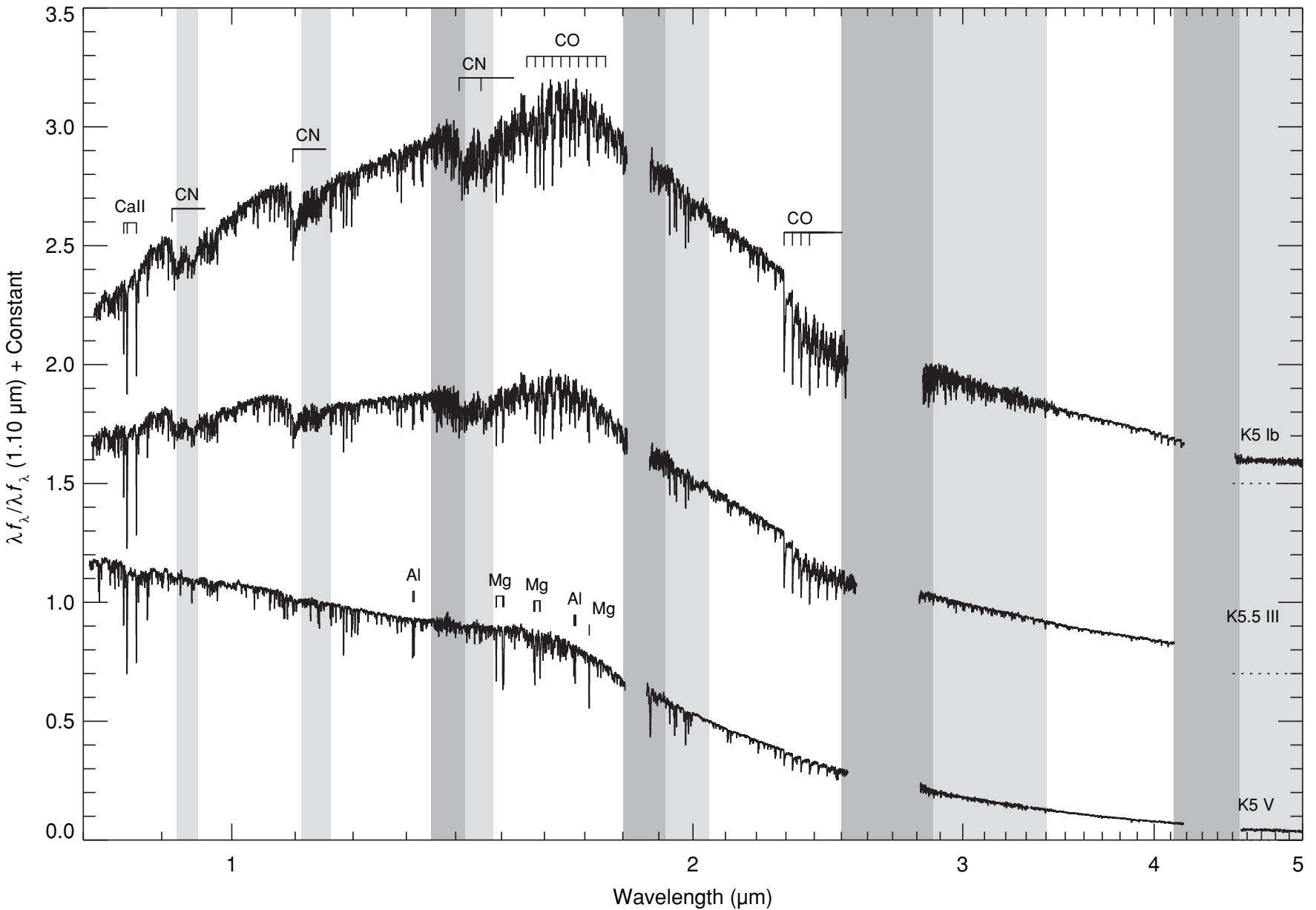


Figure 20. Luminosity effects at spectral type K. The spectra are of HD 36003 (K5 V), HD 120477 (K5.5 III), and HD 216946 (K5 Ib) and have been normalized to unity at $1.10 \mu\text{m}$ and offset by constants (dotted lines). Regions of strong (transmission $<20\%$) telluric absorption are shown in dark gray, while regions of moderate (transmission $<80\%$) telluric absorption are shown in light gray.

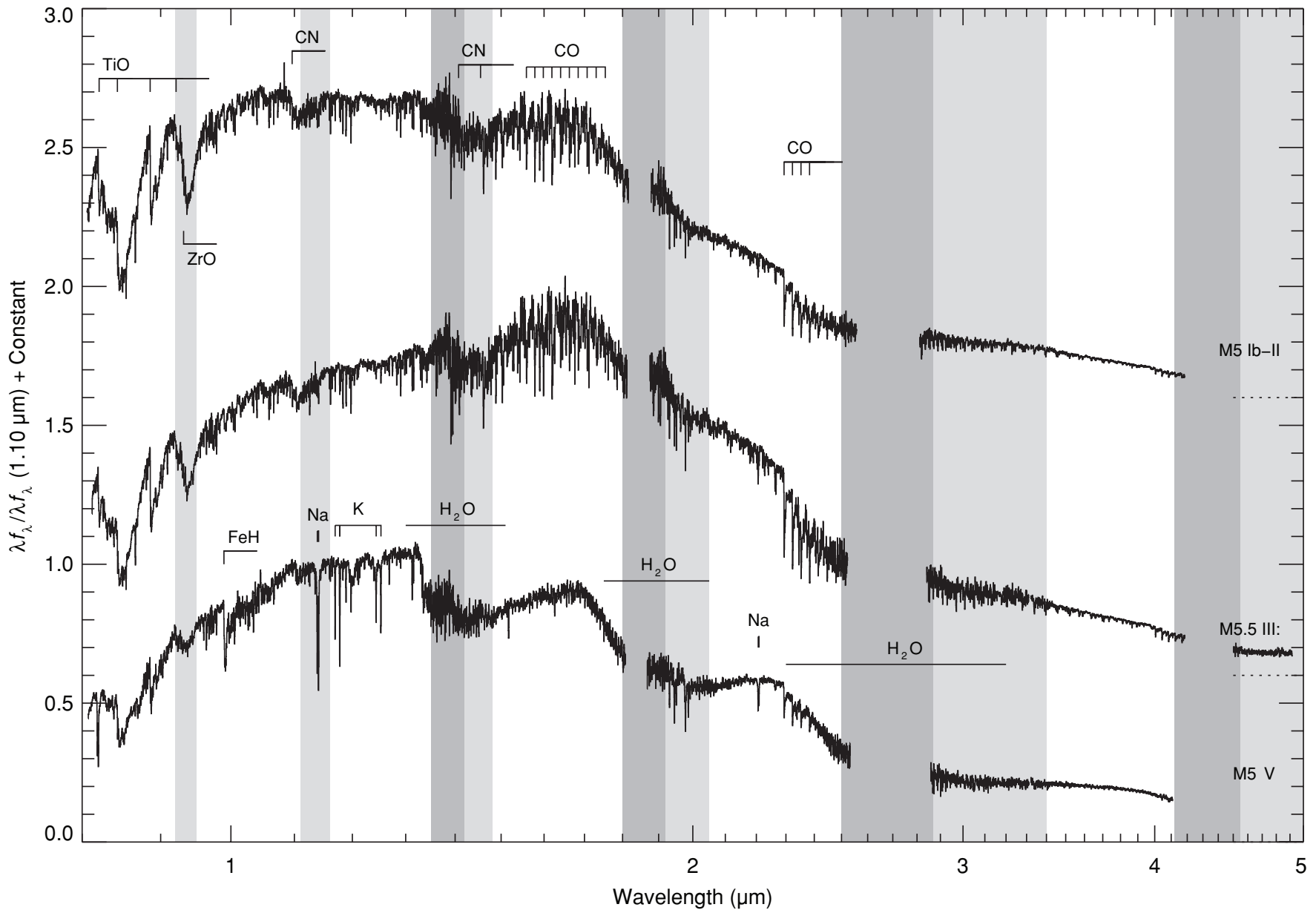


Figure 21. Luminosity effects at spectral type M. The spectra are of Gl 866ABC (M5 V), HD 94705 (M5.5 III:), and HD 156014 (M5 Ib-II) and have been normalized to unity at $1.10\ \mu\text{m}$ and offset by constants (dotted lines). Regions of strong (transmission $<20\%$) telluric absorption are shown in dark gray, while regions of moderate (transmission $<80\%$) telluric absorption are shown in light gray.

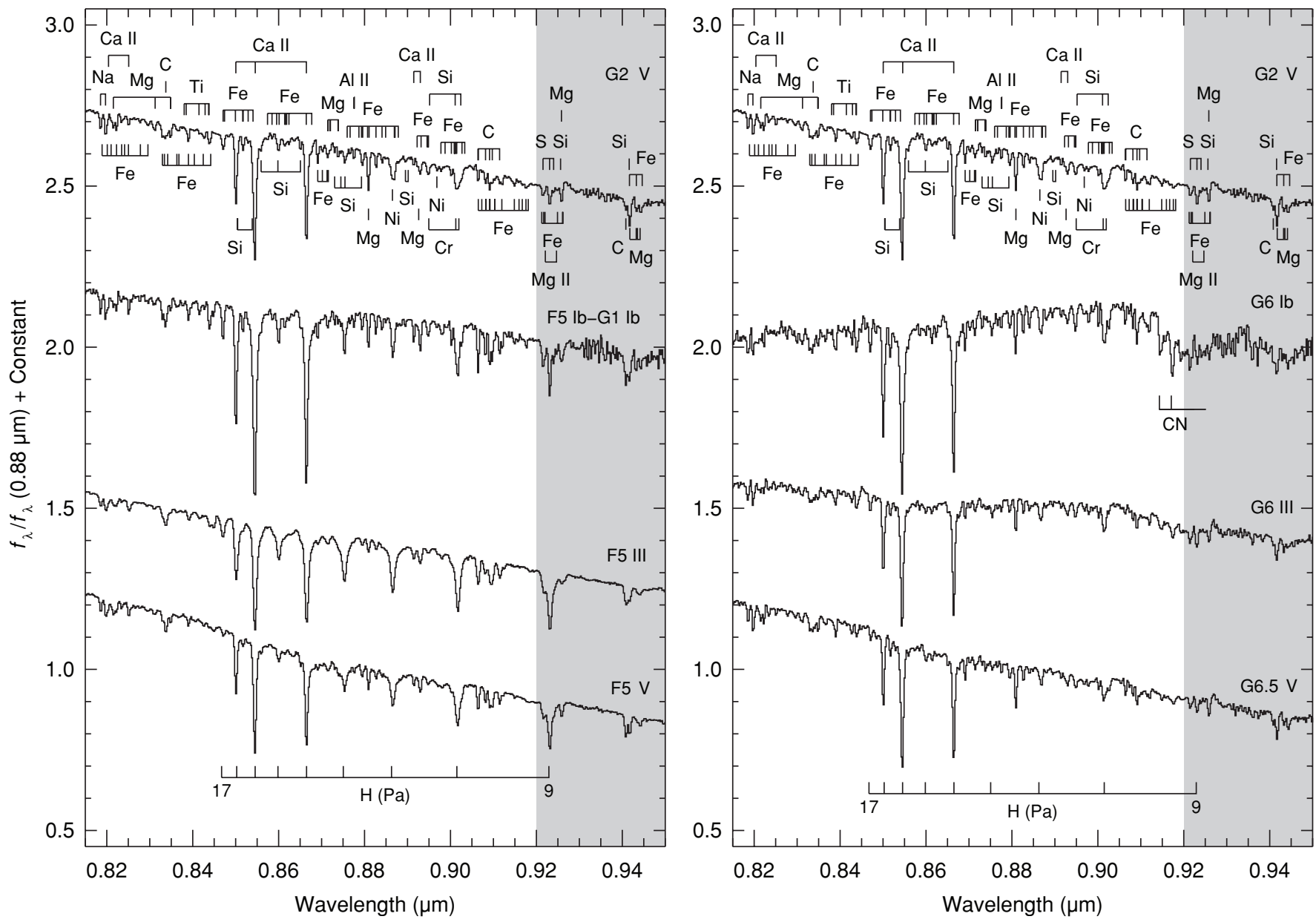


Figure 22. Luminosity effects at spectral types F5 (left) and G6 (right) plotted over the I band (0.82–0.95 μm). The spectra are of HD 213306 (F5 Ib–G1 Ib), HD 17918 (F5 III), HD 27524 (F5 V), HD 161664 (G6 Ib H_δ1), HD 27277 (G6 III), and HD 115617 (G6.5 V). The G2 V comparison star is HD 76151. The spectra have been normalized to unity at 0.88 μm and offset by constants.

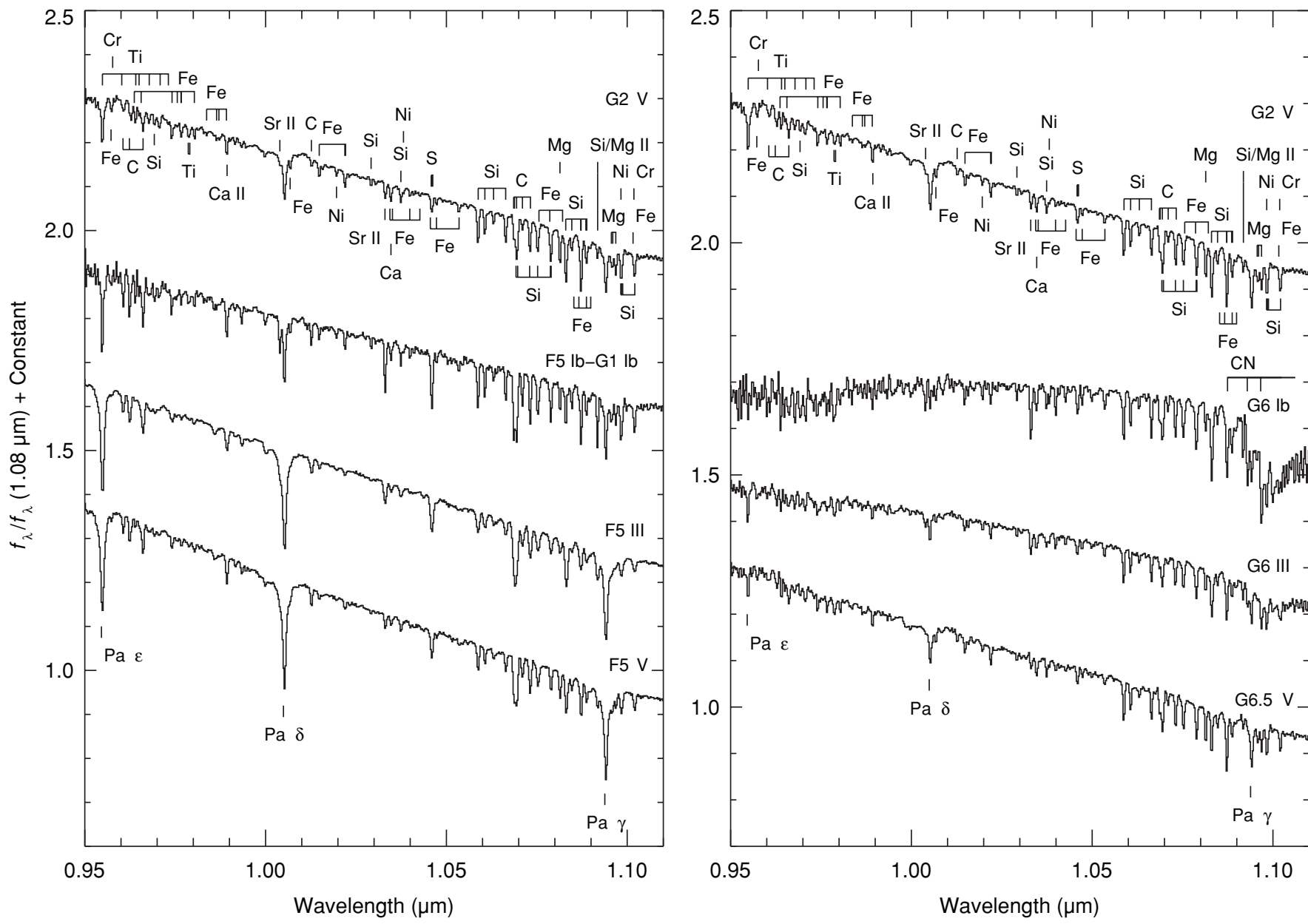


Figure 23. Same as Figure 22 except over the Y band. The spectra have been normalized to unity at $1.08 \mu\text{m}$ and offset by constants.

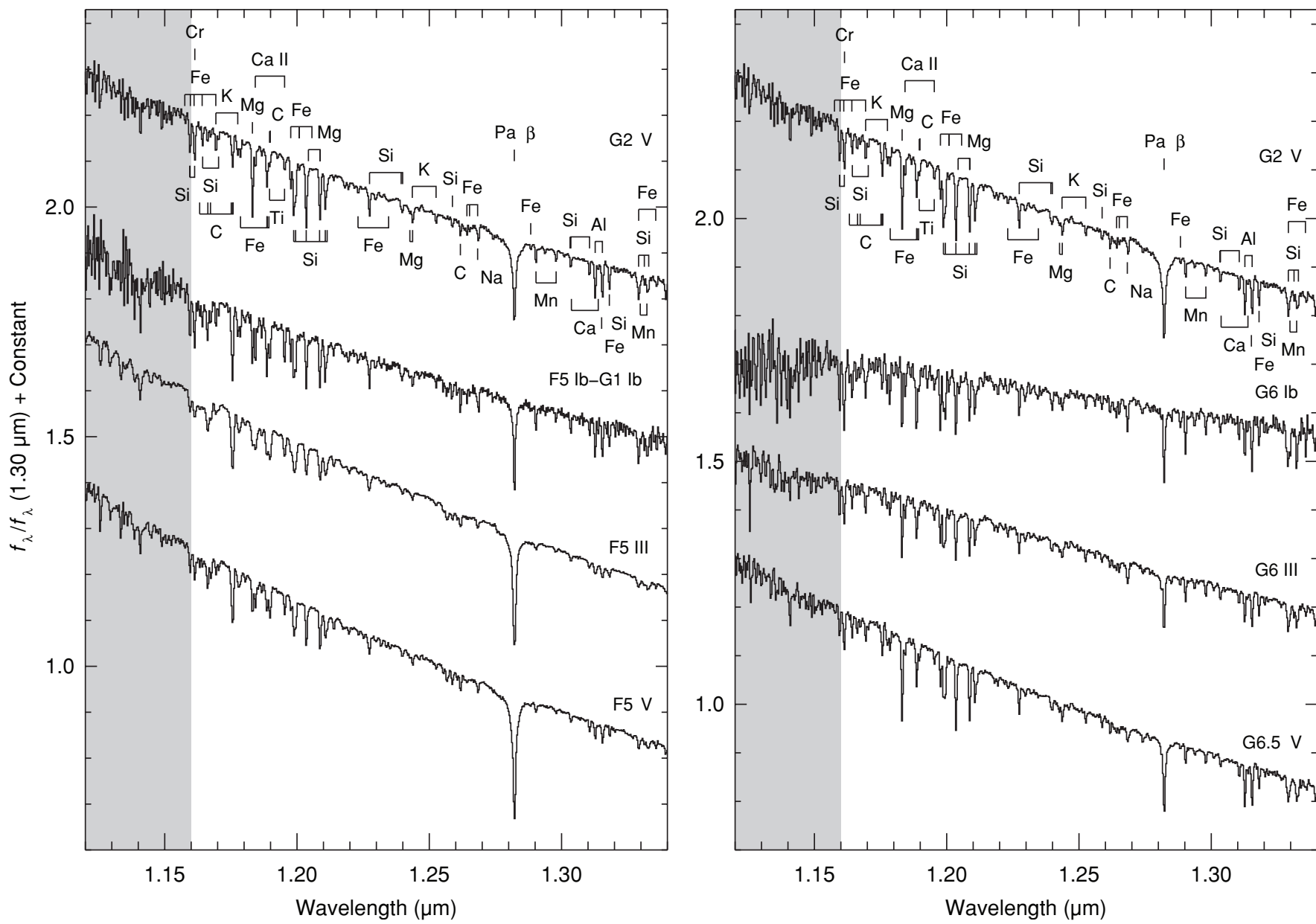


Figure 24. Same as Figure 22 except over the *J* band. The spectra have been normalized to unity at $1.30 \mu\text{m}$ and offset by constants.

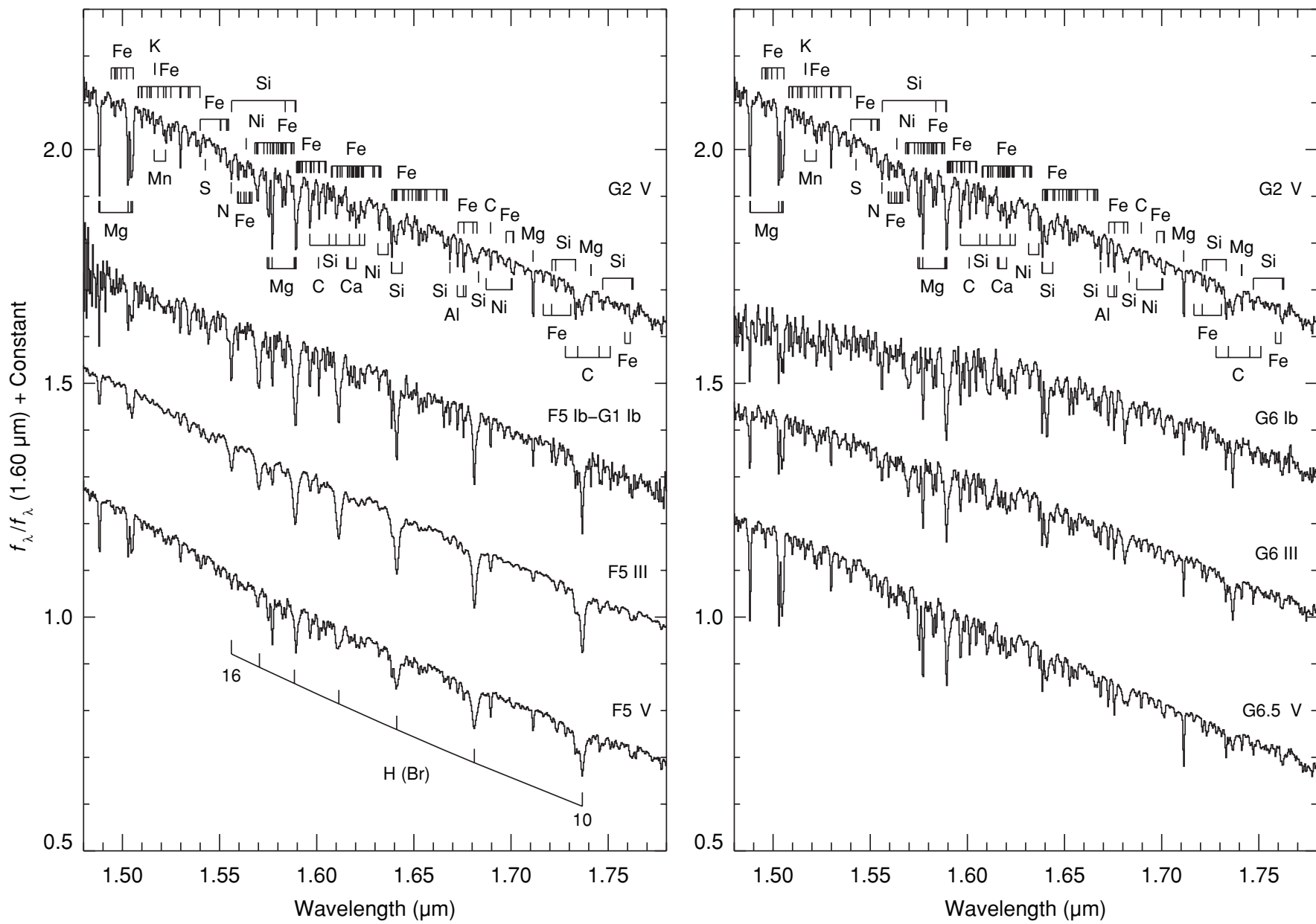


Figure 25. Same as Figure 22 except over the H band. The spectra have been normalized to unity at $1.60\ \mu\text{m}$ and offset by constants.

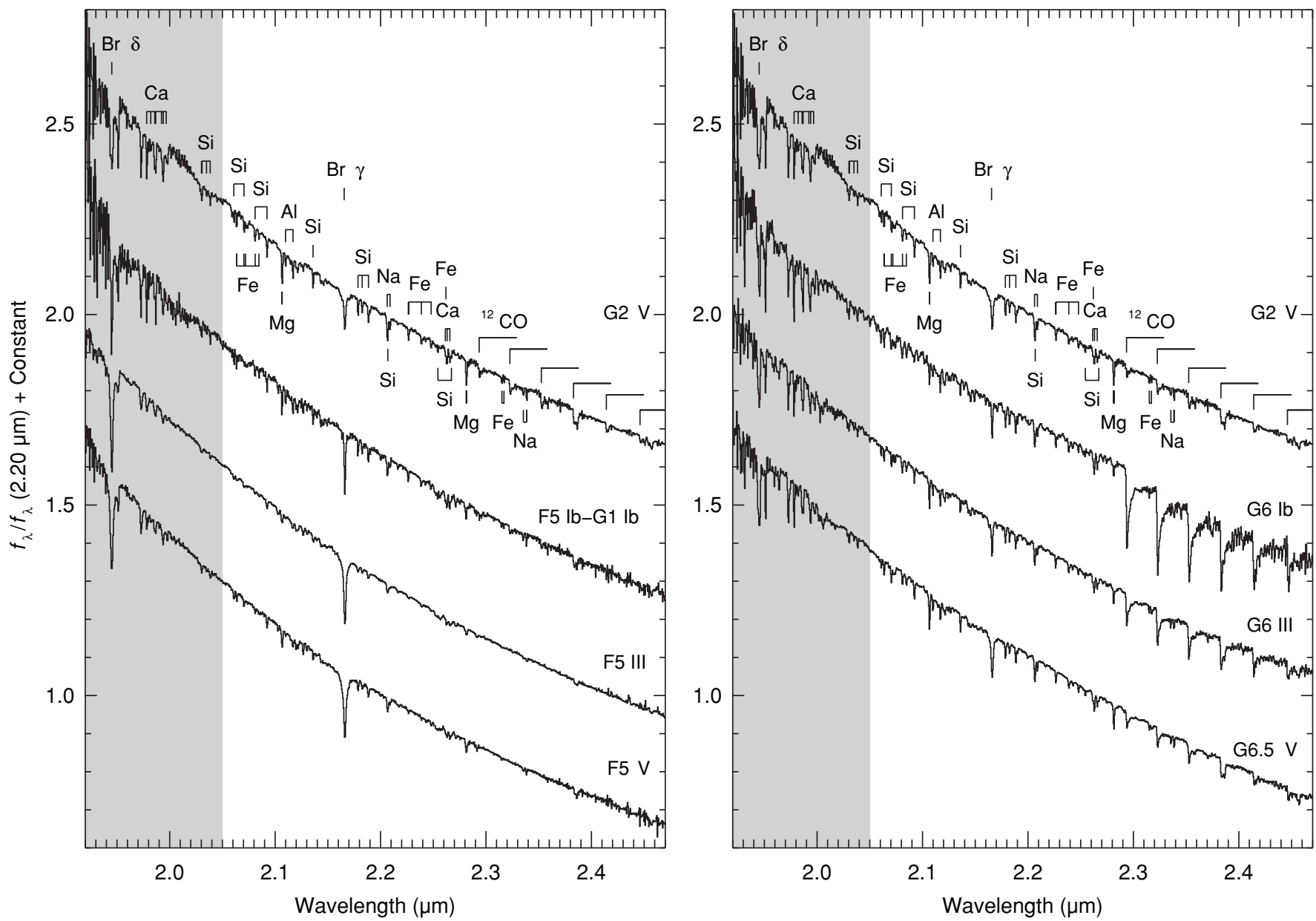


Figure 26. Same as Figure 22 except over the *K* band. The spectra have been normalized to unity at $2.20 \mu\text{m}$ and offset by constants.

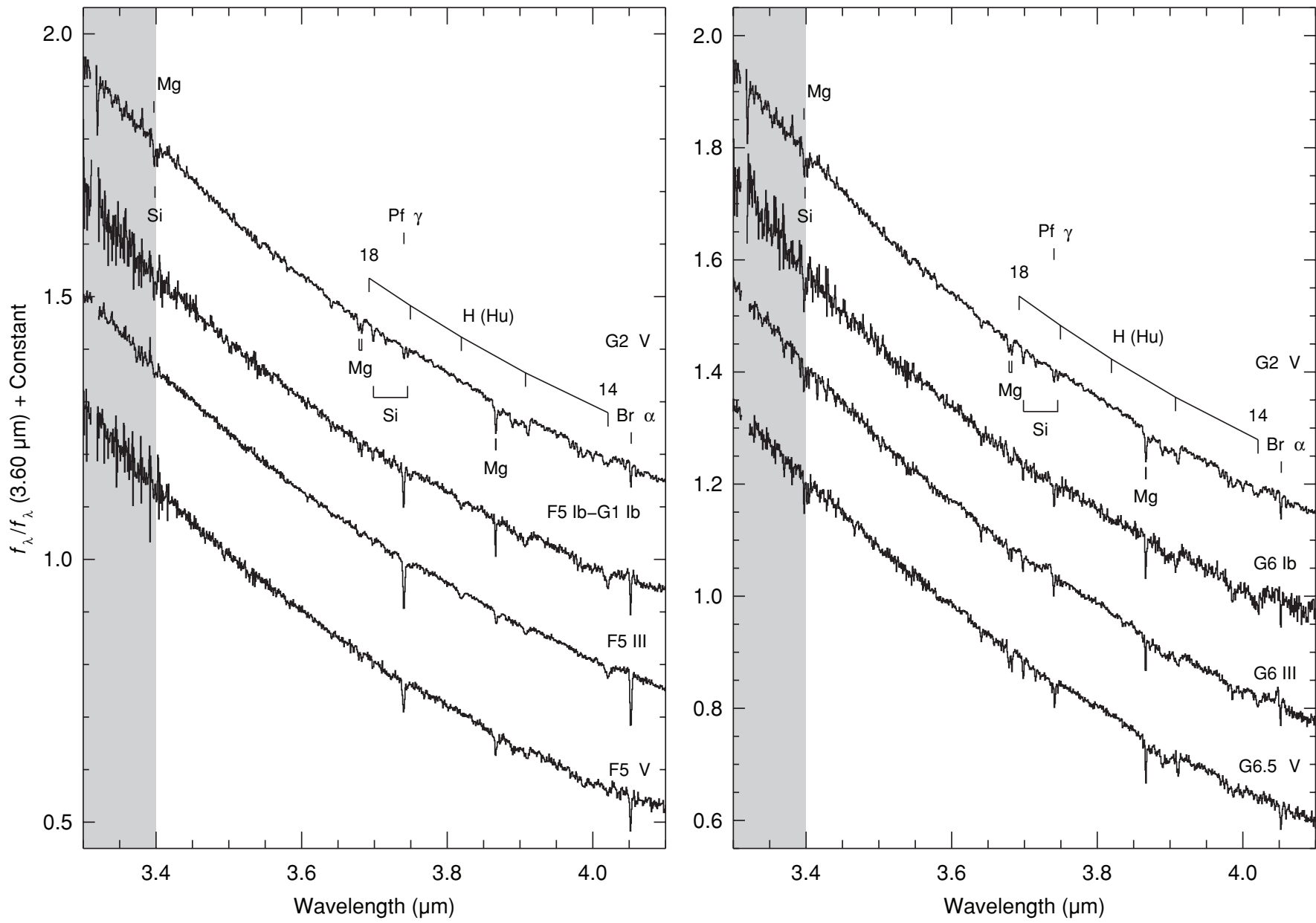


Figure 27. Same as Figure 22 except over the *L* band. The spectra have been normalized to unity at $3.60 \mu\text{m}$ and offset by constants.

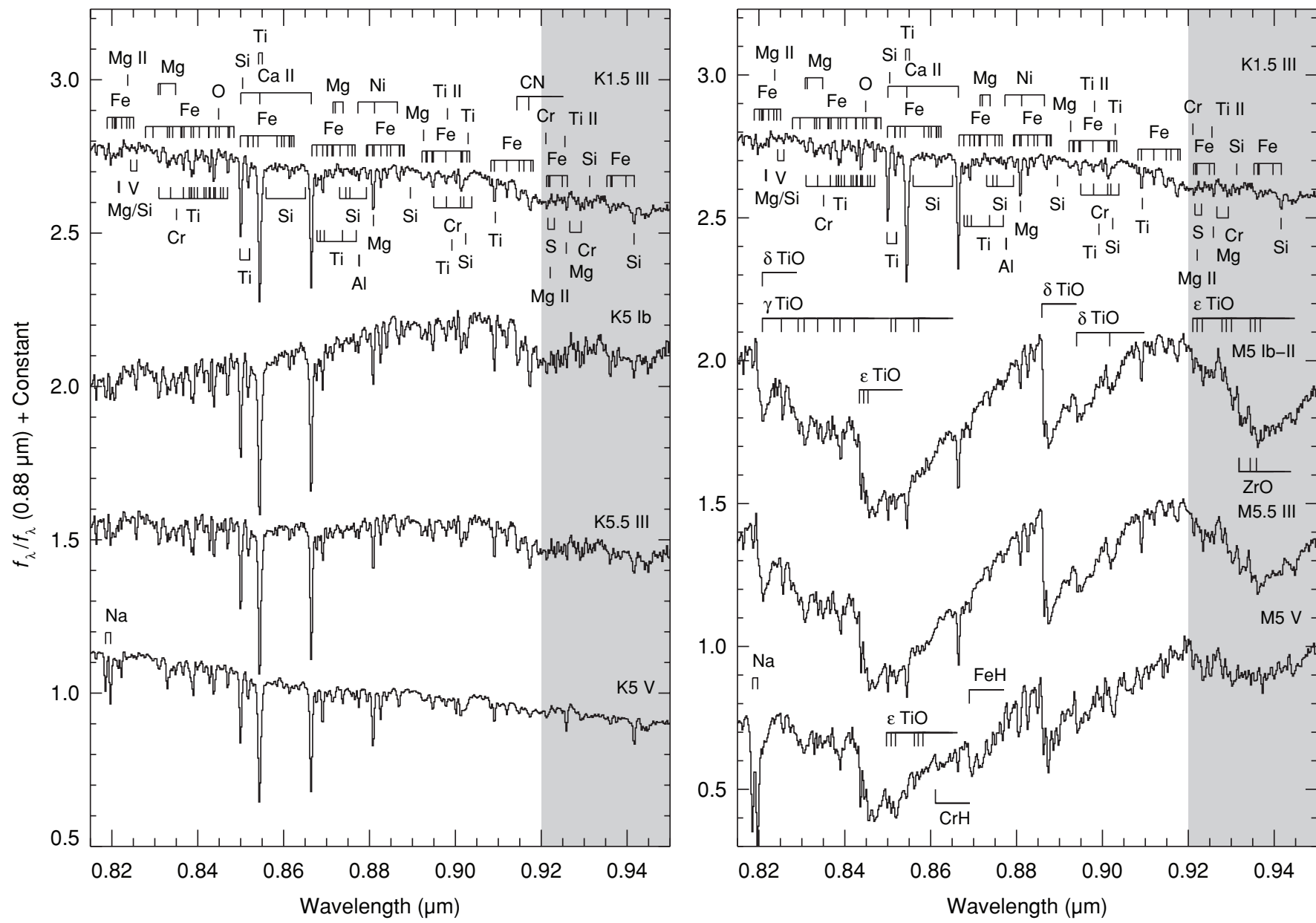


Figure 28. Luminosity effects at spectral types K5 (left) and M5 (right) plotted over the I band (0.82–0.95 μm). The spectra are of HD 216946 (K5 Ib), HD 120477 (K5.5 III), HD 36003 (K5 V), HD 156014 (M5 Ib-II), HD 94705 (M5.5 III), and Gl 866ABC (M5 V). The K1.5 III comparison star is Arcturus (HD 124897). The spectra have been normalized to unity at 0.88 μm and offset by constants.

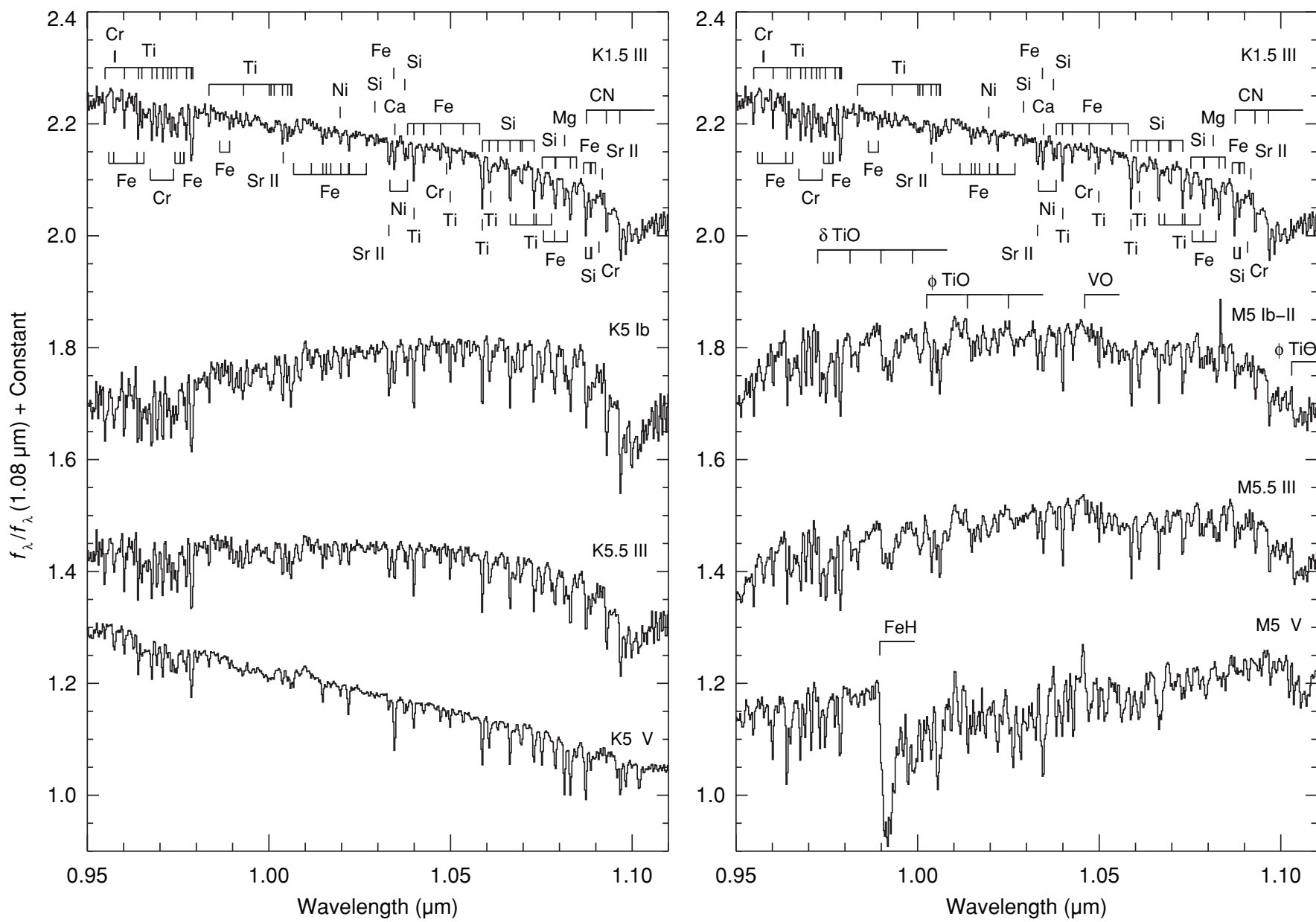


Figure 29. Same as Figure 28 except over the Y band. The spectra have been normalized to unity at $1.08\text{ }\mu\text{m}$ and offset by constants.

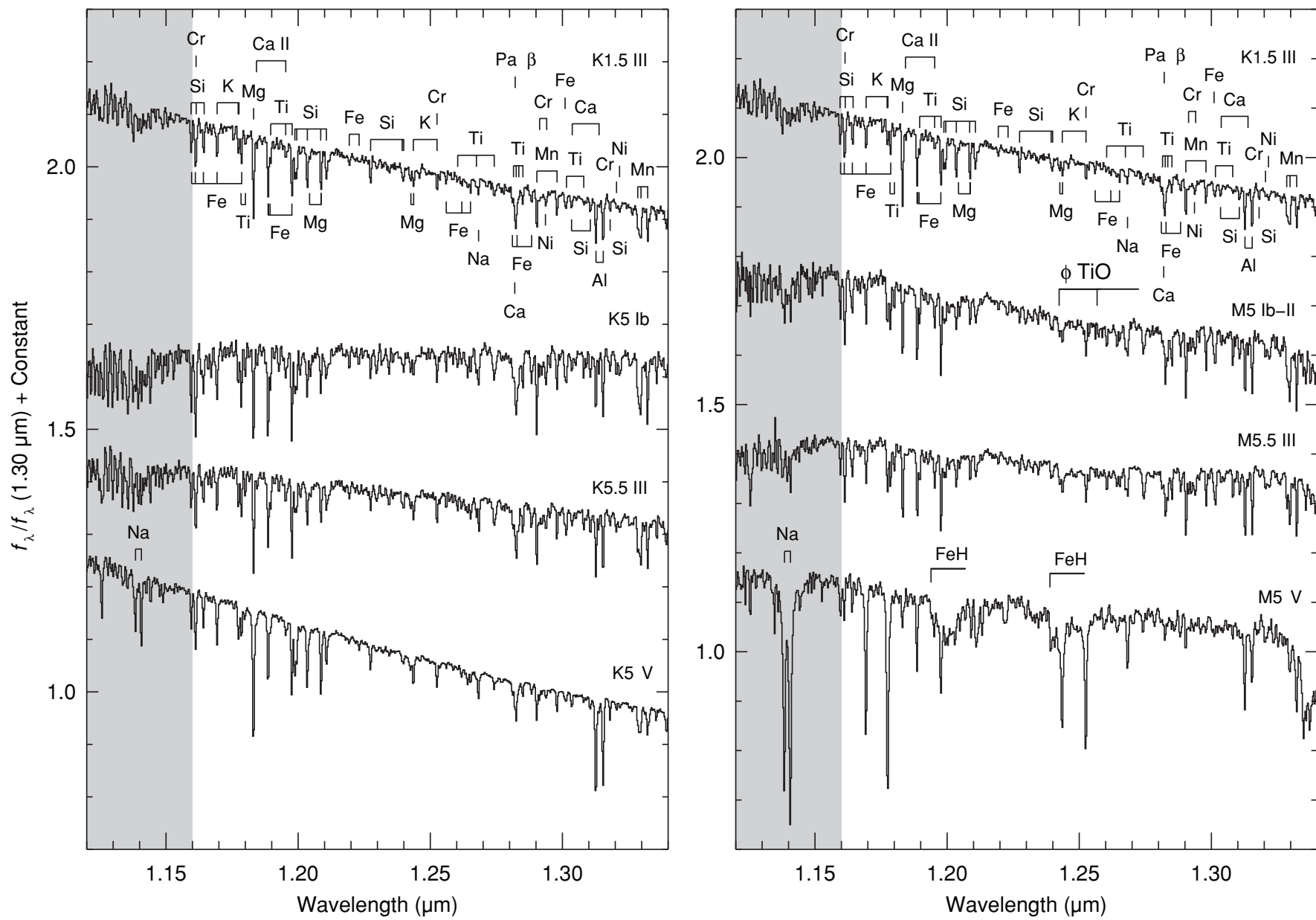


Figure 30. Same as Figure Same as Figure 28 except over the *J* band. The spectra have been normalized to unity at $1.30 \mu\text{m}$ and offset by constants.

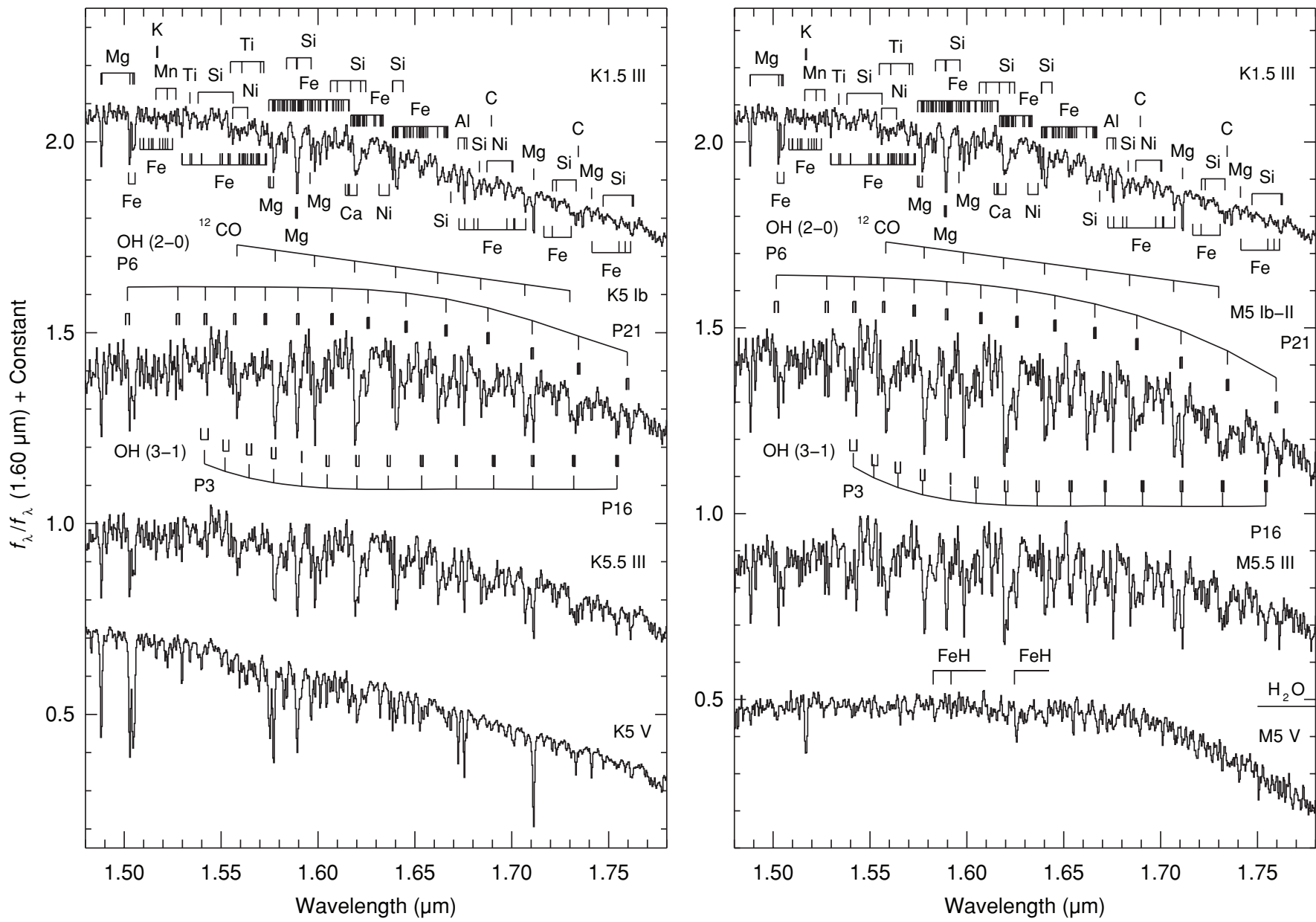


Figure 31. Same as Figure 28 except over the *H* band. The spectra have been normalized to unity at $1.60 \mu\text{m}$ and offset by constants.

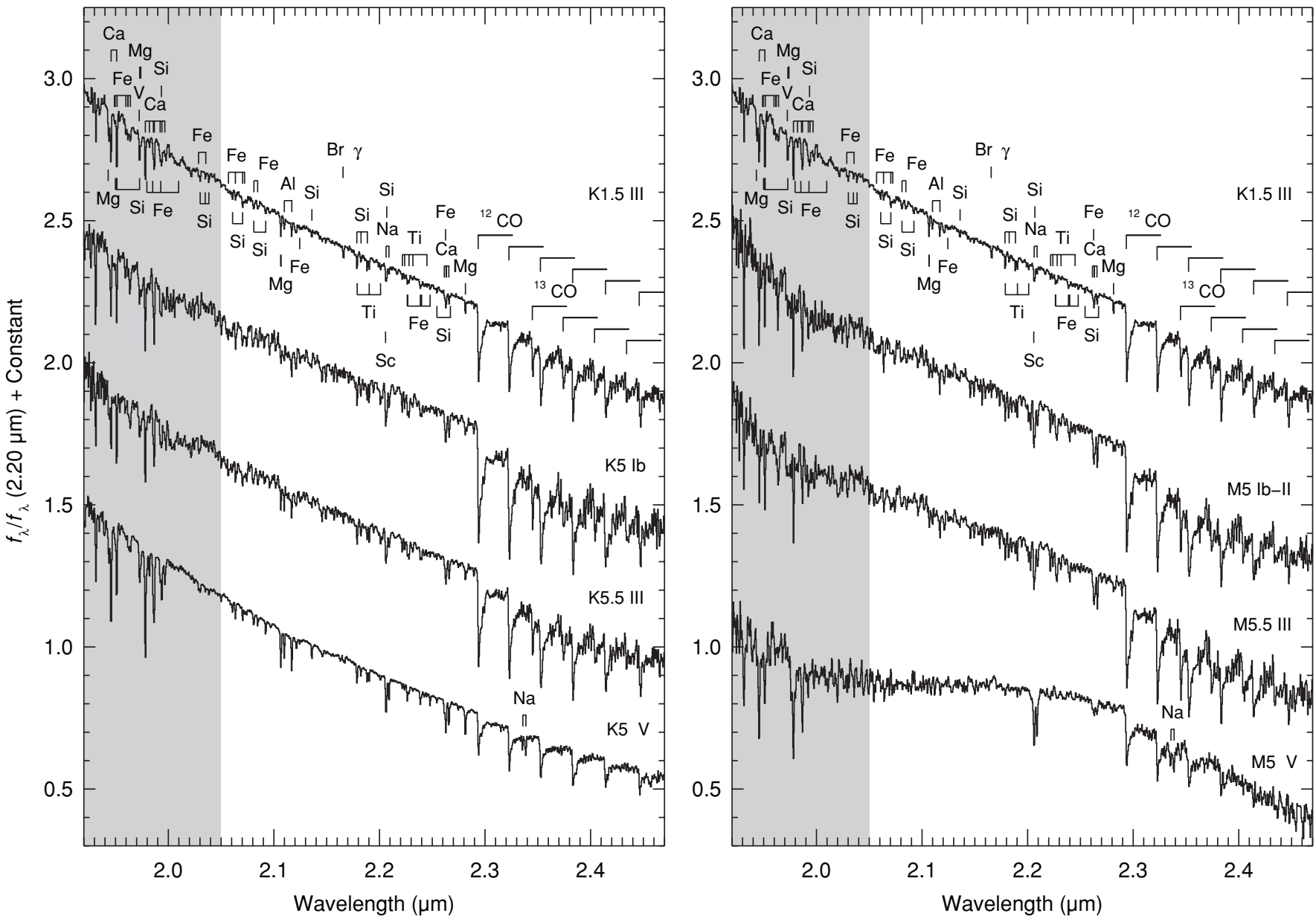


Figure 32. Same as Figure 28 except over the K band. The spectra have been normalized to unity at $2.20 \mu\text{m}$ and offset by constants.

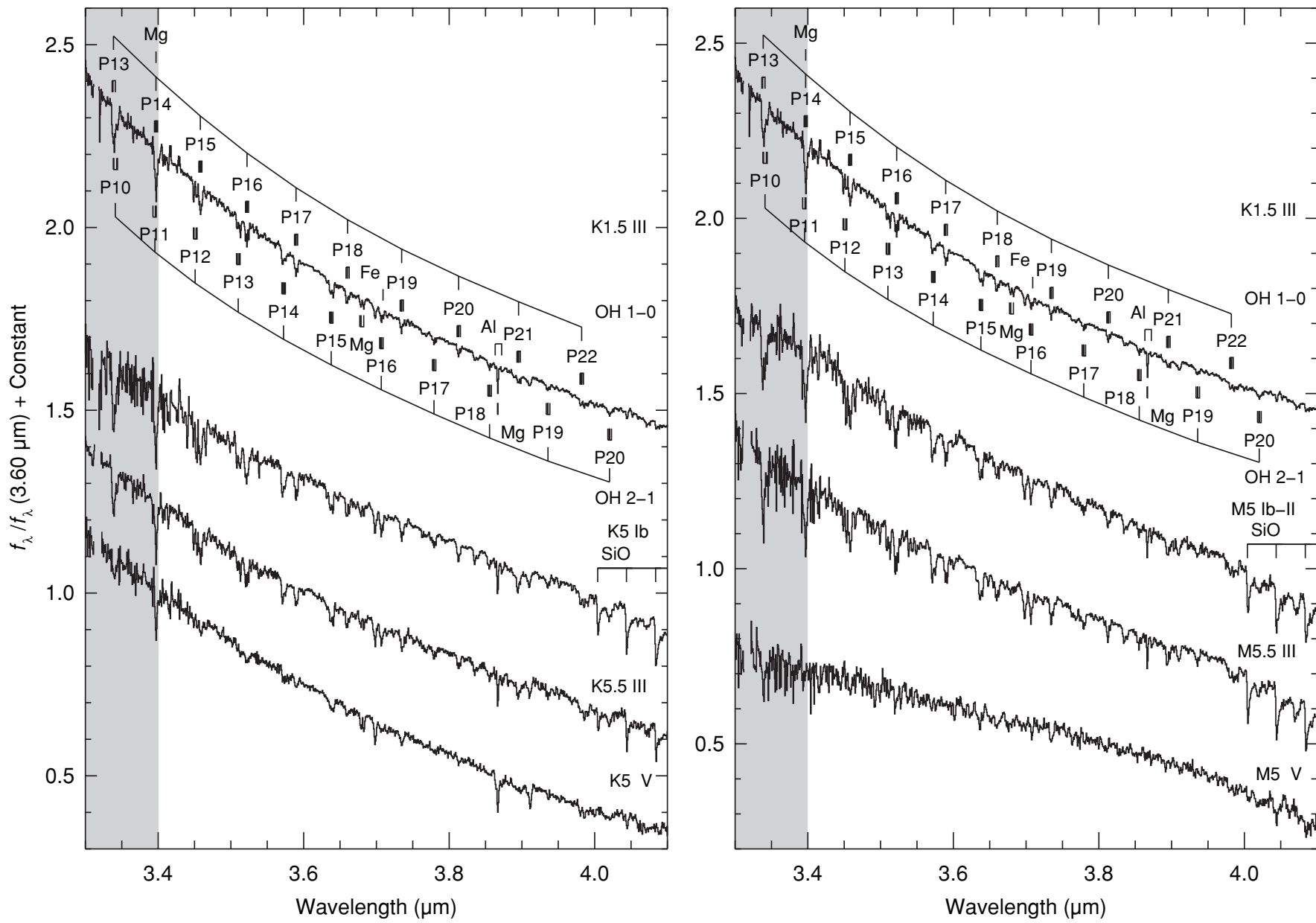


Figure 33. Same as Figure 28 except over the *L* band. The spectra have been normalized to unity at $3.60 \mu\text{m}$ and offset by constants.

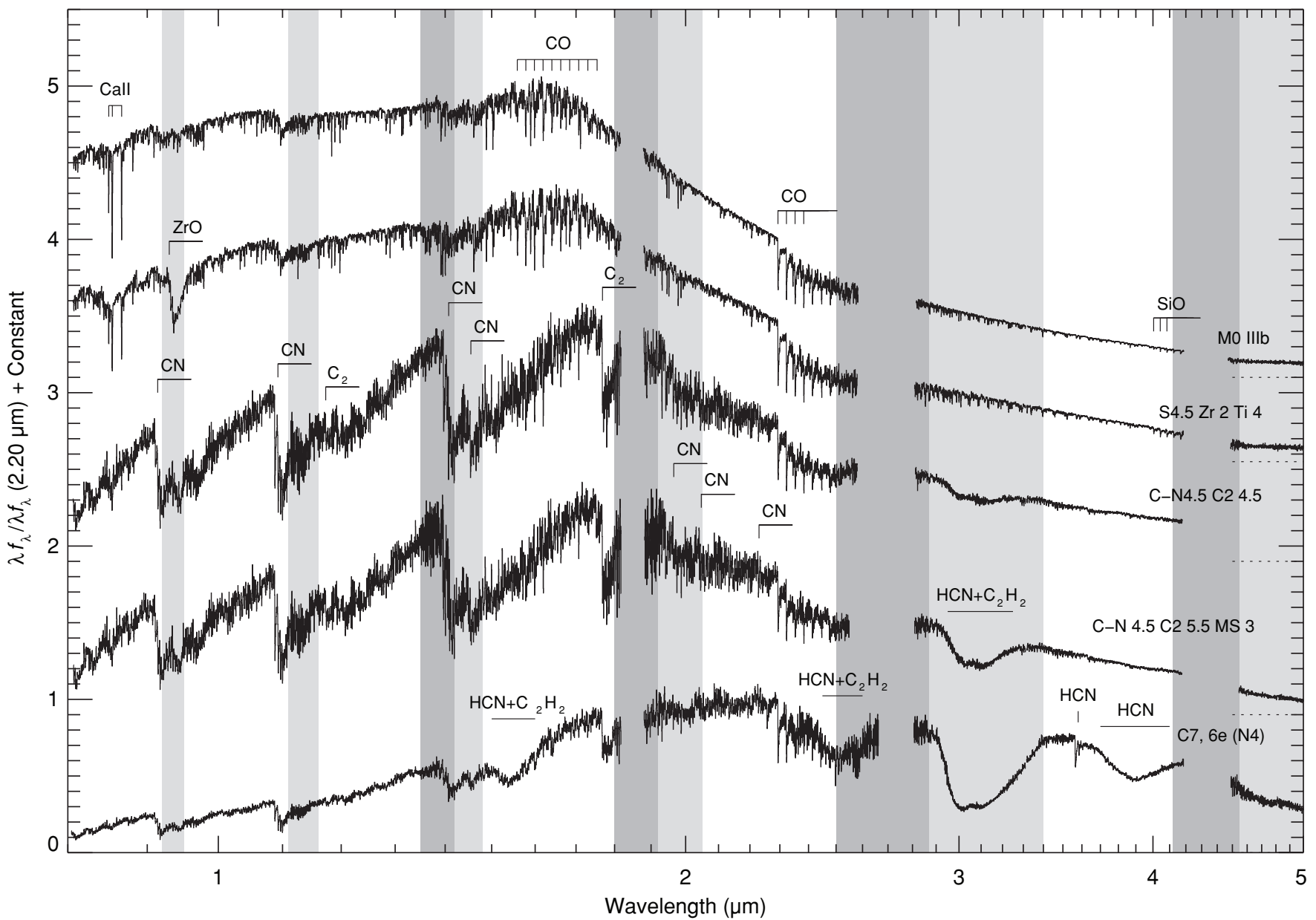


Figure 34. Sequence of M, S, and C giants of approximately the same effective temperature, illustrating the effects of increasing carbon abundance over oxygen during AGB evolution. The spectra are of HD 213893 (M0 IIIb), HD 64332 (S4.5 Zr 2 Ti 4), HD 92055 (C–N 4.5 C2 4.5), and HD 76221 (C–N 4.5 C2 5.5 MS 3) and have been normalized to unity at $1.08 \mu\text{m}$ and offset by constants (dotted lines). Also plotted is the very cool carbon star R Lep (HD 31996, C7,6e (N4)). Regions of strong (transmission $<20\%$) telluric absorption are shown in dark gray, while regions of moderate (transmission $<80\%$) telluric absorption are shown in light gray.

additional band heads of similar depths exist at 0.8508 and 0.8582 μm . Together, the six-band heads appear to form two sets of triplet band heads. The 1–1 and 2–2 bands of the ϵ system exhibit band heads at these wavelengths and therefore it is likely that these features arise from the ϵ system alone or are a combination of the γ and ϵ systems. We also note that three of the $\Delta\nu = -2$ band head classifications listed in Gatterer et al. (1957) were marked as uncertain so we have confirmed these using the theoretical line list of Schwenke (1998).

It has been known for some time that absorption bands of TiO are present in the spectra of M giant stars near 0.93 μm (Spinrad & Newburn 1965). However, to our knowledge, these bands were not detected in the spectra of M dwarfs until the work of Cushing & Vacca (2006). These band heads arise from the $\Delta\nu = -1$ band of the ϵ system. Although telluric and intrinsic H₂O absorptions make identifications in this region difficult, we nevertheless are able to identify the triplet band heads of the 0–1 (0.9211, 0.9221, 0.9233 μm), 1–2 (0.9279, 0.9289, 0.9300 μm), and 2–3 (0.9345, 0.9356, 0.9368 μm) transitions (see Figures 12 and 28). Finally, we note that while the wavelengths of the 2–3 and 3–4 band heads measured by Linton & Broida (1977) agree with our observations, they do not match the positions of the band heads predicted by Schwenke (1998).

3.3.2. VO

Absorption bands that arise from the $B^4\Pi - X^4\Sigma^+$ ⁹ and $A^4\Pi - X^4\Sigma^-$ systems of VO are present in the spectra of M stars over the 0.8–1.3 μm wavelength range. We identify only the 0–0 ($\sim 1.06 \mu\text{m}$) and 0–1 ($\sim 1.18 \mu\text{m}$) bands of the $A^4\Pi - X^4\Sigma^-$ system (see Figures 8, 13, and 29). Although there are certainly absorption features arising from the 0–1 band of $B^4\Pi - X^4\Sigma^+$ system centered near $\sim 0.85 \mu\text{m}$ in the spectra of late-type stars (Keenan & Schroeder 1952; Tinney & Reid 1998), they are simply too weak to be detected in our data.

3.3.3. ZrO

A series of four ZrO band heads arising from the 0–0 band of the system $b^3\Pi - a^3\Delta$ of ZrO (Phillips et al. 1979) are found in the spectra of M giant stars and carbon stars (see Figures 9, 21, 28, 34). Three additional band heads are also present at 0.932060, 0.934417, and 0.935860 μm but their corresponding transitions are unknown. Only three of the band heads ($R_{1(c)}$, $R_{1(d)}$, and 0.932060 μm) can be conclusively identified in the spectra given the complexity of the spectra at these wavelengths, but we include the other band heads for completeness. Additional ZrO band heads (Hammer & Davis 1981; Joyce et al. 1998) in the 1.0–1.2 μm wavelength range are not seen in our spectra.

3.4. Variations of Spectral Features with Spectral Type and Luminosity

In the following sections, we describe the variations of spectral features with spectral type and luminosity of the stars in our sample. These changes are illustrated with the representative spectra given in Figures 7–34, which include feature identifications. Technically, these identifications are only correct for Arcturus and the Sun, so we have identified the features over only Arcturus and a solar analog HD 76151 (G2 V). We caution against assuming that the same lines are

present at much earlier and later spectral types than K1.5 III and G2 V.

Many of the features and variations in their strengths have been previously recognized: Joyce et al. (1998) and Wallace et al. (2000) at J ; Meyer et al. (1998) at H ; Kleinmann & Hall (1986), Wallace & Hinkle (1996, 1997) at K ; Wallace & Hinkle (2002) and Vandebussche et al. (2002) at L ; Lançon & Rocca-Volmerange (1992) at 1.4–2.5 μm for normal stars; Lançon & Wood (2000) at 0.5–2.5 μm for luminous cool stars; and Loidl et al. (2001, 0.5–2.5 μm) and Aoki et al. (1998, 3–8 μm) for carbon stars.

The spectra are also used to compute synthetic photometric colors (see Section 4.2). Synthesized $J - H$ versus $H - K$ color-color diagrams are given in Figures 37 and 38. Figure 39 shows the spectral behavior of several late-type M giant stars plotted in Figures 37 and 38. A synthesized $Y - J$ versus $J - H$ color-color diagram is given in Figure 40. More complete spectral sequences are plotted in the Appendix (Figures 41–112) but without feature identifications.

3.4.1. F Stars

Representative F star spectra are shown in Figures 7–9, 12–18, and 22–27. The NIR spectra of F stars are dominated by the neutral hydrogen (H I) absorption lines of the Paschen ($n = 3$), Brackett ($n = 4$), Pfund ($n = 5$), and Humphreys ($n = 6$) series, in order of increasing wavelength and decreasing strength. The Brackett series (H band) is a good luminosity indicator, smoothly decreasing in strength from supergiants through giants to dwarfs (Figures 15, 18, and 25). The Pfund series (K band, series limit 2.33 μm) can also be strong in early F supergiants (Figure 9). Between the H I lines, spectra are dominated by features due to neutral metal species (e.g., Si I at 1.06–1.09 μm and 1.16–1.21 μm ; Figures 23 and 24). The strongest feature in the spectra is the Ca II triplet at 0.86 μm (Figure 22). The only indication of molecular absorption is the very weak CN feature at 1.09 μm in the latest-type F stars (Figure 9).

3.4.2. G Stars

Representative G star spectra are shown in Figures 7–9, 12–17, 19, and 22–27. H I absorption weakens significantly toward late-type G stars while the neutral metals are stronger than seen in F stars, although the strongest feature is again the Ca II triplet at 0.86 μm (Figures 7–9). The strongest neutral metal lines are those due to Mg (in the H band at about 1.50 μm , 1.58 μm , and 1.71 μm ; Figure 25). Molecular absorption due to CO and CN strengthens with decreasing effective temperature in G stars and these also provide the best luminosity indicators. The first CO overtone bands in the K band (~ 2.29 –2.5 μm) are strongest in supergiants and become progressively weaker with decreasing luminosity (Figure 26). The CN band head at 1.09 μm weakens with decreasing luminosity in mid- to late-type G stars (Figure 23).

3.4.3. K Stars

Representative K star spectra are shown in Figures 7–9, 12–17, 20, and 28–33. H I absorption becomes very weak in K stars and is effectively absent by late K (e.g., Brackett γ in Figure 16, with a slight dependence on luminosity). Neutral metal absorption features reach a maximum depth in the spectra of K and M stars and lines due to Al I at 1.31 μm , Mg I at about 1.50 μm and 1.53 μm , Al I at 1.67 μm , and Mg I at 1.71 μm are particularly strong in the spectra of K dwarfs and

⁹ This system is identified as the “C” system by Gatterer et al. (1957), Solf (1978), and Tinney & Reid (1998).

Table 6
Strong Metal Lines in the Solar Spectrum

Vacuum Wavelength (μm)	Element						
0.8185503	Na I	0.8189049	Fe I	0.8197077	Na I	0.8201178	Fe I
0.8203977	Ca II	0.8209999	Fe I	0.8215293	Mg I	0.8222636	Fe I
0.8234587	Fe I	0.8241394	Fe I	0.8250417	Fe I	0.8251063	Ca II
0.8278187	Fe I	0.8295802	Fe I	0.8312545	Mg I	0.8329342	Fe I
0.8334208	Fe I	0.8337440	C I	0.8341703	Fe I	0.8348416	Mg I
0.8363099	Fe I	0.8367942	Fe I	0.8380165	Ti I	0.8384830	Ti I
0.8390078	Fe I	0.8403729	Fe I	0.8414668	Ti I	0.8426453	Fe I
0.8428818	Ti I	0.8437274	Ti I	0.8437971	Ti I	0.8441896	Fe I
0.8446303	Si I	0.8448679	O I	0.8470736	Fe I	0.8474081	Fe I
0.8499332	Fe I	0.8500351	Ca II	0.8503886	Si I	0.8504558	Si I
0.8516415	Fe I	0.8517452	Fe I	0.8529025	Fe I	0.8538507	Si I
0.8540359	Fe I	0.8544438	Ca II	0.8559130	Si I	0.8574182	Fe I
0.8584627	Fe I	0.8595333	Fe I	0.8598319	Si I	0.8601196	Fe I
0.8614170	Fe I	0.8616300	Fe I	0.8618639	Fe I	0.8623976	Fe I
0.8650841	Si I	0.8664288	Fe I	0.8664520	Ca II	0.8677128	Fe I
0.8691012	Fe I	0.8701834	Fe I	0.8712790	Fe I	0.8715083	Mg I
0.8715584	Fe I	0.8720220	Mg I	0.8730407	Si I	0.8738417	Mg I
0.8744852	Si I	0.8754413	Si I	0.8759590	Fe I	0.8766370	Fe I
0.8775278	Al II	0.8776303	Al II	0.8786852	Fe I	0.8792801	Si I
0.8792925	Fe I	0.8795756	Fe I	0.8807058	Fe I	0.8809176	Mg I
0.8810580	Fe I	0.8826647	Fe I	0.8840858	Fe I	0.8849166	Fe I
0.8864981	Ni I	0.8869392	Fe I	0.8870855	Fe I	0.8878464	Fe I
0.8895167	Si I	0.8901676	Si I	0.8914515	Ca II	0.8922469	Fe I
0.8926021	Mg I	0.8929807	Ca II	0.8931506	Fe I	0.8945528	Fe I
0.8947657	Fe I	0.8948706	Fe I	0.8949643	Cr I	0.8951550	Si I
0.8968393	Ni I	0.8977870	Fe I	0.9002026	Fe I	0.9009236	Fe I
0.9010844	Fe I	0.9010982	Si I	0.9012314	Cr I	0.9013069	Fe I
0.9019524	Cr I	0.9024057	Si I	0.9026843	Fe I	0.9033187	Fe I
0.9063915	C I	0.9064729	Fe I	0.9064950	C I	0.9072912	Fe I
0.9080772	C I	0.9082075	Fe I	0.9082858	Fe I	0.9090810	Fe I
0.9091000	C I	0.9091901	Fe I	0.9097327	C I	0.9102910	Fe I
0.9103157	Fe I	0.9114210	C I	0.9119636	Fe I	0.9148637	Fe I
0.9159606	Fe I	0.9167071	Fe I	0.9175726	Fe I	0.9181093	Fe I
0.9212557	Fe I	0.9215392	S I	0.9217023	Fe I	0.9220099	Fe I
0.9220780	Mg II	0.9230627	S I	0.9240078	S I	0.9246802	Mg II
0.9249094	Fe I	0.9171317	Si I	0.9258316	Mg I	0.9260811	Fe I
0.9261549	Fe I	0.9293024	Cr I	0.9320690	Fe I	0.9320776	Si I
0.9352980	Fe I	0.9361990	Fe I	0.9364927	Fe I	0.9375472	Fe I
0.9390756	Fe I	0.9397251	Fe I	0.9403693	Fe I	0.9408311	C I
0.9416090	Si I	0.9416630	Fe I	0.9417544	Mg I	0.9432405	Mg I
0.9432690	Fe I	0.9435351	Mg I	0.9441373	Mg I	0.9446394	Fe I
0.9449643	Cr I	0.9465610	Fe I	0.9515871	Fe I	0.9522640	Ni I
0.9548691	Ti I	0.9572529	Fe I	0.9576939	Cr I	0.9602228	Ti I
0.9605668	C I	0.9623435	C I	0.9636864	Fe I	0.9640942	Ti I
0.9650013	Ti I	0.9655762	Fe I	0.9661080	C I	0.9678200	Ti I
0.9692054	Si I	0.9708333	Ti I	0.9731082	Ti I	0.9741243	Fe I
0.9766045	Fe I	0.9766579	Fe I	0.9786000	Ti I	0.9790378	Ti I
0.9802999	Fe I	0.9836885	Fe I	0.9864443	Fe I	0.9870889	Fe I
0.9891745	Fe I	0.9893340	Ca II	1.00394	Sr II	1.00678	Fe I
1.01266	C I	1.01484	Fe I	1.01960	Ni I	1.02191	Fe I
1.02212	Fe I	1.02918	Si I	1.03301	Sr II	1.03437	Fe I
1.03466	Ca I	1.03741	Si I	1.03814	Ni I	1.03986	Fe I
1.04266	Fe I	1.04556	Fe I	1.04583	S I	1.04596	Si I
1.04623	S I	1.04725	Fe I	1.05351	Fe I	1.05880	Si I
1.06063	Si I	1.06306	Si I	1.06639	Si I	1.06860	C I
1.06883	C I	1.06926	Si I	1.06942	C I	1.06972	Si I
1.07103	C I	1.07304	Si I	1.07325	C I	1.07523	Si I
1.07560	Fe I	1.07860	Fe I	1.07875	Si I	1.07898	Si I
1.08140	Mg I	1.08213	Fe I	1.08301	Si I	1.08468	Si I
1.08524	Fe I	1.08665	Fe I	1.08718	Si I	1.07556	Si I
1.08858	Si I	1.08872	Fe I	1.08883	Si I	1.08993	Fe I
1.09172	Mg II	1.09179	Sr II	1.09563	Mg I	1.09603	Mg I
1.09684	Mg I	1.09823	Si I	1.09828	Ni I	1.09851	Si I
1.09875	Si I	1.10163	Fe I	1.10186	Cr I	1.10210	Si I
1.11228	Fe I	1.11600	Cr I	1.11906638	Si I	1.13115	Si I

Table 6
(Continued)

Vacuum Wavelength (μm)	Element						
1.133822	C I	1.13939	Cr I	1.14069	Na I	1.14255	Fe I
1.14423	Fe I	1.14878	Cr I	1.15059	Si I	1.15757	Fe I
1.15947	Si I	1.15955	Si I	1.15963	Fe I	1.16107	Fe I
1.16137	Cr I	1.16143	Si I	1.16320	C I	1.16414	Fe I
1.16442	Si I	1.16629	C I	1.16728	C I	1.16932	Fe I
1.16934	K I	1.17035	Si I	1.17514	C I	1.17565	C I
1.17580	C I	1.17761	K I	1.17865	Fe I	1.18314	Mg I
1.18422	Ca II	1.18861	Fe I	1.18873	Fe I	1.18937	Fe I
1.1896124	Ti I	1.189617	C I	1.18990	C I	1.19530	Ca II
1.19763	Fe I	1.19875	Si I	1.19949	Si I	1.2008834	Fe I
1.2008685	Fe I	1.20348	Si I	1.20431	Mg I	1.20564	Fe I
1.20853	Si I	1.20866	Mg I	1.20870	Mg I	1.21068	Si I
1.21140	Si I	1.22305	Fe I	1.22740	Si I	1.23463	Fe I
1.23936	Si I	1.23992	Si I	1.24264	Mg I	1.24356	K I
1.24369	Mg I	1.25255	K I	1.25874	Si I	1.26175	C I
1.26422	Fe I	1.26522	Fe I	1.26826	Na I	1.28106	Fe I
1.28833	Fe I	1.29034	Mn I	1.29795	Mn I	1.30331	Si I
1.30345	Si I	1.30371	Ca I	1.31056	Si I	1.31270	Al I
1.31386	Ca I	1.31515	Fe I	1.31544	Al I	1.31805	Si I
1.32912	Si I	1.32915	Fe I	1.32975	Mn I	1.33127	Si I
1.33227	Mn I	1.33297	Si I	1.33558	Fe I	1.33958	Fe I
1.34359	Ni I	1.48761	Ni I	1.4881595	Mg I	1.4881674	Mg I
1.4881847	Mg I	1.4882243	Mg I	1.49015	Fe I	1.49422	Fe I
1.49602	Fe I	1.49633	Fe I	1.49929	Fe I	1.50218	Fe I
1.50291	Mg I	1.50218	Mg I	1.50518	Mg I	1.50559	Fe I
1.50814	Fe I	1.50988	Fe I	1.51000	Fe I	1.51265	Fe I
1.51403	Fe I	1.51482	Fe I	1.51633	Mn I	1.51672	K I
1.51725	K I	1.51824	Fe I	1.52117	Fe I	1.52219	Mn I
1.52238	Fe I	1.52491	Fe I	1.52973	Fe I	1.52987	Fe I
1.52991	Fe I	1.53396	Fe I	1.53480	Fe I	1.53811	Si I
1.53989	Fe I	1.53999	Fe I	1.54265	Si I	1.55050	Fe I
1.55056	Fe I	1.55360	Fe I	1.55385	Fe I	1.55463	Fe I
1.55594	Ni I	1.55596	Ni I	1.55620	Si I	1.55925	Fe I
1.56085	Fe I	1.56259	Fe I	1.56362	Fe I	1.56369	Ni I
1.56571	Fe I	1.56663	Fe I	1.56818	Fe I	1.56907	Fe I
1.56961	Fe I	1.56970	Fe I	1.57279	Fe I	1.57450	Mg I
1.57462	Fe I	1.57533	Mg I	1.57656	Fe I	1.57701	Mg I
1.57737	Fe I	1.57759	Fe I	1.57784	Fe I	1.57933	Fe I
1.58029	Fe I	1.58145	Fe I	1.58225	Fe I	1.58235	Fe I
1.58379	Si I	1.58395	Fe I	1.58420	Fe I	1.48681	Fe I
1.58729	Fe I	1.58828	Fe I	1.58839	Mg I	1.58888	Si I
1.58905	Mg I	1.58921	Fe I	1.58928	Si I	1.58939	Mg I
1.58968	Fe I	1.58973	Fe I	1.58996	Fe I	1.59059	Fe I
1.59087	Fe I	1.59104	Fe I	1.59157	Fe I	1.59250	Fe I
1.59462	Fe I	1.59644	Si I	1.59692	Fe I	1.59720	Fe I
1.59851	Fe I	1.60021	Fe I	1.60092	C I	1.60111	Fe I
1.60115	Fe I	1.6012453	Fe I	1.60140	Fe I	1.60422	Fe I
1.60450	Fe I	1.60471	Fe I	1.60644	Si I	1.60758	Fe I
1.60803	Fe I	1.60992	Si I	1.61047	Fe I	1.61068	Fe I
1.61204	Fe I	1.61303	Fe I	1.61552	Ca I	1.61576	Fe I
1.61610	Fe I	1.61618	Ca I	1.61681	Si I	1.61695	Fe I
1.61794	Fe I	1.61840	Fe I	1.61853	Fe I	1.61902	Fe I
1.61995	Fe I	1.62015	Ca I	1.62029	Fe I	1.62087	Fe I
1.62122	Fe I	1.62180	Fe I	1.62201	Si I	1.62301	Fe I
1.62361	Fe I	1.62404	Fe I	1.62463	Si I	1.62892	Fe I
1.62973	Fe I	1.63149	Ni I	1.63208	Fe I	1.63231	Fe I
1.63289	Fe I	1.63675	Ni I	1.63846	Si I	1.63860	Si I
1.63867	Fe I	1.63989	Fe I	1.64026	Fe I	1.64091	Fe I
1.64123	Fe I	1.64394	Si I	1.64411	Fe I	1.64493	Fe I
1.64714	Fe I	1.64912	Fe I	1.65108	Fe I	1.65217	Fe I
1.65266	Fe I	1.65290	Fe I	1.65365	Fe I	1.65565	Fe I
1.65663	Fe I	1.66173	Fe I	1.66504	Fe I	1.66581	Fe I
1.66659	Fe I	1.66700	Fe I	1.66853	Si I	1.67235	Al I
1.67278	Fe I	1.67552	Al I	1.67576	Fe I	1.67679	Al I
1.68042	Fe I	1.68251	Fe I	1.68328	Si I	1.68719	Ni I

Table 6
(Continued)

Vacuum Wavelength (μm)	Element						
1.68950	C I	1.69746	Fe I	1.70009	Ni I	1.70057	Ni I
1.70101	Fe I	1.70157	Fe I	1.71133	Mg I	1.71658	Fe I
1.72090	Fe I	1.72105	Si I	1.72303	Si I	1.69862	C I
1.73010	Fe I	1.73321	Si I	1.73433	C I	1.74123	Mg I
1.74533	C I	1.74717	Si I	1.75104	C I	1.75853	Fe I
1.76135	Fe I	1.76219	Si I	1.76282	Si I	1.94583	Ca I
1.94897	Fe I	1.94987	Si I	1.95111	Ca I	1.95114	Si I
1.95135	Si I	1.97280	Si I	1.97822	Ca I	1.98204	Ca I
1.98585	Ca I	1.98676	Ca I	1.99226	Ca I	1.99344	Si I
1.99392	Ca I	1.99673	Ca I	2.03019	Si I	2.03075	Si I
2.03494	Si I	2.03840	Si I	2.06085	Si I	2.0635328	Fe I
2.0634902	Fe I	2.07040	Fe I	2.07043	Si I	2.07226	Fe I
2.08099	Si I	2.08107	Fe I	2.08465	Fe I	2.09224	Si I
2.10655	Mg I	2.10666	Mg I	2.10988	Al I	2.11696	Al I
2.13601	Si I	2.17857	Si I	2.18257	Si I	2.18853	Si I
2.20624	Na I	2.20688	Si I	2.20897	Na I	2.22632	Fe I
2.23869	Fe I	2.24794	Fe I	2.25438	Si I	2.26141	Ca I
2.26260	Fe I	2.26311	Ca I	2.26573	Ca I	2.26720	Si I
2.28142	Mg I	2.31509	Fe I	2.33548	Na I	2.33855	Na I
2.92882	Ca I	3.15174	Si I	3.39709	Mg I	3.40135	Si I
3.67901	Mg I	3.68263	Mg I	3.69866	Si I	3.74558	Si I
3.866486	Mg I	3.86681	Mg I	3.866874	Mg I	3.866945	Mg I

early-M dwarfs (Figures 14 and 15). Lines from ionized metals weaken with progressively later spectral types (e.g., Ca II triplet at 0.86 μm ; Figures 7–9). Molecular absorption continues to strengthen in K stars as effective temperature falls. The broad *H*-band bump due to the H[−] opacity minimum at 1.6 μm first becomes evident in early-type K stars and strengthens with decreasing effective temperature (Figure 8). This feature was first observed in the pioneering balloon observations of Woolf et al. (1964). Molecular features present in the spectra of *K* stars are the second CO overtone vibration–rotation bands in the *H* band (Figure 31), the CN band head at 1.40 μm (Figures 8 and 9), OH (1–0 and 2–1) in the *L* band (Figure 33), the SiO first overtone vibration–rotation band at 4.00–4.18 μm (Figure 33), as well as the first overtone CO (*K* band; Figure 32) and CN bands (band heads at 0.91 μm and 0.94 μm ; Figure 9) that are also visible in the spectra of G stars. Molecular features weaken with decreasing luminosity class and provide some of the best surface gravity indicators in K stars; the CO, CN, and SiO features are particularly sensitive to surface gravity. Other luminosity class indicators include Mg I at 1.49 μm and 1.71 μm ; Figure 31). These lines are significantly stronger in dwarfs than in giants and supergiants of the same spectral type (see Figure 35).

3.4.4. M Stars

Representative M star spectra are shown in Figures 7–9, 12–17, 21, and 28–33. Molecular absorption features dominate the spectra of M stars. The CO (*H* band and band heads in the *K* band starting at 2.3 μm ; Figure 9), OH (band heads starting at 3.4 μm , Figures 33 and 112), and SiO absorption bands (band heads starting at 4.0 μm ; Figures 33 and 112) are strongest in early-type M supergiant stars (see Table 10). TiO (several band heads starting at 0.82 μm) and ZrO (band head at 0.93 μm) absorption also increases from mid-M to later spectral types in supergiants (Figures 21 and 97). Similar trends are seen in M giants with the addition of significant broad H₂O absorption at about 1.4 μm , 1.9 μm , and 2.7 μm , starting at about M6 III (Figures 8 and

39), and with ZrO replaced by VO (band heads at 1.03 μm and 1.17 μm ; Figure 8) in late-type M giants (TPAGB stars). The *H*-band bump first seen in the spectra of early-type K stars is strongest in mid-type M giants and supergiants (Figures 8 and 9). The *H*-band spectra of M dwarfs are dominated by numerous FeH absorption features (Figure 15, and Figure 7 of Cushing et al. 2003). In M stars the best luminosity class indicators are the FeH band head at 0.99 μm (Figure 29; Wing & Ford 1969), the second CO overtone bands in the *H* band (strong in M supergiants and giants; Figure 31), the first CO overtone bands in the *K* band (strong in M supergiants and giants; Figure 32), and the first SiO overtone bands at about 4.0 μm (strong in M supergiants and giants; Figure 33). Most neutral metal features weaken in the late-M spectral types (e.g., Ca I triplet at 2.26 μm ; Figures 16 and 108). The exceptions are the alkali lines, namely the Na I doublets at 0.82 μm , 1.14 μm , and 2.20 μm , and the K I doublets at 1.17 μm and 1.25 μm (Figures 28, 30, and 32). These lines are strong in mid- to late-type M dwarfs and weak in corresponding supergiants and giants, and are consequently excellent luminosity class or surface gravity indicators. The Ca II triplet at 0.86 μm is significantly weaker in M stars relative to earlier spectral types where it blends with TiO absorption (Figure 12) and is absent by mid- to late-type M stars (slightly dependent upon luminosity; Figures 95–97).

3.4.5. Carbon and S Stars

The sequence M–MS–S–SC–C is thought to be one of increasing carbon-to-oxygen ratio as well as increasing *s*-process element abundance during AGB evolution (Ake 1979). Our sample contains one MS, four S, five C–N, one C–R, and two C–J stars (see Table 2). In normal (oxygen-rich, C < O) M giants, some of the oxygen is used up to make CO but most of it goes into making metal oxides such as TiO. In typical carbon stars (C > O) all the oxygen is used up in the production of CO and the remaining carbon goes into carbon compounds such as C₂, CH, CN, and C₃. The TiO so characteristic of M stars is replaced by these carbon compounds. The so-called S stars

Table 7
Strong Metal Lines in the Arcturus Spectrum

Vacuum Wavelength (μm)	Element						
0.8027028	Ti I	0.8030128	Fe I	0.8030499	Fe I	0.8048243	Fe I
0.8049814	Fe I	0.8056425	Mg I	0.8070439	Ti I	0.8072310	Zr I
0.8074360	Fe I	0.8077351	Fe I	0.8082752	Fe I	0.8087374	Fe I
0.8094836	Cu I	0.8095446	Si I	0.8095706	V I	0.8096137	Co I
0.8090987	Fe I	0.8100928	Mg I	0.8110530	Fe I	0.8114371	Fe I
0.8118973	V I	0.8135217	Zr I	0.8146790	V I	0.8163294	V I
0.8185480	Na I	0.8189032	Fe I	0.8197064	Na I	0.8201155	Fe I
0.8206336	Fe I	0.8207177	Fe I	0.8209977	Fe I	0.8215279	Mg I
0.8217390	Si I	0.8222621	Fe I	0.8234564	Fe I	0.8236885	Mg II
0.8241376	Fe I	0.8243787	V I	0.8250378	Fe I	0.8258151	V I
0.8278146	Fe I	0.8295770	Fe I	0.8307854	Mg I	0.8309685	Ti I
0.8312525	Mg I	0.8329329	Fe I	0.8334191	Fe I	0.8336662	Ti I
0.8341673	Fe I	0.8348395	Mg I	0.8350545	Cr I	0.8360798	Fe I
0.8363079	Fe I	0.8366520	Ti I	0.8367910	Fe I	0.8380144	Ti I
0.8384535	Fe I	0.8384815	Ti I	0.8385065	Ti I	0.8390056	Fe I
0.8391777	Ti I	0.8399179	Ti I	0.8403690	Fe I	0.8414653	Ti I
0.8419245	Ti I	0.8425206	Fe I	0.8426436	Fe I	0.8426707	Ti I
0.8428797	Ti I	0.8437259	Ti I	0.8437950	Ti I	0.8441220	Ti I
0.8441871	Fe I	0.8448662	O I	0.8449943	Fe I	0.8453193	Ti I
0.8459405	Ti I	0.8469459	Ti I	0.8470719	Fe I	0.8474049	Fe I
0.8484293	Fe I	0.8498326	Ti I	0.8499307	Fe I	0.8500336	Ca II
0.8504538	Si I	0.8516391	Fe I	0.8517432	Fe I	0.8520352	Ti I
0.8520672	Ti I	0.8528994	Fe I	0.8540337	Fe I	0.8541677	Ti I
0.8544418	Ca II	0.8550420	Ti I	0.8559113	Si I	0.8584600	Fe I
0.8595293	Fe I	0.8601174	Fe I	0.8612958	Fe I	0.8614148	Fe I
0.8618629	Fe I	0.8623950	Fe I	0.8650827	Si I	0.8664501	Ca II
0.8666082	Fe I	0.8677115	Fe I	0.8677735	Ti I	0.8685348	Ti I
0.8690998	Fe I	0.8694700	Ti I	0.8701081	Fe I	0.8701822	Fe I
0.8712764	Fe I	0.8715065	Mg I	0.8715575	Fe I	0.8720207	Mg I
0.8730389	Si I	0.8731530	Fe I	0.8737091	Ti I	0.8738401	Mg I
0.8744834	Si I	0.8749805	Fe I	0.8754395	Si I	0.8759578	Fe I
0.8766359	Fe I	0.8769070	Ti I	0.8773071	Ni I	0.8775262	Al I
0.8776281	Al I	0.8792786	Si I	0.8792915	Fe I	0.8795737	Fe I
0.8807030	Fe I	0.8809161	Mg I	0.8810571	Fe I	0.8811812	Ni I
0.8826625	Fe I	0.8840839	Fe I	0.8849152	Fe I	0.8864966	Ni I
0.8869347	Fe I	0.8870847	Fe I	0.8878439	Fe I	0.8880660	Fe I
0.8895155	Si I	0.8922441	Fe I	0.8926003	Mg I	0.8931514	Fe I
0.8934225	Fe I	0.8945497	Fe I	0.8947629	Fe I	0.8948699	Fe I
0.8949629	Cr I	0.8977847	Fe I	0.8979327	Cr I	0.8981617	Ti II
0.8991901	Ti I	0.9012296	Cr I	0.9013046	Fe I	0.9014527	Fe I
0.9016438	Fe I	0.9019508	Cr I	0.9024039	Si I	0.9026830	Fe I
0.9029781	Ti I	0.9033171	Fe I	0.9038323	Cr I	0.9082865	Fe I
0.9090797	Fe I	0.9093169	Ti I	0.9119615	Fe I	0.9148623	Fe I
0.9159576	Fe I	0.9175701	Fe I	0.9181061	Fe I	0.9210801	Cr I
0.9212541	Fe I	0.9215371	S I	0.9217012	Fe I	0.9220072	Fe I
0.9220762	Mg II	0.9230605	S I	0.9249080	Fe I	0.9255053	Ti II
0.9258303	Mg I	0.9260793	Fe I	0.9266506	Cr I	0.9293002	Cr I
0.9148637	Fe I	0.9159606	Fe I	0.9167070	Fe I	0.9175726	Fe I
0.9181134	Fe I	0.9210817	Cr I	0.9212556	Fe I	0.9215392	S I
0.9217023	Fe I	0.9220099	Fe I	0.9230627	S I	0.9249094	Fe I
0.9258317	Mg I	0.9260811	Fe I	0.9261549	Fe I	0.9266518	Cr I
0.9293024	Cr I	0.9312817	Si I	0.9352979	Fe I	0.9361989	Fe I
0.9364927	Fe I	0.9397251	Fe I	0.9416090	Si I	0.9416630	Fe I
0.9417543	Mg I	0.9432690	Fe I	0.9435350	Mg I	0.9441373	Mg I
0.9449393	Cr I	0.9449643	Cr I	0.9456792	Fe I	0.9515871	Fe I
0.9522640	Ni I	0.9548691	Ti I	0.9559132	Fe I	0.9572530	Fe I
0.9574435	Cr I	0.9576939	Cr I	0.9602228	Ti I	0.9636863	Fe I
0.9640943	Ti I	0.9650013	Ti I	0.9655763	Fe I	0.9673135	Cr I
0.9678200	Ti I	0.9691528	Ti I	0.9708333	Ti I	0.9721622	Ti I
0.9731082	Ti I	0.9737231	Cr I	0.9741244	Fe I	0.9746277	Ti I
0.9749596	Ti I	0.9755765	Fe I	0.9766045	Fe I	0.9766579	Fe I
0.9772983	Ti I	0.9786000	Ti I	0.9786267	Ti I	0.9790378	Ti I
0.9802999	Fe I	0.9834844	Ti I	0.9864443	Fe I	0.9891744	Fe I
0.9930072	Ti I	1.0000700	Ti I	1.0005833	Ti I	1.0014491	Ti I
1.0037248	Ti I	1.0039405	Sr II	1.0051583	Ti I	1.0060489	Ti I

Table 7
(Continued)

Vacuum Wavelength (μm)	Element						
1.0062660	Ti I	1.0067806	Fe I	1.0116788	Fe I	1.0148349	Fe I
1.0157956	Fe I	1.0170261	Fe I	1.0196018	Ni I	1.0197901	Fe I
1.0219150	Fe I	1.0221207	Fe I	1.0268037	Fe I	1.0291761	Si I
1.0330141	Sr II	1.0333055	Ni I	1.0343722	Fe I	1.0346644	Ca I
1.0374111	Si I	1.0381445	Ni I	1.0381855	Fe I	1.0398643	Fe I
1.0399659	Ti I	1.0425887	Fe I	1.0426605	Fe I	1.0472531	Fe I
1.0489107	Cr I	1.0498997	Ti I	1.0535121	Fe I	1.0580062	Fe I
1.0587546	Ti I	1.0588038	Si I	1.0606332	Si I	1.0610631	Ti I
1.0630562	Si I	1.0663891	Si I	1.0664550	Ti I	1.0679972	Ti I
1.0692649	Si I	1.0697178	Si I	1.0729326	Ti I	1.0730350	Si I
1.0735811	Ti I	1.0752330	Si I	1.0755950	Fe I	1.0777825	Ti I
1.0786009	Fe I	1.0787510	Si I	1.0789814	Si I	1.0814048	Mg I
1.0821258	Fe I	1.0830059	Si I	1.0846822	Si I	1.0866494	Fe I
1.0871763	Si I	1.0872520	Si I	1.0884745	Fe I	1.0885787	Si I
1.0887246	Fe I	1.0888312	Si I	1.0899290	Fe I	1.0908706	Cr I
1.0917865	Sr II	1.0956322	Mg I	1.0960310	Mg I	1.0968449	Mg I
1.0982314	Si I	1.0982832	Ni I	1.0985065	Si I	1.0987538	Si I
1.0990231	Fe I	1.1018567	Cr I	1.1020985	Si I	1.1122839	Fe I
1.1199913	Si I	1.1292922	Si I	1.1301955	Si I	1.1313826	Cr I
1.1359061	Fe I	1.1377194	Fe I	1.1384568	Na I	1.1393868	Cr I
1.1401185	Cr I	1.1406901	Na I	1.1425449	Fe I	1.1468461	Fe I
1.1509821	Fe I	1.1525394	Mg I	1.1594684	Si I	1.1596762	Fe I
1.1610750	Fe I	1.1613739	Cr I	1.1614279	Si I	1.1641448	Fe I
1.1644164	Si I	1.1693174	Fe I	1.1693404	K I	1.1772836	K I
1.1776053	K I	1.1783770	Ti I	1.1786489	Fe I	1.1800410	Ti I
1.1831409	Mg I	1.1842238	Ca II	1.1886096	Fe I	1.1887335	Fe I
1.1893740	Fe I	1.1896127	Ti I	1.1952813	Ti I	1.1953015	Ca II
1.1976326	Fe I	1.1977134	Ti I	1.1987475	Si I	1.1994848	Si I
1.2034808	Si I	1.2043117	Mg I	1.2085302	Si I	1.2086581	Mg I
1.2086955	Mg I	1.2106853	Si I	1.2193432	Fe I	1.2230455	Fe I
1.2274054	Si I	1.2393557	Si I	1.2399229	Si I	1.2426428	Mg I
1.2435646	K I	1.2436854	Mg I	1.2525237	Cr I	1.2525537	K I
1.2560430	Fe I	1.2603718	Ti I	1.2619374	Fe I	1.2652198	Fe I
1.2674569	Ti I	1.2682612	Na I	1.2741874	Ti I	1.2810649	Fe I
1.2814987	Ti I	1.2819546	Ca I	1.2821606	H I	1.2825179	Ti I
1.2828366	Fe I	1.2834942	Ti I	1.2850548	Ti I	1.2883288	Fe I
1.2900364	Mn I	1.2913619	Cr I	1.2935865	Ni I	1.2940556	Cr I
1.2979500	Mn I	1.3010241	Fe I	1.3015456	Ti I	1.3034537	Si I
1.3037132	Ca I	1.3080848	Ti I	1.3105651	Si I	1.3127033	Al I
1.3138542	Ca I	1.3151513	Fe I	1.3154383	Al I	1.3180501	Si I
1.3204755	Cr I	1.3216071	Ni I	1.3285099	Mn I	1.3285278	Fe I
1.3291215	Si I	1.3291460	Fe I	1.3297479	Mn I	1.3312743	Si I
1.3322705	Mn I	1.3329283	Si I	1.3355823	Fe I	1.3376334	Ti I
1.3393101	Fe I	1.3395761	Fe I	1.3419361	Mn I	1.3435909	Ni I
1.4992872	Fe I	1.5021801	Fe I	1.5029104	Mg I	1.5044355	Mg I
1.5051826	Mg I	1.5055858	Fe I	1.5081407	Fe I	1.5098820	Fe I
1.5099983	Fe I	1.5126510	Fe I	1.5140258	Fe I	1.5148195	Fe I
1.5163289	Mn I	1.5167234	K I	1.5172549	K I	1.5182400	Fe I
1.5198640	Fe I	1.5211682	Fe I	1.5221899	Mn I	1.5223777	Fe I
1.5249135	Fe I	1.5266664	Mn I	1.5297316	Fe I	1.5298738	Fe I
1.5339035	Ti I	1.5339574	Fe I	1.5347990	Fe I	1.5381089	Si I
1.5398877	Fe I	1.5399925	Fe I	1.5494567	Fe I	1.5505035	Fe I
1.5505557	Fe I	1.5535998	Fe I	1.5538487	Fe I	1.5546325	Fe I
1.5548002	Ti I	1.5559624	Ni I	1.5562042	Si I	1.5592519	Fe I
1.5595753	Fe I	1.5607105	Ti I	1.5608485	Fe I	1.5615399	Fe I
1.5617894	Fe I	1.5625923	Fe I	1.5636216	Fe I	1.5636895	Ni I
1.5652785	Fe I	1.5657146	Fe I	1.5666293	Fe I	1.5681803	Fe I
1.5690306	Fe I	1.5690727	Fe I	1.5696139	Fe I	1.5697035	Fe I
1.5703273	Ti I	1.5719864	Ti I	1.5727886	Fe I	1.5734056	Fe I
1.5745006	Mg I	1.5746226	Fe I	1.5753291	Mg I	1.5765617	Fe I
1.5768629	Fe I	1.5770147	Mg I	1.5773731	Fe I	1.5774924	Fe I
1.5778378	Fe I	1.5793310	Fe I	1.5802877	Fe I	1.5814452	Fe I
1.5822462	Fe I	1.5823454	Fe I	1.5826032	Fe I	1.5827140	Fe I
1.5837954	Si I	1.5839489	Fe I	1.5841107	Ti I	1.5841966	Fe I
1.5857646	Fe I	1.5868044	Fe I	1.5872858	Fe I	1.5882785	Fe I

Table 7
(Continued)

Vacuum Wavelength (μm)	Element						
1.5883902	Mg I	1.5888811	Si I	1.5890528	Mg I	1.5892781	Si I
1.5893862	Mg I	1.5897301	Fe I	1.5899568	Fe I	1.5902364	Fe I
1.5905859	Fe I	1.5908689	Fe I	1.5910387	Fe I	1.5915647	Fe I
1.5916936	Fe I	1.5924995	Fe I	1.5946201	Fe I	1.5958447	Fe I
1.5958813	Mg I	1.5964437	Si I	1.5966916	Fe I	1.5969226	Fe I
1.5972019	Fe I	1.5985088	Fe I	1.6002094	Fe I	1.6011125	Fe I
1.6011451	Fe I	1.6012459	Fe I	1.6013985	Fe I	1.6042203	Fe I
1.6045034	Fe I	1.6047096	Fe I	1.6064409	Si I	1.6075788	Fe I
1.6080309	Fe I	1.6093127	Fe I	1.6099193	Si I	1.6104678	Fe I
1.6106802	Fe I	1.6120366	Fe I	1.6130308	Fe I	1.6141232	Ca I
1.6155175	Ca I	1.6157657	Fe I	1.6160973	Fe I	1.6161778	Ca I
1.6168131	Si I	1.6169443	Fe I	1.6179391	Fe I	1.6184003	Fe I
1.6185325	Fe I	1.6190221	Fe I	1.6199481	Fe I	1.6201500	Ca I
1.6202925	Fe I	1.6208676	Fe I	1.6212171	Fe I	1.6217965	Fe I
1.6220121	Si I	1.6230050	Fe I	1.6236082	Fe I	1.6240402	Fe I
1.6246289	Si I	1.6250896	Fe I	1.6289216	Fe I	1.6297294	Fe I
1.6314951	Ni I	1.6320779	Fe I	1.6323154	Fe I	1.6328914	Fe I
1.6335988	Fe I	1.6367558	Ni I	1.6384614	Si I	1.6385334	Fe I
1.6386023	Si I	1.6386729	Fe I	1.6388615	Fe I	1.6398865	Fe I
1.6402644	Fe I	1.6409076	Fe I	1.6412269	Fe I	1.6439419	Si I
1.6441112	Fe I	1.6444888	Fe I	1.6449307	Fe I	1.6459396	Fe I
1.6471419	Fe I	1.6478580	Fe I	1.6491168	Fe I	1.6510801	Fe I
1.6521735	Fe I	1.6526587	Fe I	1.6528981	Fe I	1.6536499	Fe I
1.6543711	Fe I	1.6545939	Fe I	1.6556516	Fe I	1.6566292	Fe I
1.6617302	Fe I	1.6650419	Fe I	1.6658076	Fe I	1.6664068	Fe I
1.6665922	Fe I	1.6670032	Fe I	1.6685326	Si I	1.6723540	Al I
1.6727843	Fe I	1.6755176	Al I	1.6757642	Fe I	1.6767949	Al I
1.6804235	Fe I	1.6825109	Fe I	1.6832772	Si I	1.6871891	Ni I
1.6894975	C I	1.6974543	Fe I	1.7000887	Ni I	1.7005669	Ni I
1.7010089	Fe I	1.7015741	Fe I	1.7072339	Fe I	1.7113303	Mg I
1.7165793	Fe I	1.7208997	Fe I	1.7210463	Si I	1.7230331	Si I
1.7307038	Fe I	1.7332059	Si I	1.7343286	C I	1.7412291	Mg I
1.7414241	Fe I	1.7471683	Si I	1.7553341	Fe I	1.7585284	Fe I
1.7613504	Fe I	1.7621891	Si I	1.7628162	Si I	1.7688737	Fe I
1.7711463	Fe I	1.7725933	Fe I	1.7726210	Fe I	1.7732942	Fe I
1.7758583	Mg I	1.7766912	Mg I	1.7775974	Fe I	1.7840949	Fe I
1.7850865	Fe I	1.7890004	Fe I	1.7935075	Fe I	1.7942698	Fe I
1.7943777	Fe I	1.7971303	Fe I	1.7984291	Fe I	1.7987210	Fe I
1.7991446	Ni I	1.8006762	Cr I	1.8045770	Ni I	1.8078612	Fe I
1.8101228	Fe I	1.8194902	Fe I	1.9430568	Mg I	1.9458301	Ca I
1.9489667	Fe I	1.9496166	Fe I	1.9498705	Si I	1.9511040	Ca I
1.9511446	Si I	1.9513500	Si I	1.9514636	Fe I	1.9598082	Fe I
1.9616920	Fe I	1.9618503	Fe I	1.9640681	Fe I	1.9723943	V I
1.9727936	Si I	1.9728928	Mg I	1.9739257	Mg I	1.9782195	Ca I
1.9797279	Fe I	1.9820428	Ca I	1.9852129	Fe I	1.9858512	Ca I
1.9867646	Ca I	1.9922628	Ca I	1.9928778	Fe I	1.9934361	Si I
1.9939170	Ca I	1.9967282	Ca I	2.0097535	Fe I	2.0286617	Fe I
2.0301933	Si I	2.0349441	Si I	2.0355272	Fe I	2.0383973	Si I
2.0569580	Fe I	2.0608501	Si I	2.0635321	Fe I	2.0703959	Fe I
2.0704272	Si I	2.0722606	Fe I	2.0809875	Si I	2.0810766	Fe I
2.0846491	Fe I	2.0922821	Si I	2.1065505	Mg I	2.1066642	Mg I
2.1098835	Al I	2.1169577	Al I	2.1244261	Fe I	2.1360087	Si I
2.1785696	Si I	2.1788888	Ti I	2.1825655	Si I	2.1885319	Si I
2.1903353	Ti I	2.2010505	Ti I	2.2057965	Sc I	2.2062447	Na I
2.2068751	Si I	2.2089689	Na I	2.2217295	Ti I	2.2238901	Ti I
2.2263176	Fe I	2.2266250	Fe I	2.2280107	Ti I	2.2316670	Ti I
2.2386901	Fe I	2.2398975	Fe I	2.2450020	Ti I	2.2479405	Fe I
2.2543838	Si I	2.2614114	Ca I	2.2626002	Fe I	2.2631137	Ca I
2.2632897	Ca I	2.2657359	Ca I	2.2671964	Si I	2.2814252	Mg I
2.2969596	Ti I	2.3150909	Fe I	2.3354795	Na I	2.3385518	Na I
2.3447857	Ti I	2.4572999	Mg I	2.4825687	Mg I	2.4867327	Mg I
3.0277195	Mg I	3.1517396	Si I	3.3970842	Mg I	3.6771872	Mg I
3.6789458	Mg I	3.6825631	Mg I	3.7091205	Fe I	3.8632832	Al I
3.8664858	Mg I	3.8669012	Mg I	3.8721194	Al I		

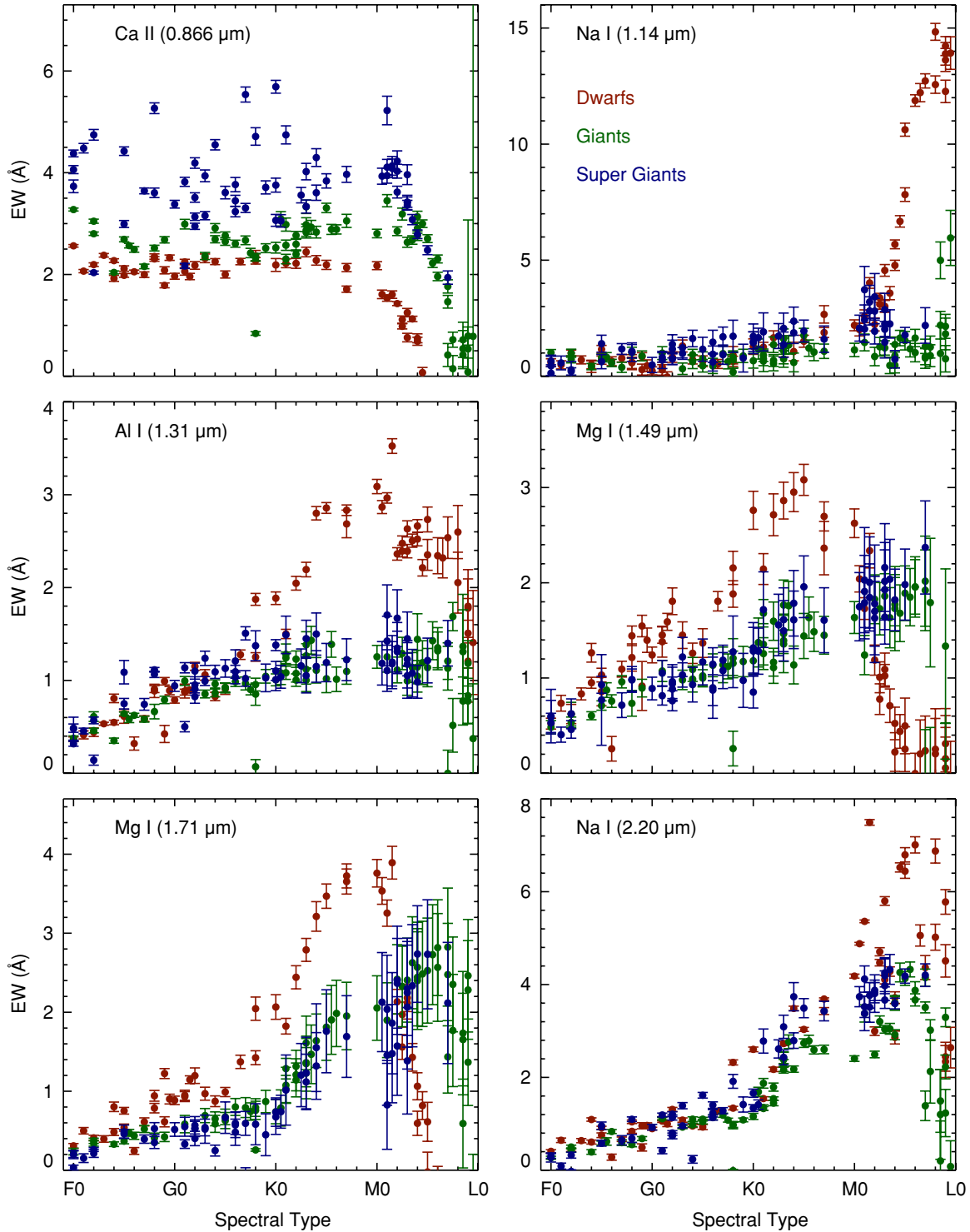


Figure 35. EWs of prominent atomic absorption lines as a function of spectral type. The Ca II EW is a good luminosity class indicator. The Na I 2.20 μm EW provides a good indication of spectral subtype, while the Na I 1.14 μm doublet EW can be used as a clear indicator of the very latest spectral subtypes.

(C \sim O) are intermediate between C stars and M giants. Zirconium has a stronger affinity for oxygen than for titanium, but is much less abundant, so in normal M stars, ZrO features are weak or absent. With increasing Zr abundance due to the *s*-process, any oxygen remaining from CO formation goes into ZrO and so in S stars ZrO predominates and TiO is weakened.

In the optical, the continuum of most carbon stars is largely obscured by absorption features from carbon compounds. Consequently, it is very difficult to use the standard atomic lines

to sort spectra into types that can be calibrated in terms of effective temperature, luminosity, and composition (i.e., a three-dimensional MK system). Nevertheless, improved optical spectra have led to a revised MK classification scheme for C stars due to Keenan (1993) and Barnbaum et al. (1996). In this scheme, the notation C-Rx, C-Jx, C-Nx, C-Lx, and C-Hx corresponds to different spectral types, where increasing digit *x* represents decreasing effective temperature. Although the spectral types probably represent different stellar populations, the types

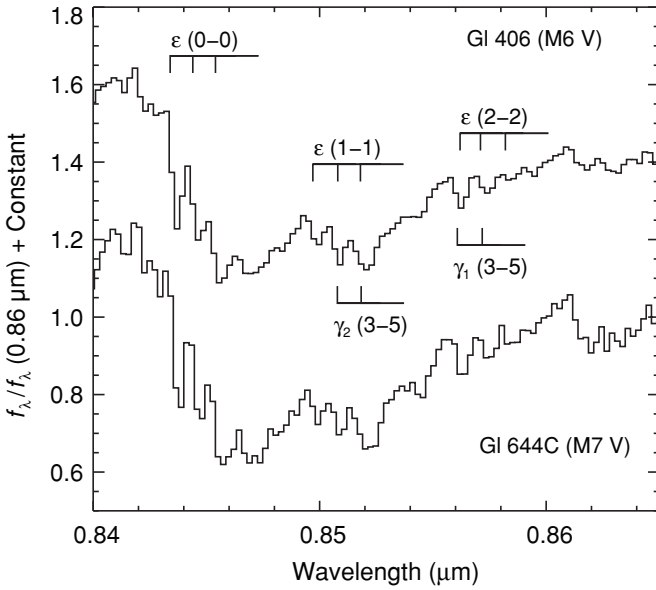


Figure 36. Spectrum of Gl 406 (M6 V) and Gl 644C (vB 8, M7 V) centered on the $\Delta\nu = 0$ system of TiO. The 0–0, 1–1, and 2–2 bands are indicated. Also indicated are the $\Delta\nu = -2$ band heads of the γ system. The set of band heads at $\sim 0.853 \mu\text{m}$ and $\sim 0.858 \mu\text{m}$ are most likely a combination of both the ϵ and γ systems even though only the γ heads are indicated in the literature.

are defined entirely by features in the observed spectra (see Table 2; Barnbaum et al. 1996). Due to differences in mass, original composition, and environment, not all carbon stars are enriched in the same way. In terms of evolutionary status, the spectral types C-R, C-J, C-N, C-L, and C-H are thought to characterize red giants, giants, TPAGB stars, PAGB stars, and binary stars undergoing mass transfer, respectively. Further symbols can be added to the notation to indicate luminosity class and composition (for details of the notation, see Barnbaum et al. 1996).

The spectral classification scheme as developed by Keenan & McNeil (1976) and revised by Ake (1979) for S stars is similar to that of C stars. The notation Sx indicates S-star effective temperature, where increasing x digit represents decreasing effective temperature. Additional symbols can be added to indicate composition. However, the effective temperature sequence of S stars relative to C stars is uncertain.

Figure 34 shows a sequence of M, S, and C-N giants, all of approximately the same effective temperature, illustrating the effects of increasing carbon enrichment and presumed AGB evolution. The M0 IIIb star shows features typical of late giant stars—strong CO absorption features in the H and K bands, the Ca II triplet and a TiO band head at about $0.85 \mu\text{m}$, a CN band head at about $1.1 \mu\text{m}$, and the SiO absorption series at about $4 \mu\text{m}$. The S star (S4.5 Zr 2 Ti 4) is similar except for a strong ZrO band head at about $0.93 \mu\text{m}$. The two carbon stars (both C-N 4.5) display the effects of increasing carbon enrichment (C2 4.5 and C2 5.5, respectively). In addition to the first overtone CO band at about $2.29 \mu\text{m}$, which is present in the M giant and S star, strong CN band heads are observed at $0.9 \mu\text{m}$, $1.1 \mu\text{m}$, and $1.4 \mu\text{m}$, together with C₂ absorption at about $1.2 \mu\text{m}$ and $1.75 \mu\text{m}$, and C₂H₂ and HCN features at about $3.1 \mu\text{m}$. The very cool carbon star R Lep (HD 31996, C7,6e (N4)) shows additional absorption features due to HCN and C₂H₂ at $1.65 \mu\text{m}$ and $2.5 \mu\text{m}$, the HCN $\nu_1 + \nu_2$ bands at $3.56 \mu\text{m}$, and the broad blend of the CS first overtone and HCN

$\nu_1 - \nu_2$ bands at $\sim 3.9 \mu\text{m}$. The HCN, C₂H₂, and CS features are identified by Goebel et al. (1980) and Aoki et al. (1998) (but are not given in Table 10).

4. EXAMPLE APPLICATIONS OF THE LIBRARY

Potential applications of the IRTF Spectral Library can take advantage of the $0.8\text{--}5 \mu\text{m}$ wavelength range at $R \sim 2000$, preserved spectral continuum shape and absolute flux calibration. For example, the library has been used to model the atmospheres of cool dwarfs (Cushing et al. 2008), confirm the presence of a gapped primordial disk around LkCa15 (Espaillat et al. 2008), and investigate the stellar populations and activity in the nuclei of Seyfert galaxies (Ramos Almeida et al. 2009). Technical applications include using the spectra to design filters and to calibrate different photometric systems. This is made possible because the system response and telluric effects are carefully removed from our spectra. Of the many potential applications, in this section we discuss just two: the measurement of equivalent widths for spectral typing, and synthetic photometry.

4.1. Equivalent Widths

As an example of the quantitative analysis that can be carried out with the spectra in our library, we have calculated the EWs of several prominent features seen in the data (Ca II, Na I, Al I, and Mg I) following the technique described by Cushing et al. (2005). The wavelength ranges used to define the continuum and the features are given in Table 8 and the EW values are given in Table 9. As Figure 35 clearly demonstrates, the Ca II EW provides a fairly good discriminator of luminosity class between spectral types F and early M; the observed ranges of Ca II EW values are seen to be remarkably narrow, particularly for the dwarfs, with little overlap among the luminosity classes. Similarly, the Na I $2.20 \mu\text{m}$ feature increases monotonically with spectral type (temperature) between early F and mid M and therefore provides an approximate means of estimating a stellar spectral type, although the uncertainty in the classification can be fairly large (\pm few spectral subtypes). The remarkably large, sudden, and monotonic increase in the Na I $1.14 \mu\text{m}$ doublet EW beginning at early M implies that this line can be used as a clear indicator of the very latest spectral subtypes. There are many other features in NIR spectra, in addition to what we have presented here, that can be used to determine spectral classes (e.g., Kleinmann & Hall 1986; Meyer et al. 1998; Wallace et al. 2000; Förster Schreiber 2000; Ivanov et al. 2004; Lançon et al. 2007; Davies et al. 2007).

4.2. Synthetic Colors

Because our spectra are flux calibrated and the spectra slopes are reliable, the IRTF Spectral Library can also be used to compute synthetic magnitudes and colors as well as transformations between various photometric systems. Table 11 gives the synthetic $Z - Y$, $Y - J$, $J - H$, $H - K$, and $K - L'$ colors of the cool stars in the library derived using Equation (5). Synthesized $J - H$ versus $H - K$ color-color diagrams for our sample of cool stars are given in Figure 37 ($0.0 < J - H < 1.2$) and Figure 38 ($-0.5 < J - H < 2.5$). Figure 39 shows the spectral behavior of several late-type M giant stars that are plotted in Figures 37 and 38. A synthesized $Y - J$ versus $J - H$ diagram of the same stars is given in Figure 40 (all stars except two very red OH/IR stars). The sample of 13 L and two T dwarfs from Cushing et al. (2005) and the eight T dwarf

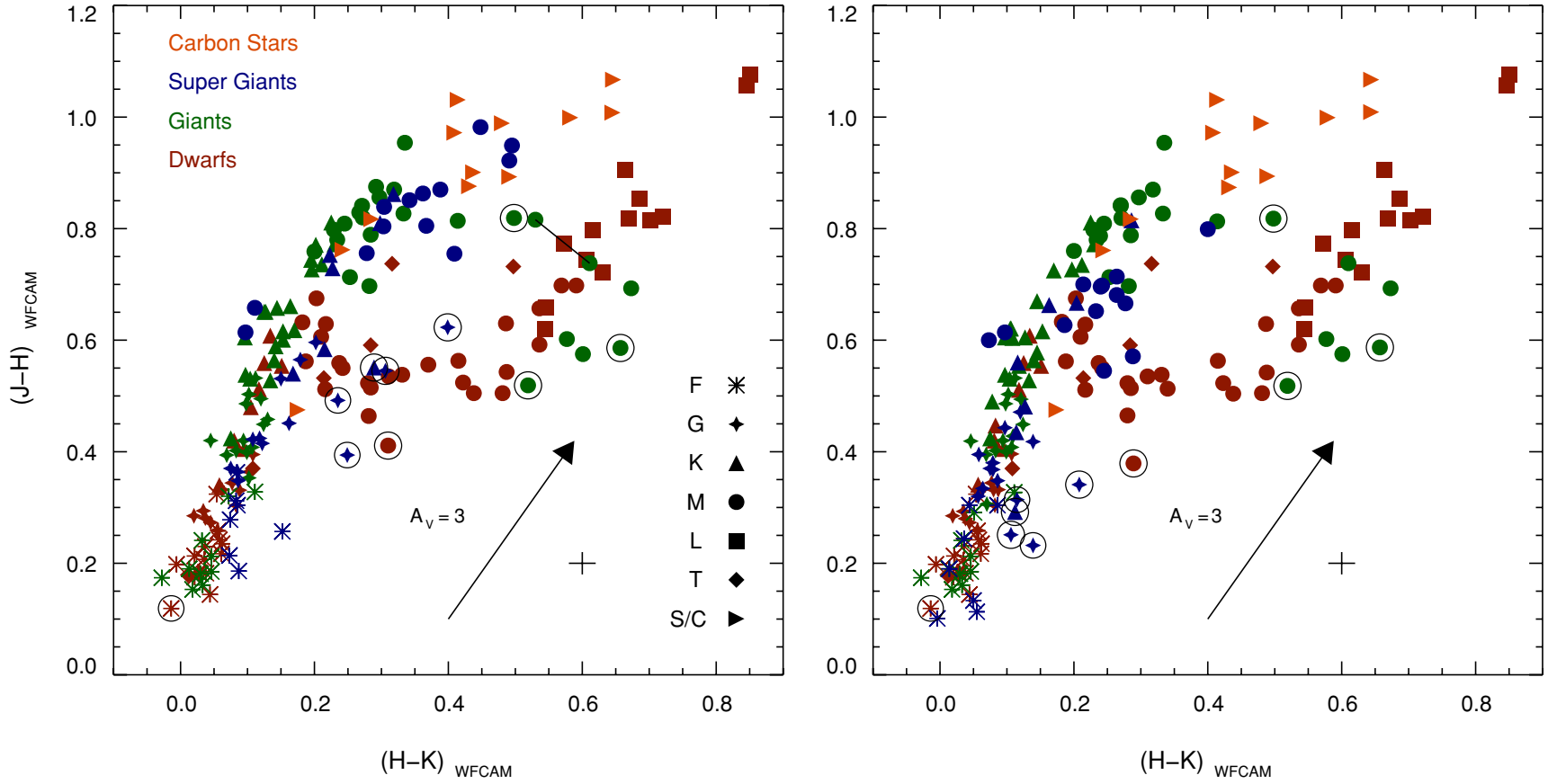


Figure 37. Left: synthesized WFCAM $J - H$ versus $H - K$ diagram for our sample of cool stars (see Table 11), plus additional L and T dwarfs from Cushing et al. (2005) and T dwarfs from Burgasser et al. (2006). Several objects with extreme colors fall outside the plotted range and are plotted in Figure 38. Note the bifurcation between dwarfs and stars of higher luminosity beyond spectral type M0 V. Stars with odd spectra are circled (see Section 4.3). HD 69243 (M6e–M9e III, Mira variable) was observed at two epochs and the change in color is indicated (see also Figure 39). The + sign indicates the accuracy of the photometry, and the arrow indicates the direction and magnitude of the reddening vector for $A_V = 3$. Right: the same plot but now with the correction for reddening included (the 66 dereddened stars are given in Table 5). Note how most M supergiant stars move closer to the main sequence.

Table 8
EW Limit Definitions

Feature	Feature Limits (μm)	First Continuum Level Limits (μm)	Second Continuum Level Limits (μm)
Ca II (0.866 μm)	0.860–0.875	0.862–0.864	0.870–0.873
Na I (1.14 μm)	1.120–1.160	1.125–1.130	1.150–1.160
Al I (1.313 μm)	1.300–1.330	1.305–1.309	1.320–1.325
Mg I (1.485 μm)	1.475–1.4975	1.4775–1.485	1.491–1.497
Mg I (1.711 μm)	1.695–1.726	1.702–1.708	1.715–1.720
Na I (2.206 μm)	2.185–2.230	2.192–2.198	2.213–2.220

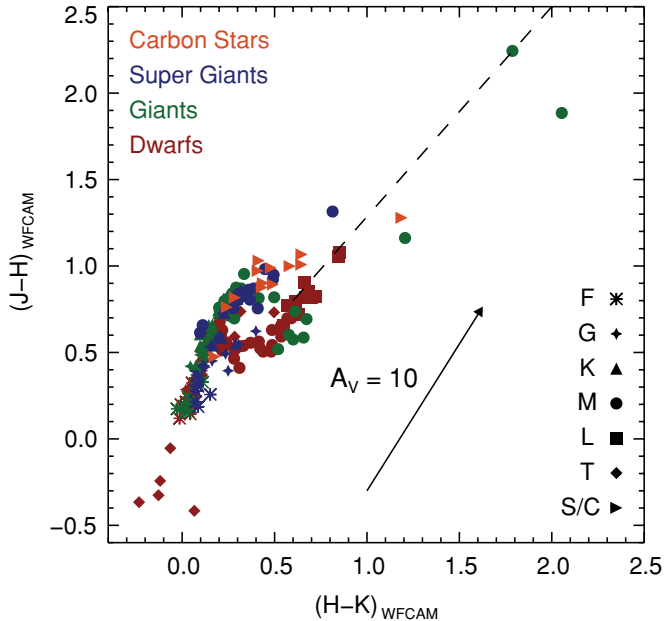


Figure 38. Same as Figure 37 except all stars are plotted. The additional stars include some very red Mira and OH/IR stars, plus several blue T dwarfs. The colors of the Mira and OH/IR stars follow the linear locus (dashed line) expected from models of circumstellar dust shells in TPAGB stars (e.g., Lewis 2006).

spectral standards from Burgasser et al. (2006) are also included in these figures and table. In addition, Figures 37 and 40 also include color–color diagrams with the corrections for reddening discussed in Section 2.3 incorporated.

The trends in the colors of the stars as a function of spectral type in the $J - H$ versus $H - K$ diagram are very similar to those presented by Bessell & Brett (1988, Figure 5) and Reid & Hawley (2005, Figure 2.22), with the slight difference that our photometry is in the NIR-MKO system. Since our photometric errors are small (at most a few percent, see Section 2.3), the scatter in these plots is due to real differences in stellar colors produced by variations in metallicity, reddening, etc. The most noticeable feature of the JHK color–color diagram is the bifurcation between M dwarfs and stars of higher luminosity classes. Stars of all luminosity classes initially show a steep rise in $J - H$ with later spectral type but starting at a spectral type of $\sim M0$, the $J - H$ colors of the dwarfs become bluer while that of the M giants and supergiants continue to become redder (Lee 1970; Glass 1975; Frogel et al. 1978). The J and H bands probe different layers (and thus different temperatures) in an atmosphere because H^- , the dominant continuum opacity source at these wavelengths, has a minimum at $\sim 1.6 \mu\text{m}$. The

turnover in the $J - H$ colors of the M dwarfs is therefore due to a change in the adiabatic temperature gradient as hydrogen is increasingly converted into H_2 in the high pressure (relative to giants) atmospheres of M dwarfs (Mould 1976). The $J - H$ colors of the M dwarfs continue to become bluer with the onset of H_2O absorption that suppresses the H - and K -band fluxes but eventually flatten out before becoming redder again for late-type M dwarfs and L dwarfs as the peak of the Planck function shifts farther into the NIR.

We note that the locus of late-M giants (Lb, SRb, and M variables; see Table 2) in the JHK color–color diagram appears to turn back down toward the location of late-type M and L dwarfs (see Figure 37). Figure 39 shows the spectral behavior of a selection of late-type M giants along the locus of decreasing $J - H$ and increasing $H - K$ color. The most distinctive features in these spectra are the broad H_2O absorption features centered at $1.4 \mu\text{m}$ and $1.9 \mu\text{m}$. H_2O absorption is observed no earlier than M6 III (see also Figure 8) and then increases in strength with later spectral types, in agreement with the trends first observed by Frogel (1971) and Hyland (1974). The turnover in $J - H$ is therefore a result of increasing H_2O line absorption which suppresses the H - and K -band fluxes more than the J -band flux. Models of Mira variables (Bessell et al. 1989, 1996) can reproduce the observed turnover in $J - H$. In these models pulsation produces extended atmospheres in which water can form in dense cool ($\leq 10^3 \text{ K}$) layers formed behind periodically outward-running shocks.

Other intrinsically red stars include late-type supergiants, carbon and S stars. The red colors are due to the cool continuum temperatures, together with molecular line blanketing from CO and CN in supergiants and from CN and C_2 in carbon stars.

One of the observable consequences of mass loss in TPAGB stars is an approximately linear locus in the JHK color–color diagram reflecting the effects of differential extinction and dust temperature in models of circumstellar shells (e.g., Lewis 2006). Less dusty Mira variables are located at the blue end of this locus at $J - H \sim 0.8$, $H - K \sim 0.6$, while the more deeply embedded OH/IR stars (optically obscured stars with 1612 MHz OH line emission) are located at the red end. The two OH/IR stars observed in our sample are located at $J - H \sim 2$, $H - K \sim 2$ (see Figure 38).

Library spectra can be used to synthesize other colors and experiment with other photometric systems. As an example, the $Y - J$ versus $J - H$ color–color diagram shown in Figure 40 illustrates the advantage of using the Y band in combination with the standard JHK bands when trying to identify T dwarfs (see also Hillenbrand et al. 2002; Hewett et al. 2006) compared to using JHK colors alone (see Figure 37). The $J - H$ color can be used as an indicator of T dwarf spectral types and is accurate to within about one subtype. For example, the UKIRT Infrared

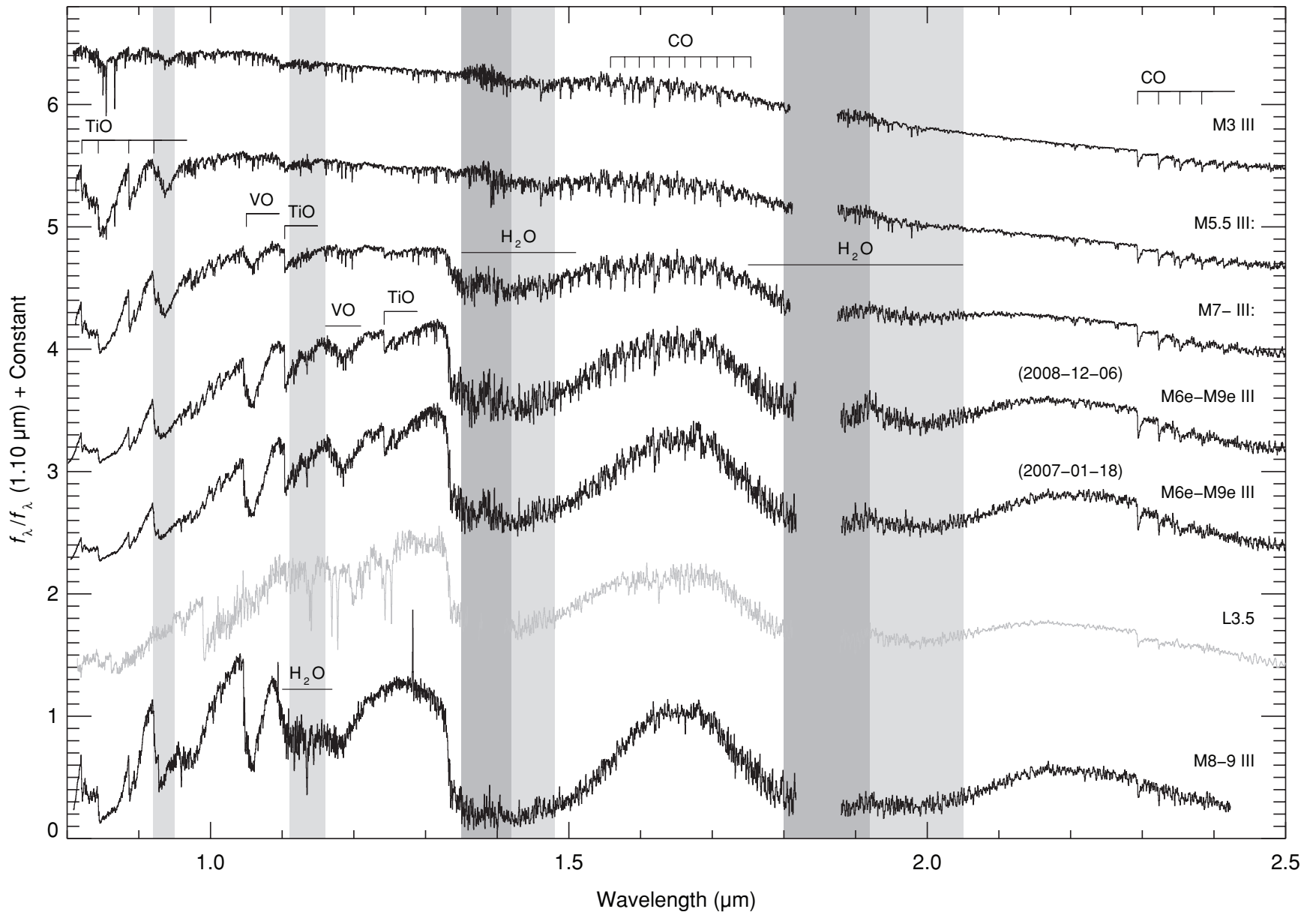


Figure 39. Spectral behavior of M giant stars along the locus of decreasing $J - H$ and increasing $H - K$ in Figure 37 (plotted from the top). Strong water absorption at $1.4 \mu\text{m}$ and $1.9 \mu\text{m}$ reduces the flux emitted at H relative to J and K . As a result, the locus of M giant stars in the $J - H$ versus $H - K$ diagram appears to turn down toward late-M and early-L dwarfs (see Section 4.2 and Figure 37). The spectra plotted (black) are HD 39045 (M3 III), HD 94705 (M5.5 III), HD 108849 (M7- III), HD 69243 (M6e–M9e III) on 2008 December 6, HD 69243 (M6e–M9e III) on 2007 January 18, and IRAS 14303–1042 (M8–9 III). Also plotted is the spectrum (gray) of 2MASS J00361617+1821104 (L3.5; Cushing et al. 2005) which has very similar JHK colors to HD 69243 (M6e–M9e III).

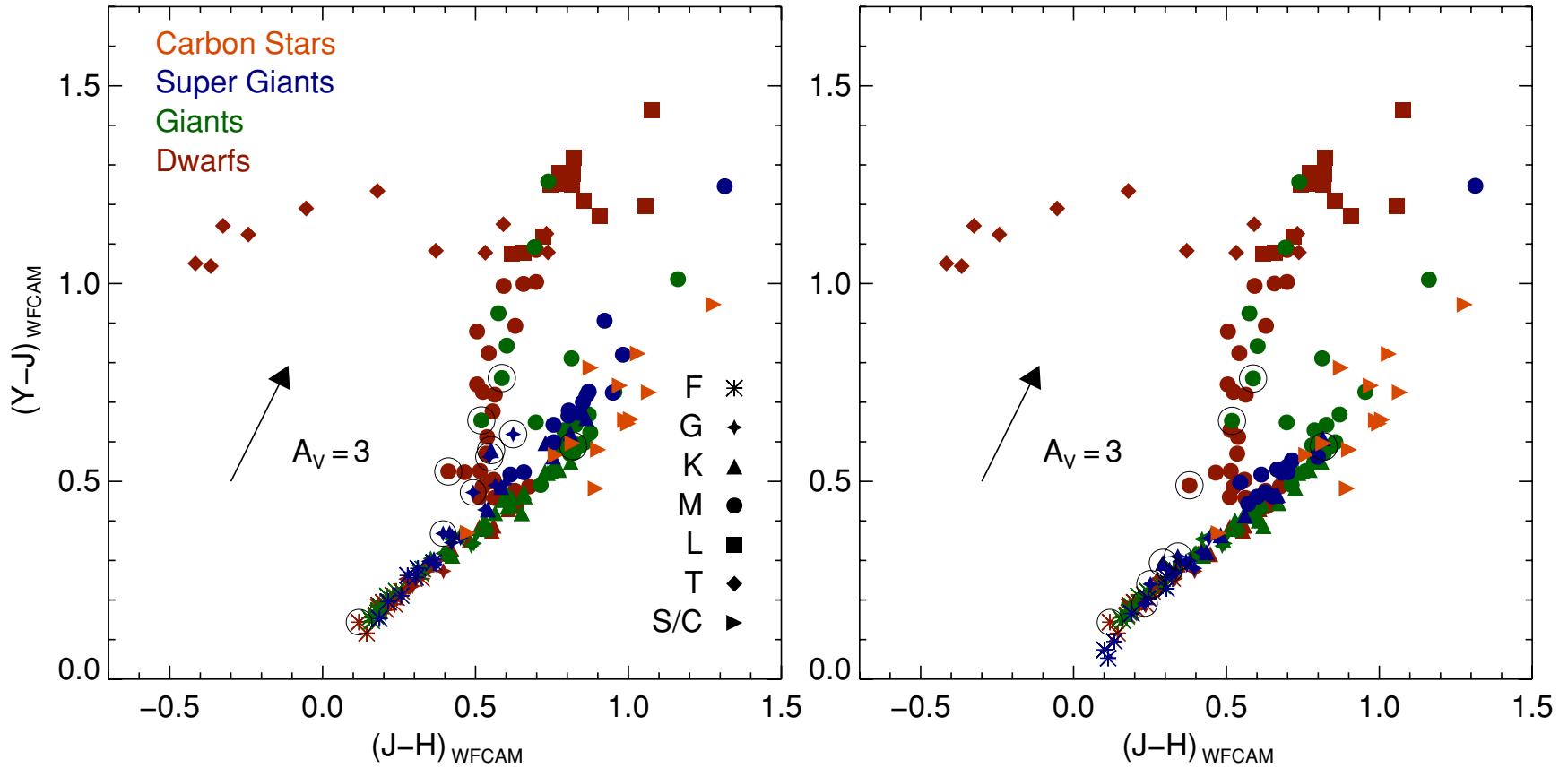


Figure 40. Left: synthesized WFCAM $Y - J$ versus $J - H$ diagram for our sample of cool stars (see Table 11), plus additional L and T dwarfs from Cushing et al. (2005) and T dwarfs from Burgasser et al. (2006). The plot illustrates the advantage of using a Y filter when trying to identify T dwarfs compared to using JHK colors (see Figure 37) and is an example of using the library to experiment with other photometric systems. Note the bifurcation between dwarfs and stars of higher luminosity beyond the spectral type M0 V. Several late-type M giants have similar colors to late-type dwarfs since both have water absorption in the NIR. Right: the same plot but now with the correction for reddening included (the 66 dereddened stars are given in Table 5). Note how most M supergiant stars move closer to the main sequence.

Table 9
EWs

Object	Spectral Type	Ca II (0.866 μm)	Na I (1.14 μm)	Al I (1.313 μm)	Mg I (1.485 μm)	Mg I (1.711 μm)	Na I (2.206 μm)
HD 7927	F0 Ia	3.73 ± 0.12	0.13 ± 0.36	0.32 ± 0.03	0.59 ± 0.18	0.03 ± 0.03	-0.12 ± 0.04
HD 135153	F0 Ib-II	4.38 ± 0.07	0.45 ± 0.41	0.48 ± 0.12	0.60 ± 0.28	0.20 ± 0.05	0.28 ± 0.10
HD 6130	F0 II	4.06 ± 0.08	0.66 ± 0.25	0.49 ± 0.05	0.53 ± 0.10	0.20 ± 0.04	0.31 ± 0.05
HD 89025	F0 IIIa	3.28 ± 0.03	1.01 ± 0.14	0.38 ± 0.03	0.48 ± 0.07	0.24 ± 0.04	0.27 ± 0.03
HD 13174	F0 III-IVn	3.05 ± 0.04	0.99 ± 0.17	0.61 ± 0.05	0.62 ± 0.12	0.37 ± 0.03	0.50 ± 0.04
HD 27397	F0 IV	2.76 ± 0.04	0.45 ± 0.23	0.41 ± 0.05	0.63 ± 0.09	0.32 ± 0.03	0.50 ± 0.05
HD 108519	F0 V(n)	2.56 ± 0.03	0.58 ± 0.17	0.37 ± 0.03	0.52 ± 0.06	0.31 ± 0.03	0.41 ± 0.04
HD 173638	F1 II	4.48 ± 0.09	0.57 ± 0.30	0.46 ± 0.03	0.41 ± 0.08	0.15 ± 0.05	0.09 ± 0.06
HD 213135	F1 V	2.07 ± 0.03	0.49 ± 0.17	0.41 ± 0.04	0.74 ± 0.08	0.50 ± 0.04	0.65 ± 0.05
BD +38 2803	F2-F5 Ib	2.04 ± 0.03	0.21 ± 0.16	0.14 ± 0.05	0.62 ± 0.16	0.26 ± 0.03	-0.02 ± 0.03
HD 182835	F2 Ib	4.74 ± 0.10	0.28 ± 0.36	0.57 ± 0.04	0.46 ± 0.09	0.21 ± 0.05	0.32 ± 0.06
HD 40535	F2 III-IV	2.80 ± 0.03	0.73 ± 0.16	0.46 ± 0.02	0.53 ± 0.06	0.34 ± 0.03	0.43 ± 0.05
HD 164136	kA9hF2mF2 (IV)	2.62 ± 0.04	0.92 ± 0.13	0.42 ± 0.04	0.52 ± 0.09	0.31 ± 0.05	0.35 ± 0.05
HD 113139	F2 V	2.19 ± 0.04	1.00 ± 0.13	0.44 ± 0.05	0.62 ± 0.10	0.41 ± 0.03	0.44 ± 0.03
HD 26015	F3 V	2.38 ± 0.04	0.70 ± 0.17	0.53 ± 0.02	0.83 ± 0.06	0.40 ± 0.04	0.64 ± 0.05
HD 21770	F4 III	2.04 ± 0.03	0.41 ± 0.14	0.35 ± 0.03	0.60 ± 0.04	0.33 ± 0.03	0.39 ± 0.05
HD 87822	F4 V	2.27 ± 0.04	0.51 ± 0.18	0.55 ± 0.02	0.95 ± 0.06	0.48 ± 0.04	0.61 ± 0.04
HD 16232	F4 V	1.92 ± 0.06	0.41 ± 0.25	0.81 ± 0.05	1.26 ± 0.10	0.80 ± 0.06	1.09 ± 0.04
HD 213306	F5 Ib - G1 Ib	4.42 ± 0.08	1.40 ± 0.37	1.09 ± 0.13	0.77 ± 0.48	0.49 ± 0.08	0.96 ± 0.08
HD 186155	F5 II-III	2.99 ± 0.07	0.63 ± 0.31	0.75 ± 0.06	0.93 ± 0.09	0.46 ± 0.05	0.58 ± 0.06
HD 17918	F5 III	2.69 ± 0.05	0.81 ± 0.14	0.64 ± 0.02	0.71 ± 0.05	0.37 ± 0.03	0.59 ± 0.04
HD 218804	F5 V	1.98 ± 0.04	1.16 ± 0.17	0.61 ± 0.08	0.86 ± 0.15	0.75 ± 0.04	0.91 ± 0.04
HD 27524	F5 V	2.12 ± 0.05	0.69 ± 0.18	0.64 ± 0.03	1.03 ± 0.07	0.54 ± 0.05	0.75 ± 0.05
HD 75555	F5.5 III-IV	2.57 ± 0.05	0.82 ± 0.20	0.58 ± 0.04	0.87 ± 0.08	0.47 ± 0.04	0.62 ± 0.08
HD 160365	F6 III-IV	2.49 ± 0.05	0.57 ± 0.16	0.62 ± 0.02	0.76 ± 0.07	0.44 ± 0.05	0.83 ± 0.04
HD 11443	F6 IV	2.24 ± 0.05	0.61 ± 0.17	0.57 ± 0.03	0.83 ± 0.06	0.46 ± 0.04	0.67 ± 0.05
HD 215648	F6 V	2.05 ± 0.03	0.65 ± 0.19	0.32 ± 0.07	0.26 ± 0.13	0.24 ± 0.04	0.28 ± 0.06
HD 201078	F7 II-	3.64 ± 0.06	1.17 ± 0.23	0.74 ± 0.06	0.71 ± 0.13	0.39 ± 0.05	0.65 ± 0.10
HD 124850	F7 III	2.16 ± 0.05	0.38 ± 0.22	0.58 ± 0.03	0.96 ± 0.06	0.52 ± 0.04	0.60 ± 0.06
HD 126660	F7 V	2.00 ± 0.05	0.78 ± 0.16	0.59 ± 0.03	1.09 ± 0.08	0.61 ± 0.05	0.67 ± 0.05
HD 190323	F8 Ia	5.27 ± 0.11	1.04 ± 0.40	1.11 ± 0.03	0.99 ± 0.14	0.35 ± 0.08	0.68 ± 0.09
HD 51956	F8 Ib	3.61 ± 0.09	1.08 ± 0.29	1.07 ± 0.03	0.98 ± 0.12	0.53 ± 0.08	1.10 ± 0.05
HD 220657	F8 III	2.52 ± 0.06	1.01 ± 0.24	0.66 ± 0.08	0.73 ± 0.14	0.41 ± 0.06	0.55 ± 0.05
HD 111844	F8 IV	2.27 ± 0.03	0.57 ± 0.20	0.45 ± 0.04	0.61 ± 0.06	0.28 ± 0.02	0.39 ± 0.05
HD 219623	F8 V	2.35 ± 0.05	0.61 ± 0.32	0.89 ± 0.07	1.22 ± 0.14	0.79 ± 0.06	0.84 ± 0.04
HD 27383	F8 V	2.31 ± 0.05	0.58 ± 0.24	0.91 ± 0.04	1.44 ± 0.10	0.94 ± 0.07	1.04 ± 0.04
HD 102870	F8.5 IV-V	2.31 ± 0.07	0.54 ± 0.27	0.83 ± 0.04	1.24 ± 0.10	0.73 ± 0.06	0.93 ± 0.04
HD 6903	F9 IIIa	2.68 ± 0.06	0.88 ± 0.21	0.79 ± 0.04	0.89 ± 0.09	0.42 ± 0.06	0.68 ± 0.04
HD 176051	F9 V	2.08 ± 0.07	0.84 ± 0.17	0.99 ± 0.04	1.55 ± 0.11	1.22 ± 0.06	0.96 ± 0.06
HD 165908	F9 V metal weak	1.79 ± 0.05	0.29 ± 0.24	0.42 ± 0.09	0.92 ± 0.26	0.61 ± 0.06	0.49 ± 0.08
HD 114710	F9.5 V	2.33 ± 0.05	0.45 ± 0.25	0.89 ± 0.04	1.40 ± 0.13	0.90 ± 0.06	0.96 ± 0.06
HD 185018	G0 Ib-II	3.38 ± 0.08	0.49 ± 0.33	0.94 ± 0.06	0.89 ± 0.12	0.52 ± 0.09	0.93 ± 0.06
HD 109358	G0 V	1.97 ± 0.06	0.23 ± 0.17	0.79 ± 0.03	1.24 ± 0.08	0.88 ± 0.05	0.90 ± 0.03
HD 74395	G1 Ib	3.82 ± 0.09	0.70 ± 0.37	1.14 ± 0.05	1.05 ± 0.13	0.55 ± 0.12	1.19 ± 0.04
HD 216219	G1 II-III: Fe-1 CH0.5	2.17 ± 0.05	0.81 ± 0.20	0.50 ± 0.05	0.81 ± 0.10	0.33 ± 0.05	0.42 ± 0.07
HD 21018	G1 III: CH-1:	2.99 ± 0.09	1.00 ± 0.28	0.99 ± 0.05	1.07 ± 0.11	0.58 ± 0.11	1.11 ± 0.03
HD 10307	G1 V	2.06 ± 0.07	0.39 ± 0.22	0.88 ± 0.08	1.38 ± 0.16	0.95 ± 0.06	1.11 ± 0.04
HD 95128	G1 V Fe-0.5	2.25 ± 0.05	0.27 ± 0.23	0.87 ± 0.03	1.45 ± 0.09	0.93 ± 0.06	1.06 ± 0.03
HD 20619	G1.5 V	1.96 ± 0.06	-0.03 ± 0.22	0.90 ± 0.03	1.59 ± 0.09	1.15 ± 0.05	1.00 ± 0.06
HD 42454	G2 Ib	4.19 ± 0.10	1.38 ± 0.41	1.10 ± 0.09	0.94 ± 0.17	0.57 ± 0.11	1.21 ± 0.05
HD 39949	G2 Ib	3.51 ± 0.09	1.17 ± 0.38	0.95 ± 0.09	0.96 ± 0.18	0.53 ± 0.11	1.14 ± 0.05
HD 3421	G2 Ib-II	3.13 ± 0.07	0.76 ± 0.26	0.91 ± 0.06	0.88 ± 0.13	0.52 ± 0.09	0.74 ± 0.06
HD 219477	G2 II-III	2.95 ± 0.06	0.75 ± 0.24	0.82 ± 0.07	0.76 ± 0.10	0.40 ± 0.09	0.80 ± 0.05
HD 126868	G2 IV	2.27 ± 0.07	0.61 ± 0.24	0.88 ± 0.06	1.22 ± 0.15	0.79 ± 0.08	0.96 ± 0.07
HD 76151	G2 V	2.18 ± 0.08	0.83 ± 0.23	1.15 ± 0.04	1.81 ± 0.14	1.20 ± 0.10	1.31 ± 0.04
HD 192713	G3 Ib-II Wk H&K comp?	3.94 ± 0.12	1.23 ± 0.44	1.24 ± 0.08	1.22 ± 0.21	0.52 ± 0.18	1.39 ± 0.07
HD 176123	G3 II	3.16 ± 0.08	0.98 ± 0.25	0.99 ± 0.05	1.03 ± 0.13	0.54 ± 0.11	0.96 ± 0.04
HD 88639	G3 IIIb Fe-1	2.36 ± 0.07	0.32 ± 0.25	0.85 ± 0.04	0.98 ± 0.10	0.69 ± 0.09	0.93 ± 0.03
HD 10697	G3 Va	2.32 ± 0.09	1.30 ± 0.26	1.06 ± 0.06	1.45 ± 0.14	0.97 ± 0.08	1.08 ± 0.05
HD 179821	G4 O-Ia	3.44 ± 0.25	0.79 ± 0.47	0.66 ± 0.05	0.83 ± 0.20	-0.44 ± 0.07	-1.75 ± 0.08
HD 6474	G4 Ia ± 4.55	0.10 ± 1.63	0.35 ± 1.09	0.07 ± 0.93	0.18 ± 0.25	0.07 ± 0.23	0.08
HD 94481	G4 III-IIIb	2.69 ± 0.07	0.93 ± 0.22	0.87 ± 0.04	1.09 ± 0.13	0.65 ± 0.09	0.98 ± 0.04
HD 108477	G4 III	2.91 ± 0.09	0.63 ± 0.30	0.96 ± 0.04	0.99 ± 0.14	0.59 ± 0.11	1.10 ± 0.05
HD 214850	G4 V	2.25 ± 0.06	0.71 ± 0.19	0.83 ± 0.05	1.26 ± 0.11	0.87 ± 0.07	0.95 ± 0.03
HD 190113	G5 Ib	3.61 ± 0.12	1.16 ± 0.52	1.13 ± 0.09	1.17 ± 0.24	0.67 ± 0.20	1.62 ± 0.06

Table 9
(Continued)

Object	Spectral Type	Ca II (0.866 μ m)	Na I (1.14 μ m)	Al I (1.313 μ m)	Mg I (1.485 μ m)	Mg I (1.711 μ m)	Na I (2.206 μ m)
HD 18474	G5: III: CN-3 CH-2 H _{δ} -1	2.65 ± 0.08	0.45 ± 0.27	0.92 ± 0.05	1.00 ± 0.09	0.68 ± 0.10	1.05 ± 0.05
HD 193896	G5 IIIa	2.76 ± 0.07	0.76 ± 0.29	0.93 ± 0.05	1.02 ± 0.12	0.63 ± 0.10	1.10 ± 0.04
HD 165185	G5 V	2.00 ± 0.07	0.64 ± 0.23	0.91 ± 0.06	1.37 ± 0.15	0.99 ± 0.06	0.93 ± 0.05
HD 161664	G6 Ib H _{δ} 1	3.77 ± 0.14	1.47 ± 0.51	1.21 ± 0.12	0.90 ± 0.32	0.48 ± 0.17	1.40 ± 0.07
HD 202314	G6 Ib-IIa Ca1 Ba0.5	3.45 ± 0.11	0.61 ± 0.39	1.03 ± 0.07	0.87 ± 0.16	0.57 ± 0.16	1.23 ± 0.08
HD 58367	G6 IIb	3.24 ± 0.10	0.95 ± 0.35	1.09 ± 0.07	1.14 ± 0.17	0.60 ± 0.14	1.13 ± 0.05
HD 27277	G6 III	2.61 ± 0.07	0.44 ± 0.33	0.99 ± 0.05	1.13 ± 0.12	0.80 ± 0.11	1.14 ± 0.05
HD 115617	G6.5 V	2.25 ± 0.06	0.53 ± 0.19	1.28 ± 0.05	1.81 ± 0.10	1.37 ± 0.08	1.27 ± 0.04
HD 333385	G7 Ia	5.54 ± 0.15	1.70 ± 0.42	1.51 ± 0.07	1.19 ± 0.16	-0.09 ± 0.12	-2.05 ± 0.13
HD 25877	G7 II	3.31 ± 0.09	0.93 ± 0.42	1.02 ± 0.08	1.08 ± 0.19	0.59 ± 0.15	1.28 ± 0.07
HD 182694	G7 IIIa	2.67 ± 0.09	0.97 ± 0.34	0.97 ± 0.07	1.14 ± 0.19	0.79 ± 0.13	1.18 ± 0.05
HD 20618	G7 IV	2.27 ± 0.08	0.66 ± 0.24	0.95 ± 0.06	1.18 ± 0.12	0.93 ± 0.09	1.12 ± 0.02
HD 114946	G7 IV	1.96 ± 0.07	0.51 ± 0.20	0.91 ± 0.03	1.25 ± 0.11	1.01 ± 0.09	1.05 ± 0.04
HD 16139	G7.5 IIIa	2.42 ± 0.09	0.63 ± 0.31	0.90 ± 0.06	1.12 ± 0.13	0.74 ± 0.11	1.08 ± 0.04
HD 208606	G8 Ib	4.71 ± 0.17	1.72 ± 0.69	1.37 ± 0.16	1.27 ± 0.38	0.58 ± 0.26	1.91 ± 0.15
HD 122563	G8: III: Fe-5	0.84 ± 0.04	0.18 ± 0.17	0.07 ± 0.08	0.26 ± 0.18	0.26 ± 0.02	-0.01 ± 0.03
HD 104979	G8 III Ba1 CN0.5 CH1	2.34 ± 0.07	0.72 ± 0.37	0.85 ± 0.12	1.21 ± 0.20	0.76 ± 0.12	0.97 ± 0.08
HD 135722	G8 III Fe-1	2.33 ± 0.07	0.80 ± 0.21	0.95 ± 0.07	1.15 ± 0.13	0.79 ± 0.11	0.98 ± 0.06
HD 101501	G8 V	2.27 ± 0.06	0.64 ± 0.22	1.25 ± 0.05	1.88 ± 0.14	1.42 ± 0.09	1.34 ± 0.04
HD 75732	G8 V	2.37 ± 0.10	0.90 ± 0.37	1.87 ± 0.06	2.16 ± 0.17	2.05 ± 0.15	2.32 ± 0.05
HD 170820	G9 II CN1 H _{δ} 1	3.71 ± 0.13	0.78 ± 0.60	1.03 ± 0.15	0.98 ± 0.28	0.45 ± 0.26	1.42 ± 0.16
HD 222093	G9 III	2.52 ± 0.09	0.88 ± 0.29	1.04 ± 0.07	1.17 ± 0.16	0.87 ± 0.14	1.09 ± 0.04
HD 165782	K0 Ia	5.69 ± 0.13	1.72 ± 0.54	1.38 ± 0.06	0.85 ± 0.17	-0.12 ± 0.09	-0.75 ± 0.12
HD 44391	K0 Ib	3.76 ± 0.14	1.44 ± 0.47	1.10 ± 0.10	1.28 ± 0.25	0.68 ± 0.22	1.66 ± 0.09
HD 179870	K0 II	3.06 ± 0.12	1.49 ± 0.42	1.01 ± 0.12	1.32 ± 0.26	0.74 ± 0.18	1.34 ± 0.07
HD 100006	K0 III	2.53 ± 0.10	0.67 ± 0.32	1.01 ± 0.06	1.18 ± 0.14	0.74 ± 0.15	1.16 ± 0.07
HD 145675	K0 V	2.19 ± 0.13	1.28 ± 0.33	1.88 ± 0.07	2.76 ± 0.20	2.07 ± 0.16	2.60 ± 0.05
HD 164349	K0.5 IIb	3.05 ± 0.12	1.66 ± 0.41	1.04 ± 0.12	1.28 ± 0.24	0.74 ± 0.21	1.41 ± 0.10
HD 9852	K0.5 III CN1	3.09 ± 0.14	1.17 ± 0.43	1.08 ± 0.12	1.37 ± 0.26	0.79 ± 0.23	1.69 ± 0.10
HD 63302	K1 Ia-Iab	4.74 ± 0.18	1.91 ± 0.82	1.49 ± 0.20	1.72 ± 0.40	1.01 ± 0.44	2.78 ± 0.26
HD 36134	K1 - III Fe-0.5	2.58 ± 0.10	0.75 ± 0.29	1.08 ± 0.07	1.26 ± 0.17	1.03 ± 0.17	1.35 ± 0.06
HD 91810	K1 - IIIb CN1.5 Ca1	2.98 ± 0.13	0.65 ± 0.45	1.28 ± 0.11	1.35 ± 0.22	1.08 ± 0.23	1.87 ± 0.10
HD 25975	K1 III	2.30 ± 0.09	0.90 ± 0.27	1.24 ± 0.06	1.68 ± 0.14	1.29 ± 0.13	1.33 ± 0.04
HD 165438	K1 IV	2.30 ± 0.10	1.03 ± 0.32	1.27 ± 0.08	1.54 ± 0.18	1.40 ± 0.14	1.52 ± 0.05
HD 142091	K1 IVa	2.38 ± 0.10	0.81 ± 0.38	1.33 ± 0.09	1.58 ± 0.20	1.35 ± 0.16	1.57 ± 0.07
HD 10476	K1 V	2.22 ± 0.09	1.25 ± 0.21	1.50 ± 0.05	2.14 ± 0.16	1.82 ± 0.10	1.54 ± 0.04
HD 212466	K2 O-Ia	6.13 ± 0.22	3.22 ± 1.05	1.81 ± 0.17	1.88 ± 0.42	0.53 ± 0.27	1.29 ± 0.14
HD 2901	K2 III Fe-1	2.40 ± 0.06	0.68 ± 0.25	1.00 ± 0.07	1.17 ± 0.15	1.32 ± 0.20	1.54 ± 0.04
HD 132935	K2 III	2.77 ± 0.08	0.55 ± 0.32	1.08 ± 0.09	1.11 ± 0.17	1.14 ± 0.21	1.45 ± 0.06
HD 137759	K2 III	2.60 ± 0.11	1.36 ± 0.33	1.23 ± 0.09	1.60 ± 0.20	1.21 ± 0.20	1.79 ± 0.09
HD 3765	K2 V	2.22 ± 0.10	1.66 ± 0.30	2.05 ± 0.07	2.71 ± 0.22	2.44 ± 0.15	2.17 ± 0.05
HD 23082	K2.5 II	3.56 ± 0.15	1.73 ± 0.54	1.16 ± 0.18	1.56 ± 0.32	1.20 ± 0.40	2.61 ± 0.20
HD 187238	K3 Iab-Ib	4.02 ± 0.16	2.06 ± 0.66	1.45 ± 0.20	1.61 ± 0.34	1.23 ± 0.45	3.09 ± 0.25
HD 16068	K3 II-III	3.34 ± 0.13	1.36 ± 0.54	1.05 ± 0.19	1.50 ± 0.32	1.12 ± 0.35	2.43 ± 0.16
HD 221246	K3 III	3.33 ± 0.13	1.34 ± 0.39	1.26 ± 0.13	1.39 ± 0.22	1.23 ± 0.32	2.26 ± 0.13
HD 178208	K3 III	2.87 ± 0.12	1.62 ± 0.42	1.38 ± 0.14	1.77 ± 0.26	1.36 ± 0.31	2.42 ± 0.12
HD 35620	K3 III Fe1	2.98 ± 0.14	1.09 ± 0.56	1.12 ± 0.16	1.36 ± 0.30	1.35 ± 0.35	2.38 ± 0.16
HD 99998	K3+ III Fe-0.5	2.83 ± 0.11	0.75 ± 0.36	1.00 ± 0.12	1.46 ± 0.21	1.61 ± 0.34	2.16 ± 0.07
HD 114960	K3.5 IIIb CN0.5 CH0.5	2.93 ± 0.14	1.35 ± 0.39	1.43 ± 0.15	1.76 ± 0.25	1.47 ± 0.37	2.77 ± 0.15
HD 219134	K3 V	2.44 ± 0.09	1.29 ± 0.46	2.19 ± 0.08	2.86 ± 0.19	2.79 ± 0.14	2.73 ± 0.04
HD 185622	K4 Ib	4.30 ± 0.17	2.37 ± 0.61	1.50 ± 0.23	1.78 ± 0.34	1.55 ± 0.56	3.74 ± 0.30
HD 201065	K4 Ib-II	3.61 ± 0.15	1.87 ± 0.46	1.15 ± 0.17	1.61 ± 0.30	1.32 ± 0.42	2.79 ± 0.17
HD 207991	K4- III	2.83 ± 0.12	0.59 ± 0.40	1.11 ± 0.14	1.14 ± 0.20	1.64 ± 0.34	2.18 ± 0.07
HD 45977	K4 V	2.28 ± 0.09	1.06 ± 0.40	2.80 ± 0.07	2.95 ± 0.20	3.21 ± 0.19	3.49 ± 0.05
HD 216946	K5 Ib	3.84 ± 0.14	1.95 ± 0.47	1.19 ± 0.21	1.96 ± 0.32	1.76 ± 0.52	3.49 ± 0.21
HD 181596	K5 III	3.31 ± 0.09	1.76 ± 0.30	1.02 ± 0.15	1.44 ± 0.24	1.81 ± 0.42	2.74 ± 0.09
HD 36003	K5 V	2.19 ± 0.09	1.51 ± 0.26	2.86 ± 0.06	3.08 ± 0.16	3.47 ± 0.15	3.03 ± 0.04
HD 120477	K5.5 III	2.89 ± 0.10	1.21 ± 0.35	1.39 ± 0.14	1.63 ± 0.22	1.90 ± 0.44	2.79 ± 0.12
HD 3346	K6 IIIa	2.89 ± 0.09	1.04 ± 0.37	1.01 ± 0.13	1.49 ± 0.21	1.99 ± 0.42	2.59 ± 0.09
HD 181475	K7 IIa	3.97 ± 0.16	1.60 ± 0.57	1.22 ± 0.22	1.61 ± 0.34	1.69 ± 0.52	3.43 ± 0.21
HD 194193	K7 III	3.05 ± 0.13	1.08 ± 0.31	1.10 ± 0.14	1.45 ± 0.20	1.95 ± 0.43	2.60 ± 0.09
HD 237903	K7 V	2.13 ± 0.08	1.88 ± 0.21	2.83 ± 0.06	2.70 ± 0.15	3.65 ± 0.16	3.69 ± 0.02
HD 201092	K7 V	1.71 ± 0.06	2.66 ± 0.38	2.68 ± 0.15	2.36 ± 0.28	3.72 ± 0.15	3.43 ± 0.07
HD 213893	M0 IIIb	2.81 ± 0.08	1.13 ± 0.29	1.25 ± 0.12	1.63 ± 0.17	2.05 ± 0.41	2.40 ± 0.06
HD 19305	M0 V	2.17 ± 0.08	2.19 ± 0.23	3.09 ± 0.08	2.62 ± 0.15	3.76 ± 0.17	4.18 ± 0.04
HD 236697	M0.5 Ib	3.93 ± 0.16	2.07 ± 0.56	1.18 ± 0.23	1.75 ± 0.36	2.13 ± 0.63	3.74 ± 0.22

Table 9
(Continued)

Object	Spectral Type	Ca II (0.866 μ m)	Na I (1.14 μ m)	Al I (1.313 μ m)	Mg I (1.485 μ m)	Mg I (1.711 μ m)	Na I (2.206 μ m)
HD 209290	M0.5 V	1.61 \pm 0.08	2.01 \pm 0.27	2.87 \pm 0.07	2.04 \pm 0.14	3.54 \pm 0.17	4.88 \pm 0.03
HD 339034	M1 Ia	5.22 \pm 0.28	3.73 \pm 1.00	1.70 \pm 0.32	2.03 \pm 0.55	0.83 \pm 0.56	3.38 \pm 0.37
HD 14404	M1–Iab–Ib	4.11 \pm 0.15	2.04 \pm 0.58	1.11 \pm 0.22	1.79 \pm 0.38	1.46 \pm 0.63	3.52 \pm 0.23
HD 39801	M1–M2 Ia–Iab	3.94 \pm 0.15	2.43 \pm 0.64	1.42 \pm 0.27	1.91 \pm 0.38	2.04 \pm 0.68	4.12 \pm 0.28
HD 204724	M1+ III	3.45 \pm 0.12	1.46 \pm 0.36	1.25 \pm 0.17	1.24 \pm 0.21	1.90 \pm 0.47	3.38 \pm 0.18
HD 42581	M1 V	1.54 \pm 0.06	2.58 \pm 0.28	2.96 \pm 0.06	1.73 \pm 0.11	3.25 \pm 0.17	5.36 \pm 0.03
HD 35601	M1.5 Iab–Ib	4.14 \pm 0.18	3.20 \pm 0.71	1.20 \pm 0.29	2.00 \pm 0.48	1.86 \pm 0.64	3.77 \pm 0.28
BD +60 265	M1.5 Ib	4.09 \pm 0.18	2.81 \pm 0.61	1.18 \pm 0.24	1.85 \pm 0.35	1.48 \pm 0.62	3.51 \pm 0.33
HD 36395	M1.5 V	1.60 \pm 0.07	4.02 \pm 0.23	3.52 \pm 0.08	2.34 \pm 0.18	3.89 \pm 0.21	7.49 \pm 0.06
HD 206936	M2–Ia	4.23 \pm 0.20	3.42 \pm 1.00	1.67 \pm 0.31	1.78 \pm 0.62	1.57 \pm 0.62	3.81 \pm 0.41
HD 10465	M2 Ib	4.03 \pm 0.14	2.81 \pm 0.55	1.35 \pm 0.28	1.63 \pm 0.38	2.40 \pm 0.69	3.88 \pm 0.22
HD 23475	M2 II	3.62 \pm 0.12	1.94 \pm 0.55	1.31 \pm 0.22	1.70 \pm 0.37	2.37 \pm 0.57	3.82 \pm 0.22
HD 120052	M2 III	2.85 \pm 0.09	0.85 \pm 0.40	1.11 \pm 0.14	1.83 \pm 0.26	2.42 \pm 0.44	2.49 \pm 0.07
HD 95735	M2 V	1.43 \pm 0.04	2.23 \pm 0.28	2.36 \pm 0.07	1.19 \pm 0.16	2.13 \pm 0.16	3.00 \pm 0.09
Gl 806	M2 V	1.25 \pm 0.08	3.01 \pm 0.26	2.39 \pm 0.07	1.02 \pm 0.12	2.18 \pm 0.17	4.11 \pm 0.09
HD 219734	M2.5 III Ba0.5	3.19 \pm 0.12	1.27 \pm 0.40	1.29 \pm 0.17	1.73 \pm 0.28	2.33 \pm 0.51	3.20 \pm 0.12
Gl 381	M2.5 V	1.11 \pm 0.07	3.10 \pm 0.21	2.48 \pm 0.08	1.01 \pm 0.16	1.97 \pm 0.16	4.47 \pm 0.07
Gl 581	M2.5 V	0.98 \pm 0.05	3.38 \pm 0.19	2.39 \pm 0.06	0.78 \pm 0.16	1.56 \pm 0.16	4.71 \pm 0.09
RW Cyg	M3 to M4 Ia–Iab	3.96 \pm 0.19	2.87 \pm 0.70	1.45 \pm 0.29	1.93 \pm 0.42	1.38 \pm 0.67	4.19 \pm 0.39
CD –31 4916	M3 Iab–Ia	3.42 \pm 0.14	1.47 \pm 0.68	1.05 \pm 0.24	2.02 \pm 0.41	2.25 \pm 0.69	3.98 \pm 0.32
HD 14469	M3–M4 Iab	3.42 \pm 0.10	2.26 \pm 0.54	1.17 \pm 0.26	2.16 \pm 0.46	2.07 \pm 0.78	4.25 \pm 0.30
HD 40239	M3 IIb	3.36 \pm 0.10	2.02 \pm 0.33	1.23 \pm 0.18	1.64 \pm 0.28	2.30 \pm 0.60	3.67 \pm 0.18
HD 39045	M3 III	2.63 \pm 0.10	1.22 \pm 0.31	1.00 \pm 0.16	1.86 \pm 0.23	2.41 \pm 0.53	3.04 \pm 0.08
Gl 388	M3 V	0.76 \pm 0.08	4.56 \pm 0.25	2.63 \pm 0.09	1.09 \pm 0.17	2.12 \pm 0.20	5.80 \pm 0.09
HD 14488	M3.5 Iab Fe–1 var?	3.08 \pm 0.10	2.25 \pm 0.61	1.08 \pm 0.26	2.04 \pm 0.42	2.34 \pm 0.77	4.33 \pm 0.32
HD 28487	M3.5 III Ca–0.5	2.68 \pm 0.08	0.46 \pm 0.35	1.14 \pm 0.16	1.63 \pm 0.32	2.63 \pm 0.58	3.05 \pm 0.12
Gl 273	M3.5 V	1.13 \pm 0.05	3.58 \pm 0.28	2.51 \pm 0.07	0.71 \pm 0.18	1.43 \pm 0.17	4.28 \pm 0.10
HD 19058	M4+ IIIa	2.79 \pm 0.09	0.73 \pm 0.38	0.98 \pm 0.18	1.82 \pm 0.32	2.74 \pm 0.61	3.59 \pm 0.12
HD 214665	M4+ III	2.91 \pm 0.10	0.88 \pm 0.51	1.44 \pm 0.28	1.73 \pm 0.44	2.40 \pm 0.62	3.61 \pm 0.16
HD 4408	M4 III	3.14 \pm 0.11	1.37 \pm 0.32	1.14 \pm 0.18	1.77 \pm 0.28	2.44 \pm 0.62	3.60 \pm 0.14
HD 27598	M4– III	2.76 \pm 0.09	0.47 \pm 0.33	1.04 \pm 0.17	1.82 \pm 0.27	2.57 \pm 0.57	2.92 \pm 0.11
Gl 213	M4 V	0.69 \pm 0.08	4.78 \pm 0.22	2.52 \pm 0.07	0.52 \pm 0.17	1.06 \pm 0.17	3.72 \pm 0.13
Gl 299	M4 V	0.75 \pm 0.09	5.68 \pm 0.19	2.66 \pm 0.07	0.22 \pm 0.20	0.59 \pm 0.15	2.86 \pm 0.14
HD 204585	M4.5 IIIa	3.00 \pm 0.08	1.64 \pm 0.33	1.19 \pm 0.24	1.68 \pm 0.30	2.48 \pm 0.67	4.26 \pm 0.20
Gl 268AB	M4.5 V	0.07 \pm 0.10	6.67 \pm 0.25	2.21 \pm 0.09	0.44 \pm 0.18	0.82 \pm 0.18	6.52 \pm 0.10
HD 156014	M5 Ib–II	2.48 \pm 0.09	1.78 \pm 0.33	1.21 \pm 0.24	1.98 \pm 0.37	2.73 \pm 0.69	4.18 \pm 0.15
HD 175865	M5 III	2.70 \pm 0.08	1.53 \pm 0.40	1.14 \pm 0.21	1.89 \pm 0.29	2.53 \pm 0.67	4.13 \pm 0.15
Gl 51	M5 V	-0.60 \pm 0.14	7.82 \pm 0.29	2.73 \pm 0.13	0.50 \pm 0.29	0.61 \pm 0.25	6.79 \pm 0.15
Gl 866ABC	M5 V	-0.54 \pm 0.17	10.62 \pm 0.28	2.35 \pm 0.17	0.25 \pm 0.23	-0.02 \pm 0.25	6.44 \pm 0.15
HD 94705	M5.5 III:	2.22 \pm 0.09	1.18 \pm 0.35	1.43 \pm 0.20	1.85 \pm 0.30	2.73 \pm 0.63	4.33 \pm 0.16
HD 196610	M6 III	1.96 \pm 0.08	1.65 \pm 0.37	1.35 \pm 0.22	1.96 \pm 0.29	2.57 \pm 0.68	3.67 \pm 0.13
HD 18191	M6– III:	2.31 \pm 0.08	1.02 \pm 0.40	1.32 \pm 0.20	1.96 \pm 0.32	2.82 \pm 0.61	3.88 \pm 0.19
Gl 406	M6 V	-0.86 \pm 0.21	11.88 \pm 0.25	2.34 \pm 0.19	-0.00 \pm 0.21	-0.25 \pm 0.30	7.01 \pm 0.17
GJ 1111	M6.5 V	-1.62 \pm 0.24	12.22 \pm 0.39	2.32 \pm 0.22	0.20 \pm 0.36	-0.46 \pm 0.31	5.06 \pm 0.23
HD 14386	M5e–M9e III	0.42 \pm 0.23	0.78 \pm 0.44	-0.00 \pm 0.25	-0.09 \pm 0.55	1.43 \pm 0.46	1.39 \pm 0.32
HD 108849	M7– III:	1.46 \pm 0.12	0.84 \pm 0.34	1.13 \pm 0.23	2.02 \pm 0.47	2.82 \pm 0.75	4.15 \pm 0.19
HD 207076	M7– III:	1.76 \pm 0.13	1.29 \pm 0.31	1.21 \pm 0.20	1.92 \pm 0.42	2.48 \pm 0.65	3.51 \pm 0.12
Gl 644C	M7 V	-1.75 \pm 0.27	12.72 \pm 0.31	2.54 \pm 0.22	0.24 \pm 0.37	-0.57 \pm 0.34	4.37 \pm 0.26
MY Cep	M7–M7.5 I	1.94 \pm 0.13	2.19 \pm 0.77	1.40 \pm 0.25	2.37 \pm 0.49	2.12 \pm 0.77	4.20 \pm 0.24
HD 69243	M6e–M9e III	0.15 \pm 0.26	1.26 \pm 0.47	0.52 \pm 0.29	-0.47 \pm 0.95	1.77 \pm 0.71	2.13 \pm 0.68
BRI B2339–0447	M7–8 III	0.72 \pm 0.15	0.88 \pm 0.47	1.69 \pm 0.15	1.79 \pm 0.68	2.35 \pm 0.60	3.02 \pm 0.22
IRAS 01037+1219	M8 III	0.54 \pm 2.54	1.82 \pm 0.68	0.83 \pm 0.30	-0.32 \pm 0.84	1.37 \pm 0.55	2.22 \pm 0.26
Gl 752B	M8 V	-1.45 \pm 0.30	12.56 \pm 0.38	2.05 \pm 0.33	0.25 \pm 0.43	-0.62 \pm 0.40	5.02 \pm 0.28
LP 412–31	M8 V	-2.63 \pm 0.31	14.84 \pm 0.36	2.60 \pm 0.29	0.20 \pm 0.37	-0.80 \pm 0.40	6.88 \pm 0.26
IRAS 21284–0747	M8–9 III	0.42 \pm 0.27	2.20 \pm 0.60	0.78 \pm 0.26	-1.25 \pm 1.06	1.65 \pm 0.59	1.49 \pm 0.68
IRAS 14436–0703	M8–9 III	0.54 \pm 0.36	4.99 \pm 0.79	1.31 \pm 0.45	-4.24 \pm 1.78	1.74 \pm 0.78	1.20 \pm 0.97
IRAS 14303–1042	M8–9 III	0.72 \pm 0.35	0.98 \pm 1.18	1.37 \pm 0.56	-4.68 \pm 1.66	0.59 \pm 0.56	0.20 \pm 0.86
IRAS 15060+0947	M9 III	0.08 \pm 0.27	2.15 \pm 0.52	1.18 \pm 0.24	1.34 \pm 0.81	2.46 \pm 0.71	3.29 \pm 0.20
BRI B1219–1336	M9 III	0.79 \pm 0.18	0.75 \pm 0.57	0.78 \pm 0.24	-0.52 \pm 0.67	2.28 \pm 0.62	1.23 \pm 0.51
DENIS–P J104814.7–395606.1	M9 V	-2.79 \pm 0.35	13.89 \pm 0.49	1.51 \pm 0.37	0.15 \pm 0.53	-1.17 \pm 0.48	2.44 \pm 0.31
LP 944–20	M9 V	-1.62 \pm 0.57	12.27 \pm 0.48	1.21 \pm 0.44	-0.08 \pm 0.46	-1.12 \pm 0.53	2.34 \pm 0.34
LHS 2065	M9 V	-1.41 \pm 0.38	14.23 \pm 0.41	1.78 \pm 0.31	0.31 \pm 0.30	-1.30 \pm 0.48	5.78 \pm 0.26
LHS 2924	M9 V	-1.20 \pm 0.44	13.62 \pm 0.50	1.80 \pm 0.40	0.05 \pm 0.43	-1.18 \pm 0.52	4.51 \pm 0.35
BRI B0021–0214	M9.5 V	-4.46 \pm 0.87	13.92 \pm 0.70	1.41 \pm 0.56	-0.24 \pm 0.58	-1.54 \pm 0.65	2.64 \pm 0.44
IRAS 14086–0703	M10+ III	0.78 \pm 6.59	5.96 \pm 1.19	0.37 \pm 0.59	-2.43 \pm 1.02	-0.35 \pm 0.55	0.08 \pm 0.55

Table 10
Molecular Features in FGKM Spectra

Wavelength (μm) (1)	Transition (2)	References (3)
TiO		
0.82009172 <i>R</i> head	1–0 band of δ ($b^1\Pi - a^1\Delta$)	1
0.82081 <i>R</i> ₃ head	0–2 band of γ ($A^3\Phi - X^3\Delta$)	2
0.82523 <i>R</i> ₂ head	0–2 band of γ ($A^3\Phi - X^3\Delta$)	2
0.82720357 <i>R</i> head	2–1 band of δ ($b^1\Pi - a^1\Delta$)	1
0.82913 <i>R</i> ₃ head	1–3 band of γ ($A^3\Phi - X^3\Delta$)	2
0.83052 <i>R</i> ₁ head	0–2 band of γ ($A^3\Phi - X^3\Delta$)	2
0.83368 <i>R</i> ₂ head	1–3 band of γ ($A^3\Phi - X^3\Delta$)	2
0.83748 <i>R</i> ₃ head	2–4 band of γ ($A^3\Phi - X^3\Delta$)	2
0.83888 <i>R</i> ₁ head	1–3 band of γ ($A^3\Phi - X^3\Delta$)	2
0.84195 <i>R</i> ₂ head	2–4 band of γ ($A^3\Phi - X^3\Delta$)	2
0.8434 <i>R</i> ₁ head	0–0 band of ϵ ($E^3\Pi - X^3\Delta$)	3
0.8444 <i>R</i> ₂ head	0–0 band of ϵ ($E^3\Pi - X^3\Delta$)	3
0.8454 <i>R</i> ₃ head	0–0 band of ϵ ($E^3\Pi - X^3\Delta$)	3
0.8497 <i>R</i> ₁ head	1–1 band of ϵ ($E^3\Pi - X^3\Delta$)	3
0.85078 <i>R</i> ₂ head	3–5 band of γ ($A^3\Phi - X^3\Delta$)	2
0.8508 <i>R</i> ₂ head	1–1 band of ϵ ($E^3\Pi - X^3\Delta$)	3
0.8518 <i>R</i> ₃ head	1–1 band of ϵ ($E^3\Pi - X^3\Delta$)	3
0.85183 <i>Q</i> ₂ head	3–5 band of γ ($A^3\Phi - X^3\Delta$)	2
0.85608 <i>R</i> ₁ head	3–5 band of γ ($A^3\Phi - X^3\Delta$)	2
0.8562 <i>R</i> ₁ head	2–2 band of ϵ ($E^3\Pi - X^3\Delta$)	3
0.8571 <i>R</i> ₂ head	2–2 band of ϵ ($E^3\Pi - X^3\Delta$)	3
0.85718 <i>Q</i> ₁ head	3–5 band of γ ($A^3\Phi - X^3\Delta$)	2
0.8582 <i>R</i> ₃ head	2–2 band of ϵ ($E^3\Pi - X^3\Delta$)	3
0.886207 <i>R</i> head	0–0 band of δ ($b^1\Pi - a^1\Delta$)	4
0.887093 <i>Q</i> head	0–0 band of δ ($b^1\Pi - a^1\Delta$)	4
0.893983 <i>R</i> head	1–1 band of δ ($b^1\Pi - a^1\Delta$)	4
0.90171 <i>R</i> head	2–2 band of δ ($b^1\Pi - a^1\Delta$)	4
0.9211 <i>R</i> ₁ head	0–1 band of ϵ ($E^3\Pi - X^3\Delta$)	2
0.9221 <i>R</i> ₂ head	0–1 band of ϵ ($E^3\Pi - X^3\Delta$)	2
0.9233 <i>R</i> ₃ head	0–1 band of ϵ ($E^3\Pi - X^3\Delta$)	2
0.9279 <i>R</i> ₁ head	1–2 band of ϵ ($E^3\Pi - X^3\Delta$)	2
0.9289 <i>R</i> ₂ head	1–2 band of ϵ ($E^3\Pi - X^3\Delta$)	2
0.9300 <i>R</i> ₃ head	1–2 band of ϵ ($E^3\Pi - X^3\Delta$)	2
0.9345 <i>R</i> ₁ head	2–3 band of ϵ ($E^3\Pi - X^3\Delta$)	2
0.9356 <i>R</i> ₂ head	2–3 band of ϵ ($E^3\Pi - X^3\Delta$)	2
0.9368 <i>R</i> ₃ head	2–3 band of ϵ ($E^3\Pi - X^3\Delta$)	2
0.9728 <i>R</i> head	0–1 band of δ ($b^1\Pi - a^1\Delta$)	5
0.9817 <i>R</i> head	1–2 band of δ ($b^1\Pi - a^1\Delta$)	5
0.9902 <i>R</i> head	2–3 band of δ ($b^1\Pi - a^1\Delta$)	5
0.9989 <i>R</i> head	3–4 band of δ ($b^1\Pi - a^1\Delta$)	5
1.0027652 <i>R</i> head	1–0 band of Φ ($b^1\Pi - d^1\Sigma$)	6
1.0140301 <i>R</i> head	2–1 band of Φ ($b^1\Pi - d^1\Sigma$)	6
1.0254435 <i>R</i> head	3–2 band of Φ ($b^1\Pi - d^1\Sigma$)	6
1.1032539 <i>R</i> head	0–0 band of Φ ($b^1\Pi - d^1\Sigma$)	6
1.1160977 <i>R</i> head	1–1 band of Φ ($b^1\Pi - d^1\Sigma$)	6
1.2423352 <i>R</i> head	0–1 band of Φ ($b^1\Pi - d^1\Sigma$)	6
1.2567493 <i>R</i> head	1–2 band of Φ ($b^1\Pi - d^1\Sigma$)	6
CN		
0.91092 ⁵ R ₂₁ head	1–0 band of $A^2\Pi - X^2\Sigma^+$	7, 8
0.91431 <i>R</i> ₂ head	1–0 band of $A^2\Pi - X^2\Sigma^+$	7, 8
0.91709 <i>R</i> ₁ head	1–0 band of $A^2\Pi - X^2\Sigma^+$	7, 8
0.91920 <i>Q</i> ₁ head	1–0 band of $A^2\Pi - X^2\Sigma^+$	7, 8
1.0875 ⁵ R ₂₁ head	0–0 band of $A^2\Pi - X^2\Sigma^+$	7, 8
1.0929 <i>R</i> ₂ head	0–0 band of $A^2\Pi - X^2\Sigma^+$	7, 8
1.0966 <i>R</i> ₁ head	0–0 band of $A^2\Pi - X^2\Sigma^+$	7, 8
1.0999 <i>Q</i> ₁ head	0–0 band of $A^2\Pi - X^2\Sigma^+$	7, 8
1.4078 <i>R</i> ₂ head	0–1 band of $A^2\Pi - X^2\Sigma^+$	7, 9
1.4138 <i>R</i> ₁ head	0–1 band of $A^2\Pi - X^2\Sigma^+$	7, 9
1.4549 <i>R</i> ₂ head	1–2 band of $A^2\Pi - X^2\Sigma^+$	7, 9
1.9649 <i>R</i> ₂ head	3–5 band of $A^2\Pi - X^2\Sigma^+$	10
2.0470 <i>R</i> ₂ head	3–5 band of $A^2\Pi - X^2\Sigma^+$	10
2.1349 <i>R</i> ₂ head	3–5 band of $A^2\Pi - X^2\Sigma^+$	10
2.2236 <i>R</i> ₂ head	3–5 band of $A^2\Pi - X^2\Sigma^+$	10

Table 10
(Continued)

Wavelength (μm) (1)	Transition (2)	References (3)
CrH		
0.8613 head	0–0 band of $A^6\Sigma^+ - X^6\Sigma^+$	8
FeH		
0.8964 <i>R</i> head	1–0 band of $F^4\Delta - X^4\Delta$	11
0.9899 <i>R</i> head	0–0 band of $F^4\Delta - X^4\Delta$	11
1.1942 <i>R</i> head	0–1 band of $F^4\Delta - X^4\Delta$	11
1.2392 <i>R</i> head	1–2 band of $F^4\Delta - X^4\Delta$	11
1.58306 head	$E^4\Pi - A^4\Pi$	12
1.59161 head	$E^4\Pi - A^4\Pi$	12
1.62501 head	$E^4\Pi - A^4\Pi$	12
H ₂ O		
0.89–0.99	$3\nu_3, \nu_1 + 2\nu_3, 2\nu_1 + \nu_3, 3\nu_1, \nu_1 + 2\nu_2 + \nu_3, 2\nu_1 + 2\nu_2$	13
1.09–1.20	$\nu_2 + 2\nu_3, \nu_1 + \nu_2 + \nu_3, 2\nu_1 + \nu_2, 3\nu_2 + \nu_3, \nu_1 + 2\nu_2$	13
1.3–1.51	$2\nu_3, \nu_1 + \nu_2, 2\nu_1, 2\nu_2 + \nu_3, \nu_1 + 2\nu_2$	13
1.75–2.05	$\nu_2 + \nu_3, \nu_1 + \nu_2, 3\nu_2$	13
2.3–3.2	$\nu_1, \nu_3, 2\nu_2$	13
ZrO		
0.93019 <i>R</i> ₃ head	0–0 band of $b^3\Pi - a^3\Delta$	14
0.931801 <i>R</i> _(c) head	0–0 band of $b^3\Pi - a^3\Delta$	14
0.931845 <i>R</i> _(d) head	0–0 band of $b^3\Pi - a^3\Delta$	14
0.932060 head	unknown	14
0.93317 <i>R</i> ₂ head	0–0 band of $b^3\Pi - a^3\Delta$	14
0.934417 head	unknown	14
0.935860 head	unknown	14
VO		
1.04626 ⁵ R ₄₃ head	0–0 band of $A^4\Pi - X^4\Sigma^-$	15, 16
1.04822 ⁵ Q ₄₃ head	0–0 band of $A^4\Pi - X^4\Sigma^-$	15, 16
1.45092 <i>R</i> ₃ head	0–0 band of $A^4\Pi - X^4\Sigma^-$	15, 16
1.45300 ⁵ Q ₂₁ head	0–0 band of $A^4\Pi - X^4\Sigma^-$	15, 16
1.17–1.20	0–1 band of $A^4\Pi - X^4\Sigma^-$	16
C ₂		
1.1727 head	2–0 band of $A' ^3\Sigma_g^- - X' ^3\Pi_u$	17
1.7680 head	0–0 band of $A' ^3\Sigma_g^- - X' ^3\Pi_u$	17
¹² CO		
1.5582 <i>R</i> head	3–0 band of $X^1\Sigma^+ - X^1\Sigma^+$	18
1.5779 <i>R</i> head	4–1 band of $X^1\Sigma^+ - X^1\Sigma^+$	18
1.5982 <i>R</i> head	5–2 band of $X^1\Sigma^+ - X^1\Sigma^+$	18
1.6189 <i>R</i> head	6–3 band of $X^1\Sigma^+ - X^1\Sigma^+$	18
1.6401 <i>R</i> head	7–4 band of $X^1\Sigma^+ - X^1\Sigma^+$	18
1.6618 <i>R</i> head	8–5 band of $X^1\Sigma^+ - X^1\Sigma^+$	18
1.6840 <i>R</i> head	9–6 band of $X^1\Sigma^+ - X^1\Sigma^+$	18
1.7067 <i>R</i> head	10–7 band of $X^1\Sigma^+ - X^1\Sigma^+$	18
1.7230 <i>R</i> head	11–8 band of $X^1\Sigma^+ - X^1\Sigma^+$	18
1.7538 <i>R</i> head	12–9 band of $X^1\Sigma^+ - X^1\Sigma^+$	18
2.2935 <i>R</i> head	2–0 band of $X^1\Sigma^+ - X^1\Sigma^+$	18
2.3227 <i>R</i> head	3–1 band of $X^1\Sigma^+ - X^1\Sigma^+$	18
2.3525 <i>R</i> head	4–2 band of $X^1\Sigma^+ - X^1\Sigma^+$	18
2.3830 <i>R</i> head	5–3 band of $X^1\Sigma^+ - X^1\Sigma^+$	18
2.4141 <i>R</i> head	6–4 band of $X^1\Sigma^+ - X^1\Sigma^+$	18
¹³ CO		
2.3448 <i>R</i> head	2–0 band of $X^1\Sigma^+ - X^1\Sigma^+$	18
2.3739 <i>R</i> head	3–1 band of $X^1\Sigma^+ - X^1\Sigma^+$	18
2.4037 <i>R</i> head	4–2 band of $X^1\Sigma^+ - X^1\Sigma^+$	18
2.4341 <i>R</i> head	5–3 band of $X^1\Sigma^+ - X^1\Sigma^+$	18
OH		
3.4–4.2 series	1–0 bands of $X^2\Pi - X^2\Pi$	19
3.4–4.2 series	2–1 bands of $X^2\Pi - X^2\Pi$	19
SiO		
4.0042 <i>R</i> head	2–0 band of $X^1\Sigma^+ - X^1\Sigma^+$	20
4.0437 <i>R</i> head	3–1 band of $X^1\Sigma^+ - X^1\Sigma^+$	20

Table 10
(Continued)

Wavelength (μm)	Transition	References
(1)	(2)	(3)
4.0838 <i>R</i> head	4–2 band of $X^1\Sigma^+ - X^1\Sigma^+$	20
4.1247 <i>R</i> head	5–3 band of $X^1\Sigma^+ - X^1\Sigma^+$	20
4.1663 <i>R</i> head	5–3 band of $X^1\Sigma^+ - X^1\Sigma^+$	20

References. (1) Valenti et al. 1998; (2) Gatterer et al. 1957; (3) Linton & Broida 1977; (4) Phillips 1950; (5) Lockwood 1973; (6) Galehouse et al. 1980; (7) Pearse & Gaydon 1965; (8) Pearse & Gaydon 1976; (9) Herzberg & Phillips 1948; (10) Brocklehurst et al. 1971; (11) Phillips et al. 1987; (12) Wallace & Hinkle 2001; (13) Auman 1967; (14) Phillips et al. 1979; (15) Lagerqvist & Selin (1957); (16) Cheung et al. (1982); (17) Ballik & Ramsay 1963; (18) Goorvitch 1994; (19) Hinkle et al. 1995; (20) Beer et al. (1974).

Deep Sky Survey (UKIDSS) is using YJH photometry in a wide area survey for T dwarfs and cooler objects (Pinfield et al. 2008). Note also the bifurcation between M dwarfs and stars of higher luminosity, which is also seen in the JHK plot. Starting at M0 V, dwarfs initially become bluer in $J - H$ with constant $Y - J$ constant, due to the change in adiabatic temperature gradient (Figure 40). This trend ends at about M4 V at which point dwarfs become redder in $Y - J$ and $J - H$ with decreasing effective temperature. The effect of increasing H_2O absorption in these late-type dwarfs is to decrease the amount of $J - H$ reddening compared with the locus of higher luminosity stars. Late-type M giants have similar colors to late-type dwarfs since both have H_2O absorption in the NIR.

4.3. Notes on Individual Objects

Ten of the 212 stars in the library have spectra and/or $J - H$ versus $H - K$ colors that are different from those expected based on their spectral type. Five of these stars are supergiants displaying emission lines and with redder than normal continua that cannot be explained by standard interstellar reddening (reddening not in the direction of the extinction vector). As explained below, most of these stars are probably PAGB stars. Three of the unusual stars are emission-line Mira variables (TPAGB stars). Of the two remaining unusual stars, one is an M subdwarf misclassified as an M dwarf and the other is an F dwarf with weak emission in some metal lines.

Unusual objects are circled in the $J - H$ versus $H - K$ diagram (see Figure 37):

HD 26015 is classified as F3 V by Gray et al. (2001). The spectrum is normal up to 2.22 μm but at longer wavelengths some metal lines go into weak emission (Ca I doublet at 2.263 and 2.267 μm , Mg I at 2.280 μm , Na I at 2.339 μm , and Mg I at 3.867 μm). The continuum is also slightly bluer than normal for a spectral type of F3V. The star is classified as variable (of unspecified type) in the GCVS and is slightly metal rich ([Fe/H] = 0.2, average from SIMBAD).

HD 179821 is classified as G4 O–Ia by Keenan & McNeil (1989). Strong emission in the Na I doublet at 2.205 and 2.209 μm is seen together with very strong Pfund series absorption longward of the series limit at about 2.33 μm . The expected first CO overtone bands in the K band are absent. From its location in the JHK color–color diagram, the star has a significant NIR excess. The star is classified as a semiregular

variable giant or supergiant (type SRd) in the GCVS. Optical *Hubble Space Telescope (HST)* images of HD 179821 reveal a bright star embedded in faint extended nebulosity (Ueta et al. 2000). Kipper (2008) reviews observations of HD 179821 some of which are consistent with an intermediate-mass PAGB star, while others point to a high-mass post-red-supergiant star.

HD 6474 is classified as G4 Ia by Keenan & McNeil (1989). The spectral continuum is redder than normal, and the JHK colors indicate a NIR excess. Spectral features in the K band appear subdued probably due to veiling and Si I at 3.745 μm is in emission. The star is classified as a semiregular variable (type SRd) in the GCVS and as a UU Her-type variable by Zsoldos (1993). Szczerba et al. (2007) classify UU Her-type variables with NIR excess due to circumstellar dust as probable PAGB stars.

HD 333385 (BD +29° 3865) is classified as G7 Ia by Keenan & McNeil (1989). The star is classified as a slow irregular variable (type L) in the GCVS. The spectrum is clearly unusual showing a number of metal lines in emission, particularly in the K band, where the Na I doublet at 2.205 and 2.209 μm is strong. The first CO overtone bands in the K band appear sharper than those in other late-type G supergiants. Si I at 3.745 μm is in emission. The JHK colors indicate a large NIR excess. Using high-dispersion optical echelle spectra, Klochkova et al. (2000) conclude that HD 333385 is probably a PAGB star.

HD 165782 is classified as K0 Ia by Keenan & McNeil (1989). The spectrum shows weak absorption features in the K band probably due to veiling, and the Na I doublet at 2.205 and 2.209 μm is in emission. The first CO overtone bands in the K band appear sharp and Si I at 3.745 μm is in emission. The JHK colors indicate a NIR excess. The star is classified as a semiregular variable (type SRd) in the GCVS. An OH maser is reported by Nyman et al. (1998), and Omont et al. (1993) classify HD 165782 as a PAGB star.

HD 212466 is classified as K2 O–Ia by Keenan & McNeil (1989). The spectrum shows SiO in emission at 4.00, 4.04, and 4.08 μm , and the first CO overtone bands in the K band appear sharp. The JHK colors indicate a large NIR excess. The star is classified as a semiregular variable (type SRd) in the GCVS. A Si emission feature at 10 μm is cited as evidence of mass loss by Sylvester et al. (1998).

Gl 299 is classified as M4 V by Henry et al. (1994). However, its location below the locus of M dwarfs in the $J - H$ versus $H - K$ plot is more consistent with an M subdwarf (Bessell & Brett 1988, Figure A3). This is confirmed by its spectrum that shows weak CO overtone absorption at 2.29 μm , a weak Na I doublet at 2.205 and 2.209 μm , and weak K I at 1.516 μm , compared with a normal M4 V (e.g., Cushing & Vacca 2006).

HD 14386 (Mira) is classified as M5e-M9e III and as a Mira variable (type M) in the GCVS. This archetypal variable star was observed on three occasions. On 2003 January 14 the emission line due to Paβ (1.28 μm , EW –0.4 Å) was detected, on 2003 September 20 emission lines due to Paγ (1.094 μm , EW –0.9 Å) and Paβ (1.282 μm , EW –0.7 Å) were detected, and on 2003 November 6 the emission line due to Na I (1.269 μm , EW –1.0 Å) was detected. (Nondetections of these lines are roughly EW > –0.2 Å.) Mira-type variables can emit in a variety of metal and hydrogen lines, probably originating in atmospheric shock waves resulting from pulsation (e.g., Richter

Table 11
Synthetic WFCAM Colors

Object (1)	Spectral Type (2)	Z - Y (mag) (3)	Y - J (mag) (4)	J - H (mag) (5)	H - K (mag) (6)	K - L' (mag) (7)
HD 7927	F0 Ia	+0.161	+0.211	+0.257	+0.152	+0.208
HD 135153	F0 Ib-II	+0.113	+0.153	+0.186	+0.087	+0.044
HD 6130	F0 II	+0.147	+0.193	+0.225	+0.090	+0.128
HD 89025	F0 IIIa	+0.052	+0.147	+0.161	+0.033	+0.058
HD 13174	F0 III-IVn	+0.066	+0.155	+0.153	+0.018	+0.053
HD 27397	F0 IV	+0.058	+0.115	+0.107	-0.011	-0.018
HD 108519	F0 V(n)	+0.043	+0.116	+0.144	+0.044	+0.018
HD 173638	F1 II	+0.187	+0.200	+0.222	+0.083	+0.088
HD 213135	F1 V	+0.045	+0.162	+0.175	+0.021	+0.028
BD +38 2803	F2-F5 Ib	+0.106	+0.257	+0.304	+0.085	+0.096
HD 182835	F2 Ib	+0.158	+0.196	+0.214	+0.073	...
HD 40535	F2 III-IV	+0.079	+0.173	+0.185	+0.046	+0.065
HD 164136	kA9hF2mF2 (IV)	+0.080	+0.197	+0.210	+0.031	+0.110
HD 113139	F2 V	+0.084	+0.187	+0.184	+0.026	-0.092
HD 26015	F3 V	+0.061	+0.144	+0.119	-0.014	-0.045
HD 21770	F4 III	+0.050	+0.168	+0.181	+0.030	+0.068
HD 87822	F4 V	+0.065	+0.182	+0.182	+0.038	+0.052
HD 16232	F4 V	+0.050	+0.175	+0.207	+0.035	+0.113
HD 213306	F5 Ib - G1 Ib	+0.181	+0.295	+0.363	+0.084	+0.029
HD 186155	F5 II-III	+0.047	+0.159	+0.158	+0.039	-0.007
HD 17918	F5 III	+0.082	+0.184	+0.190	+0.013	+0.019
HD 218804	F5 V	+0.082	+0.206	+0.242	+0.058	+0.073
HD 27524	F5 V	+0.036	+0.173	+0.183	+0.028	+0.045
HD 75555	F5.5 III-IV	+0.088	+0.210	+0.212	+0.046	...
HD 160365	F6 III-IV	+0.033	+0.159	+0.174	-0.028	+0.012
HD 11443	F6 IV	+0.065	+0.184	+0.243	+0.088	-0.009
HD 215648	F6 V	+0.072	+0.212	+0.230	+0.037	...
HD 201078	F7 II-	+0.099	+0.201	+0.231	+0.081	...
HD 124850	F7 III	+0.093	+0.222	+0.241	+0.032	...
HD 126660	F7 V	+0.055	+0.194	+0.217	+0.061	+0.042
HD 190323	F8 Ia	+0.174	+0.262	+0.278	+0.074	+0.067
HD 51956	F8 Ib	+0.144	+0.280	+0.312	+0.083	+0.003
HD 220657	F8 III	+0.119	+0.278	+0.328	+0.111	+0.122
HD 111844	F8 IV	+0.044	+0.119	+0.105	+0.009	...
HD 219623	F8 V	+0.103	+0.222	+0.258	+0.056	-0.012
HD 27383	F8 V	+0.086	+0.194	+0.213	+0.021	-0.017
HD 102870	F8.5 IV-V	+0.076	+0.220	+0.251	+0.043	+0.033
HD 6903	F9 IIIa	+0.127	+0.268	+0.320	+0.072	+0.043
HD 176051	F9 V	+0.089	+0.254	+0.324	+0.054	-0.037
HD 165908	F9 V metal weak	+0.036	+0.189	+0.235	+0.062	+0.058
HD 114710	F9.5 V	+0.060	+0.194	+0.198	-0.006	+0.025
HD 185018	G0 Ib-II	+0.173	+0.303	+0.364	+0.085	+0.007
HD 109358	G0 V	+0.079	+0.235	+0.294	+0.034	+0.010
HD 74395	G1 Ib	+0.175	+0.298	+0.348	+0.086	+0.062
HD 216219	G1 II-III: Fe-1 CH0.5	+0.096	+0.232	+0.274	+0.054	+0.061
HD 21018	G1 III: CH-1:	+0.175	+0.305	+0.353	+0.102	+0.066
HD 10307	G1 V	+0.092	+0.233	+0.281	+0.037	+0.029
HD 95128	G1 - V Fe-0.5	+0.110	+0.253	+0.273	+0.045	...
HD 20619	G1.5 V	+0.122	+0.278	+0.344	+0.077	+0.053
HD 42454	G2 Ib	+0.264	+0.369	+0.415	+0.122	...
HD 39949	G2 Ib	+0.250	+0.361	+0.424	+0.118	...
HD 3421	G2 Ib-II	+0.175	+0.289	+0.370	+0.075	+0.076
HD 219477	G2 II-III	+0.125	+0.269	+0.320	+0.065	...
HD 126868	G2 IV	+0.107	+0.246	+0.318	+0.074	+0.090
HD 76151	G2 V	+0.100	+0.250	+0.304	+0.083	+0.044
HD 192713	G3 Ib-II Wk H&K comp?	+0.226	+0.345	+0.422	+0.108	+0.085
HD 176123	G3 II	+0.211	+0.345	+0.410	+0.089	+0.098
HD 88639	G3 IIIb Fe-1	+0.169	+0.318	+0.394	+0.069	+0.112
HD 10697	G3 Va	+0.140	+0.279	+0.331	+0.088	+0.082
HD 179821	G4 O-Ia	+0.301	+0.368	+0.394	+0.249	+0.239
HD 6474	G4 Ia	+0.408	+0.472	+0.492	+0.235	+0.217
HD 94481	G4 III-IIIb	+0.163	+0.311	+0.402	+0.083	...
HD 108477	G4 III	+0.181	+0.319	+0.399	+0.099	+0.096
HD 214850	G4 V	+0.103	+0.273	+0.395	+0.108	+0.059

Table 11
(Continued)

Object (1)	Spectral Type (2)	Z - Y (mag) (3)	Y - J (mag) (4)	J - H (mag) (5)	H - K (mag) (6)	K - L' (mag) (7)
HD 190113	G5 Ib	+0.300	+0.428	+0.531	+0.150	+0.133
HD 18474	G5: III: CN-3 CH-2 H _δ -1	+0.162	+0.313	+0.420	+0.045	+0.074
HD 193896	G5 IIIa	+0.229	+0.363	+0.449	+0.124	...
HD 165185	G5 V	+0.056	+0.218	+0.259	+0.055	-0.014
HD 161664	G6 Ib H _δ 1	+0.397	+0.490	+0.565	+0.179	+0.185
HD 202314	G6 Ib-IIa Ca1 Ba0.5	+0.239	+0.357	+0.451	+0.162	+0.161
HD 58367	G6 IIb	+0.203	+0.335	+0.434	+0.099	+0.131
HD 27277	G6 III	+0.238	+0.354	+0.420	+0.094	+0.093
HD 115617	G6.5 V	+0.086	+0.232	+0.285	+0.020	-0.031
HD 333385	G7 Ia	+0.557	+0.562	+0.545	+0.306	+0.594
HD 25877	G7 II	+0.206	+0.328	+0.400	+0.076	+0.081
HD 182694	G7 IIIa	+0.157	+0.318	+0.408	+0.107	+0.044
HD 20618	G7 IV	+0.181	+0.331	+0.439	+0.098	+0.093
HD 114946	G7 IV	+0.165	+0.328	+0.451	+0.094	+0.120
HD 16139	G7.5 IIIa	+0.226	+0.357	+0.458	+0.130	+0.078
HD 208606	G8 Ib	+0.411	+0.494	+0.596	+0.202	+0.099
HD 122563	G8: III: Fe-5	+0.204	+0.374	+0.532	+0.112	+0.051
HD 104979	G8 III Ba1 CN0.5 CH1	+0.184	+0.337	+0.486	+0.098	+0.132
HD 135722	G8 III Fe-1	+0.185	+0.343	+0.495	+0.120	-0.006
HD 101501	G8 V	+0.133	+0.270	+0.332	+0.062	+0.012
HD 75732	G8 V	+0.148	+0.290	+0.364	+0.103	+0.071
HD 170820	G9 II CN1 H _δ 1	+0.455	+0.541	+0.613	+0.221	+0.157
HD 222093	G9 III	+0.202	+0.367	+0.503	+0.102	+0.070
HD 165782	K0 Ia	+0.584	+0.579	+0.551	+0.289	...
HD 44391	K0 Ib	+0.303	+0.429	+0.540	+0.168	+0.117
HD 179870	K0 II	+0.274	+0.386	+0.439	+0.048	-0.016
HD 100006	K0 III	+0.235	+0.380	+0.531	+0.104	+0.109
HD 145675	K0 V	+0.140	+0.290	+0.340	+0.058	-0.017
HD 164349	K0.5 IIb	+0.250	+0.371	+0.470	+0.074	...
HD 9852	K0.5 III CN1	+0.348	+0.472	+0.601	+0.153	+0.092
HD 63302	K1 Ia-Iab	+0.383	+0.486	+0.584	+0.215	+0.205
HD 36134	K1- III Fe-0.5	+0.229	+0.390	+0.538	+0.097	+0.097
HD 91810	K1- IIIb CN1.5 Ca1	+0.263	+0.401	+0.528	+0.134	+0.138
HD 25975	K1 III	+0.149	+0.312	+0.424	+0.075	+0.042
HD 165438	K1 IV	+0.194	+0.350	+0.454	+0.098	...
HD 142091	K1 IVa	+0.199	+0.341	+0.454	+0.084	...
HD 10476	K1 V	+0.147	+0.317	+0.405	+0.095	+0.031
HD 124897	K1.5 III Fe-0.5	+0.246	+0.420	+0.651	+0.127	+0.076
HD 212466	K2 O-Ia	+0.635	+0.619	+0.623	+0.399	+0.302
HD 2901	K2 III Fe-1	+0.284	+0.436	+0.605	+0.096	+0.125
HD 132935	K2 III	+0.298	+0.462	+0.661	+0.164	+0.127
HD 137759	K2 III	+0.264	+0.420	+0.564	+0.140	...
HD 3765	K2 V	+0.166	+0.330	+0.420	+0.080	+0.049
HD 23082	K2.5 II	+0.457	+0.550	+0.699	+0.204	+0.199
HD 187238	K3 Iab-Ib	+0.553	+0.597	+0.729	+0.227	+0.254
HD 16068	K3 II-III	+0.440	+0.538	+0.706	+0.173	+0.223
HD 221246	K3 III	+0.332	+0.472	+0.658	+0.144	+0.178
HD 178208	K3 III	+0.315	+0.453	+0.589	+0.142	...
HD 35620	K3 III Fe1	+0.326	+0.459	+0.618	+0.170	+0.061
HD 99998	K3+ III Fe-0.5	+0.347	+0.526	+0.744	+0.195	+0.144
HD 114960	K3.5 IIIb CN0.5 CH0.5	+0.314	+0.443	+0.616	+0.153	+0.072
HD 219134	K3 V	+0.245	+0.384	+0.512	+0.117	+0.086
HD 185622	K4 Ib	+0.546	+0.622	+0.810	+0.298	...
HD 201065	K4 Ib-II	+0.444	+0.563	+0.753	+0.223	+0.181
HD 207991	K4- III	+0.384	+0.533	+0.771	+0.202	+0.058
HD 45977	K4 V	+0.192	+0.351	+0.480	+0.105	...
HD 216946	K5 Ib	+0.562	+0.660	+0.862	+0.318	+0.211
HD 181596	K5 III	+0.385	+0.525	+0.727	+0.196	+0.154
HD 36003	K5 V	+0.221	+0.388	+0.559	+0.125	+0.021
HD 120477	K5.5 III	+0.372	+0.521	+0.736	+0.211	+0.164
HD 3346	K6 IIIa	+0.364	+0.529	+0.772	+0.230	...
HD 181475	K7 IIa	+0.574	+0.660	+0.853	+0.308	...
HD 194193	K7 III	+0.401	+0.549	+0.811	+0.225	+0.106
HD 237903	K7 V	+0.271	+0.430	+0.608	+0.134	+0.112

Table 11
(Continued)

Object (1)	Spectral Type (2)	Z - Y (mag) (3)	Y - J (mag) (4)	J - H (mag) (5)	H - K (mag) (6)	K - L' (mag) (7)
HD 201092	K7 V	+0.212	+0.374	+0.554	+0.151	...
HD 213893	M0 IIIb	+0.390	+0.526	+0.759	+0.200	+0.086
HD 19305	M0 V	+0.287	+0.437	+0.632	+0.182	+0.074
HD 236697	M0.5 Ib	+0.579	+0.673	+0.839	+0.304	+0.273
HD 209290	M0.5 V	+0.336	+0.476	+0.629	+0.217	+0.195
HD 339034	M1 Ia	+0.983	+0.906	+0.922	+0.491	+0.516
HD 14404	M1–Iab–Ib	+0.613	+0.666	+0.804	+0.303	+0.337
HD 39801	M1–M2 Ia–Iab	+0.474	+0.523	+0.658	+0.111	+0.616
HD 204724	M1+ III	+0.394	+0.491	+0.713	+0.253	+0.085
HD 42581	M1 V	+0.332	+0.456	+0.606	+0.210	+0.199
HD 35601	M1.5 Iab–Ib	+0.638	+0.717	+0.863	+0.362	+0.253
BD +60 265	M1.5 Ib	+0.655	+0.727	+0.870	+0.388	+0.355
HD 36395	M1.5 V	+0.360	+0.487	+0.675	+0.203	+0.104
HD 206936	M2–Ia	+0.603	+0.643	+0.755	+0.409	+0.462
HD 10465	M2 Ib	+0.528	+0.599	+0.756	+0.278	+0.163
HD 23475	M2 II	+0.473	+0.571	+0.813	+0.256	...
HD 120052	M2 III	+0.427	+0.589	+0.841	+0.271	+0.087
HD 95735	M2 V	+0.339	+0.460	+0.512	+0.216	+0.310
Gl 806	M2 V	+0.340	+0.458	+0.562	+0.187	...
HD 219734	M2.5 III Ba0.5	+0.446	+0.570	+0.809	+0.245	+0.084
Gl 381	M2.5 V	+0.398	+0.500	+0.550	+0.242	+0.263
Gl 581	M2.5 V	+0.406	+0.486	+0.523	+0.280	+0.301
RW Cyg	M3 to M4 Ia–Iab	+0.839	+0.820	+0.982	+0.448	+0.356
CD –31 4916	M3 Iab–Ia	+0.637	+0.700	+0.851	+0.342	+0.395
HD 14469	M3–M4 Iab	+0.705	+0.679	+0.805	+0.367	+0.284
HD 40239	M3 IIb	+0.530	+0.626	+0.862	+0.300	+0.212
HD 39045	M3 III	+0.466	+0.593	+0.829	+0.267	+0.172
Gl 388	M3 V	+0.421	+0.504	+0.559	+0.237	+0.249
HD 14488	M3.5 Iab Fe–1 var?	+0.727	+0.724	+0.949	+0.495	+0.331
HD 28487	M3.5 III Ca–0.5	+0.550	+0.623	+0.875	+0.292	+0.165
Gl 273	M3.5 V	+0.476	+0.526	+0.515	+0.284	+0.311
HD 19058	M4+ IIIa	+0.551	+0.603	+0.878	+0.297	+0.075
HD 214665	M4+ III	+0.694	+0.726	+0.954	+0.335	+0.031
HD 4408	M4 III	+0.521	+0.598	+0.856	+0.297	+0.027
HD 27598	M4– III	+0.500	+0.572	+0.820	+0.272	+0.165
Gl 213	M4 V	+0.500	+0.523	+0.464	+0.281	+0.368
Gl 299	M4 V	+0.485	+0.525	+0.411	+0.310	+0.464
HD 204585	M4.5 IIIa	+0.621	+0.590	+0.780	+0.234	...
Gl 268AB	M4.5 V	+0.552	+0.570	+0.535	+0.311	+0.392
HD 156014	M5 Ib–II	+0.647	+0.517	+0.614	+0.097	+0.188
HD 175865	M5 III	+0.648	+0.601	+0.798	+0.229	...
Gl 51	M5 V	+0.601	+0.612	+0.538	+0.331	+0.335
Gl 866ABC	M5 V	+0.727	+0.677	+0.556	+0.370	+0.457
HD 94705	M5.5 III:	+0.755	+0.643	+0.827	+0.333	+0.175
HD 196610	M6 III	+0.851	+0.629	+0.789	+0.284	-0.091
HD 18191	M6– III:	+0.794	+0.669	+0.870	+0.319	-0.012
Gl 406	M6 V	+0.824	+0.719	+0.563	+0.415	+0.513
GJ 1111	M6.5 V	+0.841	+0.726	+0.524	+0.422	+0.516
HD 14386	M5e–M9e III	+1.213	+0.654	+0.519	+0.519	+0.600
HD 108849	M7– III:	+1.151	+0.811	+0.814	+0.414	+0.204
HD 207076	M7– III:	+1.007	+0.649	+0.697	+0.282	+0.498
Gl 644C	M7 V	+0.861	+0.745	+0.505	+0.438	+0.544
MY Cep	M7–M7.5 I	+1.469	+1.246	+1.315	+0.814	+0.919
HD 69243	M6e–M9e III	+1.533	+1.258	+0.738	+0.611	+0.707
BRI B2339–0447	M7 – 8 III	+0.701	+0.589	+0.819	+0.498	+0.590
IRAS 01037+1219	M8 III	+2.767	+2.545	+2.244	+1.787	+2.288
Gl 752B	M8 V	+1.039	+0.824	+0.543	+0.487	+0.590
LP 412–31	M8 V	+1.030	+0.893	+0.630	+0.486	+0.612
IRAS 21284–0747	M8 – 9 III	+1.536	+1.092	+0.693	+0.673	+0.822
IRAS 14436–0703	M8 – 9 III	+1.437	+0.925	+0.575	+0.601	...
IRAS 14303–1042	M8 – 9 III	+1.251	+0.761	+0.586	+0.657	...
IRAS 15060+0947	M9 III	+1.350	+1.011	+1.162	+1.206	...
BRI B1219–1336	M9 III	+1.273	+0.843	+0.602	+0.577	...
DENIS–P J104814.7–395606.1	M9 V	+1.101	+0.879	+0.505	+0.481	+0.681

Table 11
(Continued)

Object (1)	Spectral Type (2)	Z – Y (mag) (3)	Y – J (mag) (4)	J – H (mag) (5)	H – K (mag) (6)	K – L' (mag) (7)
LP 944–20	M9 V	+1.253	+0.994	+0.592	+0.536	+0.750
LHS 2065	M9 V	+1.209	+1.004	+0.698	+0.569	...
LHS 2924	M9 V	+1.209	+0.999	+0.657	+0.536	...
BRI B0021–0214	M9.5 V	+1.244	+1.085	+0.698	+0.591	+0.661
IRAS 14086–0703	M10+ III	+2.219	+2.128	+1.885	+2.054	...
HD 142143	M6.5S to M7S III:	+0.975	+0.787	+0.876	+0.431	+0.256
BD +44 2267	S2.5 Zr 2	+0.456	+0.566	+0.762	+0.242	+0.245
HD 64332	S4.5 Zr 2 Ti 4	+0.488	+0.596	+0.817	+0.285	+0.219
HD 44544	SC5.5 Zr 0.5	+0.812	+0.823	+1.031	+0.414	+0.494
HD 62164	S5–S6 Zr 3 to 4 Ti 0	+0.661	+0.742	+0.972	+0.409	+0.315
HD 76846	C–R2+ IIIa: C2 2.5	+0.374	+0.370	+0.475	+0.175	+0.240
HD 31996	C7,6e(N4)	+0.649	+0.947	+1.279	+1.187	+1.152
HD 44984	C–N4 C2 3.5	+0.638	+0.580	+0.901	+0.437	+0.403
HD 76221	C–N 4.5 C2 5.5 MS 3	+0.620	+0.657	+1.008	+0.645	+0.593
HD 92055	C–N4.5 C2 4.5	+0.651	+0.655	+0.989	+0.480	+0.493
HD 70138	C–J4.5 IIIa: C2 6 j 6	+0.657	+0.482	+0.893	+0.491	+0.622
HD 48664	C–N5 C2 6	+0.745	+0.725	+1.067	+0.646	+0.643
HD 57160	C–J5–C2 5–j 4	+0.627	+0.646	+0.999	+0.582	+0.625

& Wood 2001). The lines are known to come and go depending upon cycle and phase (e.g., Lançon & Wood 2000, in the NIR).

BRI B2339–0447 is classified as M7–8 III by Kirkpatrick et al. (1997) and as a Mira variable (type M) in the GCVS. The spectrum shows Pa γ (1.094 μ m, EW 1.2 \AA), Pa β (1.282 μ m, EW 0.8 \AA), and Br γ (2.166 μ m, EW 0.5 \AA) in emission. Pa δ (1.005 μ m) in emission was also detected but blended with a TiO band head.

IRAS 1403–1042 is classified as M8–9 III by Kirkpatrick et al. (1997) and as a Mira variable (type M) in the GCVS. The spectrum shows Pa γ (1.094 μ m, EW 1.9 \AA) and Pa β (1.282 μ m, EW 4.8 \AA) in emission (see Figure 37). Pa δ (1.005 μ m) in emission was also detected but blended with a TiO band head.

5. SUMMARY

We have constructed a medium resolution ($R \sim 2000$) near-infrared (0.8–5 μ m) spectral library of 210 cool stars. The stars all have well established MK classifications and have near-solar metallicities. The sample covers F, G, K, and M stars with luminosity classes between I and V, and includes some AGB, carbon, and S stars. Sample selection, data reduction, and data calibration are carefully described. The continuum shape of the spectra is measured to an accuracy of a few percent, and the spectra are absolutely flux calibrated using 2MASS photometry. Synthesized color–color diagrams are constructed from the spectra and their use demonstrated. Spectral features are described and detailed lists of atomic and molecular features are tabulated. Several unusual stars in the sample are identified and described. The library is available in digital form from the IRTF Web site.

Observations for the IRTF Spectral Library required a significant investment in telescope time and the authors would like to thank IRTF Director, Alan Tokunaga, and the IRTF TAC for their support. Observing was ably assisted by telescope

operators Bill Golisch, Dave Griep, and Paul Sears. We would also like to thank the IRTF day crew and engineering staff for excellent maintenance of the telescope and instrumentation. Natasha Förster-Schreiber helped us with sample selection during the early stages of the project. J.T.R. would like to thank Katelyn Allers for providing observations of five late-type M giants. M.C.C. acknowledges financial support from the IRTF and by the National Aeronautics and Space Administration through the *Spitzer Space Telescope* Fellowship Program through a contract issued by the Jet Propulsion Laboratory, California Institute of Technology, under a contract with NASA. W.D.V. and M.C.C. acknowledge financial support from IRTF during several trips to Honolulu. This publication makes use of data from the Two Micron All Sky Survey, which is a joint project of the University of Massachusetts and the Infrared Processing and Analysis Center and is funded by NASA and the National Science Foundation. This research has made use of the SIMBAD database, operated at CDS, Strasbourg, France; NASA's Astrophysics Data System Bibliographic Services; and the SpeX Prism Spectral Libraries, maintained by Adam Burgasser.¹⁰ We thank the anonymous referee for a thorough reading of the manuscript and insightful suggestions for improving it.

Facilities: IRTF (SpeX)

APPENDIX

SPECTRAL SEQUENCES

More complete spectral sequences are plotted in this section: F stars (bands I , Y , J , H , K , and L') in Figures 41–58; G stars (bands I , Y , J , H , K , and L') in Figures 59–76; K stars (bands I , Y , J , H , K , and L') in Figures 77–94; and M stars (bands I , Y , J , H , K , and L') in Figures 95–112. For feature identifications see the partial spectral sequences plotted in Figures 7–34.

¹⁰ <http://www.brownndwarfs.org/spexprism>

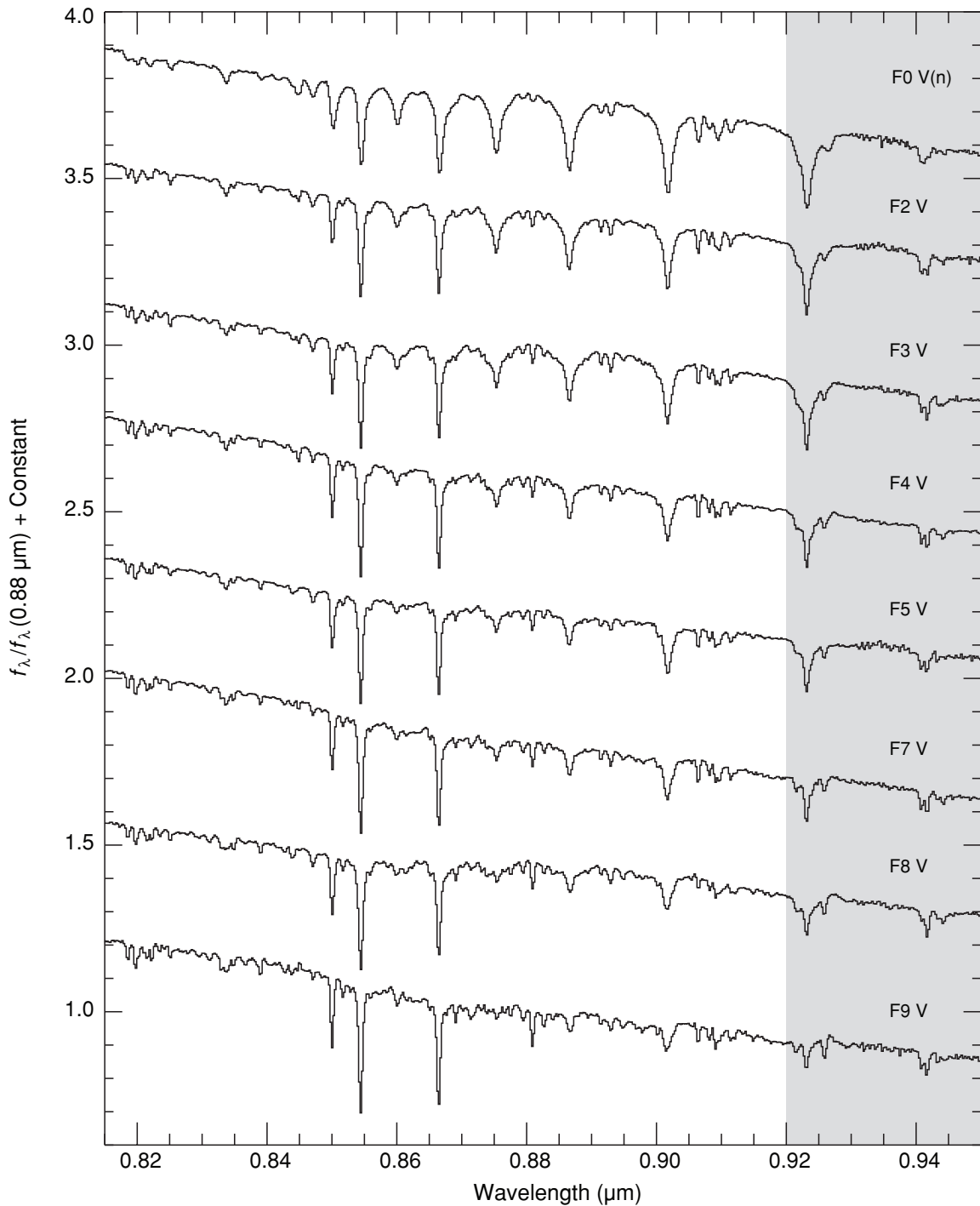


Figure 41. Sequence of F dwarf stars plotted over the I band (0.82 – $0.95 \mu\text{m}$). The spectra are of HD 108519 F0 V(n), HD 113139 (F2 V), HD 26015 (F3 V), HD 87822 (F4 V), HD 218804 (F5 V), HD 126660 (F7 V), HD 27393 (F8 V), and HD 176051 (F9 V). The spectra have been normalized to unity at $0.88 \mu\text{m}$ and offset by constants.

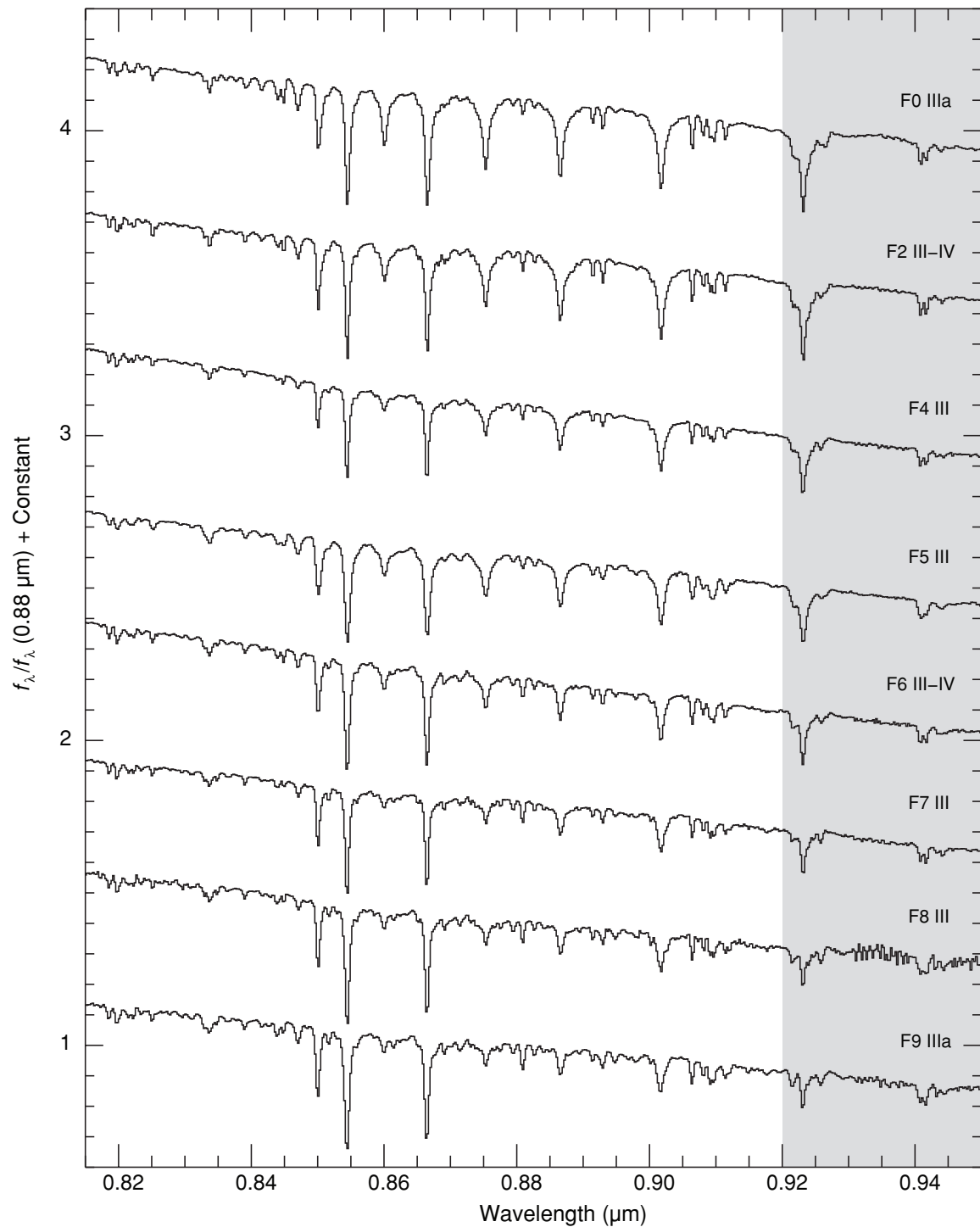


Figure 42. Sequence of F giant stars plotted over the I band (0.82–0.95 μm). The spectra are of HD 89025 (F0 IIIa), HD 40535 (F2 III–IV), HD 21770 (F4 III), HD 17918 (F5 III), HD 160365 (F6 III–IV), HD 124850 (F7 III), HD 220657 (F8 III), and HD 6903 (F9 IIIa). The spectra have been normalized to unity at 0.88 μm and offset by constants.

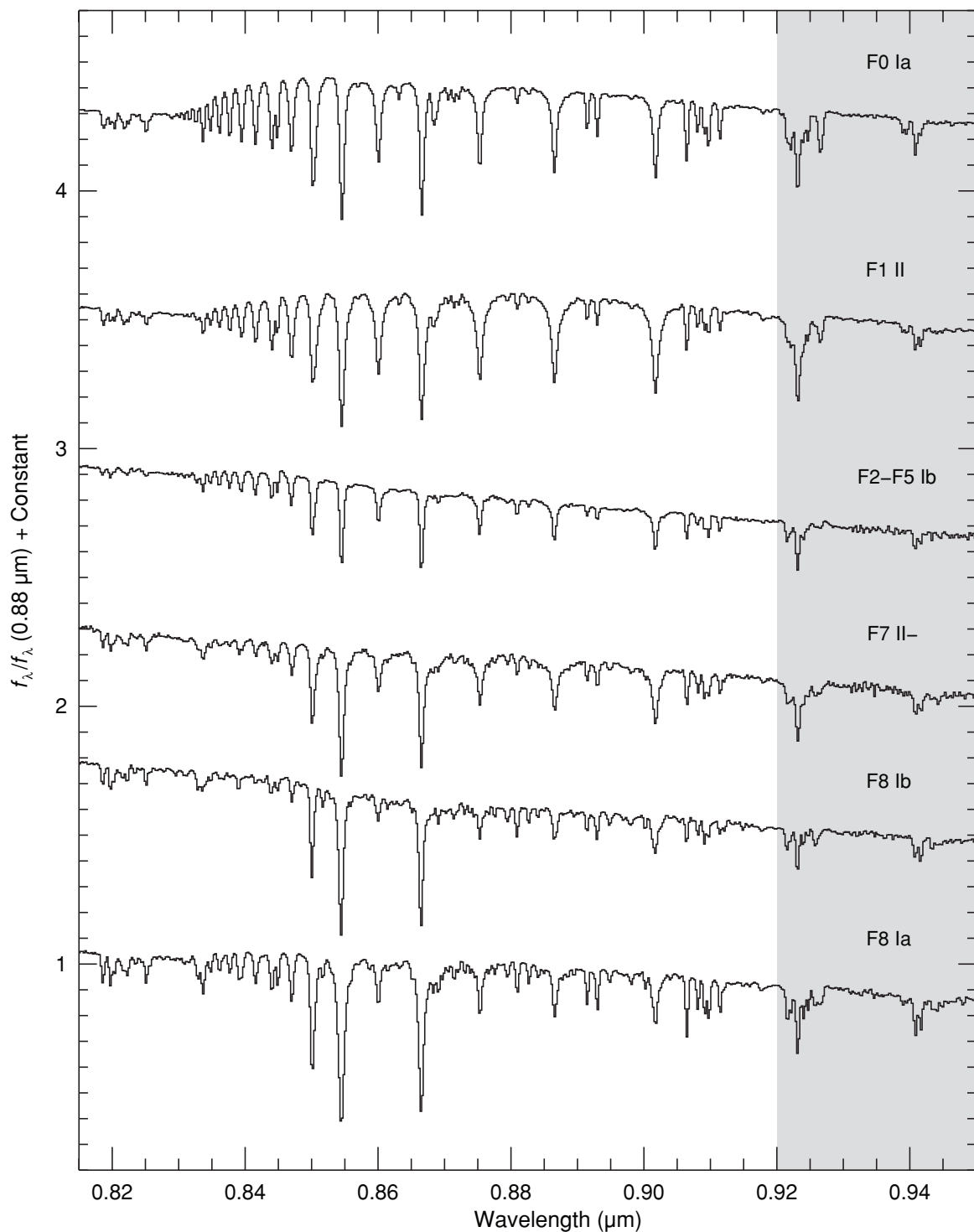


Figure 43. Sequence of F supergiant stars plotted over the I band (0.82–0.95 μm). The spectra are of HD 7927 (F0 Ia), HD 173638 (F1 II), BD +38 2803 (F2–F5 Ib), HD 201078 (F7 II-), HD 51956 (F8 Ib) and HD 190323 (F8 Ia). The spectra have been normalized to unity at 0.88 μm and offset by constants.

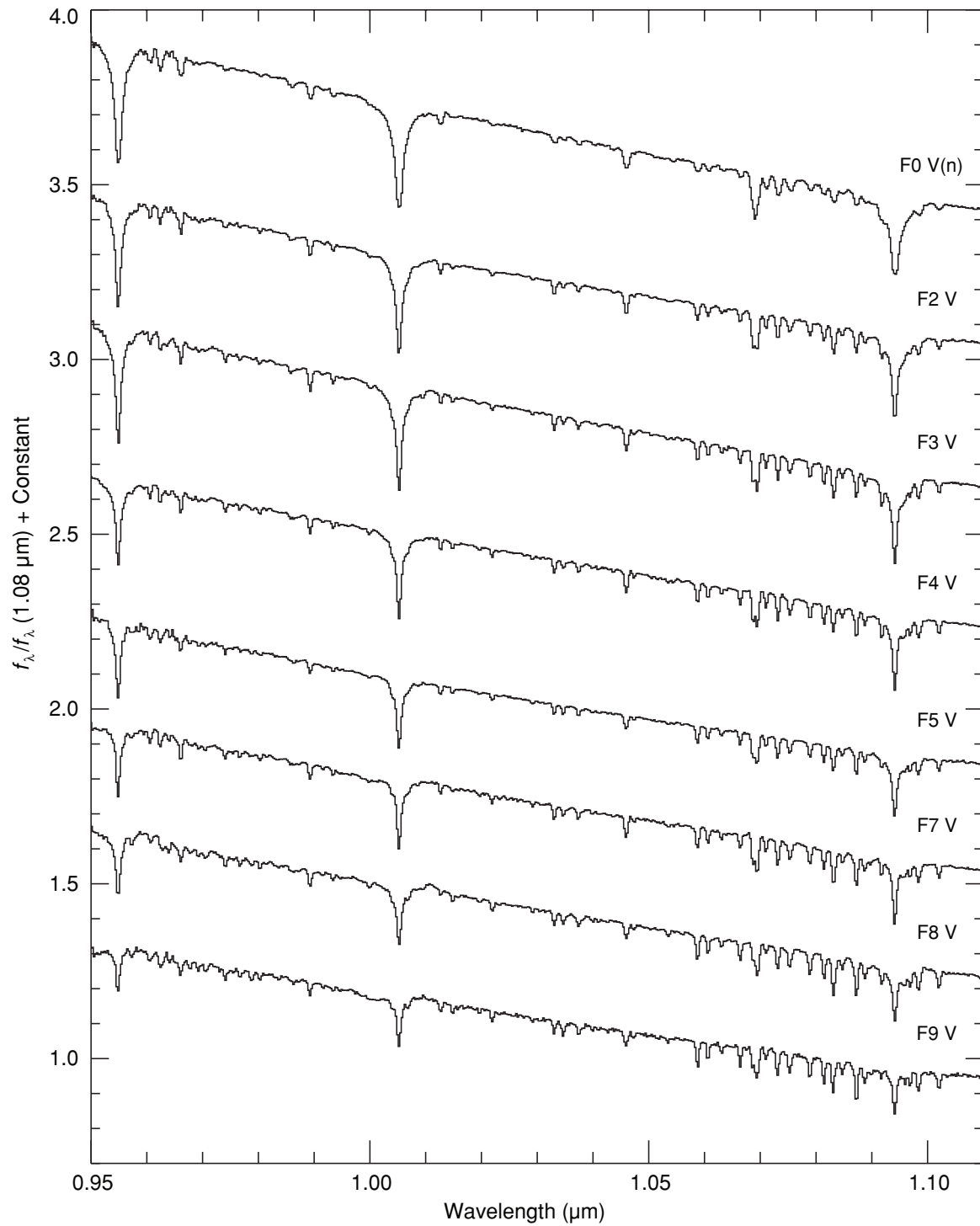


Figure 44. Sequence of F dwarf stars plotted over the Y band (0.95 – $1.10 \mu\text{m}$). The spectra are of HD 108519 F0 V(n), HD 113139 (F2 V), HD 26015 (F3 V), HD 87822 (F4 V), HD 218804 (F5 V), HD 126660 (F7 V), HD 27393 (F8 V), and HD 176051 (F9 V). The spectra have been normalized to unity at $1.08 \mu\text{m}$ and offset by constants.

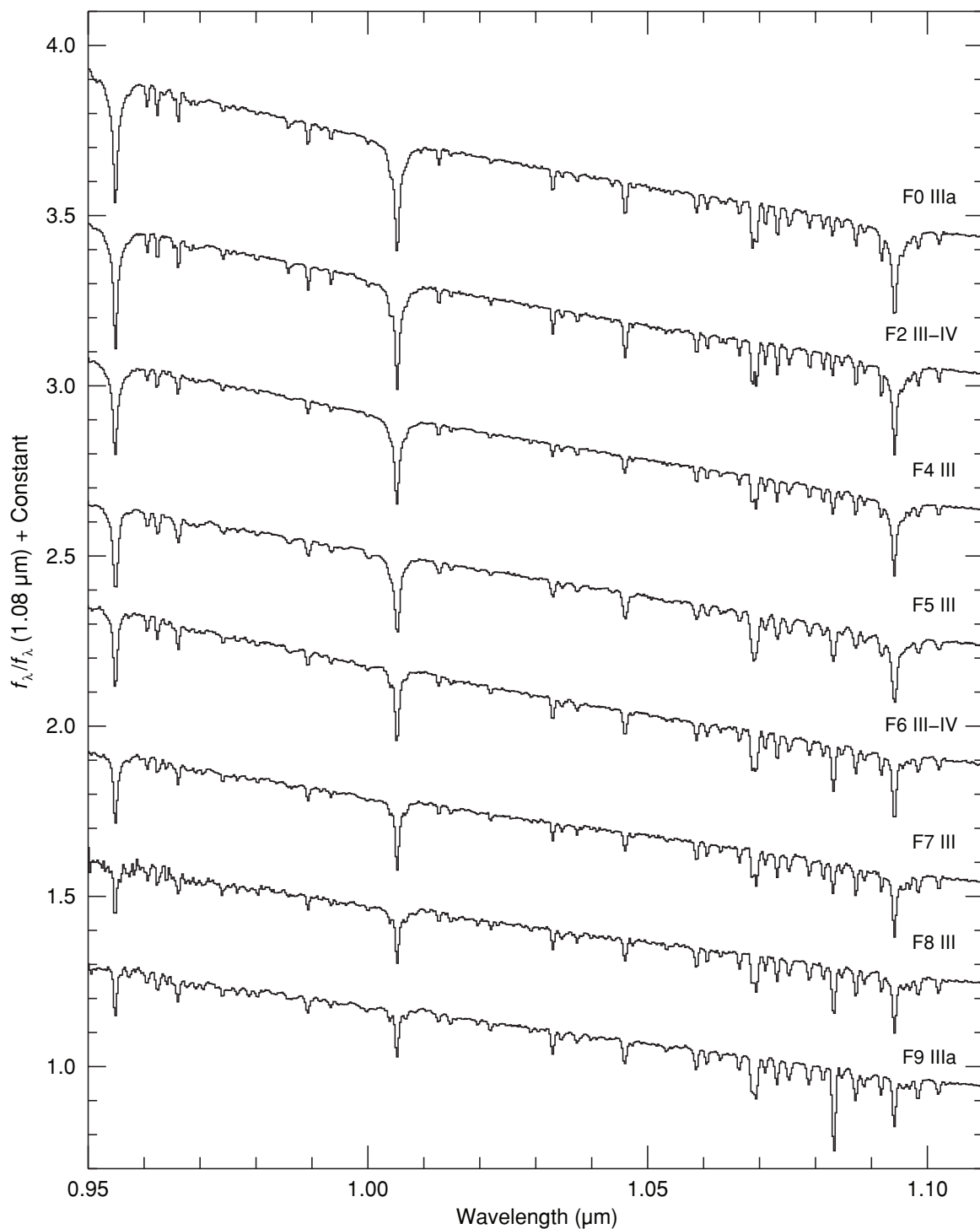


Figure 45. Sequence of F giant stars plotted over the Y band (0.95–1.10 μm). The spectra are of HD 89025 (F0 IIIa), HD 40535 (F2 III-IV), HD 21770 (F4 III), HD 17918 (F5 III), HD 160365 (F6 III-IV), HD 124850 (F7 III), HD 220657 (F8 III), and HD 6903 (F9 IIIa). The spectra have been normalized to unity at 1.08 μm and offset by constants.

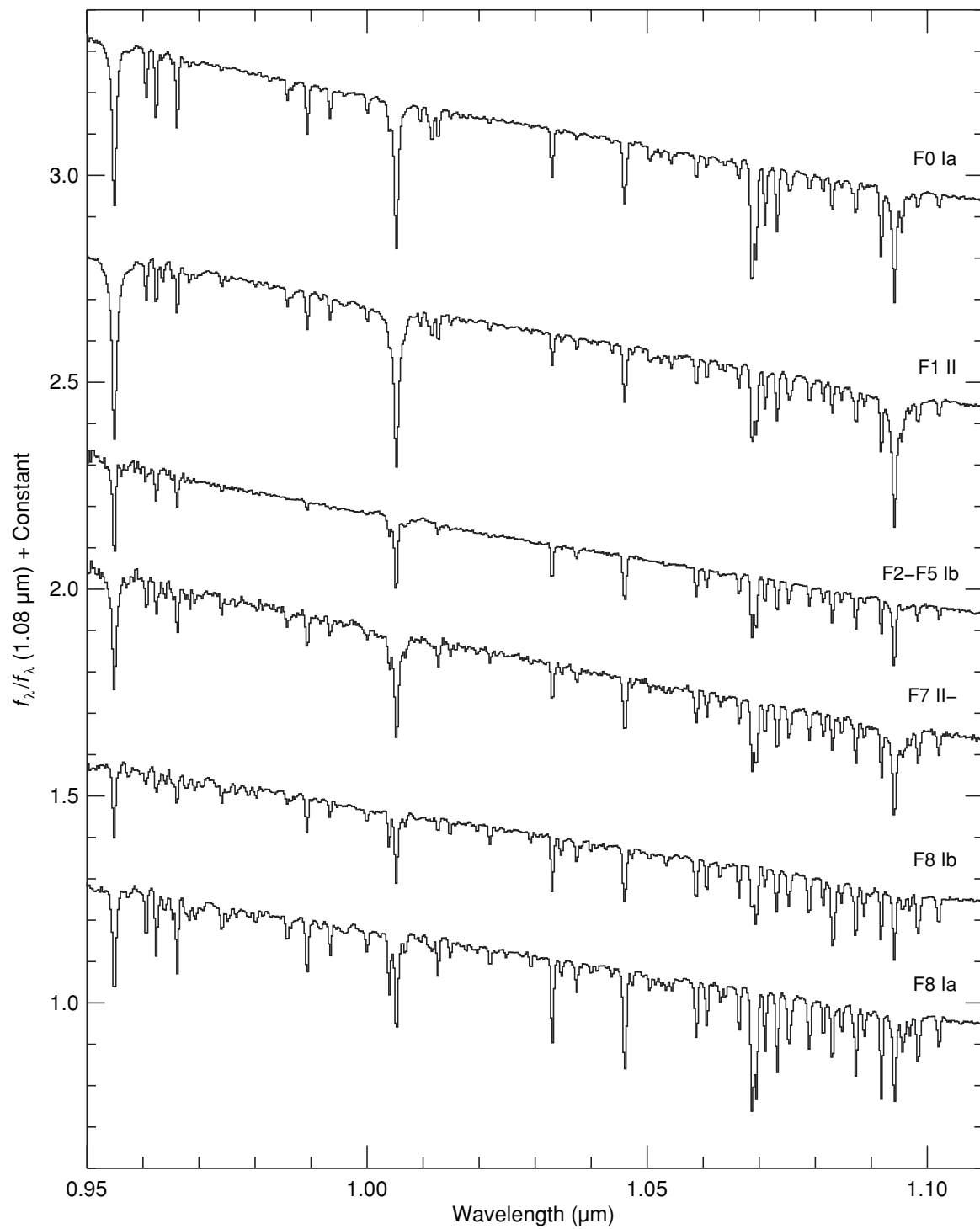


Figure 46. Sequence of F supergiant stars plotted over the *Y* band (0.95–1.10 μm). The spectra are of HD 7927 (F0 Ia), HD 173638 (F1 II), BD +38 2803 (F2–F5 Ib), HD 51956 (F6 IbII), HD 201078 (F7 II–), and HD 190323 (F8 Ia). The spectra have been normalized to unity at 1.08 μm and offset by constants.

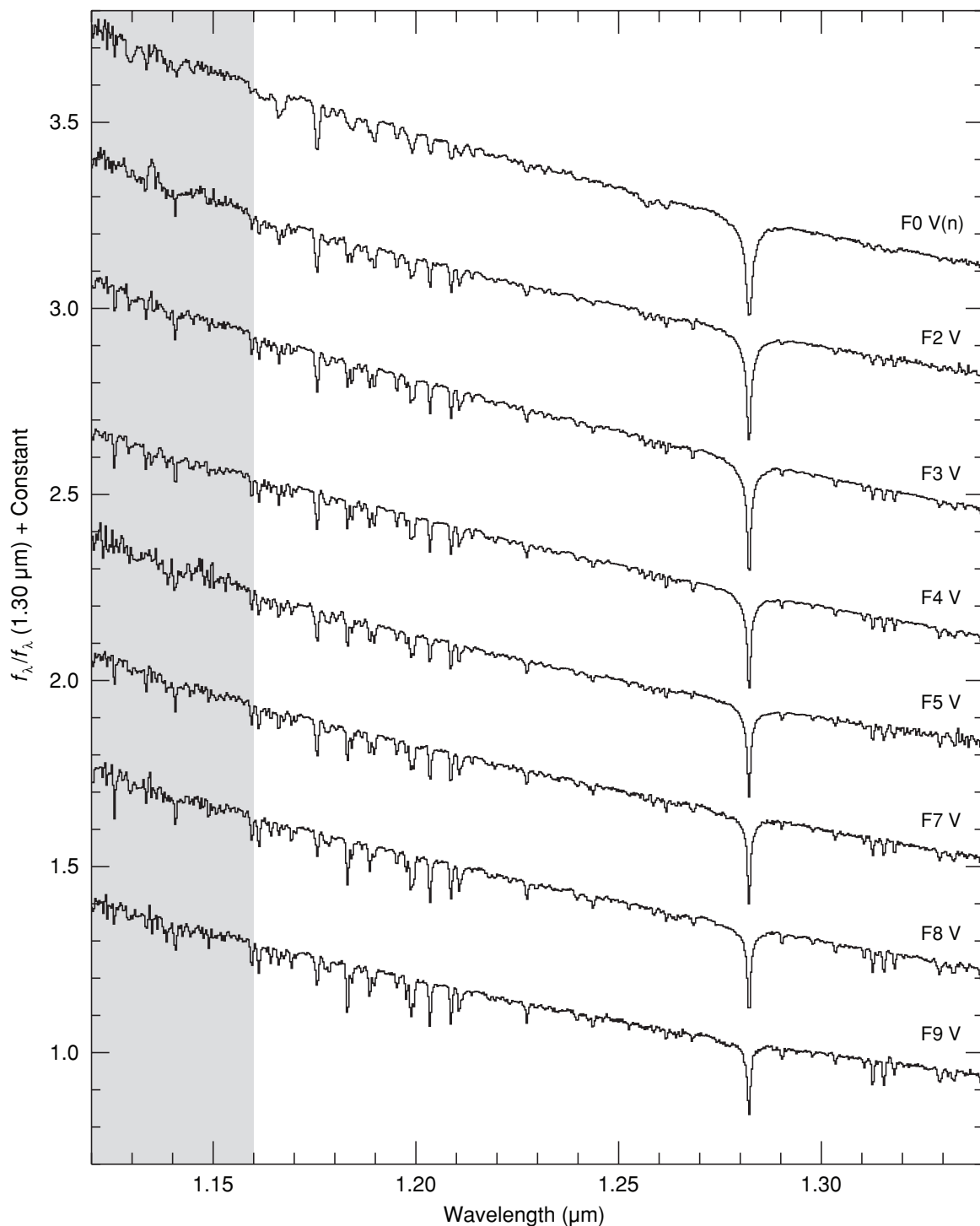


Figure 47. Sequence of F dwarf stars plotted over the *J* band (1.12–1.34 μm). The spectra are of HD 108519 F0 V(n), HD 113139 (F2 V), HD 26015 (F3 V), HD 87822 (F4 V), HD 218804 (F5 V), HD 126660 (F7 V), HD 27393 (F8 V), and HD 176051 (F9 V). The spectra have been normalized to unity at 1.30 μm and offset by constants.

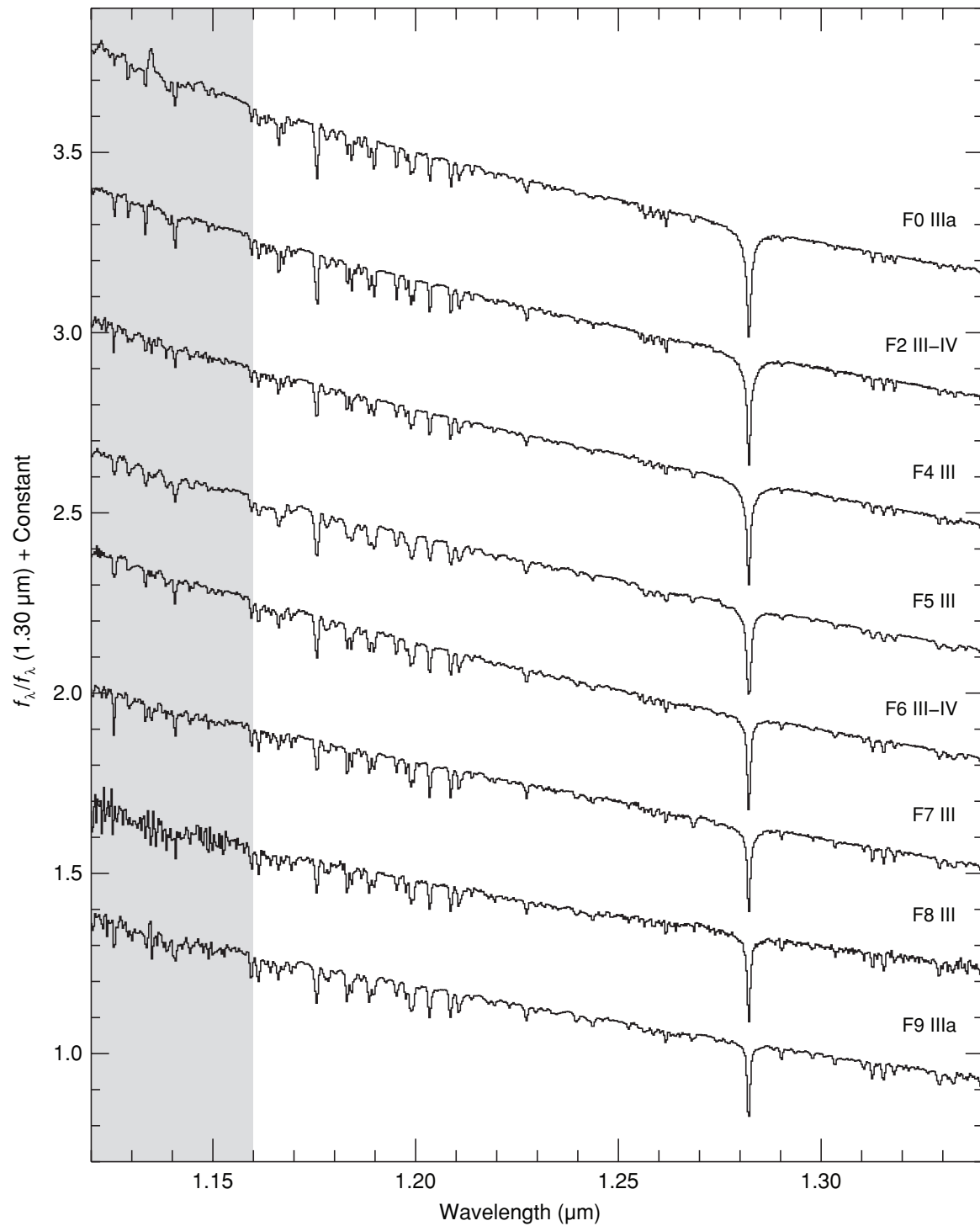


Figure 48. Sequence of F giant stars plotted over the *J* band (1.12–1.34 μm). The spectra are of HD 89025 (F0 IIIa), HD 40535 (F2 III-IV), HD 21770 (F4 III), HD 17918 (F5 III), HD 160365 (F6 III-IV), HD 124850 (F7 III), HD 220657 (F8 III), and HD 6903 (F9 IIIa). The spectra have been normalized to unity at 1.30 μm and offset by constants.

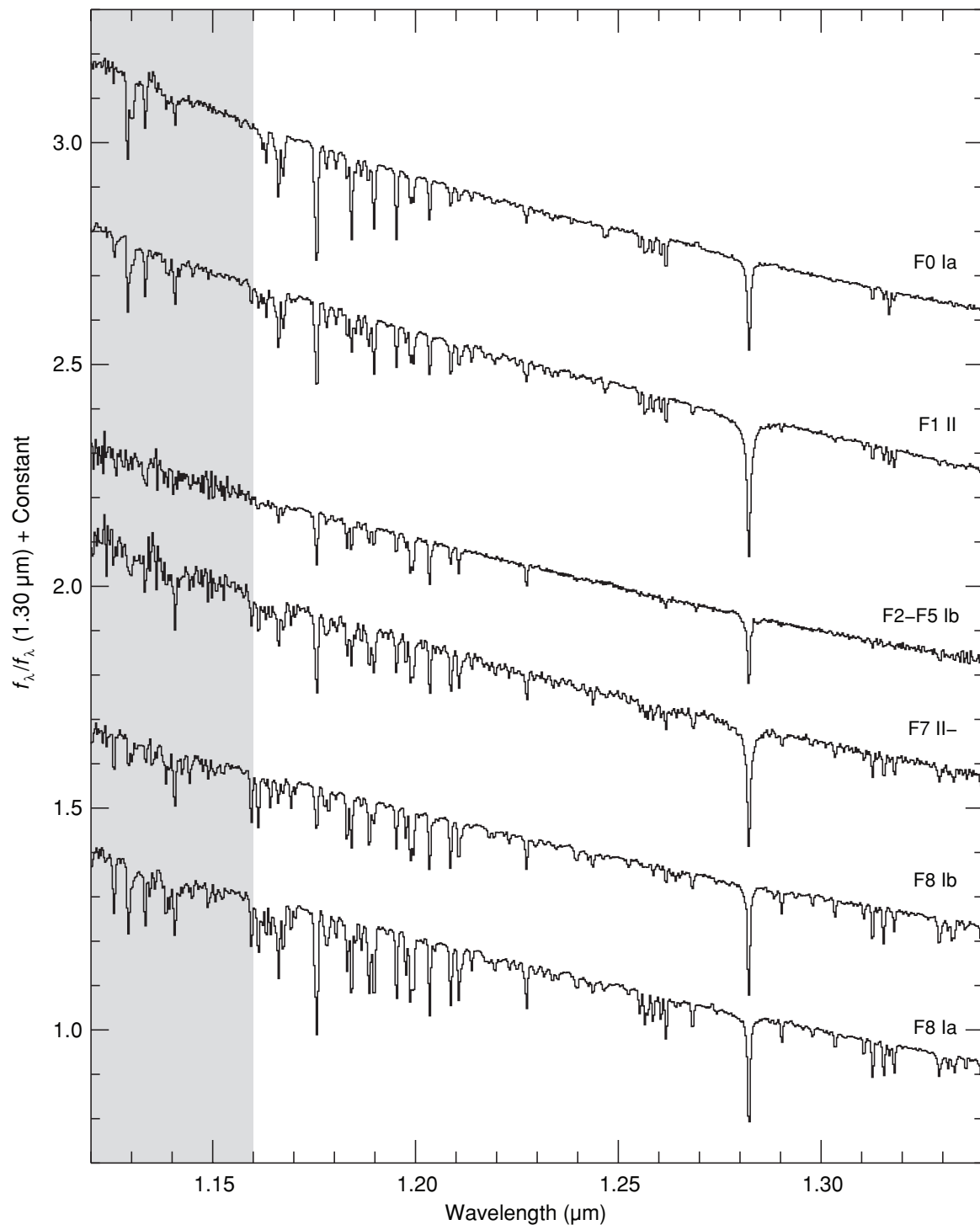


Figure 49. Sequence of F supergiant stars plotted over the *J* band (1.12–1.34 μm). The spectra are of HD 7927 (F0 Ia), HD 173638 (F1 II), BD +38 2803 (F2–F5 Ib), HD 201078 (F7 II-), HD 51956 (F8 Ib) and HD 190323 (F8 Ia). The spectra have been normalized to unity at 1.30 μm and offset by constants.

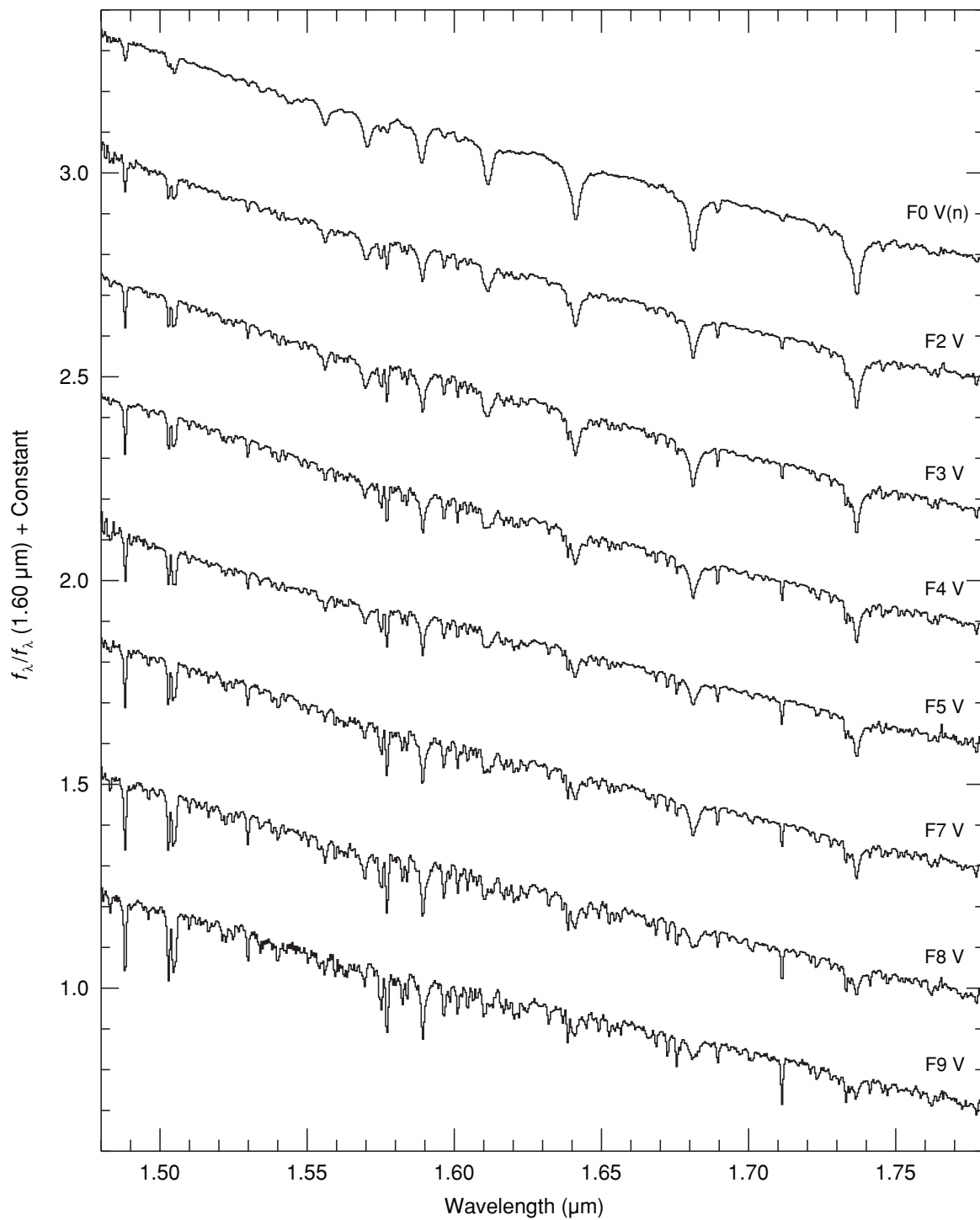


Figure 50. Sequence of F dwarf stars plotted over the *H* band (1.78–1.78 μm). The spectra are of HD 108519 F0 V(n), HD 113139 (F2 V), HD 26015 (F3 V), HD 87822 (F4 V), HD 218804 (F5 V), HD 126660 (F7 V), HD 27393 (F8 V), and HD 176051 (F9 V). The spectra have been normalized to unity at 1.60 μm and offset by constants.

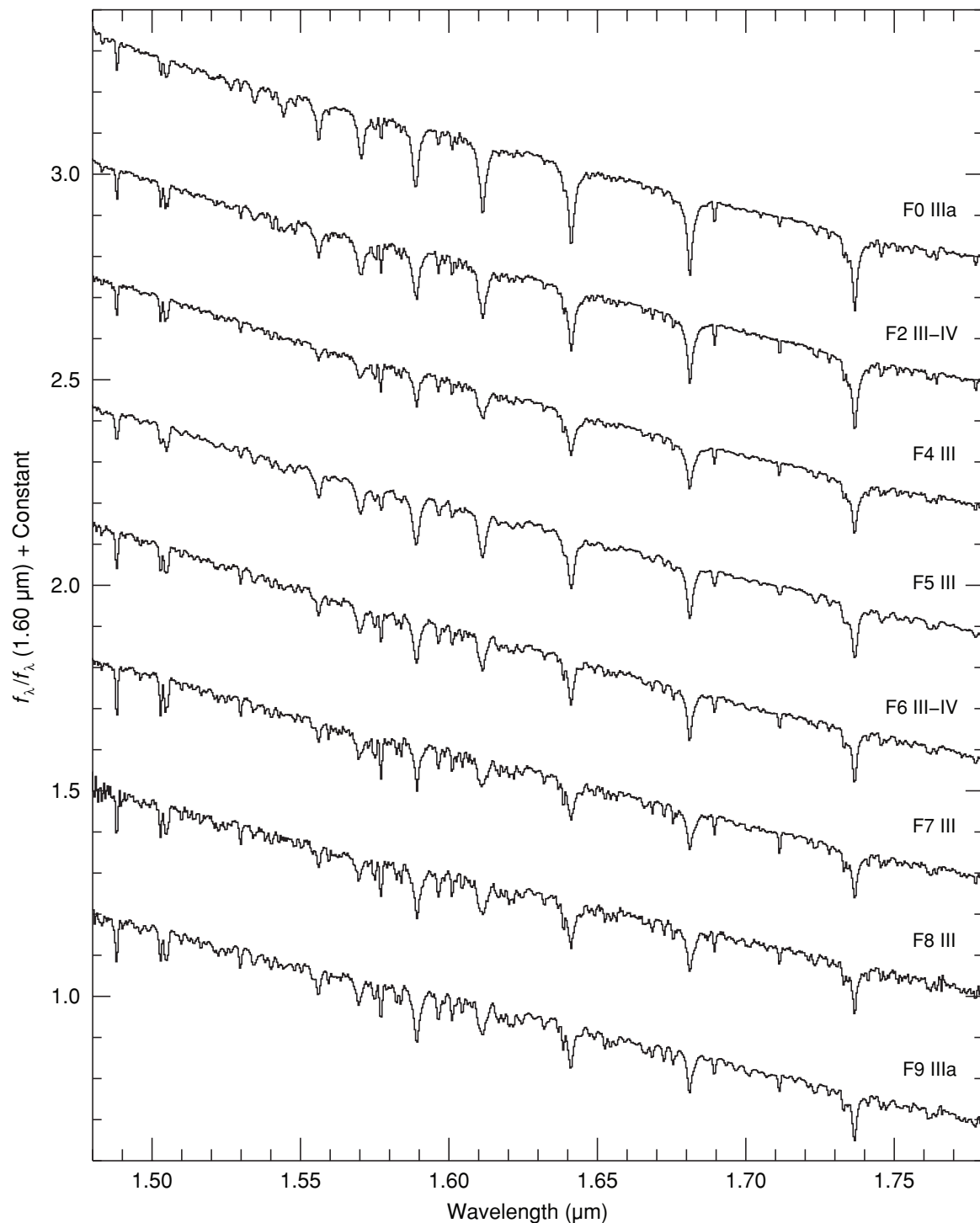


Figure 51. Sequence of F giant stars plotted over the *H* band (1.48–1.78 μm). The spectra are of HD 89025 (F0 IIIa), HD 40535 (F2 III-IV), HD 21770 (F4 III), HD 17918 (F5 III), HD 160365 (F6 III-IV), HD 124850 (F7 III), HD 220657 (F8 III), HD 6903 (F9 IIIa). The spectra have been normalized to unity at 1.60 μm and offset by constants.

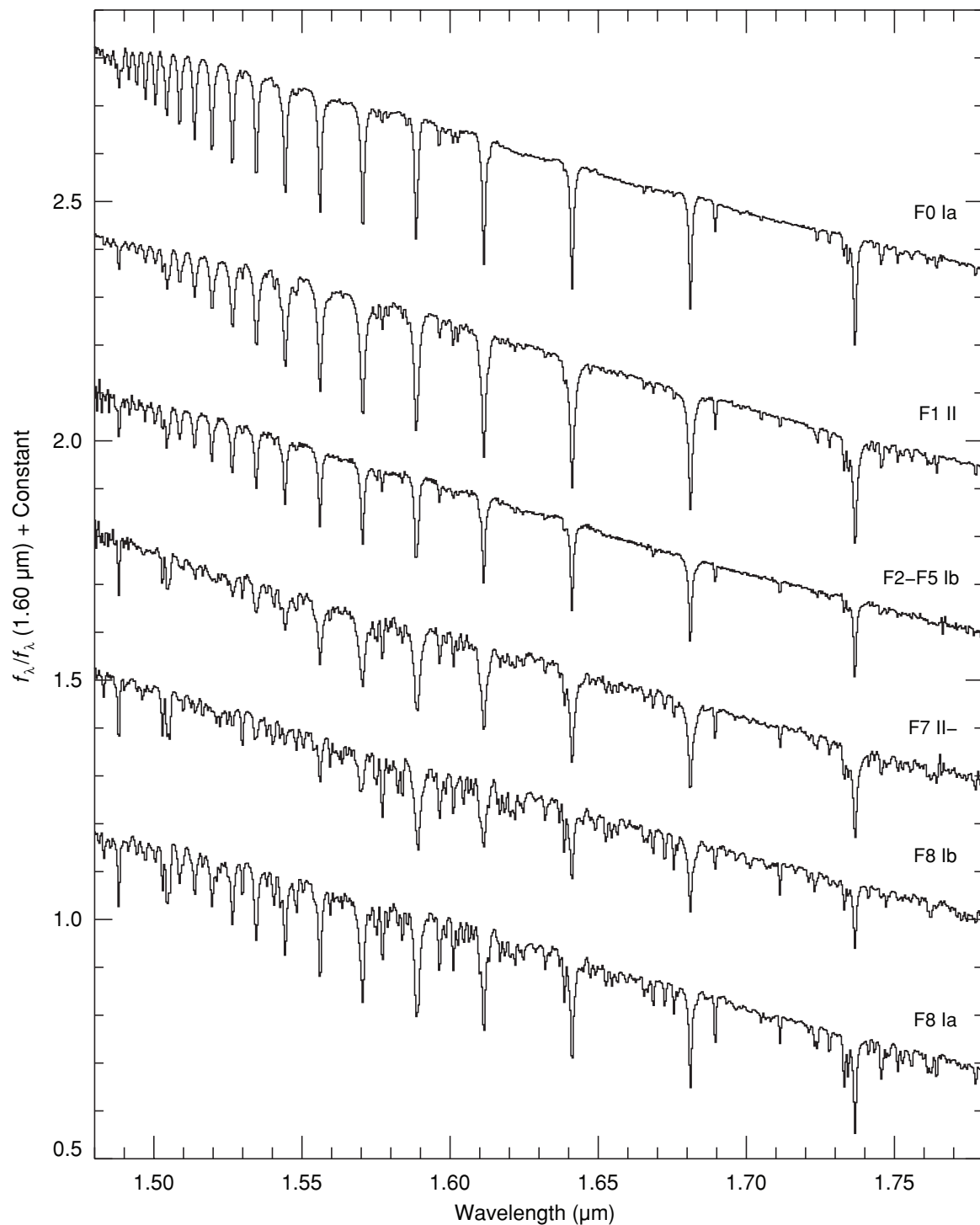


Figure 52. Sequence of F supergiant stars plotted over the *H* band (1.48–1.78 μm). The spectra are of HD 7927 (F0 Ia), HD 173638 (F1 II), BD +38 2803 (F2–F5 Ib), HD 51956 (F6 IbII), HD 201078 (F7 II–), and HD 190323 (F8 Ia). The spectra have been normalized to unity at 1.60 μm and offset by constants.

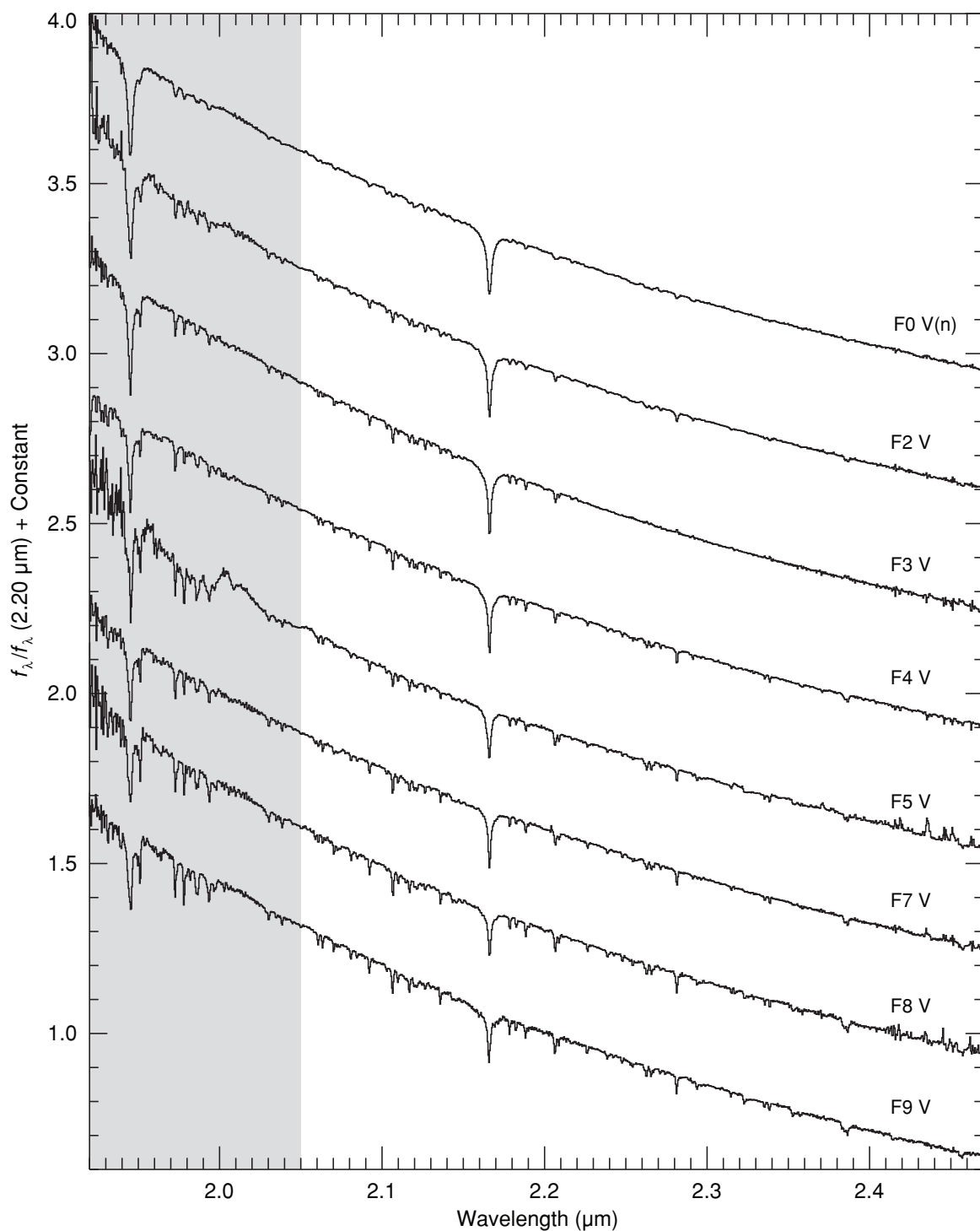


Figure 53. Sequence of F dwarf stars plotted over the K band (1.92 – $2.5 \mu\text{m}$). The spectra are of HD 108519 F0 V(n), HD 113139 (F2 V), HD 26015 (F3 V), HD 87822 (F4 V), HD 218804 (F5 V), HD 126660 (F7 V), HD 27393 (F8 V), and HD 176051 (F9 V). The spectra have been normalized to unity at $2.20 \mu\text{m}$ and offset by constants.

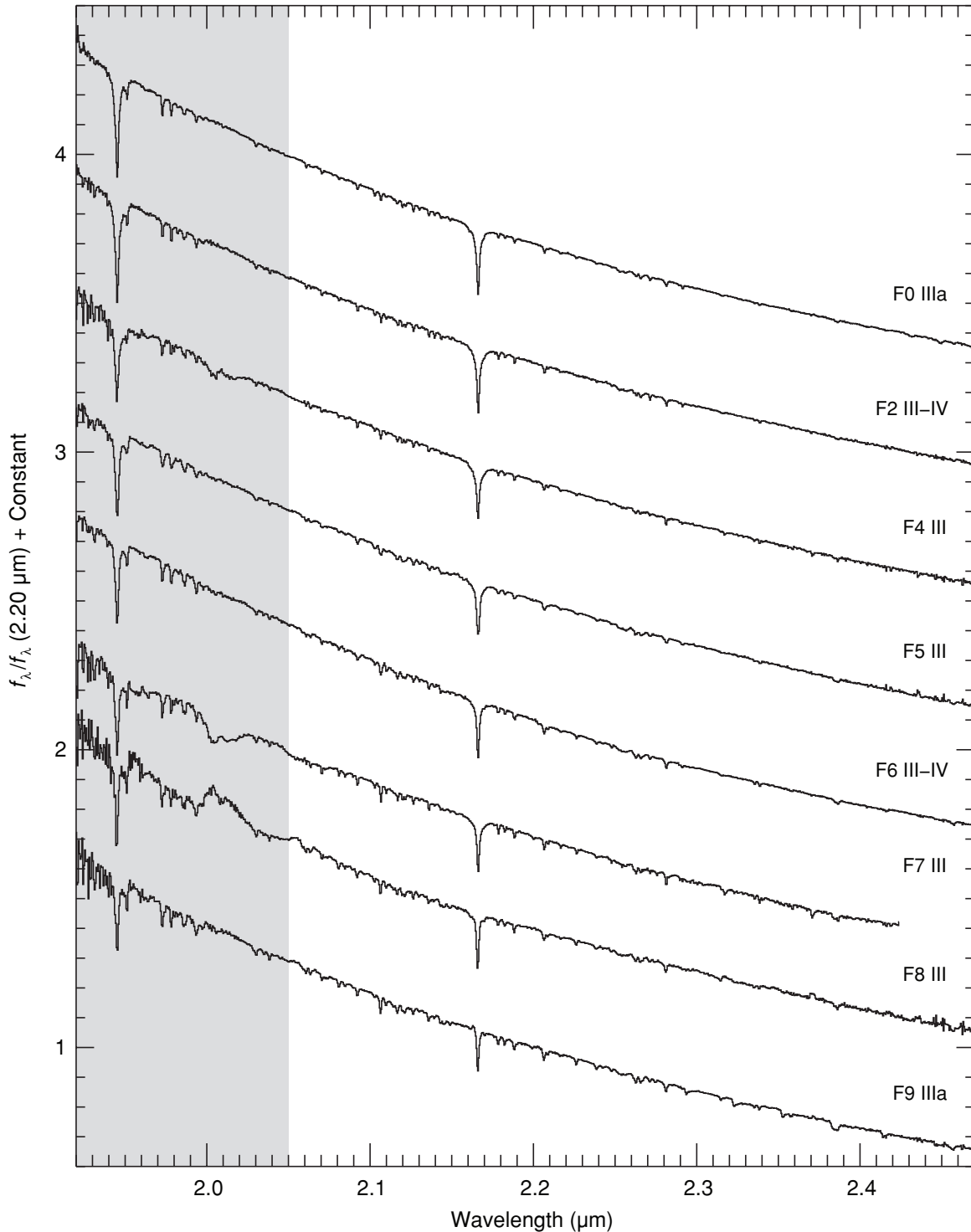


Figure 54. Sequence of F giant stars plotted over the K band ($1.92\text{--}2.5 \mu\text{m}$). The spectra are of HD 89025 (F0 IIIa), HD 40535 (F2 III-IV), HD 21770 (F4 III), HD 17918 (F5 III), HD 160365 (F6 III-IV), HD 124850 (F7 III), HD 220657 (F8 III), HD 6903 (F9 IIIa). The spectra have been normalized to unity at $2.20 \mu\text{m}$ and offset by constants. Note the relatively poor correction of telluric CO_2 at $\sim 2.02 \mu\text{m}$ in the F7 III and F8 III stars (see Section 2.2).

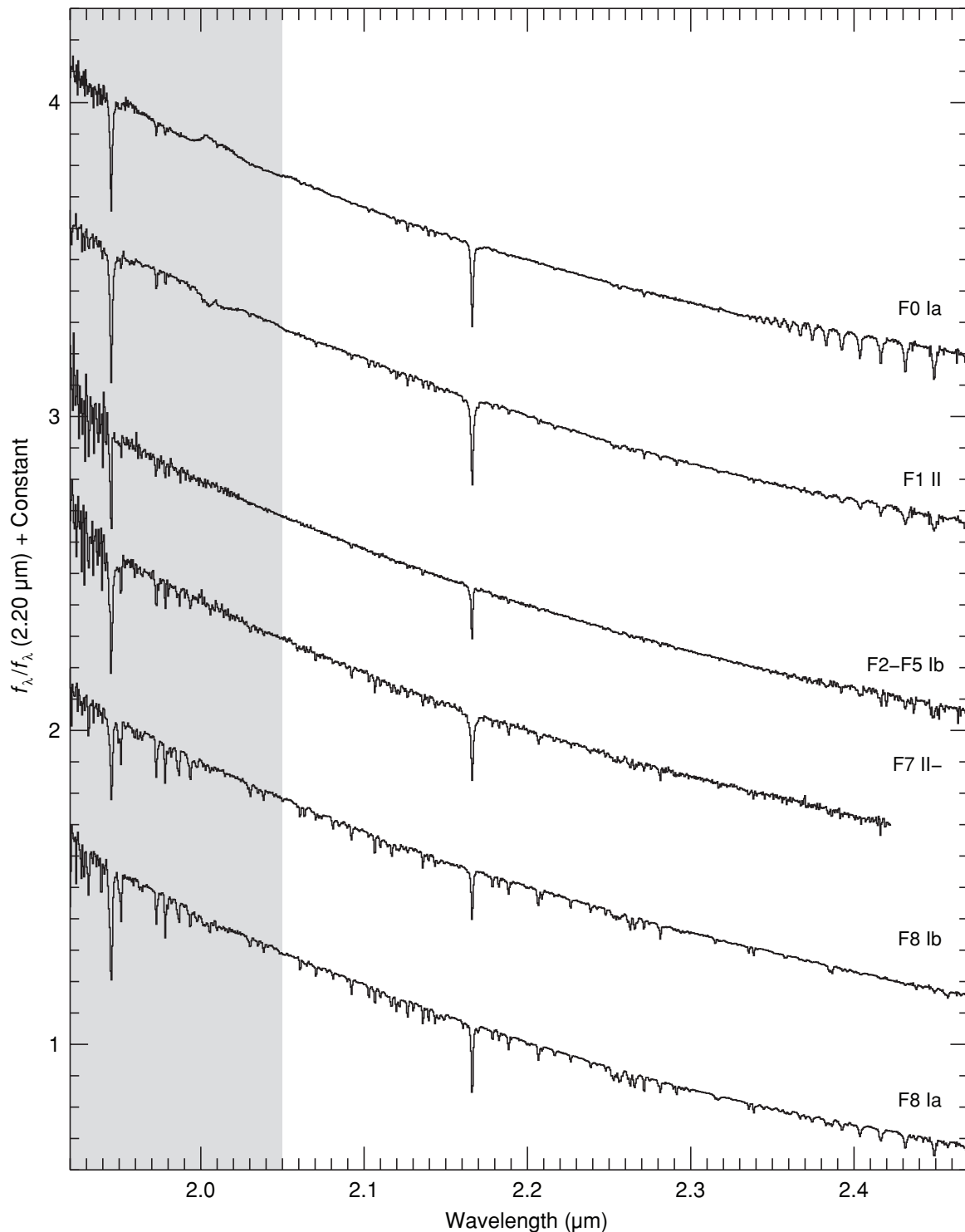


Figure 55. Sequence of F supergiant stars plotted over the K band (1.92 – $2.5 \mu\text{m}$). The spectra are of HD 7927 (F0 Ia), HD 173638 (F1 II), BD +38 2803 (F2–F5 Ib), HD 51956 (F6 IbII), HD 201078 (F7 II–), and HD 190323 (F8 Ia). The spectra have been normalized to unity at $2.20 \mu\text{m}$ and offset by constants.

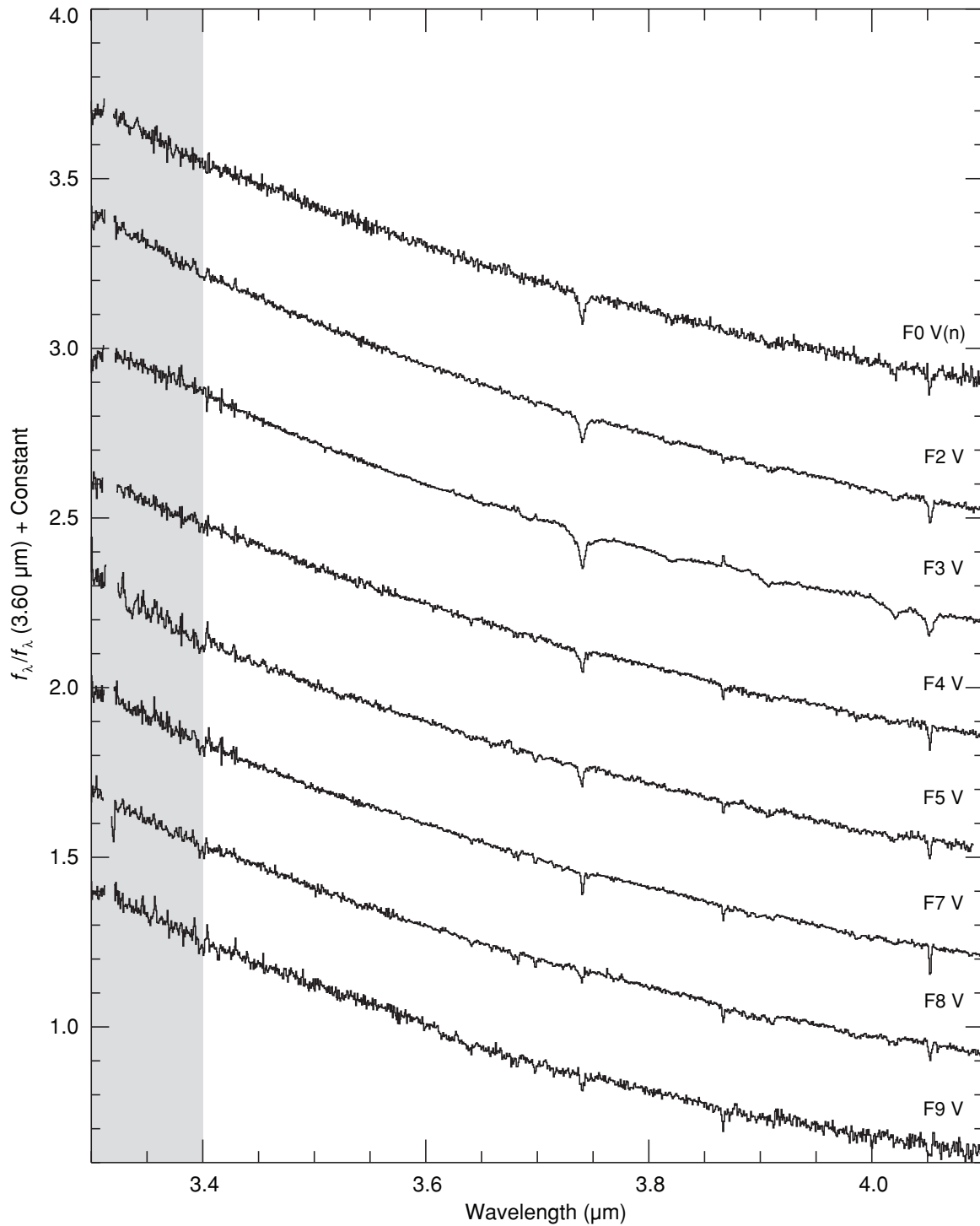


Figure 56. Sequence of F dwarf stars plotted over the L' band ($3.3\text{--}4.1\,\mu\text{m}$). The spectra are of HD 108519 F0 V(n), HD 113139 (F2 V), HD 26015 (F3 V), HD 87822 (F4 V), HD 218804 (F5 V), HD 126660 (F7 V), HD 27393 (F8 V), and HD 176051 (F9 V). The spectra have been normalized to unity at $3.6\,\mu\text{m}$ and offset by constants.

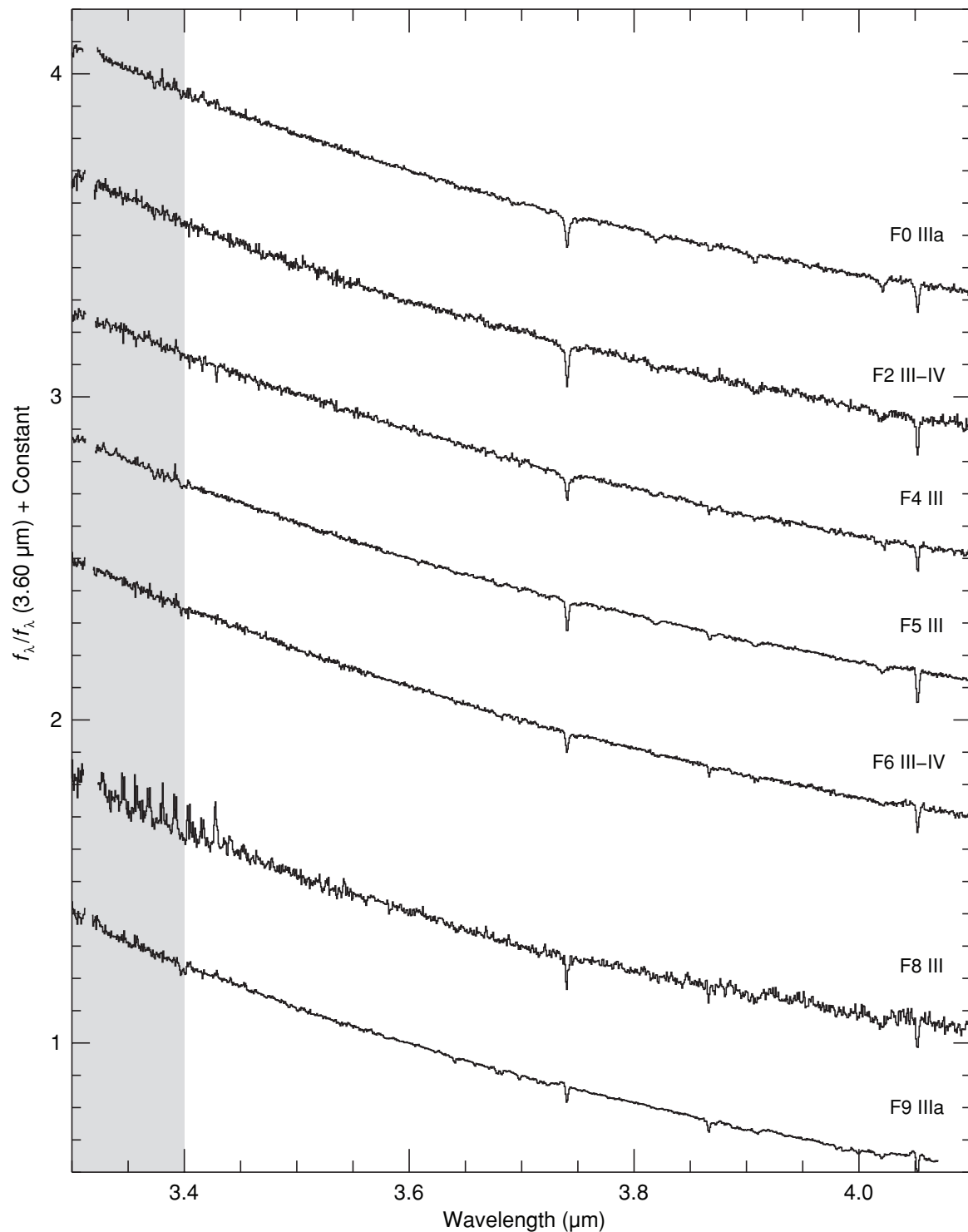


Figure 57. Sequence of F giant stars plotted over the L' band ($3.3\text{--}4.1 \mu\text{m}$). The spectra are of HD 89025 (F0 IIIa), HD 40535 (F2 III-IV), HD 21770 (F4 III), HD 17918 (F5 III), HD 160365 (F6 III-IV), HD 124850 (F7 III), HD 220657 (F8 III), and HD 6903 (F9 IIIa). The spectra have been normalized to unity at $3.6 \mu\text{m}$ and offset by constants.

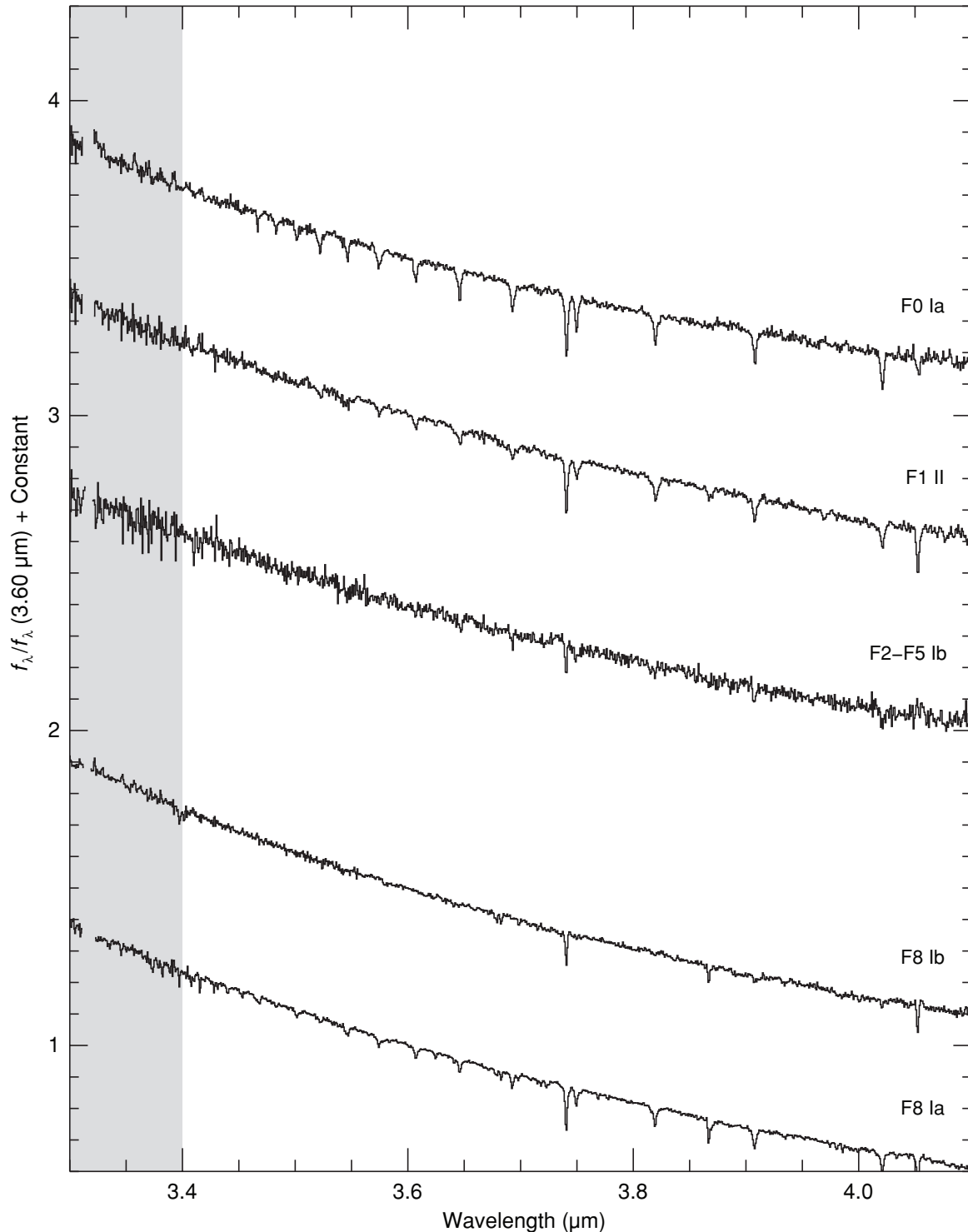


Figure 58. Sequence of F supergiant stars plotted over the L' band (1.92 – $2.5 \mu\text{m}$). The spectra are of HD 7927 (F0 Ia), HD 173638 (F1 II), BD +38 2803 (F2–F5 Ib), HD 51956 (F6 IbII), HD 201078 (F7 II–), and HD 190323 (F8 Ia). The spectra have been normalized to unity at $3.6 \mu\text{m}$ and offset by constants.

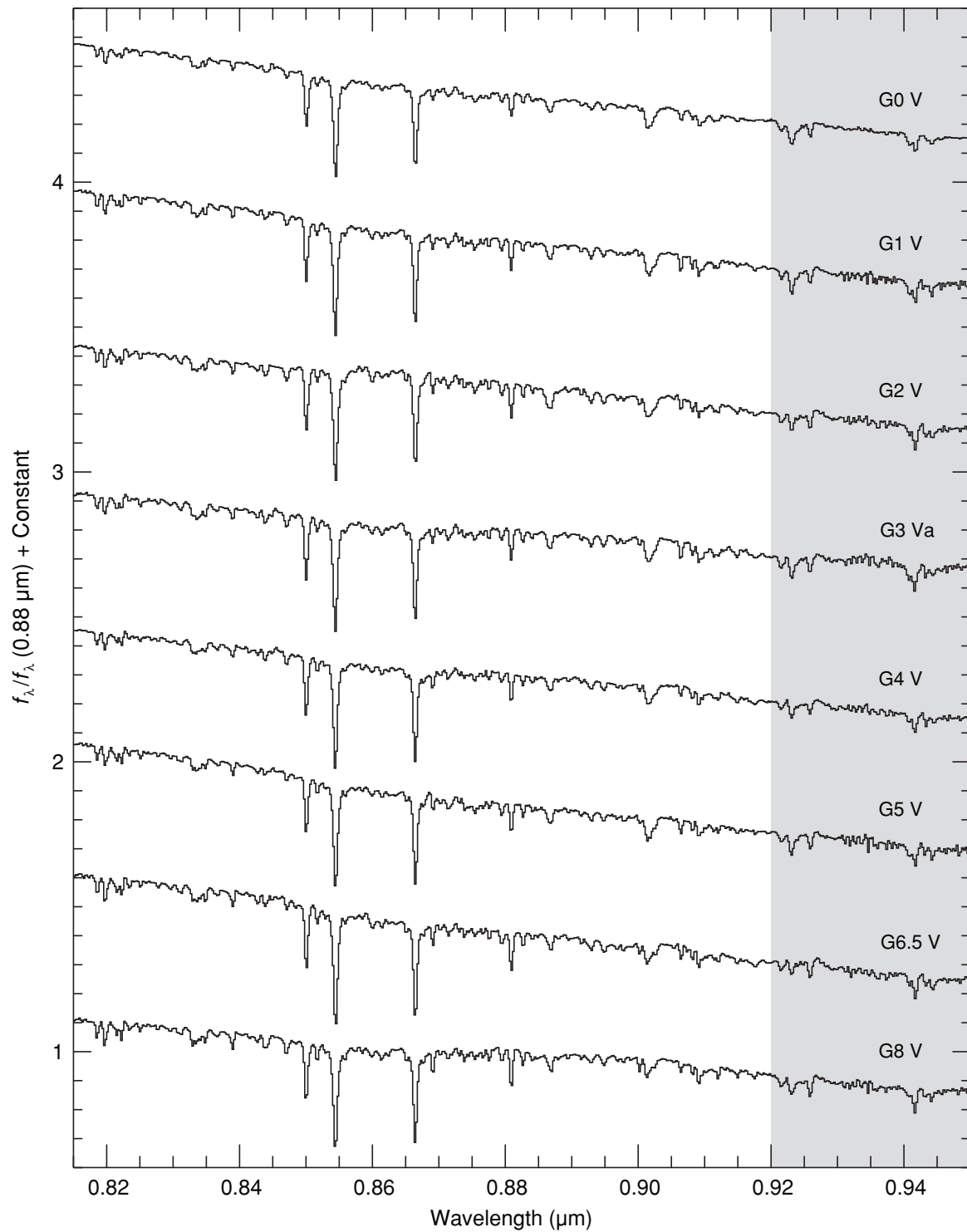


Figure 59. Sequence of G dwarf stars plotted over the I band ($0.82\text{--}0.95 \mu\text{m}$). The spectra are of HD 109358 (G0 V), HD 10307 (G1 V), HD 76151 (G2 V), HD 10697 (G3 Va), HD 214850 (G4 V), HD 165185 (G5 V), HD 115617 (G6.5 V), and HD 101501 (G8 V). The spectra have been normalized to unity at $0.88 \mu\text{m}$ and offset by constants.

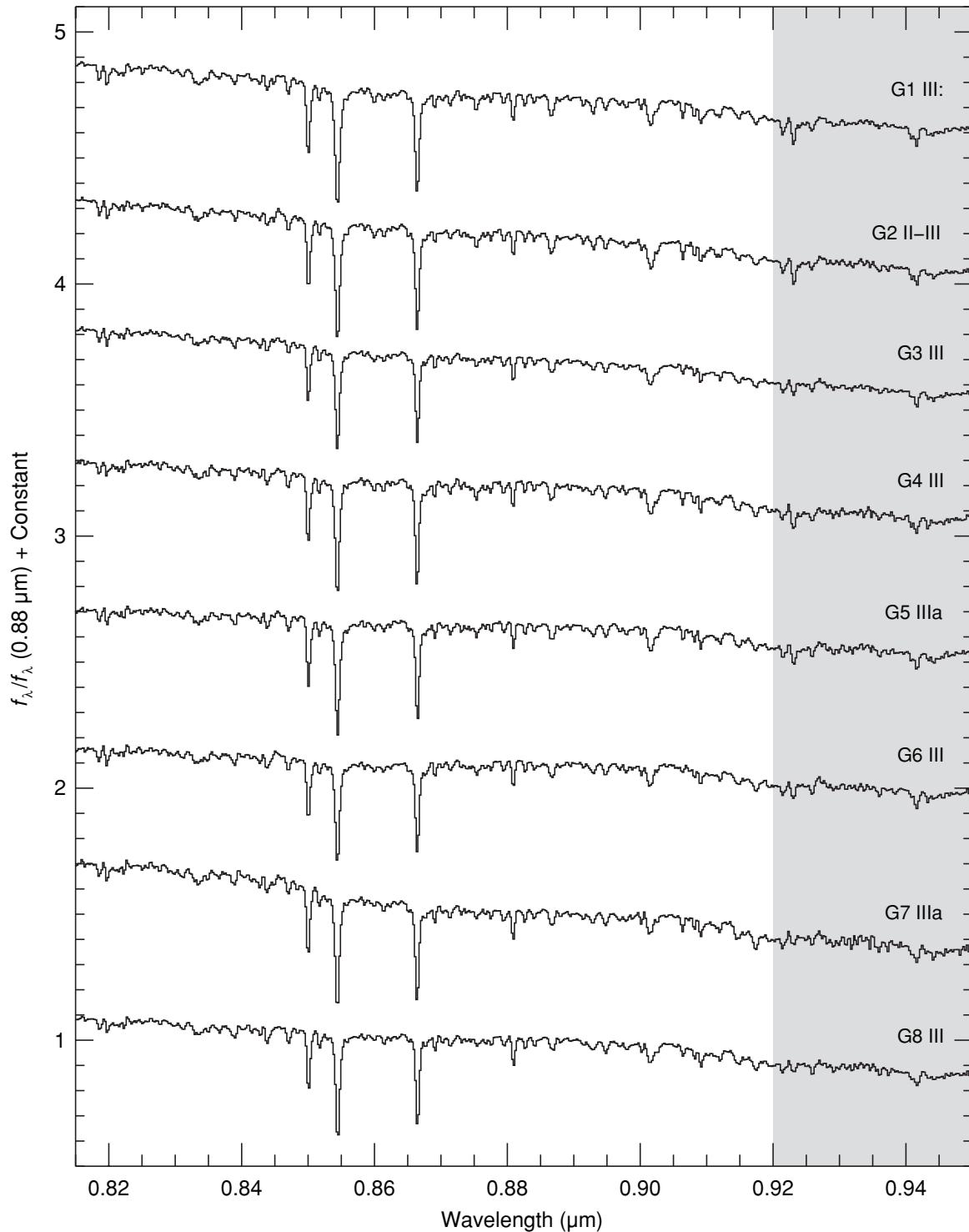


Figure 60. Sequence of G giant stars plotted over the I band (0.82–0.95 μm). The spectra are of HD 21018 (G1 III:CH-1:), HD 219477 (G2 II-III), HD 88639 (G3 IIIb Fe-1), HD 108477 (G4 III), HD 193896 (G5 IIIa), HD 27277 (G6 III), HD 182694 (G7 IIIa), and HD 135722 (G8 III Fe-1). The spectra have been normalized to unity at 0.88 μm and offset by constants.

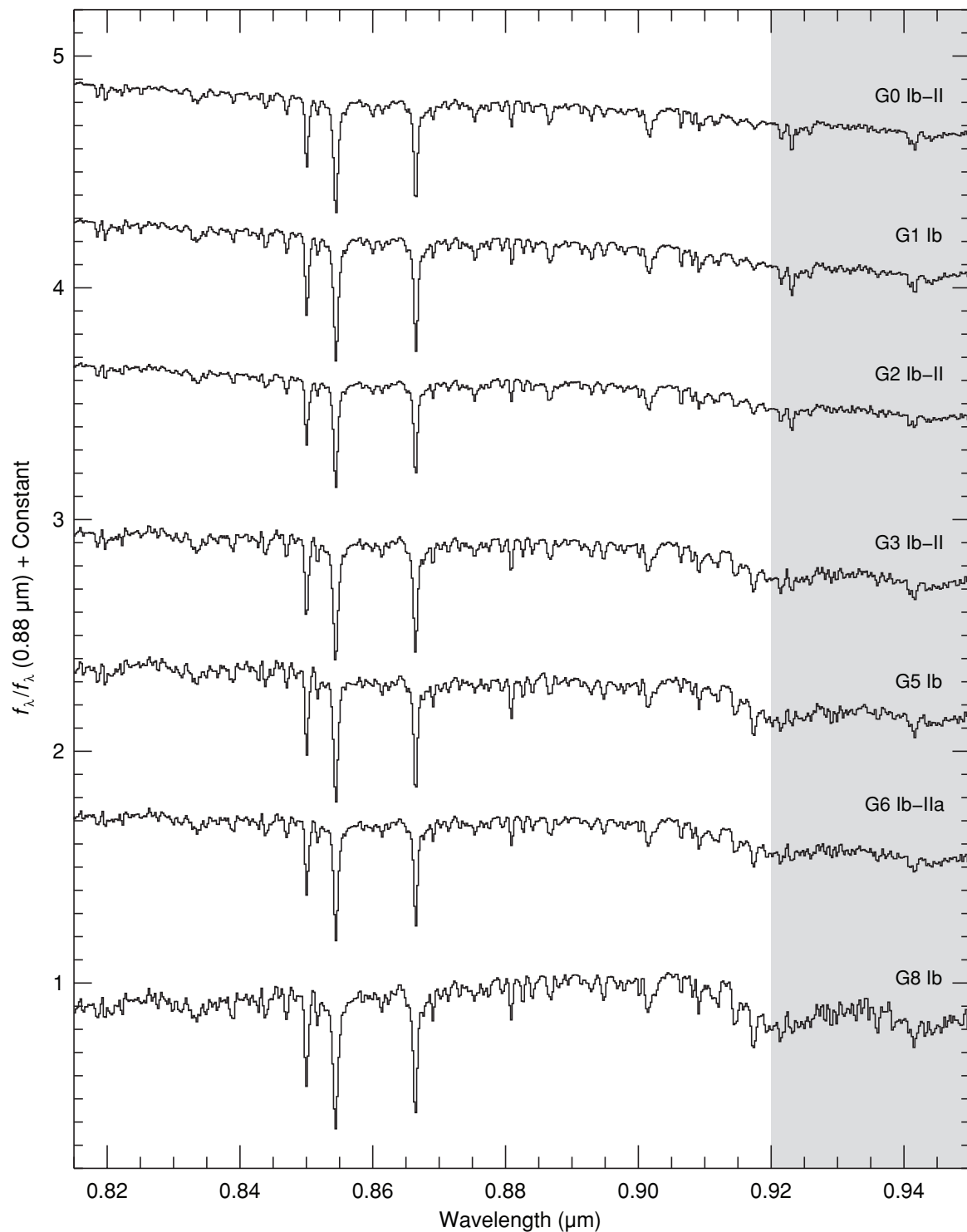


Figure 61. Sequence of G supergiant stars plotted over the I band (0.82 – $0.95 \mu\text{m}$). The spectra are of HD 185018 (G0 Ib-II), HD 74395 (G1 Ib), HD 3421 (G2 Ib-II), HD 192713 (G3 Ib-II Wk H&K comp?), HD 190113 (G5 Ib), HD 202314 (G6 Ib-IIa Ca1 B0.5), and HD 208606 (G8 Ib). The spectra have been normalized to unity at $0.88 \mu\text{m}$ and offset by constants.

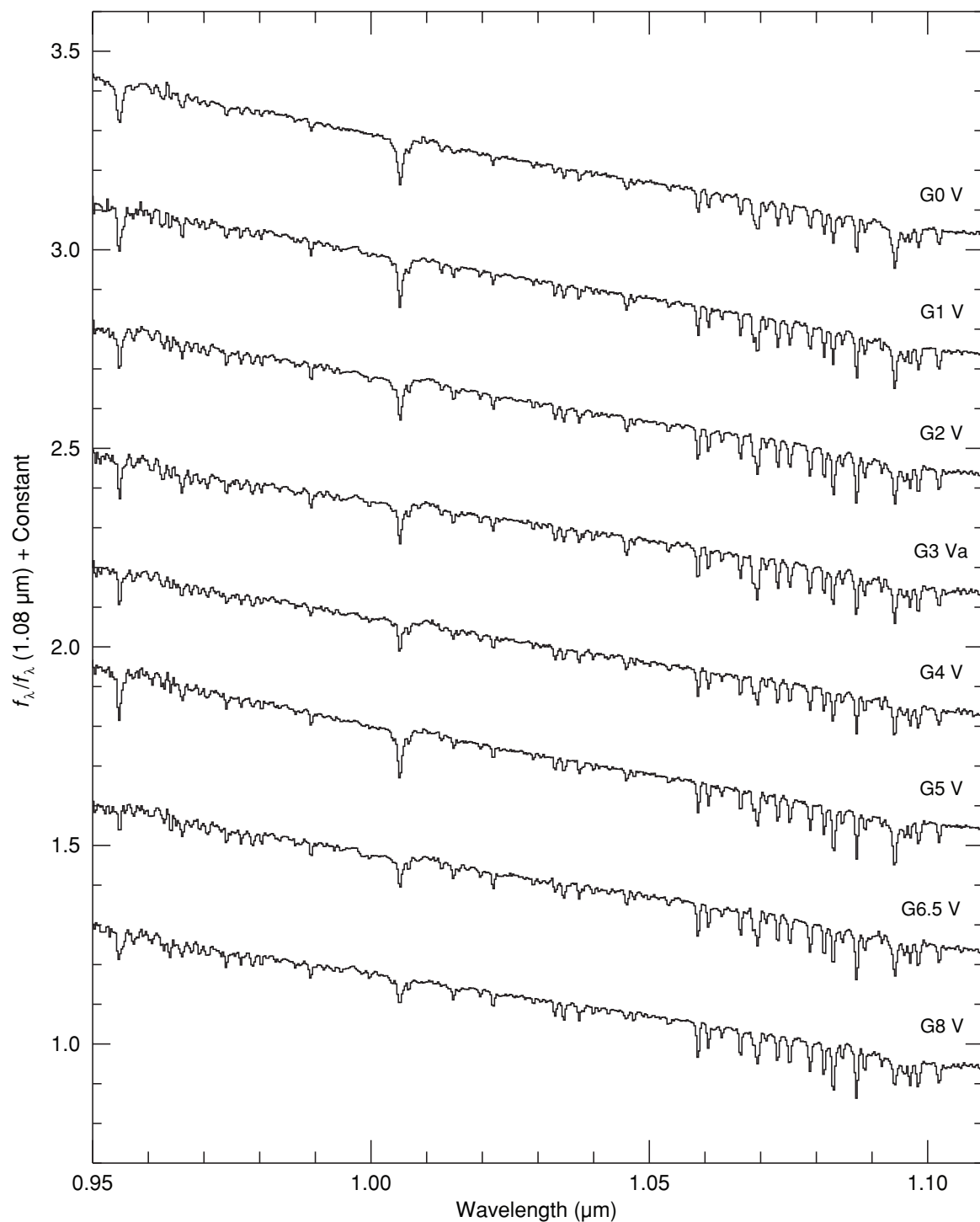


Figure 62. Sequence of G dwarf stars plotted over the Y band (0.95 – $1.10 \mu\text{m}$). The spectra are of HD 109358 (G0 V), HD 10307 (G1 V), HD 76151 (G2 V), HD 10697 (G3 Va), HD 214850 (G4 V), HD 165185 (G5 V), HD 115617 (G6.5 V), and HD 101501 (G8 V). The spectra have been normalized to unity at $1.08 \mu\text{m}$ and offset by constants.

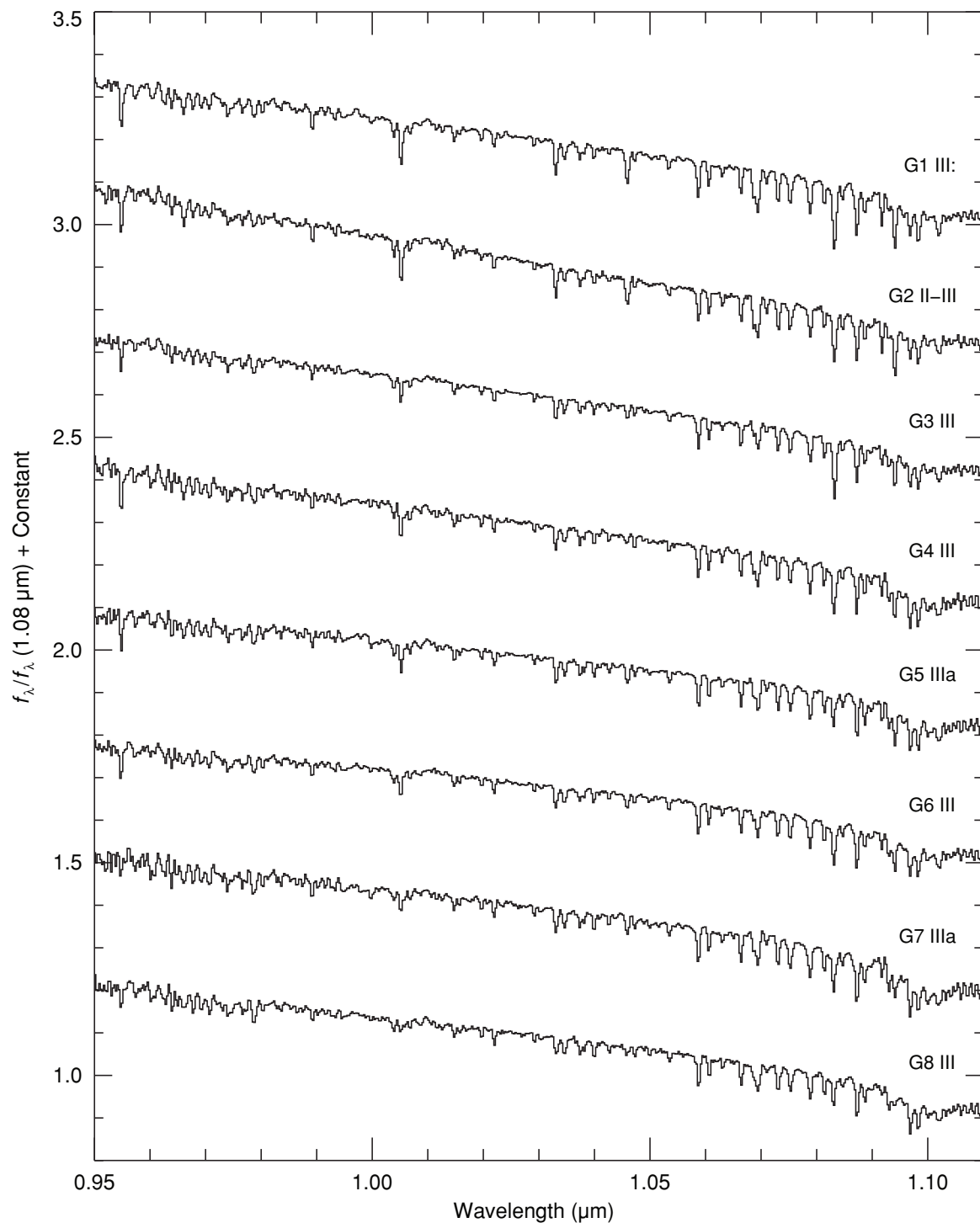


Figure 63. Sequence of G giant stars plotted over the Y band (0.95–1.10 μm). The spectra are of HD 21018 (G1 III:CH-1:), HD 219477 (G2 II-III), HD 88639 (G3b III Fe-1), HD 108477 (G4 III), HD 193896 (G5 IIIa), HD 27277 (G6 III), HD 182694 (G7 IIIa), and HD 135722 (G8 III Fe-1). The spectra have been normalized to unity at 1.08 μm and offset by constants.

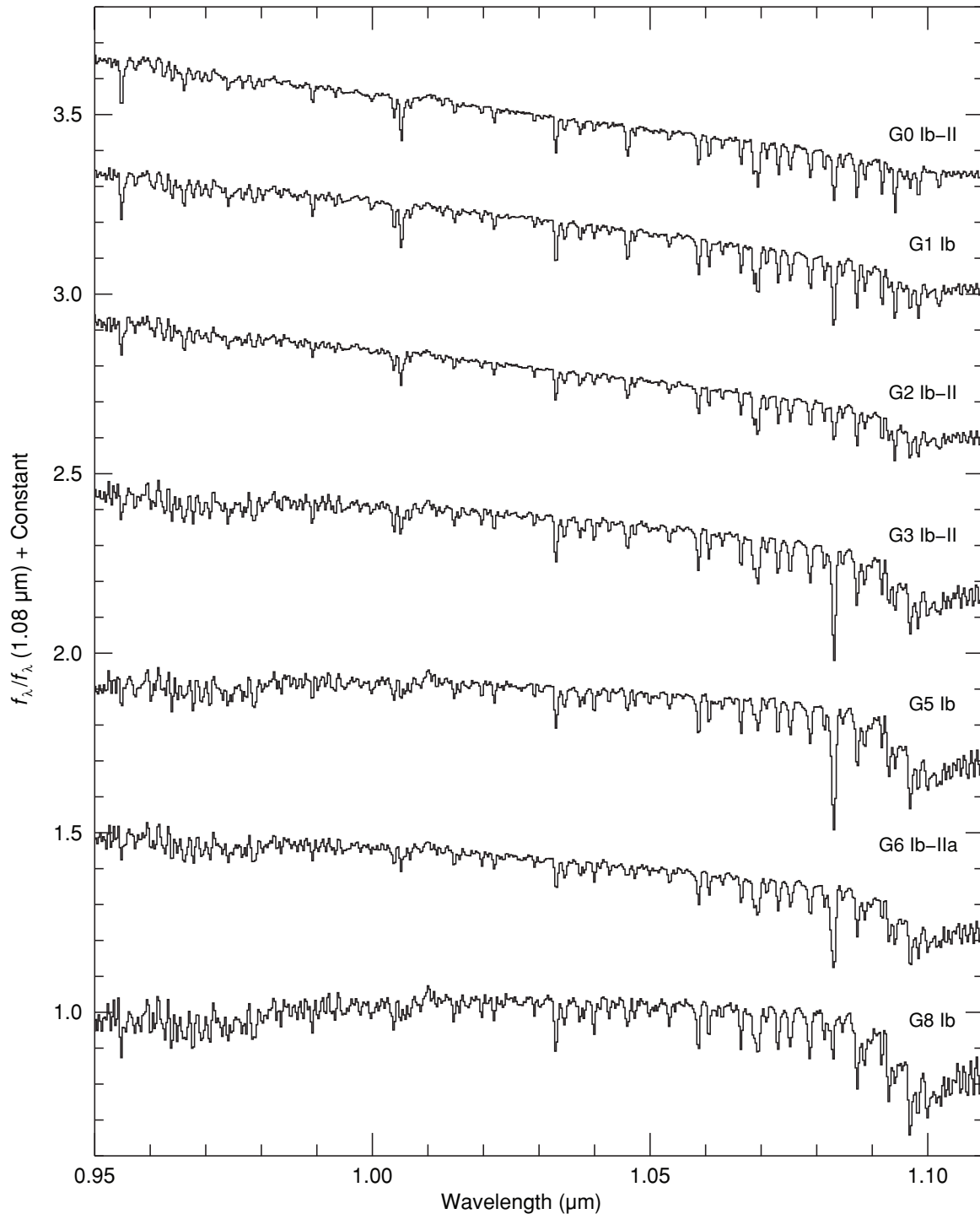


Figure 64. Sequence of G supergiant stars plotted over the Y band (0.95 – $1.10 \mu\text{m}$). The spectra are of HD 185018 (G0 Ib-II), HD 74395 (G1 Ib), HD 3421 (G2 Ib-II), HD 192713 (G3 Ib-II Wk H&K comp?), HD 190113 (G5 Ib), HD 202314 (G6 Ib-IIa Ca1 B0.5), and HD 208606 (G8 Ib). The spectra have been normalized to unity at $1.08 \mu\text{m}$ and offset by constants.

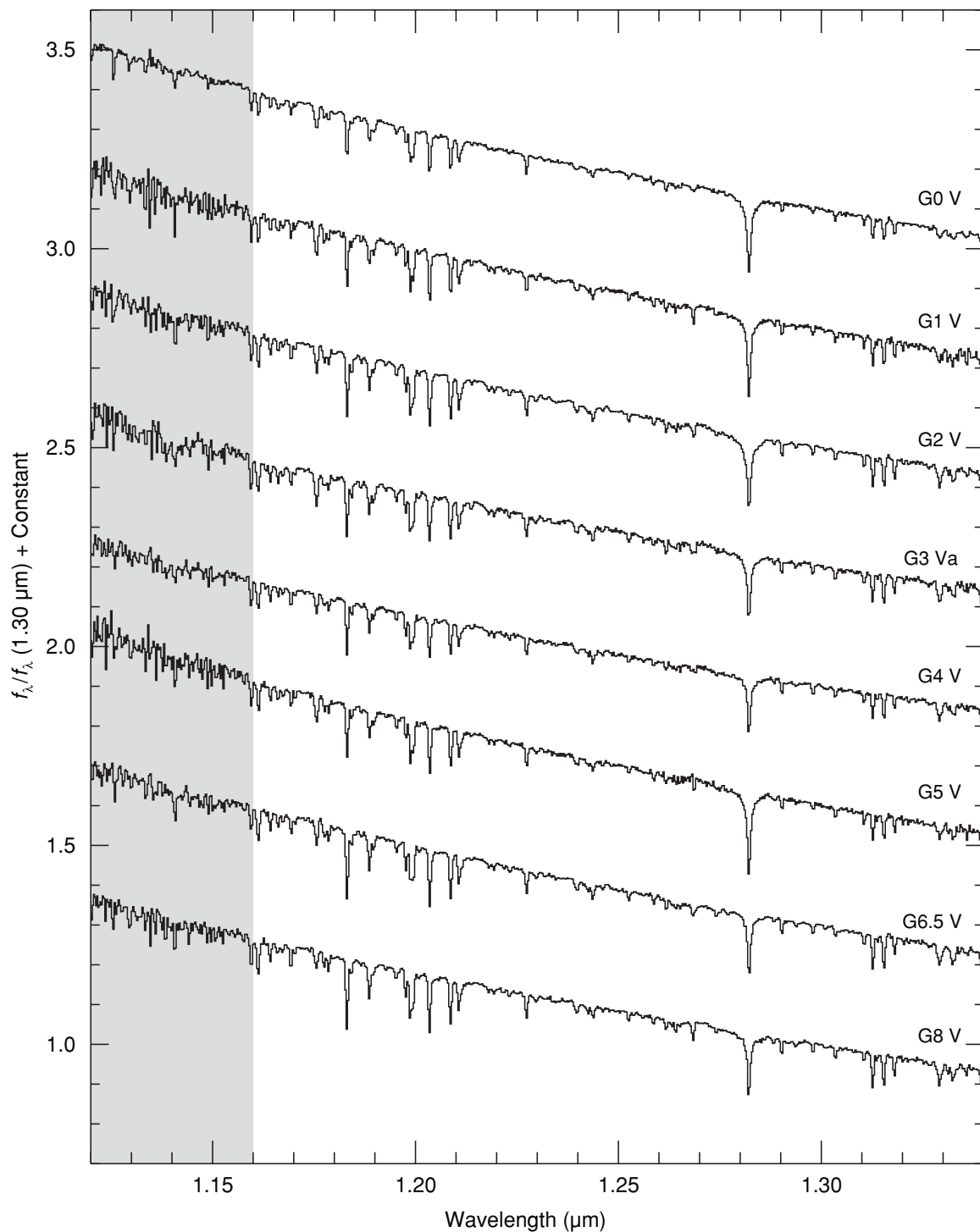


Figure 65. Sequence of G dwarf stars plotted over the *J* band (1.12–1.34 μm). The spectra are of HD 109358 (G0 V), HD 10307 (G1 V), HD 76151 (G2 V), HD 10697 (G3 Va), HD 214850 (G4 V), HD 165185 (G5 V), HD 115617 (G6.5 V), and HD 101501 (G8 V). The spectra have been normalized to unity at 1.30 μm and offset by constants.

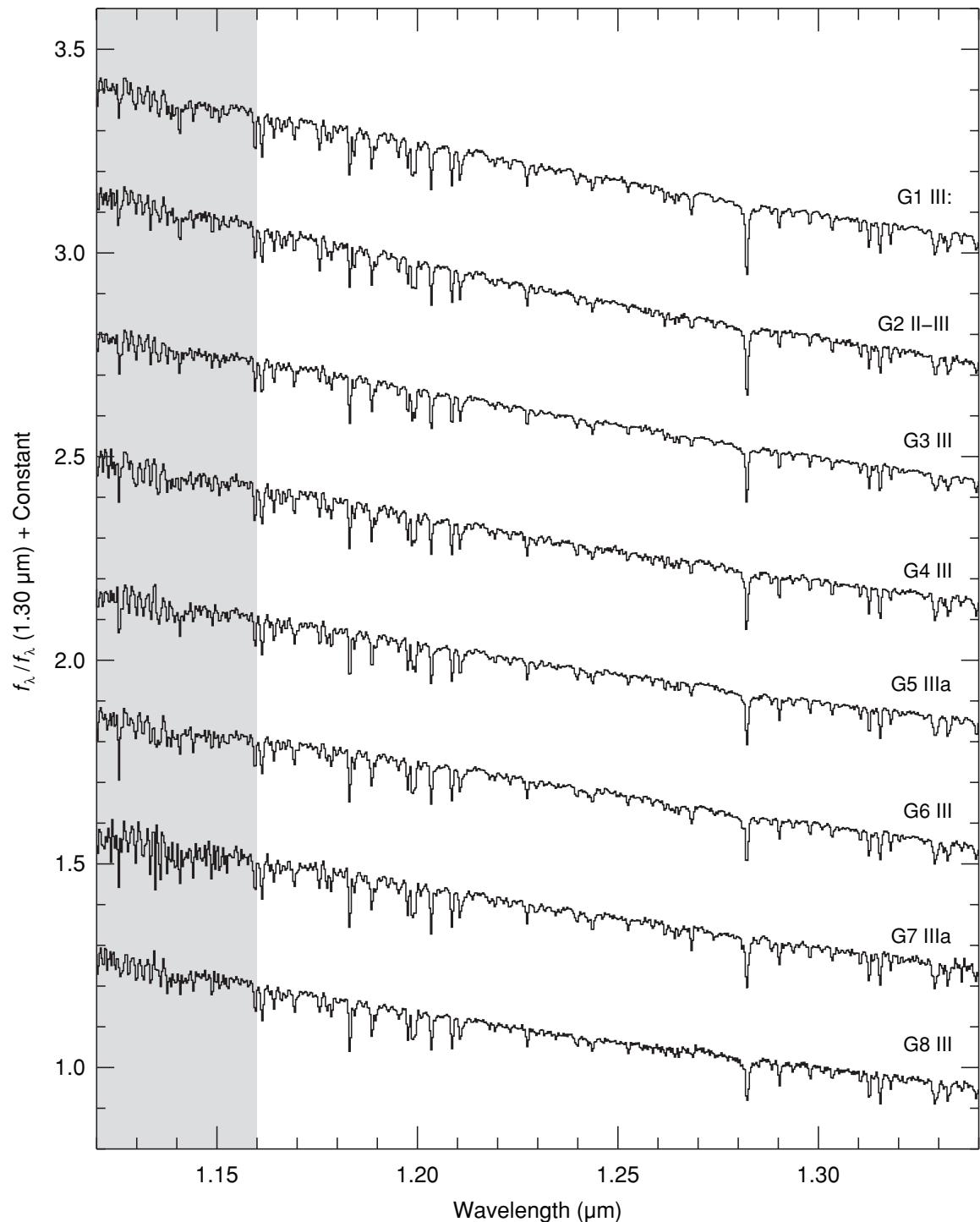


Figure 66. Sequence of G giant stars plotted over the *J* band (1.12–1.34 μm). The spectra are of HD 21018 (G1 III:CH-1:), HD 219477 (G2 II-III), HD 88639 (G3b III Fe-1), HD 108477 (G4 III), HD 193896 (G5 IIIa), HD 27277 (G6 III), HD 182694 (G7 IIIa), and HD 135722 (G8 III Fe-1). The spectra have been normalized to unity at 1.30 μm and offset by constants.

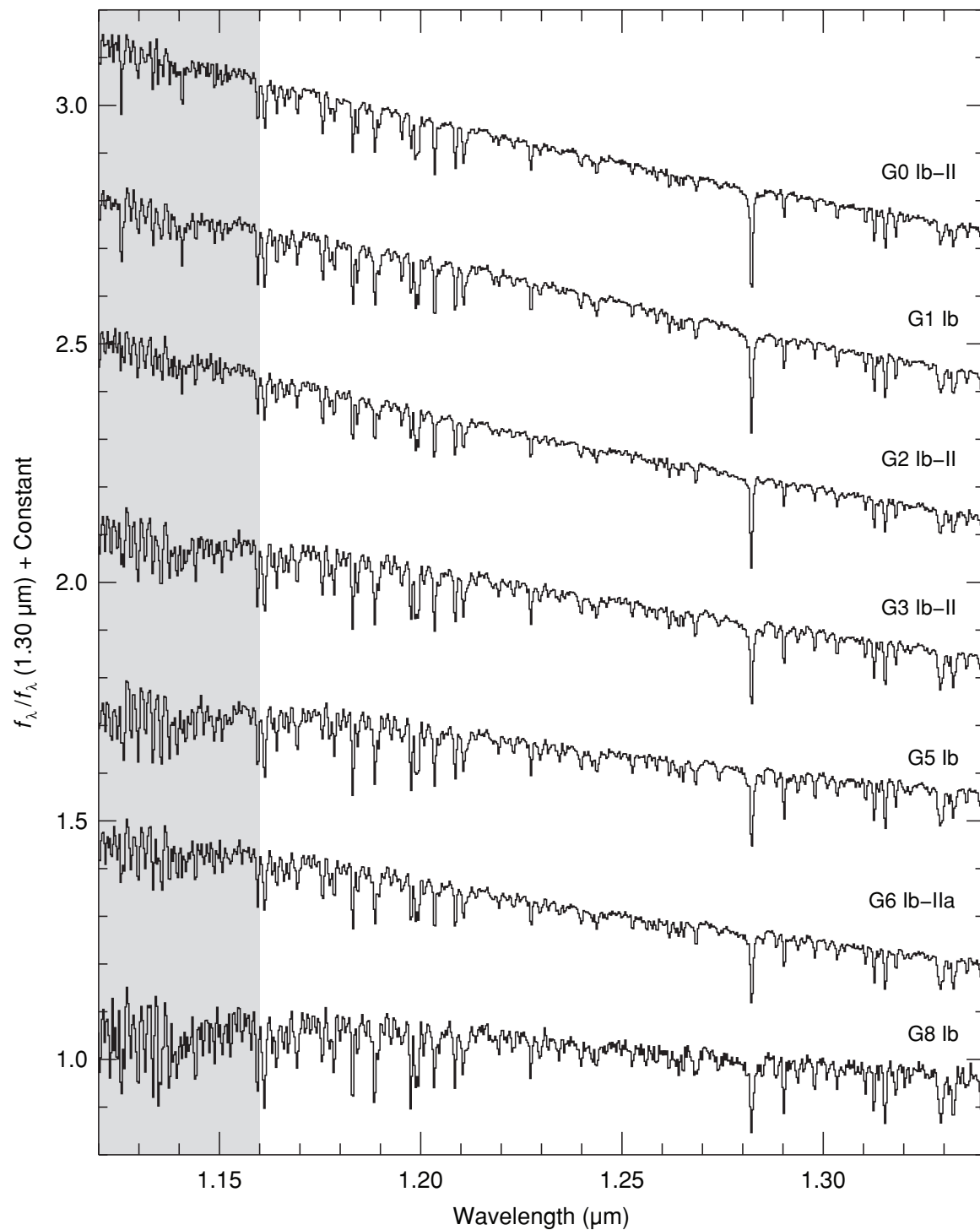


Figure 67. Sequence of G supergiant stars plotted over the J band (1.12–1.34 μm). The spectra are of HD 185018 (G0 Ib-II), HD 74395 (G1 Ib), HD 3421 (G2 Ib-II), HD 192713 (G3 Ib-II Wk H&K comp?), HD 190113 (G5 Ib), HD 202314 (G6 Ib-IIa CaI B0.5), and HD 208606 (G8 Ib). The spectra have been normalized to unity at 1.30 μm and offset by constants.

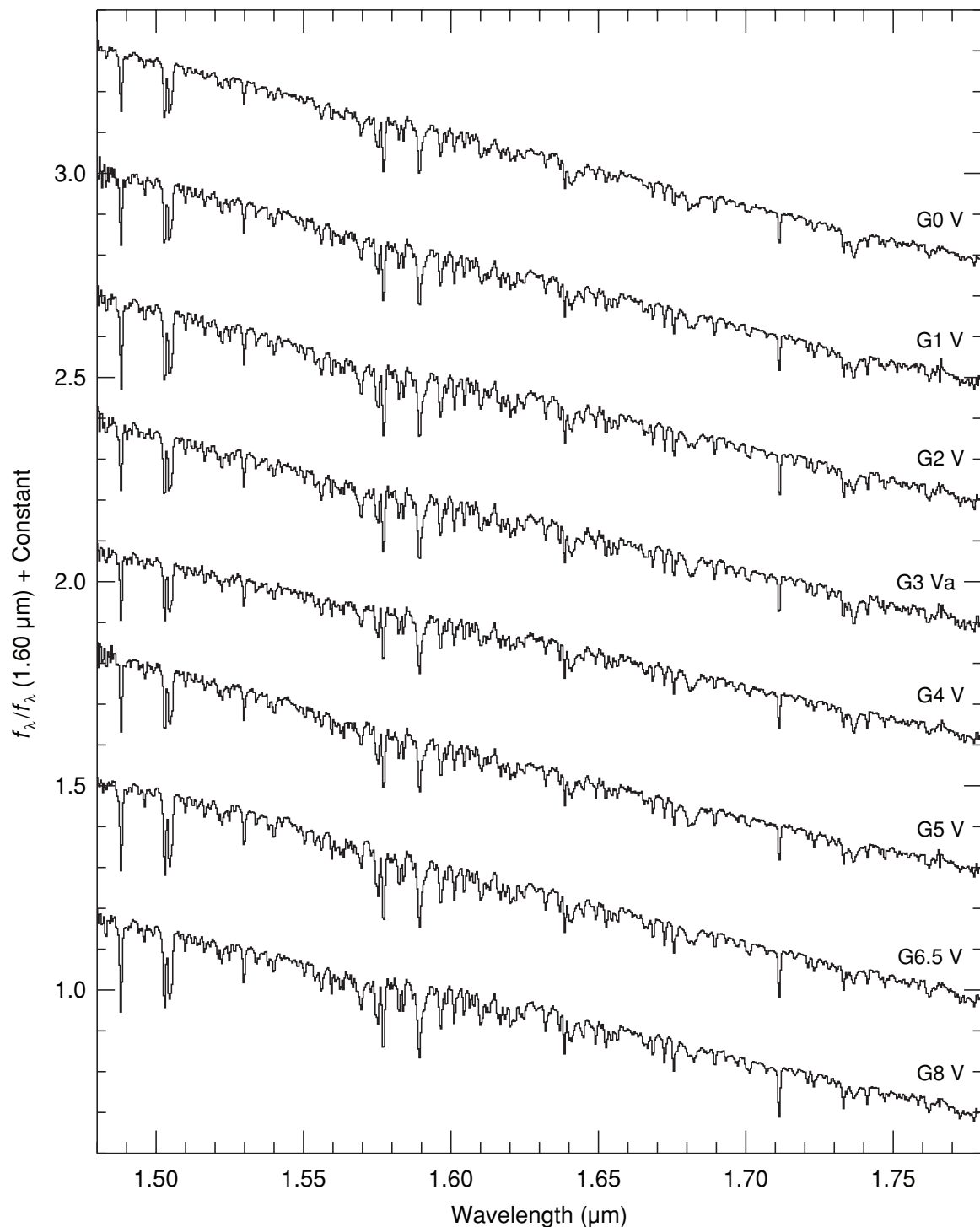


Figure 68. Sequence of G dwarf stars plotted over the *H* band (1.48–1.78 μm). The spectra are of HD 109358 (G0 V), HD 10307 (G1 V), HD 76151 (G2 V), HD 10697 (G3 Va), HD 214850 (G4 V), HD 165185 (G5 V), HD 115617 (G6.5 V), and HD 101501 (G8 V). The spectra have been normalized to unity at 1.60 μm and offset by constants.

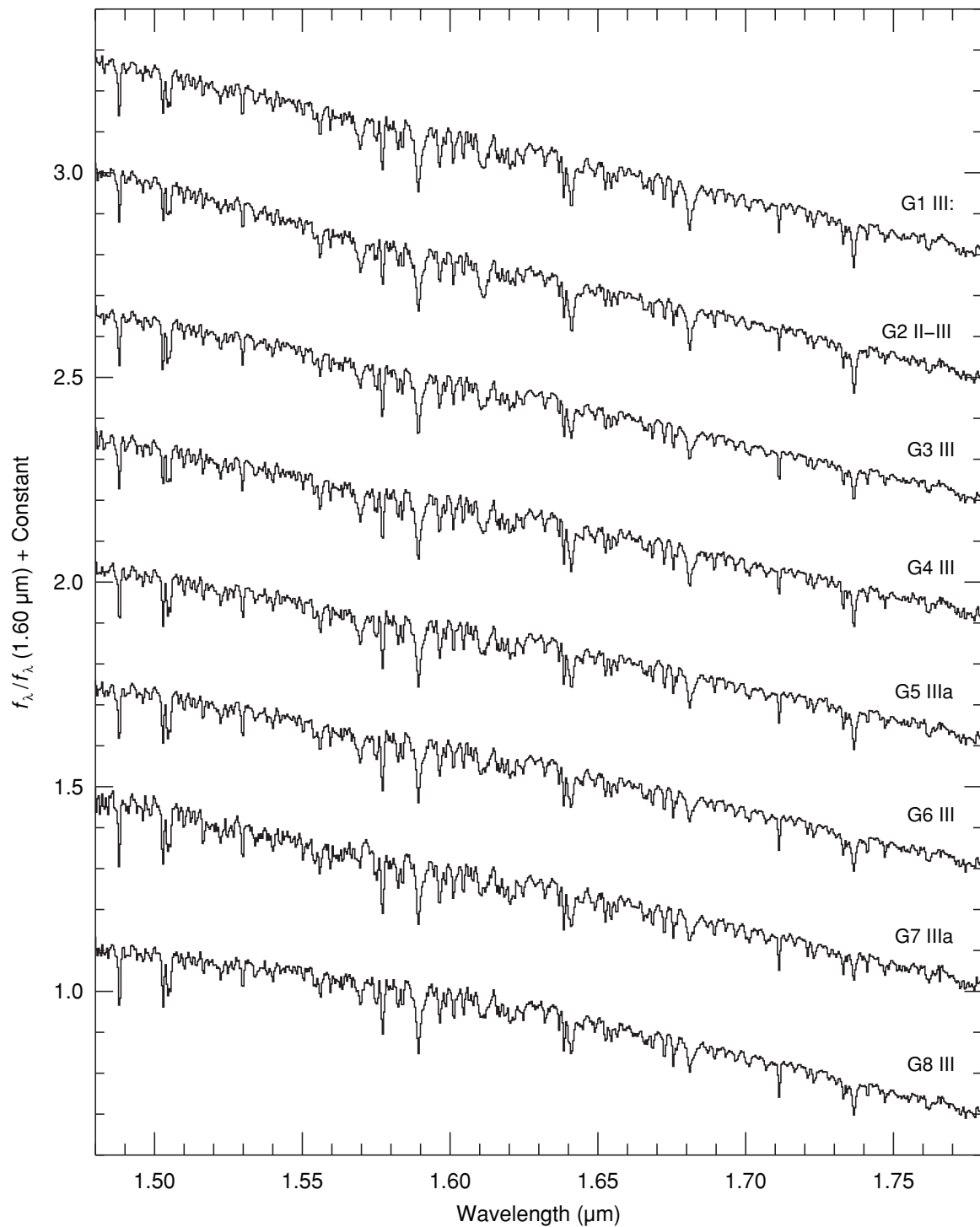


Figure 69. Sequence of G giant stars plotted over the *H* band (1.48–1.78 μm). The spectra are of HD 21018 (G1 III:CH-1:), HD 219477 (G2 II-III), HD 88639 (G3b III Fe-1), HD 108477 (G4 III), HD 193896 (G5 IIIa), HD 27277 (G6 III), HD 182694 (G7 IIIa), and HD 135722 (G8 III Fe-1). The spectra have been normalized to unity at 1.60 μm and offset by constants.

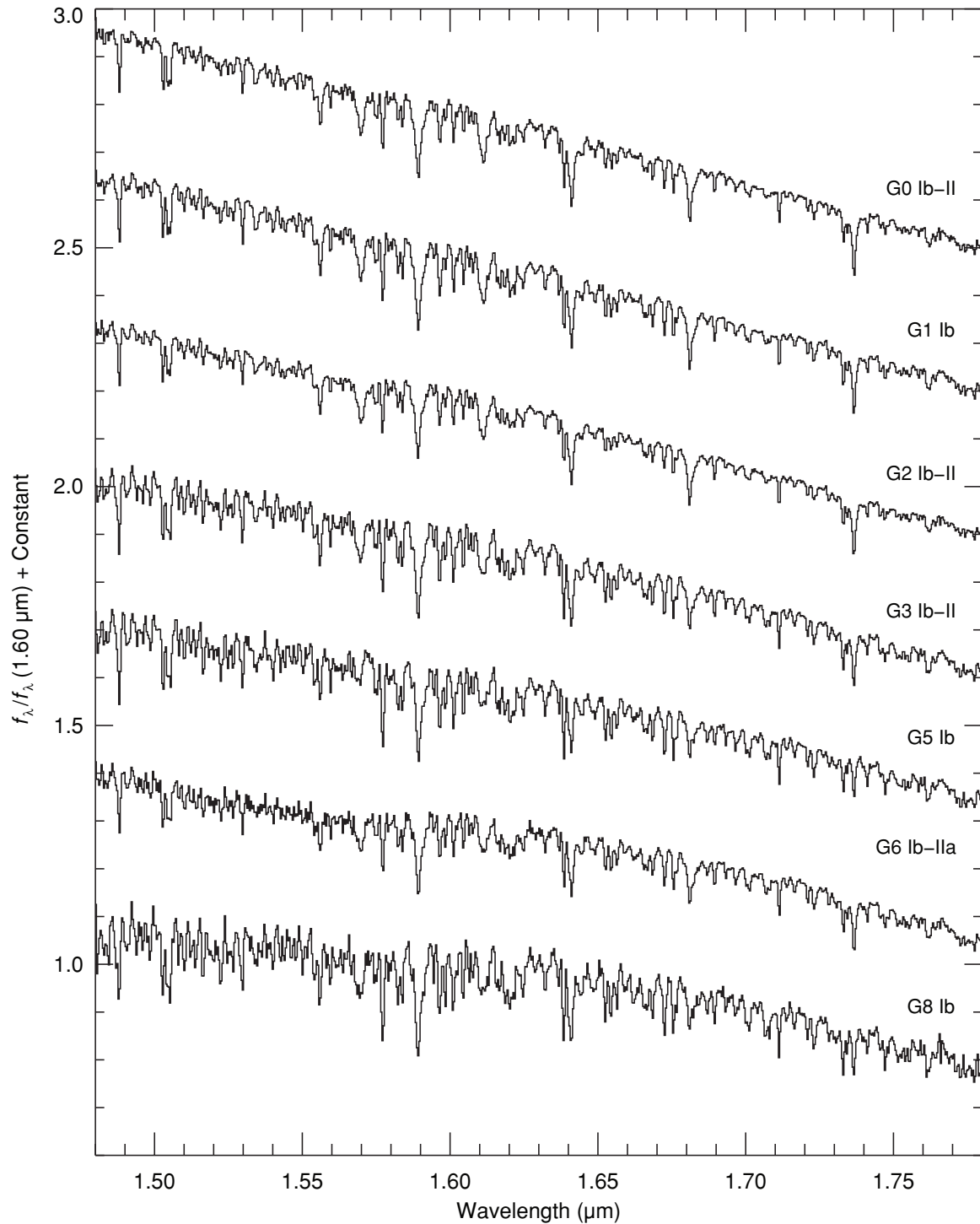


Figure 70. Sequence of G supergiant stars plotted over the *H* band (1.48–1.78 μm). The spectra are of HD 185018 (G0 Ib-II), HD 74395 (G1 Ib), HD 3421 (G2 Ib-II), HD 192713 (G3 Ib-II Wk H&K comp?), HD 190113 (G5 Ib), HD 202314 (G6 Ib-IIa Cal B0.5), and HD 208606 (G8 Ib). The spectra have been normalized to unity at $1.60 \mu\text{m}$ and offset by constants.

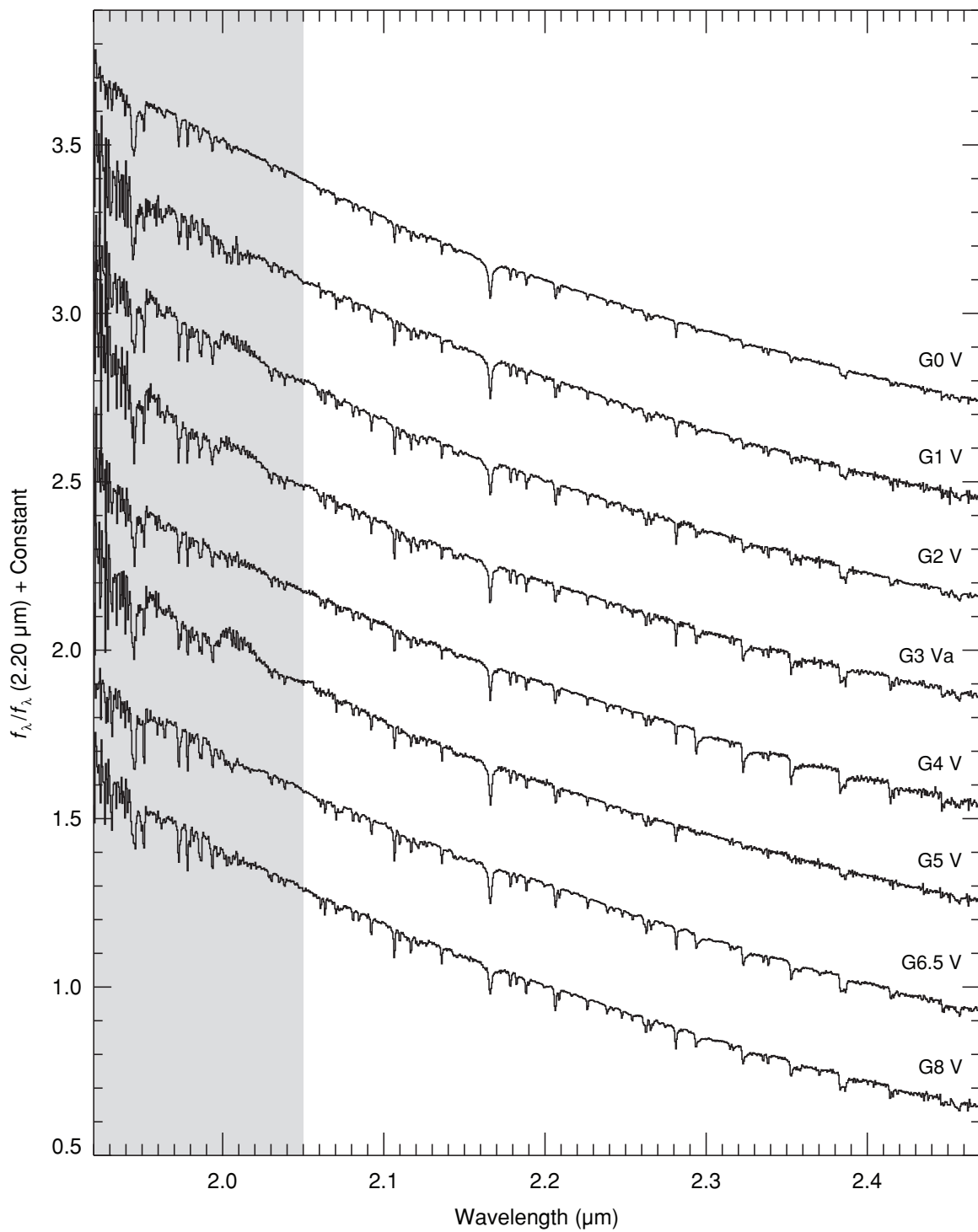


Figure 71. Sequence of G dwarf stars plotted over the *K* band (1.92–2.58 μm). The spectra are of HD 109358 (G0 V), HD 10307 (G1 V), HD 76151 (G2 V), HD 10697 (G3 Va), HD 214850 (G4 V), HD 165185 (G5 V), HD 115617 (G6.5 V), and HD 101501 (G8 V). The spectra have been normalized to unity at 2.20 μm and offset by constants.

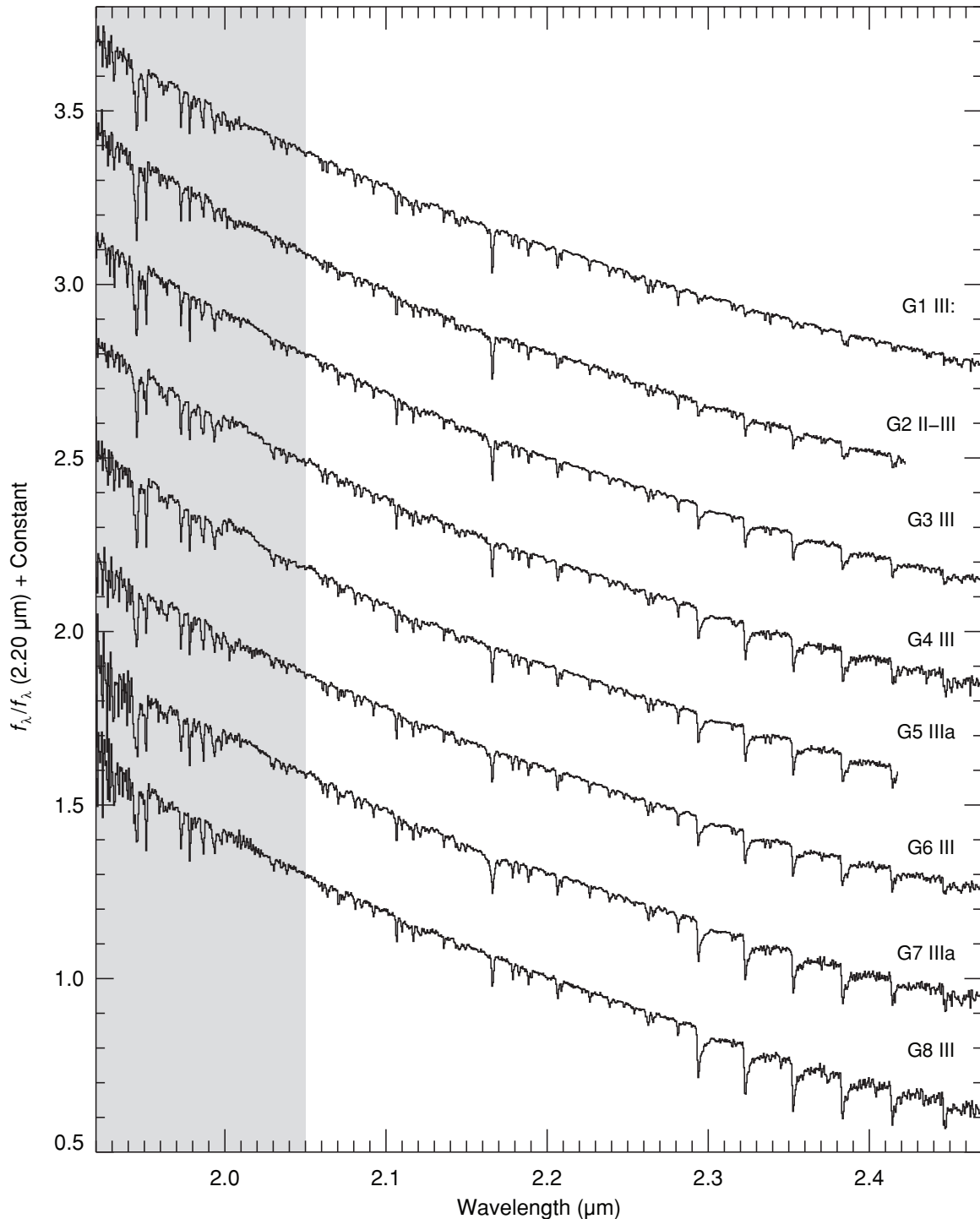


Figure 72. Sequence of G giant stars plotted over the K band (1.92–2.5 μm). The spectra are of HD 21018 (G1 III:CH-1:), HD 219477 (G2 II-III), HD 88639 (G3b III Fe-1), HD 108477 (G4 III), HD 193896 (G5 IIIa), HD 27277 (G6 III), HD 182694 (G7 IIIa), and HD 135722 (G8 III Fe-1). The spectra have been normalized to unity at 2.20 μm and offset by constants.

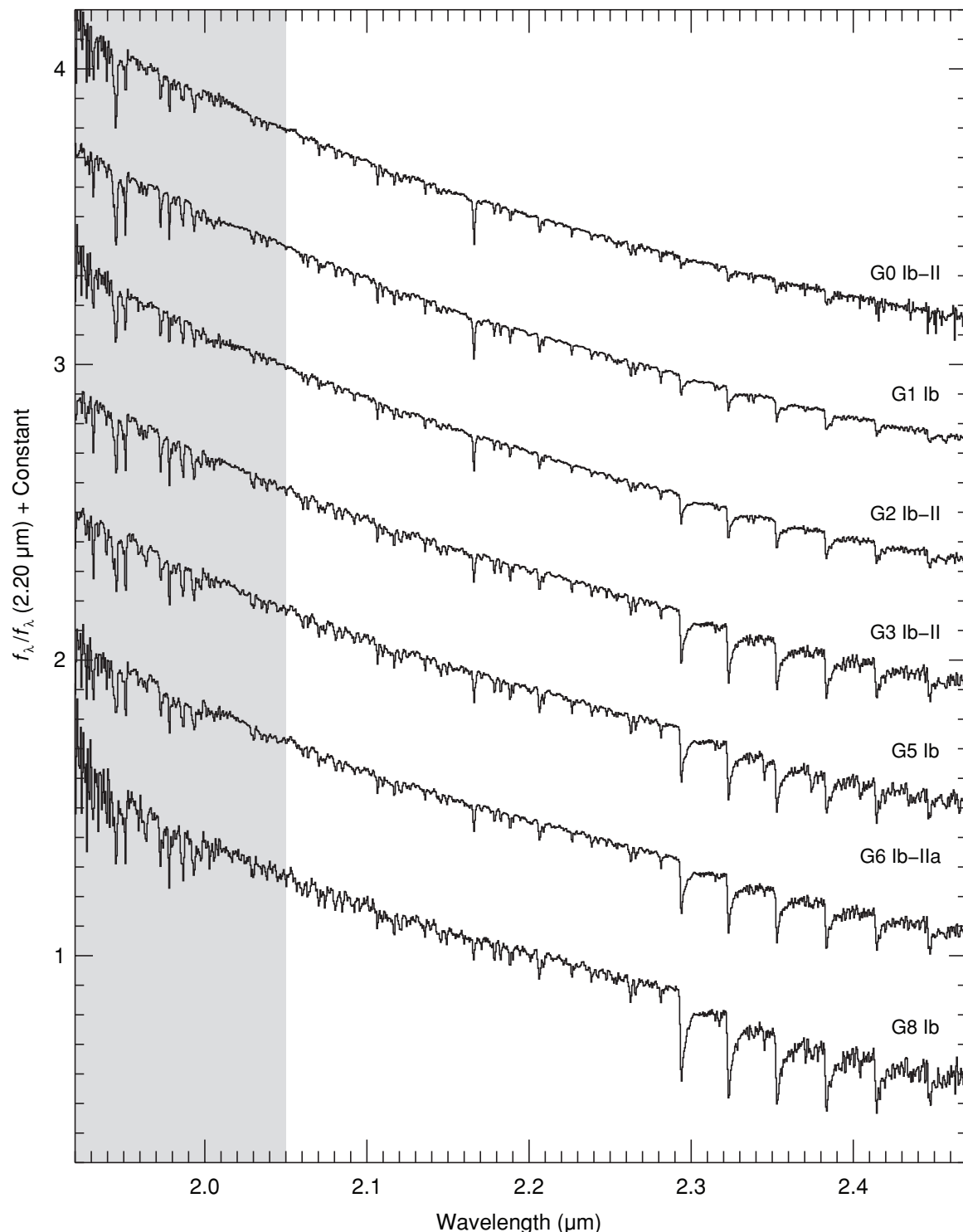


Figure 73. Sequence of G supergiant stars plotted over the K band ($1.92\text{--}2.5\,\mu\text{m}$). The spectra are of HD 185018 (G0 Ib-II), HD 74395 (G1 Ib), HD 3421 (G2 Ib-II), HD 192713 (G3 Ib-II Wk H&K comp?), HD 190113 (G5 Ib), HD 202314 (G6 Ib-IIa Ca1 B0.5), and HD 208606 (G8 Ib). The spectra have been normalized to unity at $2.20\,\mu\text{m}$ and offset by constants.

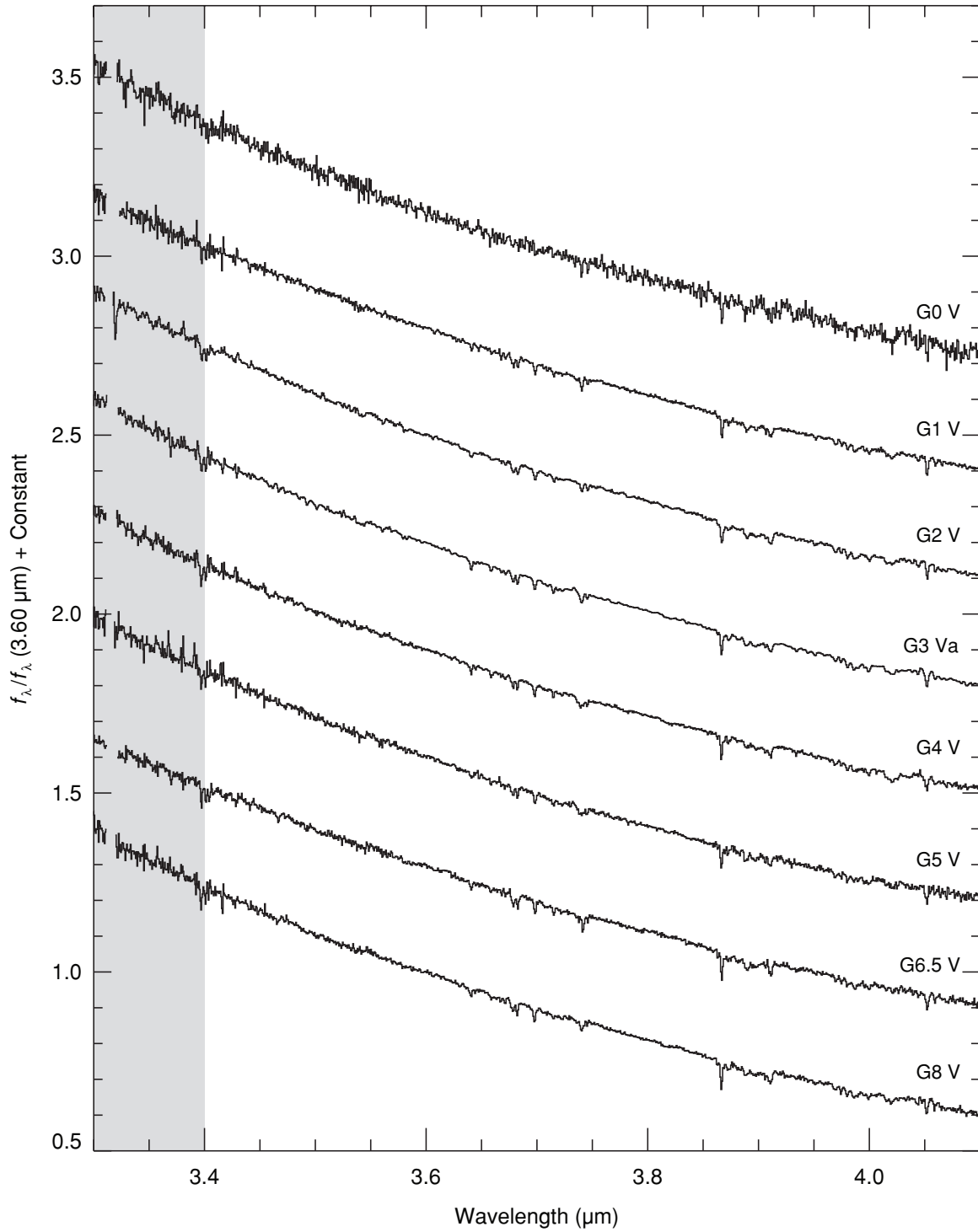


Figure 74. Sequence of G dwarf stars plotted over the L' band ($3.3\text{--}4.1 \mu\text{m}$). The spectra are of HD 109358 (G0 V), HD 10307 (G1 V), HD 76151 (G2 V), HD 10697 (G3 Va), HD 214850 (G4 V), HD 165185 (G5 V), HD 115617 (G6.5 V), and HD 101501 (G8 V). The spectra have been normalized to unity at $3.6 \mu\text{m}$ and offset by constants.

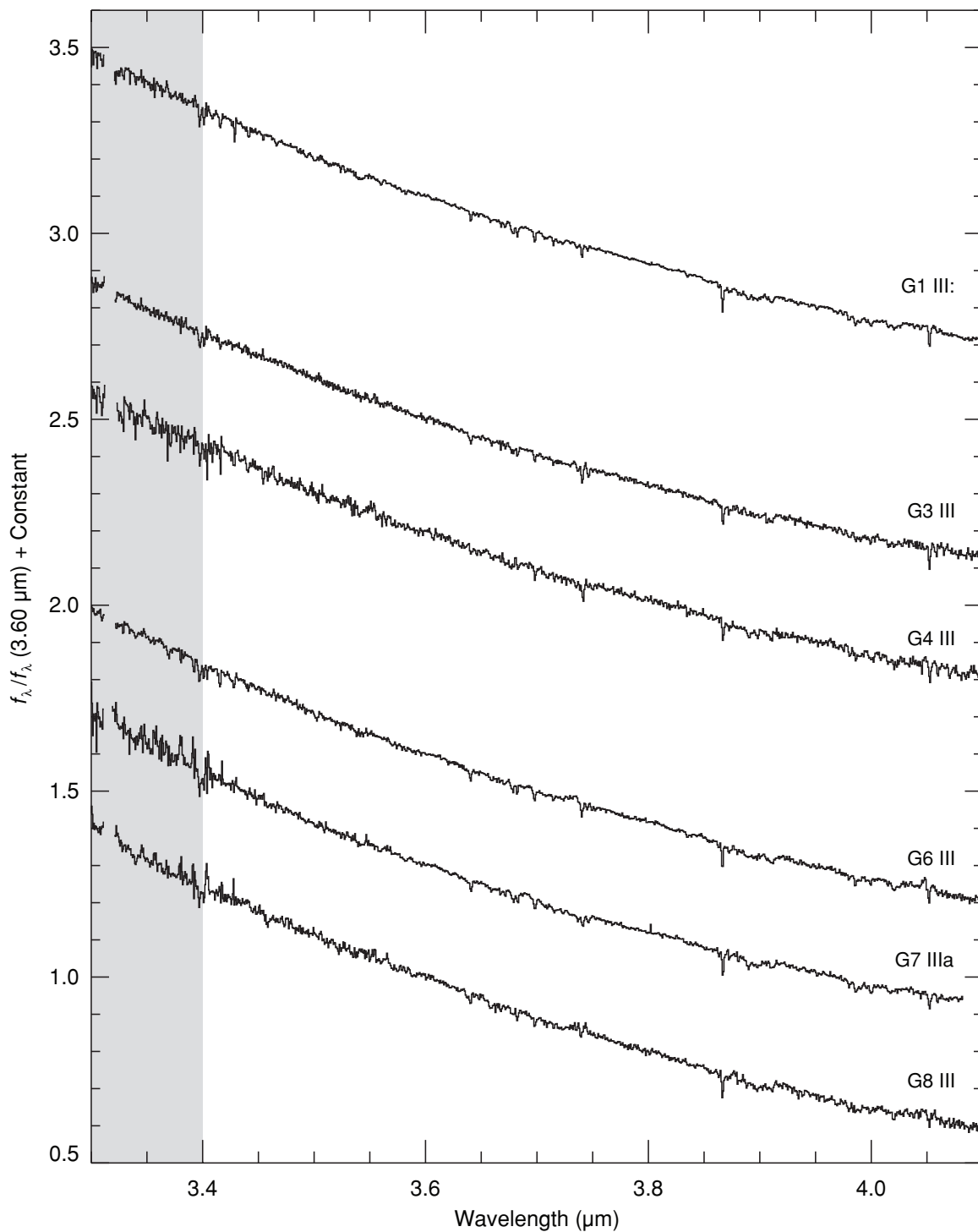


Figure 75. Sequence of G giant stars plotted over the L' band (3.6–4.1 μm). The spectra are of HD 21018 (G1 III:CH–1), HD 219477 (G2 II–III), HD 88639 (G3b III Fe–1), HD 108477 (G4 III), HD 193896 (G5 IIIa), HD 27277 (G6 III), HD 182694 (G7 IIIa), and HD 135722 (G8 III Fe–1). The spectra have been normalized to unity at 3.6 μm and offset by constants.

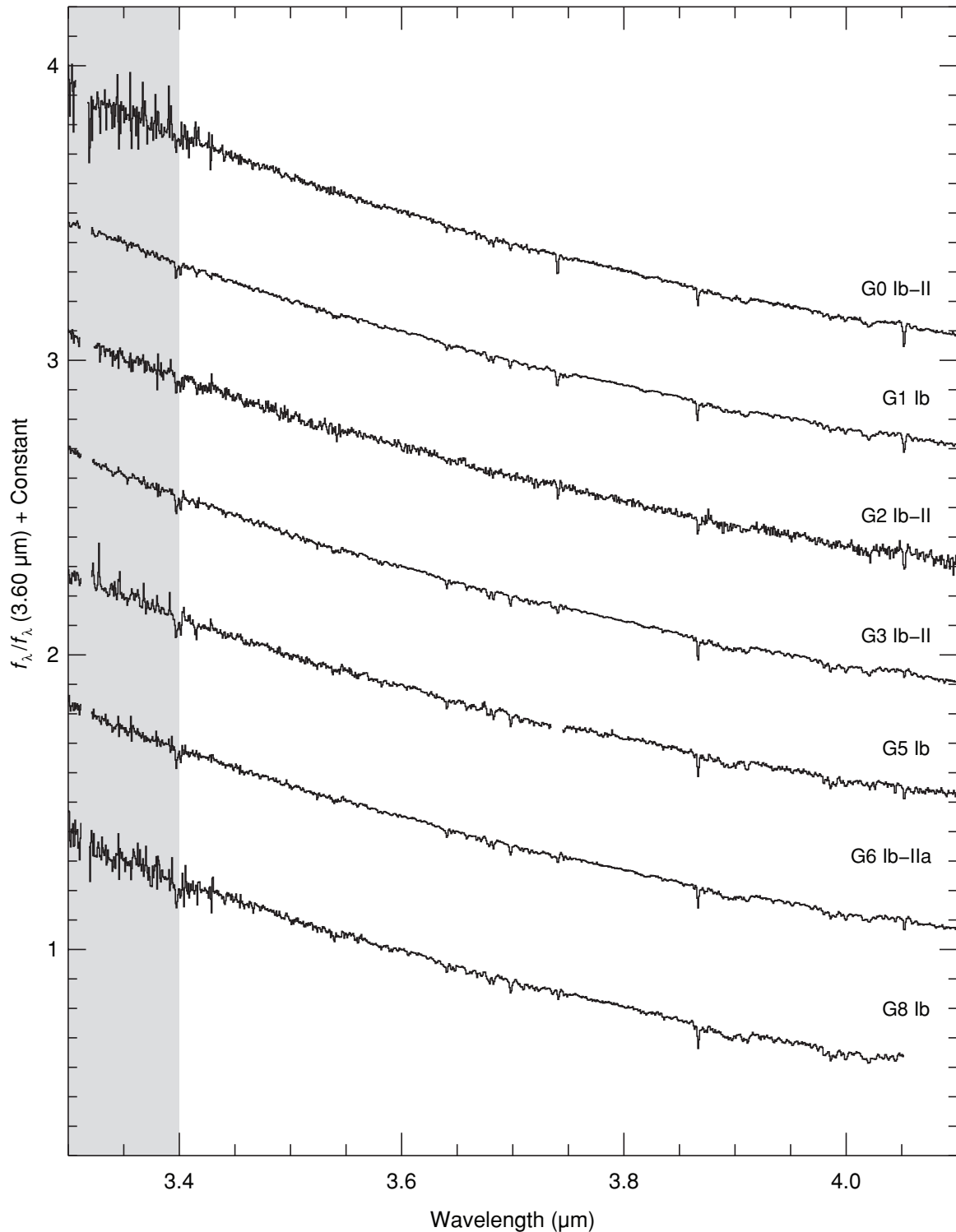


Figure 76. Sequence of G supergiant stars plotted over the L' band (3.6–4.1 μm). The spectra are of HD 185018 (G0 Ib-II), HD 74395 (G1 Ib), HD 3421 (G2 Ib-II), HD 192713 (G3 Ib-II Wk H&K comp?), HD 190113 (G5 Ib), HD 202314 (G6 Ib-IIa Ca1 B0.5), and HD 208606 (G8 Ib). The spectra have been normalized to unity at 3.6 μm and offset by constants.

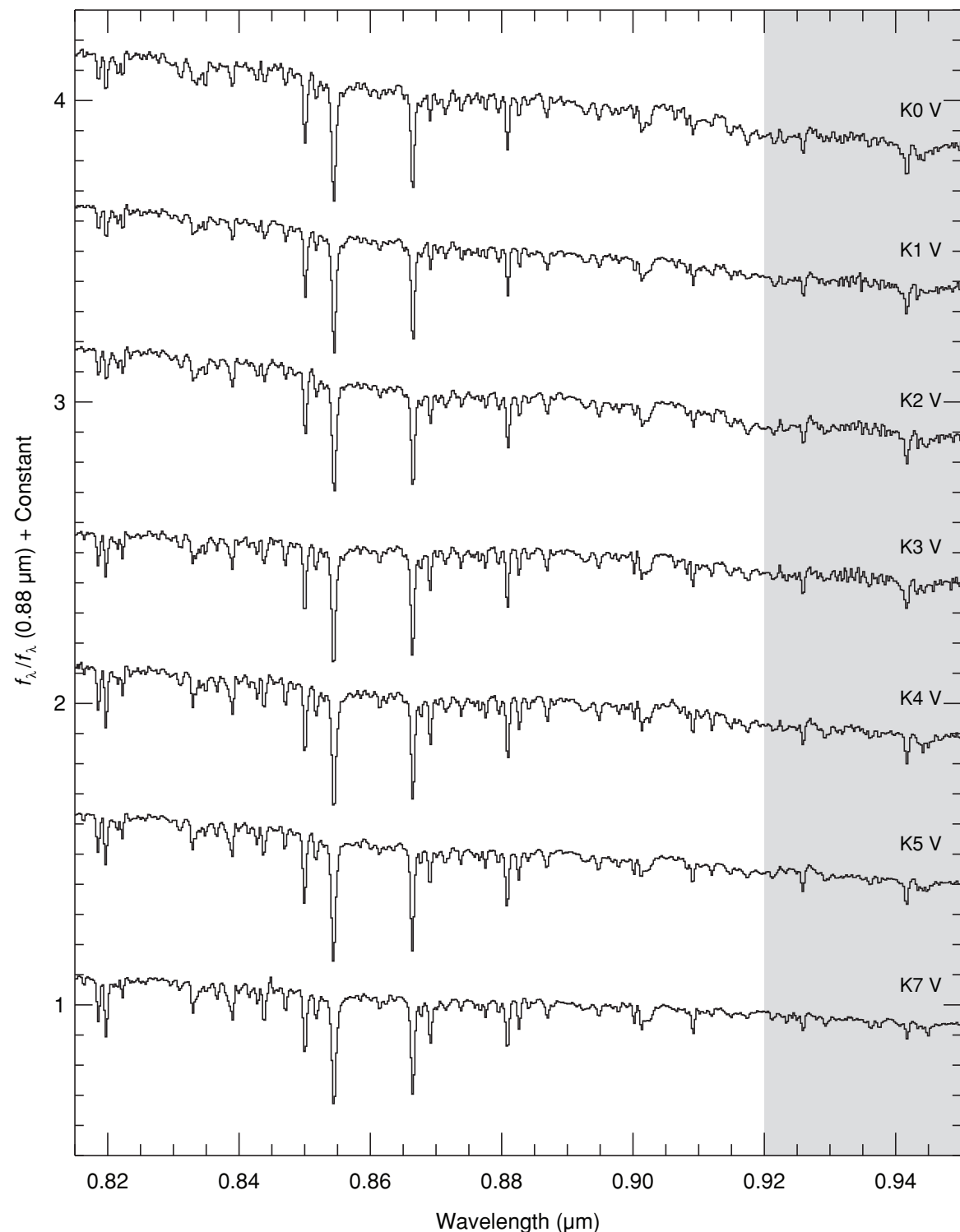


Figure 77. Sequence of K dwarf stars plotted over the I band ($0.82\text{--}0.95 \mu\text{m}$). The spectra are of HD 145675 (K0 V), HD 10476 (K1 V), HD 3765 (K2 V), HD 219134 (K3 V), HD 45977 (K4 V), HD 36003 (K5 V), and HD 237903 (K7 V). The spectra have been normalized to unity at $0.88 \mu\text{m}$ and offset by constants.

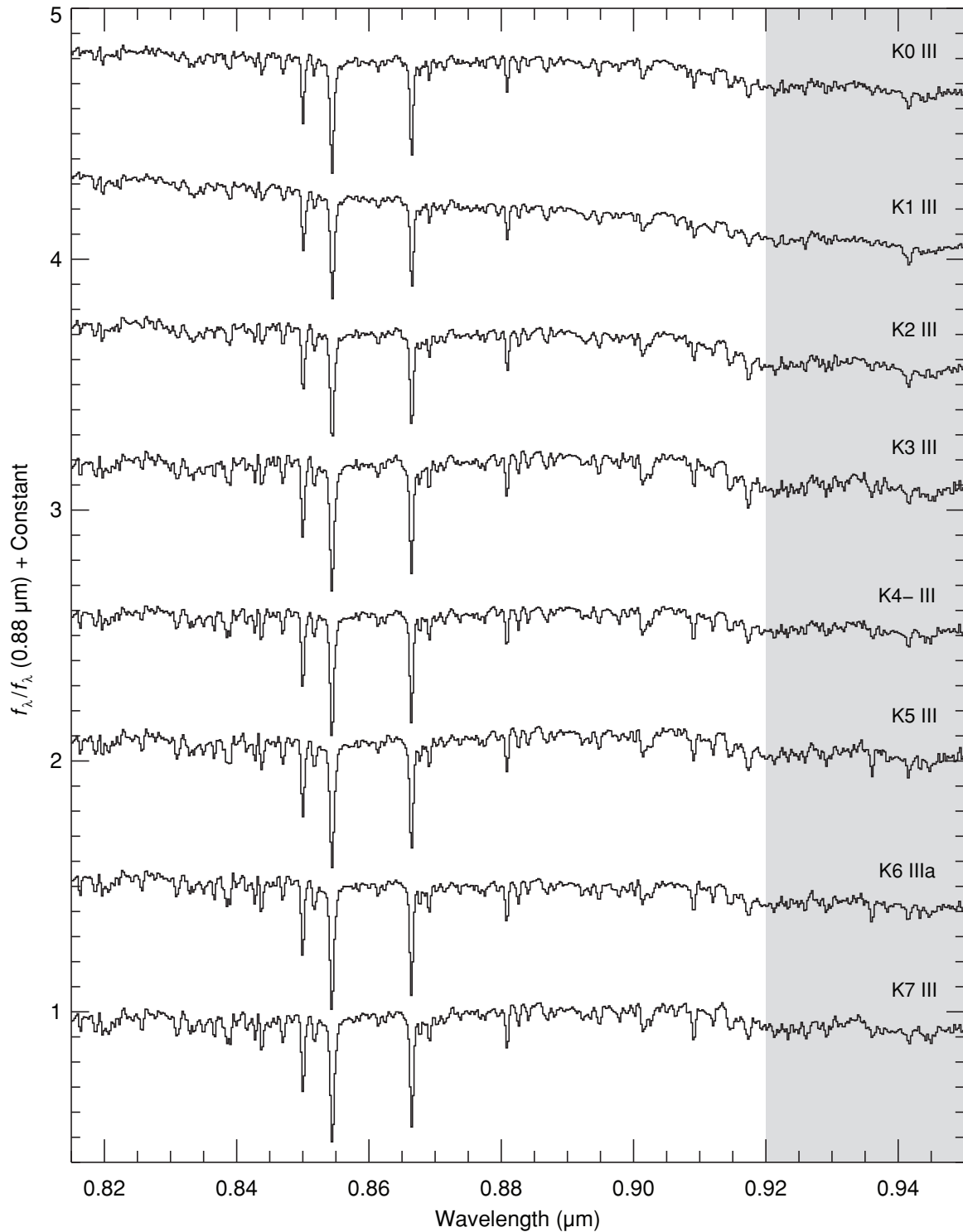


Figure 78. Sequence of K giant stars plotted over the I band (0.82–0.95 μm). The spectra are of HD 100006 (K0 III), HD 25975 (K1 III), HD 137759 (K2 III), HD 221246 (K3 III), HD 207991 (K4- III), HD 181596 (K5 III), HD 3346 (K6 IIIa), and HD 194193 (K7 III). The spectra have been normalized to unity at 0.88 μm and offset by constants.

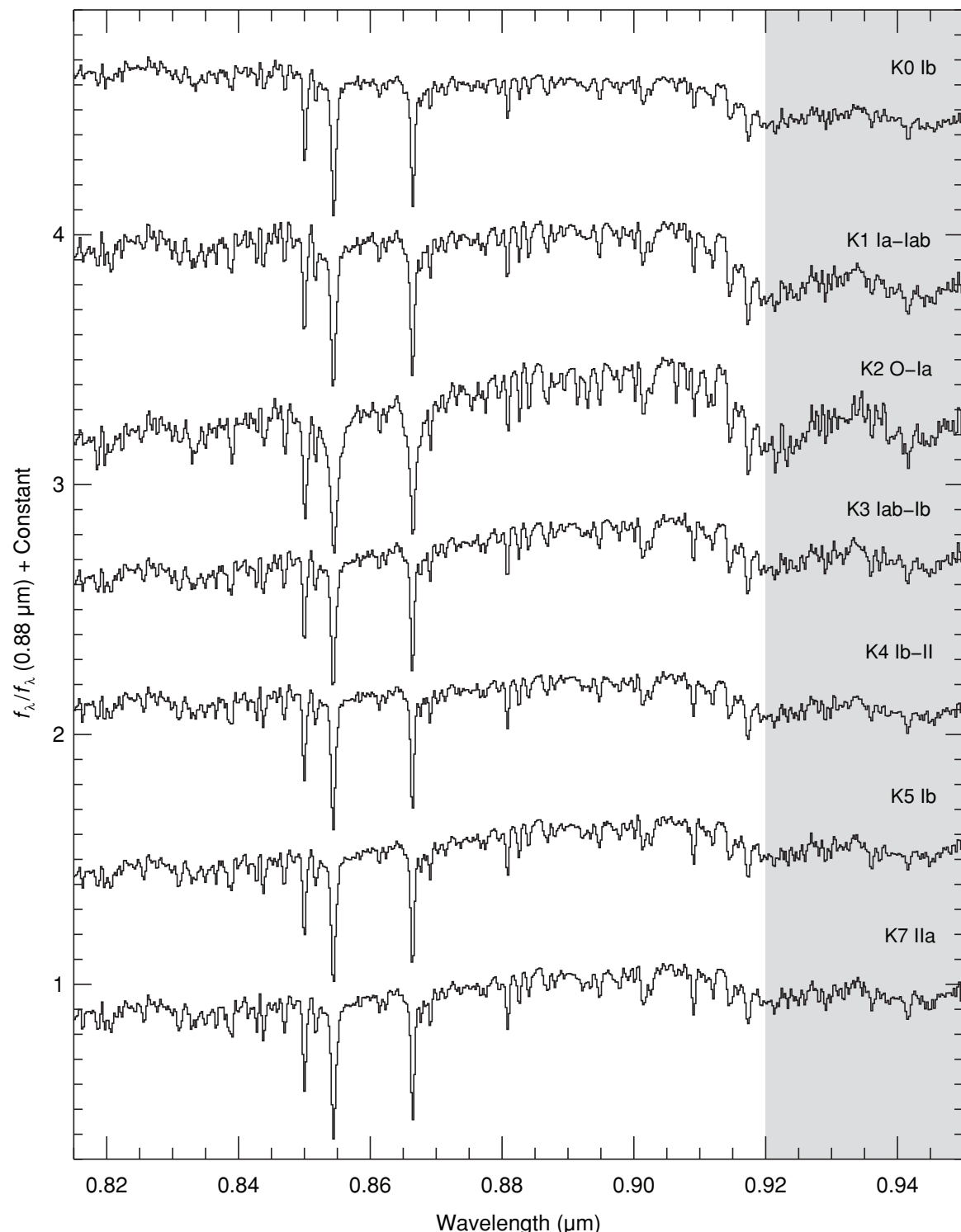


Figure 79. Sequence of K supergiant stars plotted over the I band (0.82–0.95 μm). The spectra are of HD 44391 (K0 Ib), HD 63302 (K1 Ia–Iab), HD 212466 (K2 O–Ia), HD 187238 (K3 Iab–Ib), HD 201065 (K4 Ib–II), HD 216946 (K5 Ib), and HD 181475 (K7 IIa). The spectra have been normalized to unity at 0.88 μm and offset by constants.

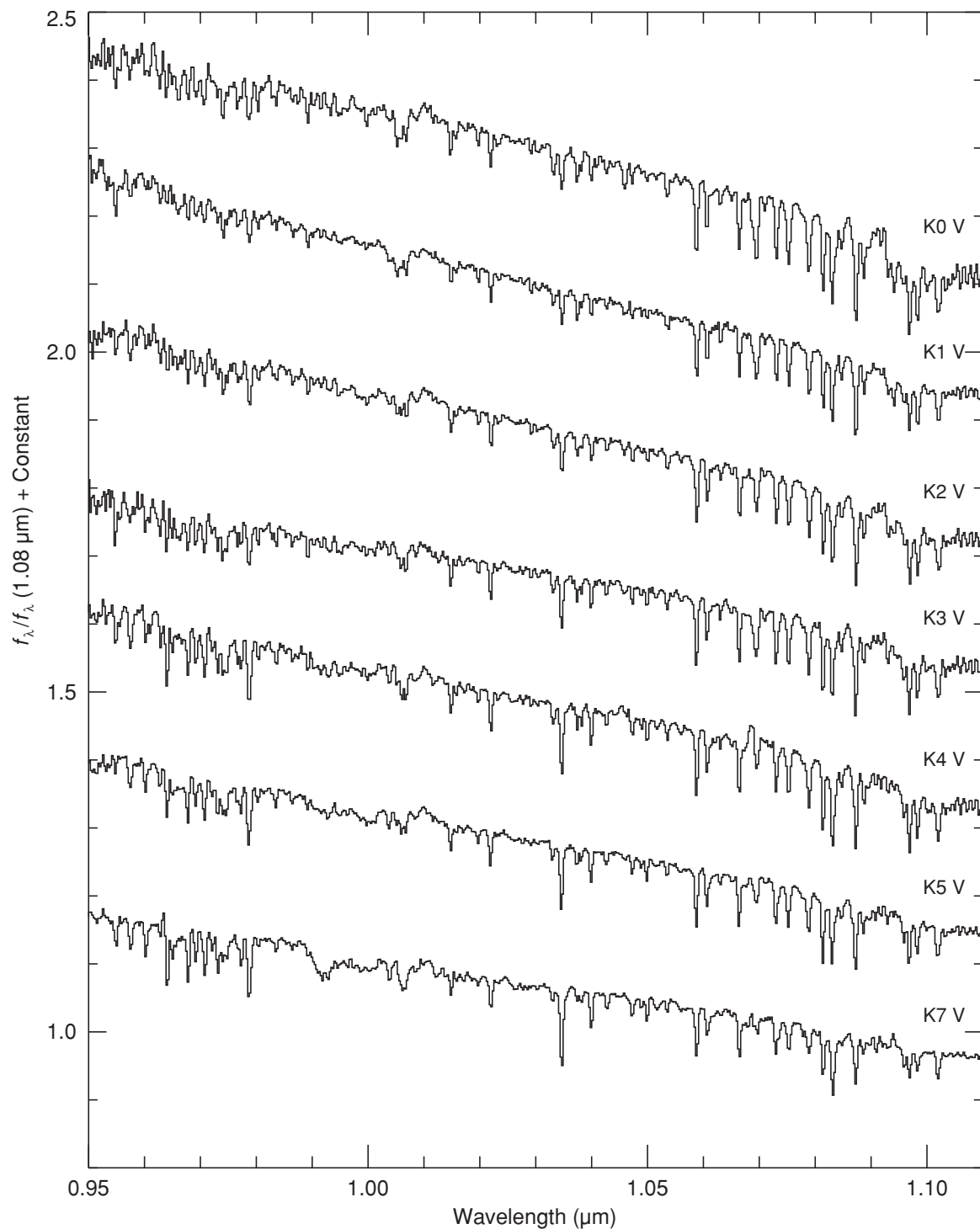


Figure 80. Sequence of K dwarf stars plotted over the Y band ($0.95\text{--}0.10\,\mu\text{m}$). The spectra are of HD 145675 (K0 V), HD 10476 (K1 V), HD 3765 (K2 V), HD 219134 (K3 V), HD 45977 (K4 V), HD 36003 (K5 V), and HD 237903 (K7 V). The spectra have been normalized to unity at $1.08\,\mu\text{m}$ and offset by constants.

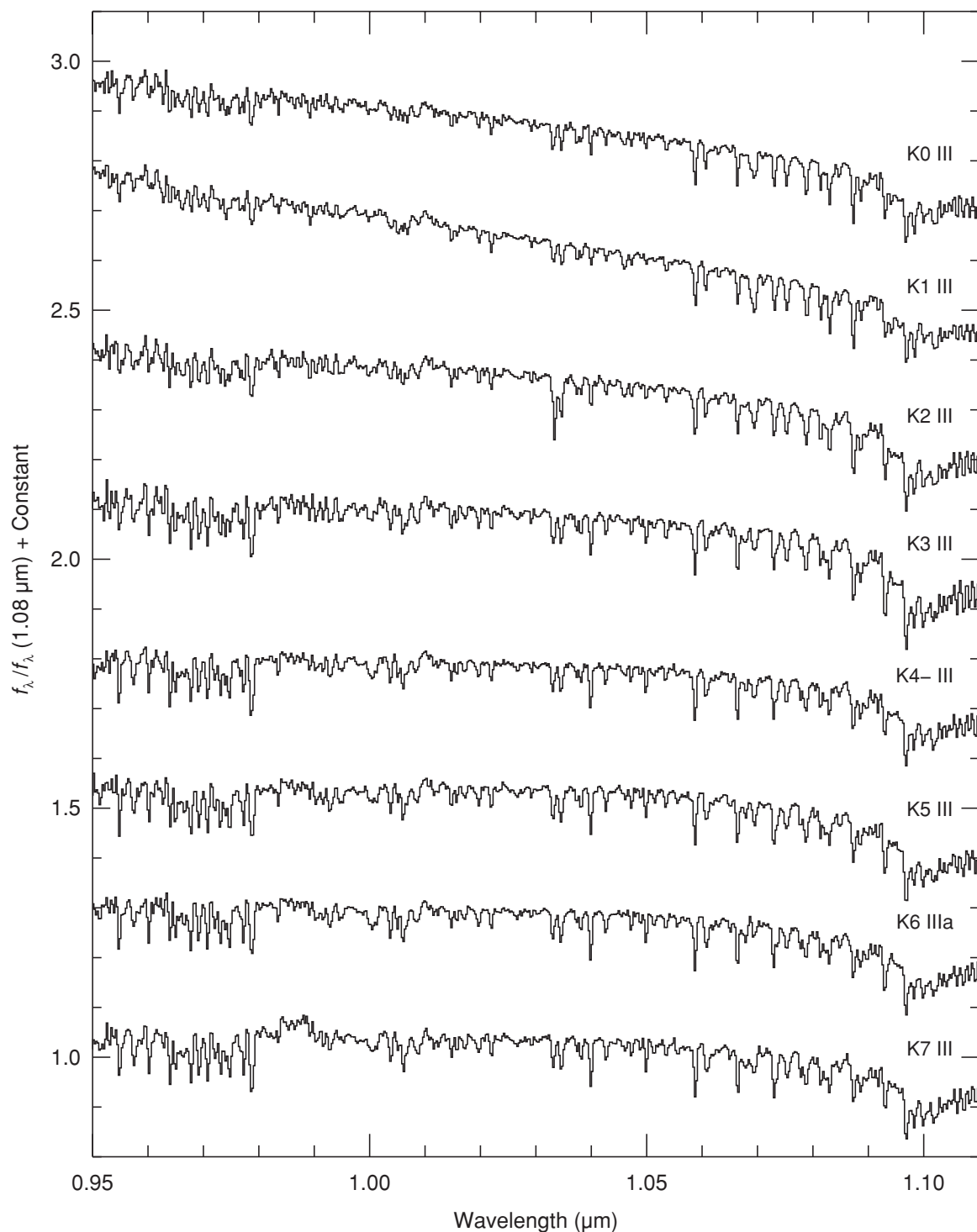


Figure 81. Sequence of K giant stars plotted over the Y band (0.95–1.10 μm). The spectra are of HD 100006 (K0 III), HD 25975 (K1 III), HD 137759 (K2 III), HD 221246 (K3 III), HD 207991 (K4– III), HD 181596 (K5 III), HD 3346 (K6 IIIa), and HD 194193 (K7 III). The spectra have been normalized to unity at 1.08 μm and offset by constants.

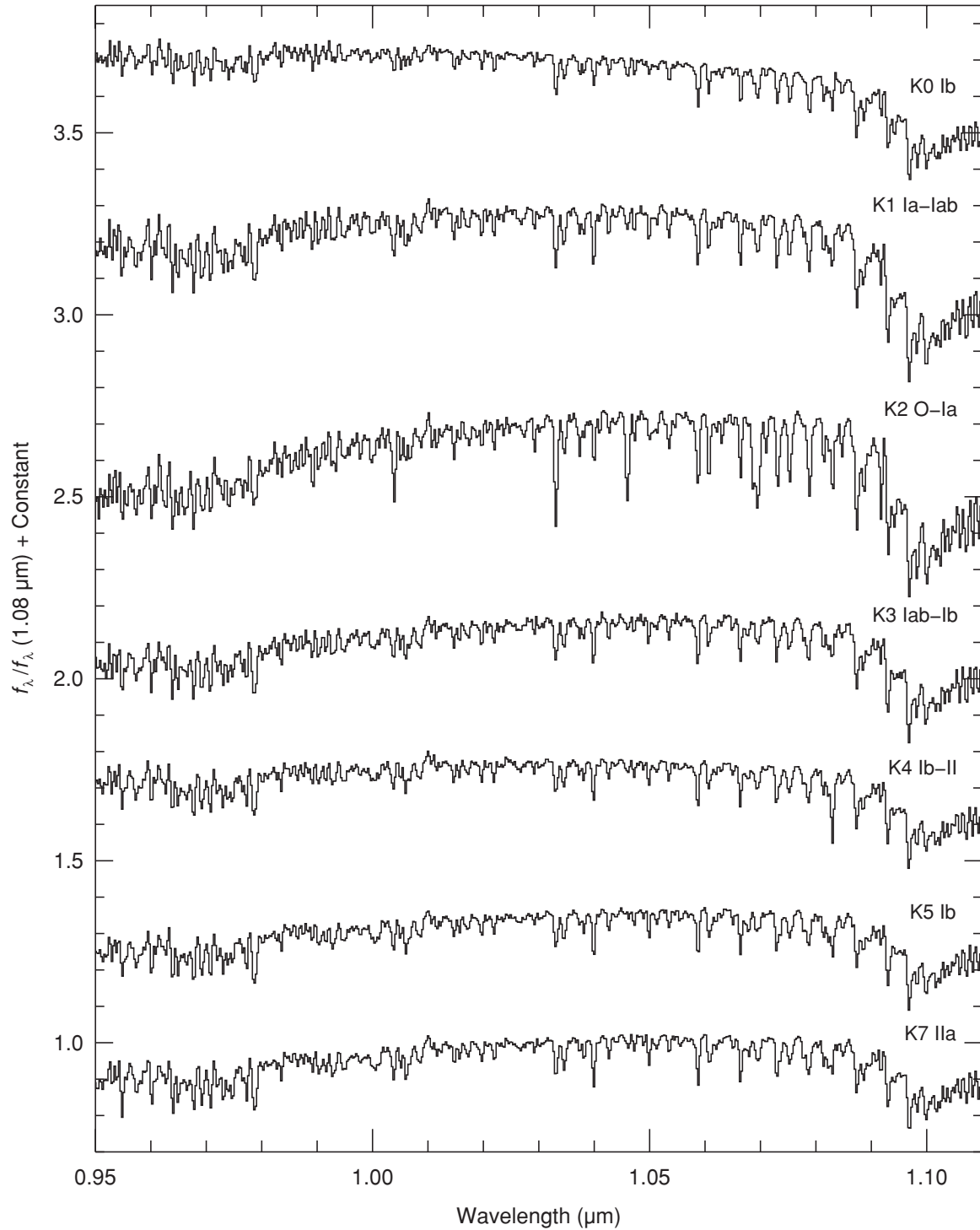


Figure 82. Sequence of K supergiant stars plotted over the Y band (0.95–1.10 μm). The spectra are of HD 44391 (K0 Ib), HD 63302 (K1 Ia–Iab), HD 212466 (K2 O–Ia), HD 187238 (K3 Iab–Ib), HD 201065 (K4 Ib–II), HD 216946 (K5 Ib), and HD 181475 (K7 IIa). The spectra have been normalized to unity at 1.08 μm and offset by constants.

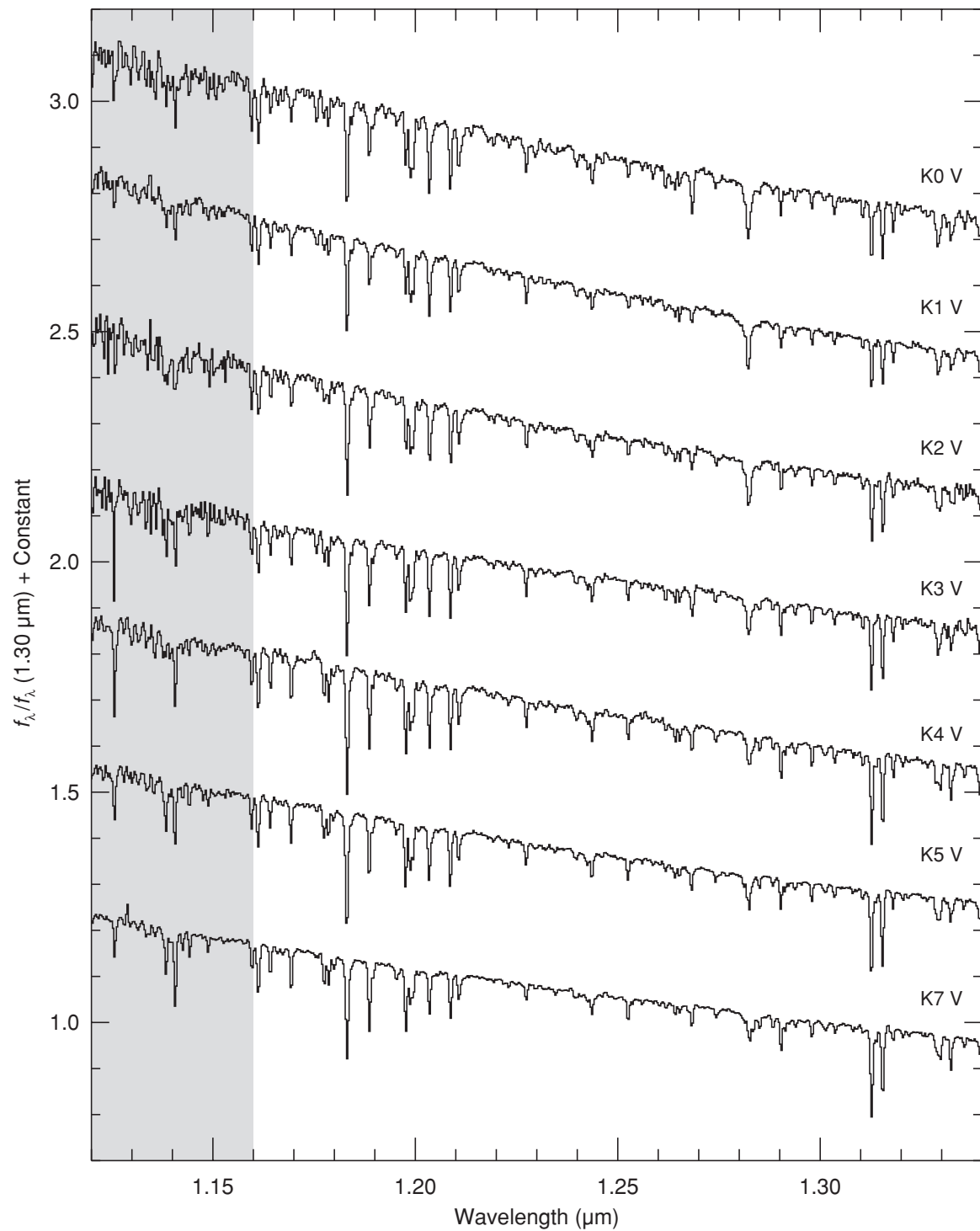


Figure 83. Sequence of K dwarf stars plotted over the *J* band (1.12–1.34 μm). The spectra are of HD 145675 (K0 V), HD 10476 (K1 V), HD 3765 (K2 V), HD 219134 (K3 V), HD 45977 (K4 V), HD 36003 (K5 V), and HD 237903 (K7 V). The spectra have been normalized to unity at 1.30 μm and offset by constants.

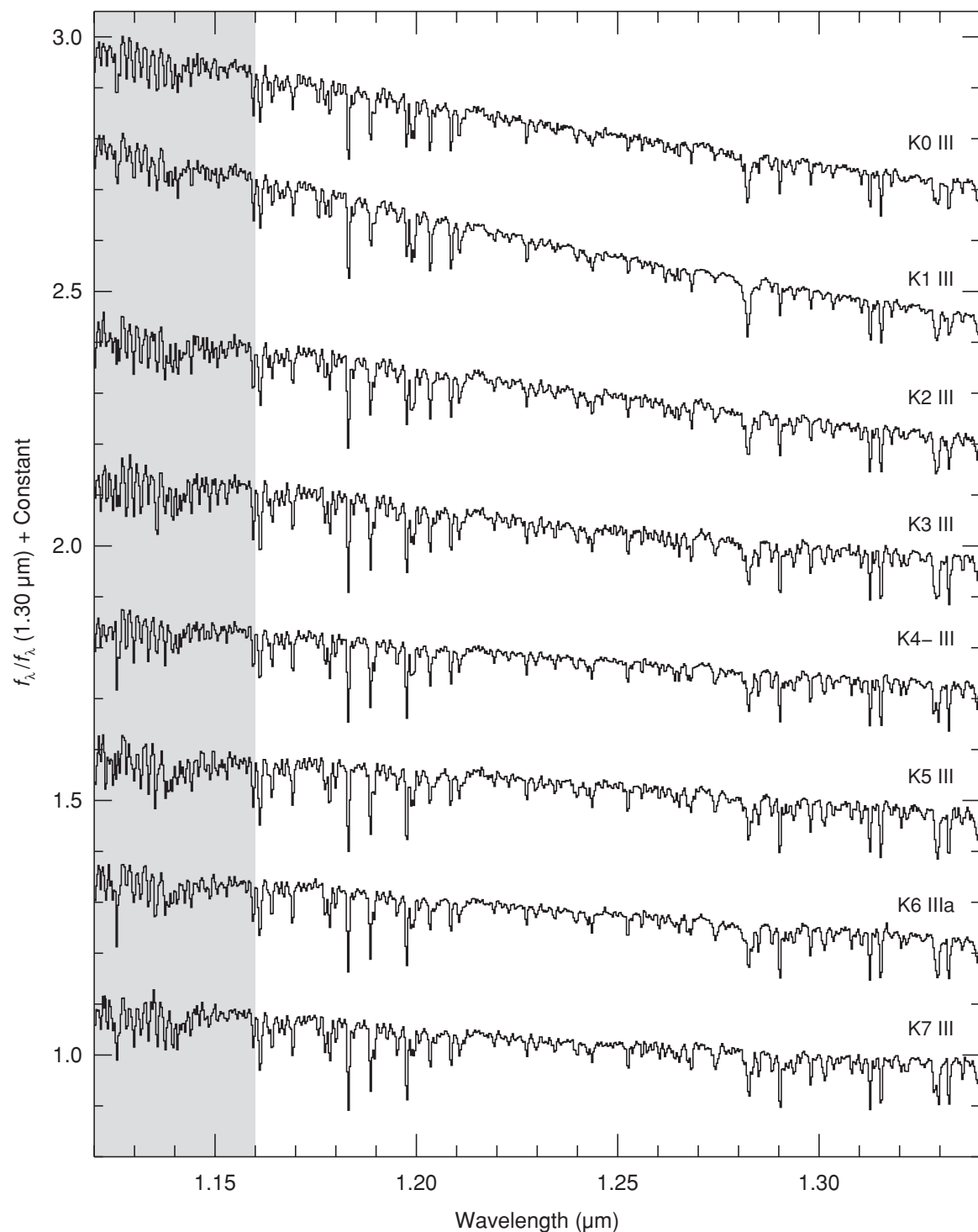


Figure 84. Sequence of K giant stars plotted over the J band (1.12–1.34 μm). The spectra are of HD 100006 (K0 III), HD 25975 (K1 III), HD 137759 (K2 III), HD 221246 (K3 III), HD 207991 (K4– III), HD 181596 (K5 III), HD 3346 (K6 IIIa), and HD 194193 (K7 III). The spectra have been normalized to unity at 1.30 μm and offset by constants.

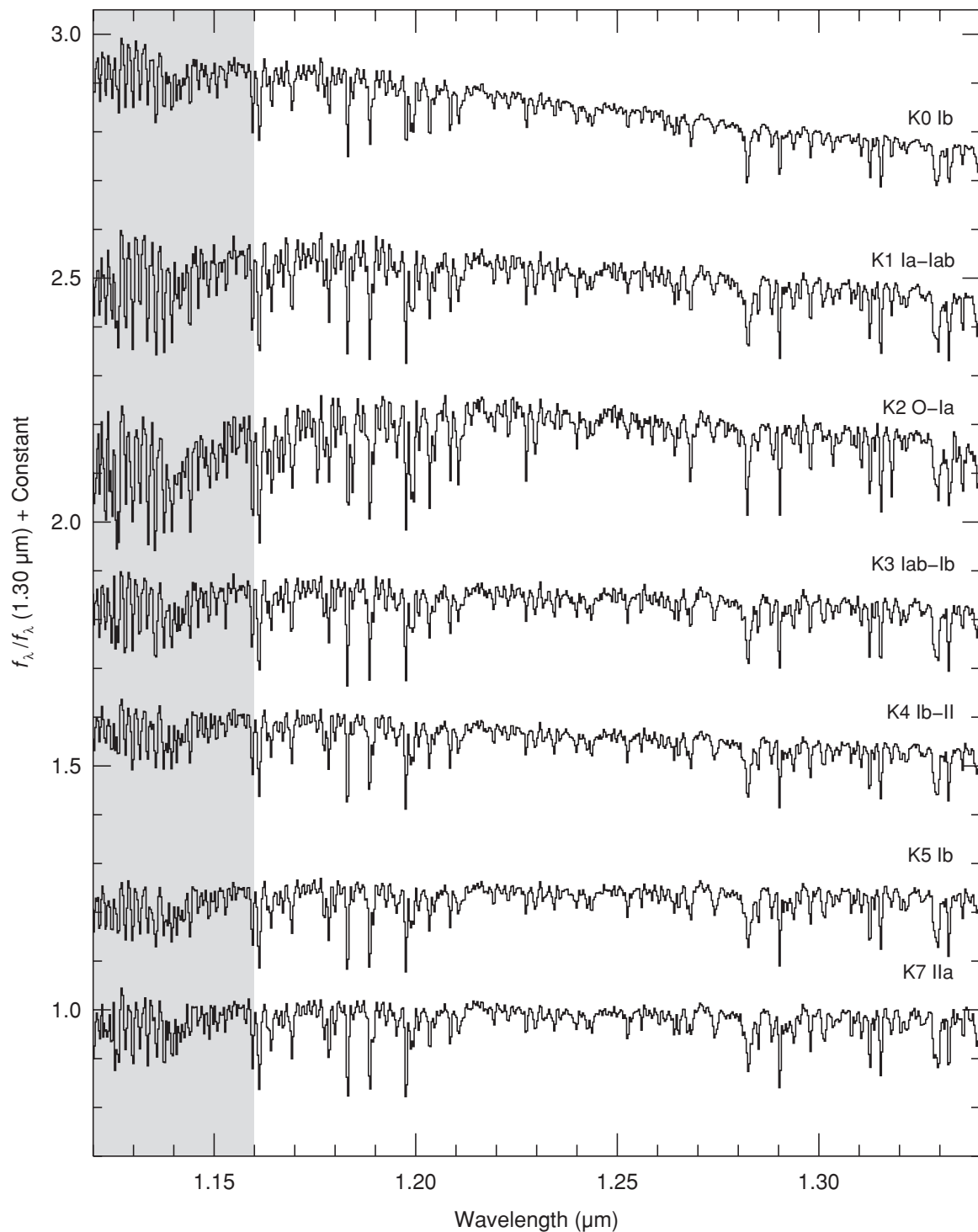


Figure 85. Sequence of K supergiant stars plotted over the J band (1.12–1.34 μm). The spectra are of HD 44391 (K0 Ib), HD 63302 (K1 Ia–Iab), HD 212466 (K2 O–Ia), HD 187238 (K3 Iab–Ib), HD 201065 (K4 Ib–II), HD 216946 (K5 Ib), and HD 181475 (K7 IIa). The spectra have been normalized to unity at 1.30 μm and offset by constants.

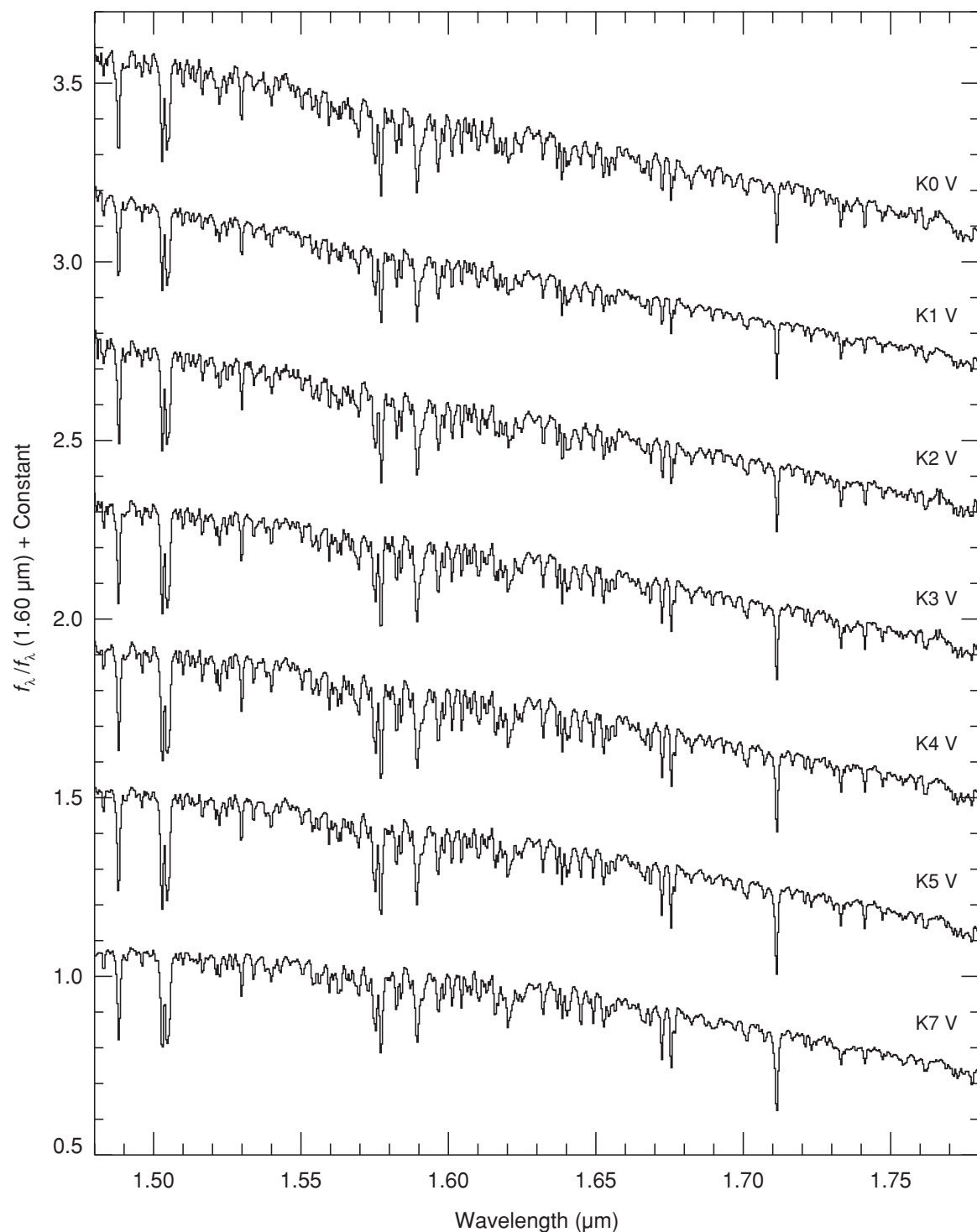


Figure 86. Sequence of K dwarf stars plotted over the *H* band (1.48–1.78 μm). The spectra are of HD 145675 (K0 V), HD 10476 (K1 V), HD 3765 (K2 V), HD 219134 (K3 V), HD 45977 (K4 V), HD 36003 (K5 V), and HD 237903 (K7 V). The spectra have been normalized to unity at 1.60 μm and offset by constants.

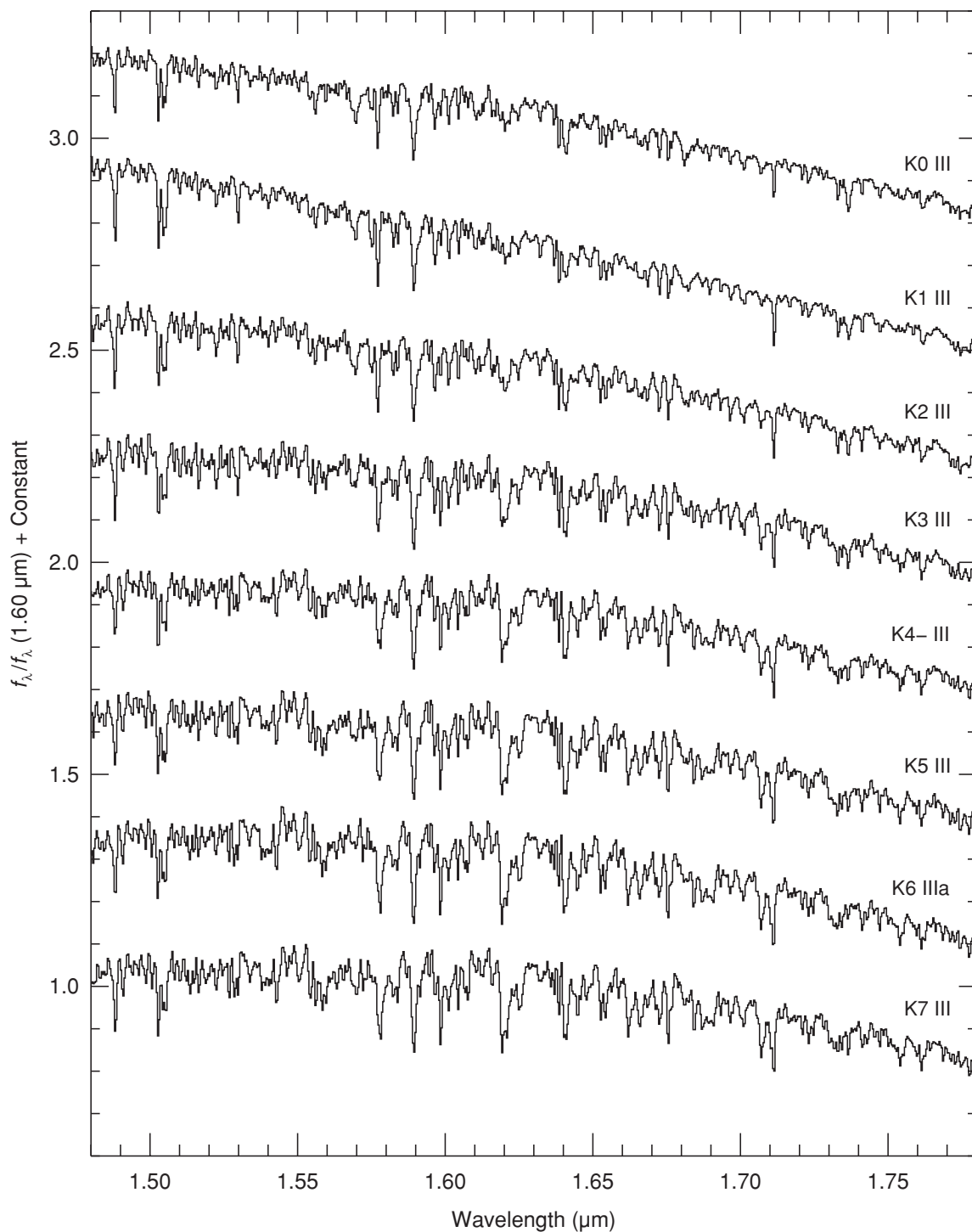


Figure 87. Sequence of K giant stars plotted over the *H* band (1.48–1.78 μm). The spectra are of HD 100006 (K0 III), HD 25975 (K1 III), HD 137759 (K2 III), HD 221246 (K3 III), HD 207991 (K4– III), HD 181596 (K5 III), HD 3346 (K6 IIIa), and HD 194193 (K7 III). The spectra have been normalized to unity at 1.60 μm and offset by constants.

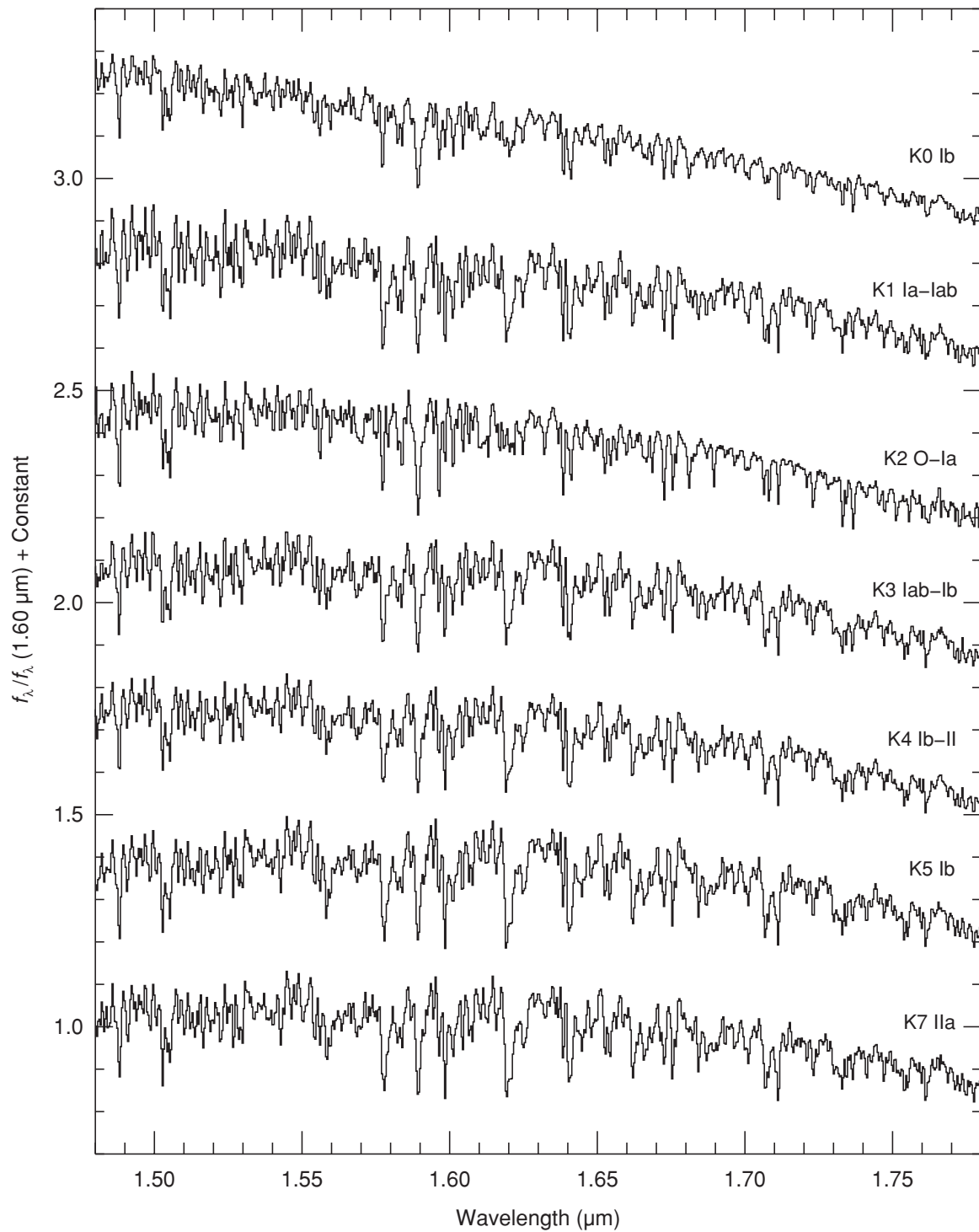


Figure 88. Sequence of K supergiant stars plotted over the H band (1.48–1.78 μm). The spectra are of HD 44391 (K0 Ib), HD 63302 (K1 Ia–Iab), HD 212466 (K2 O–Ia), HD 187238 (K3 Iab–Ib), HD 201065 (K4 Ib–II), HD 216946 (K5 Ib), and HD 181475 (K7 IIa). The spectra have been normalized to unity at 1.60 μm and offset by constants.

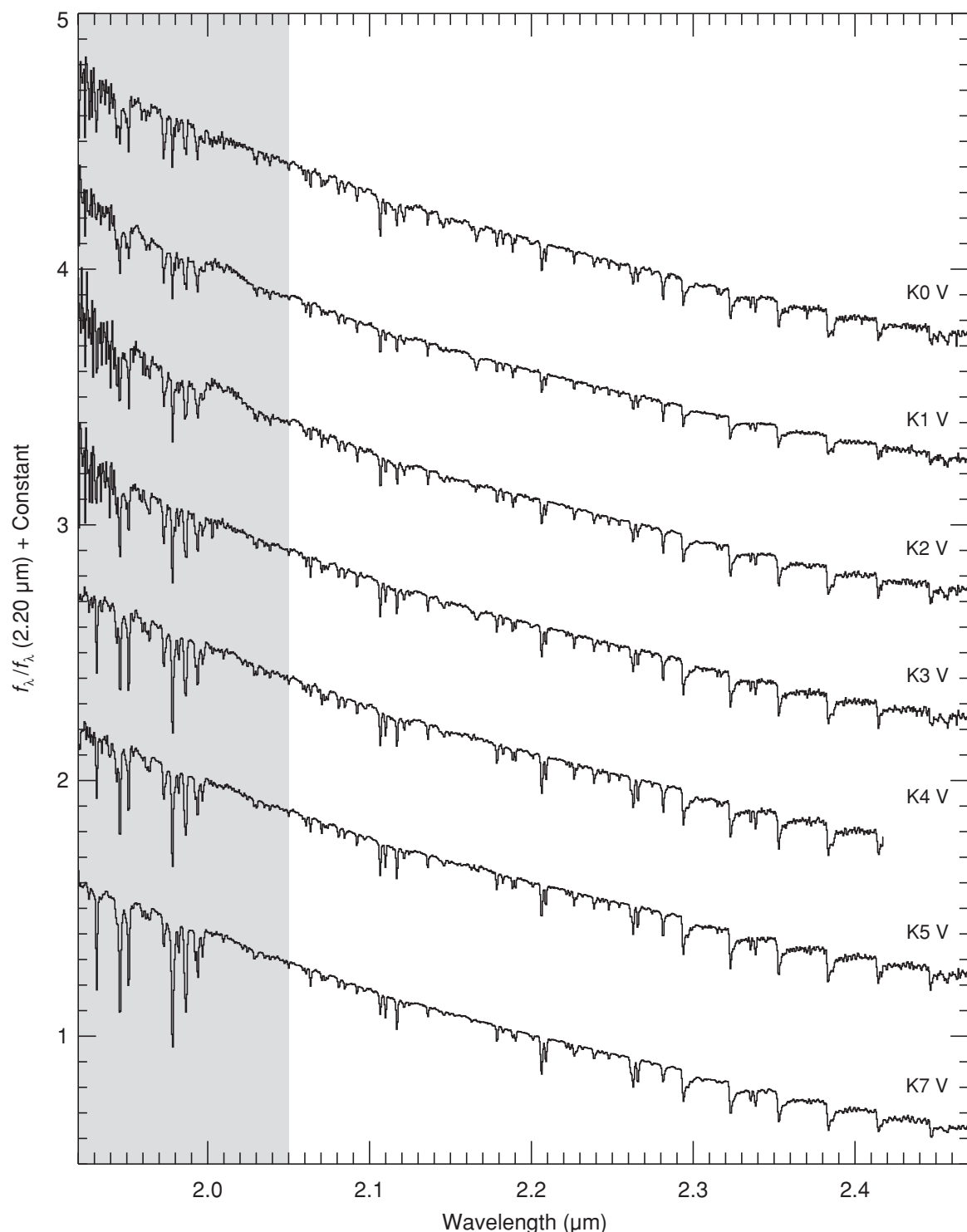


Figure 89. Sequence of K dwarf stars plotted over the K band ($1.92\text{--}2.5\,\mu\text{m}$). The spectra are of HD 145675 (K0 V), HD 10476 (K1 V), HD 3765 (K2 V), HD 219134 (K3 V), HD 45977 (K4 V), HD 36003 (K5 V), and HD 237903 (K7 V). The spectra have been normalized to unity at $2.20\,\mu\text{m}$ and offset by constants.

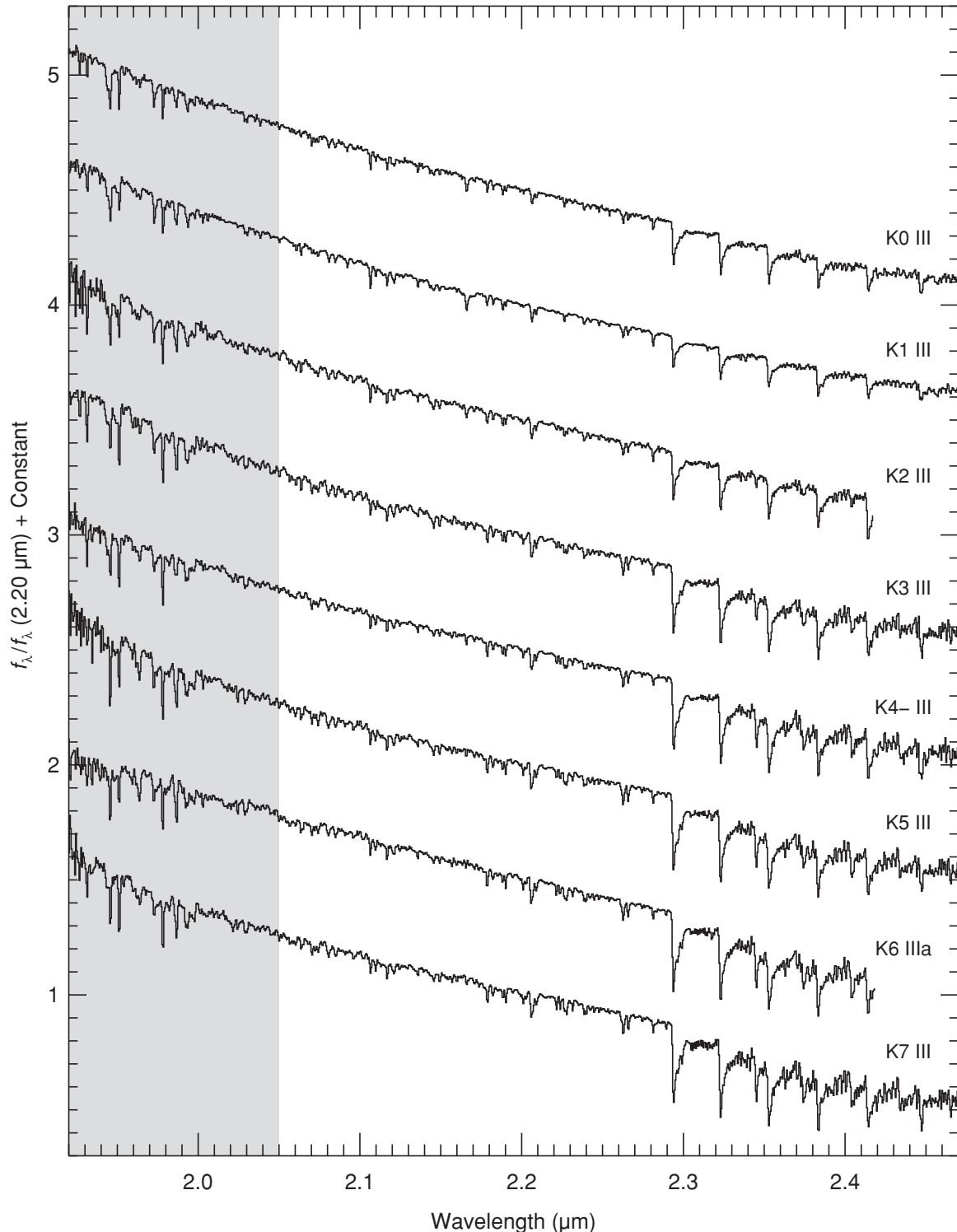


Figure 90. Sequence of K giant stars plotted over the K band (1.92–2.5 μm). The spectra are of HD 100006 (K0 III), HD 25975 (K1 III), HD 137759 (K2 III), HD 221246 (K3 III), HD 207991 (K4- III), HD 181596 (K5 III), HD 3346 (K6 IIIa), and HD 194193 (K7 III). The spectra have been normalized to unity at 2.20 μm and offset by constants.

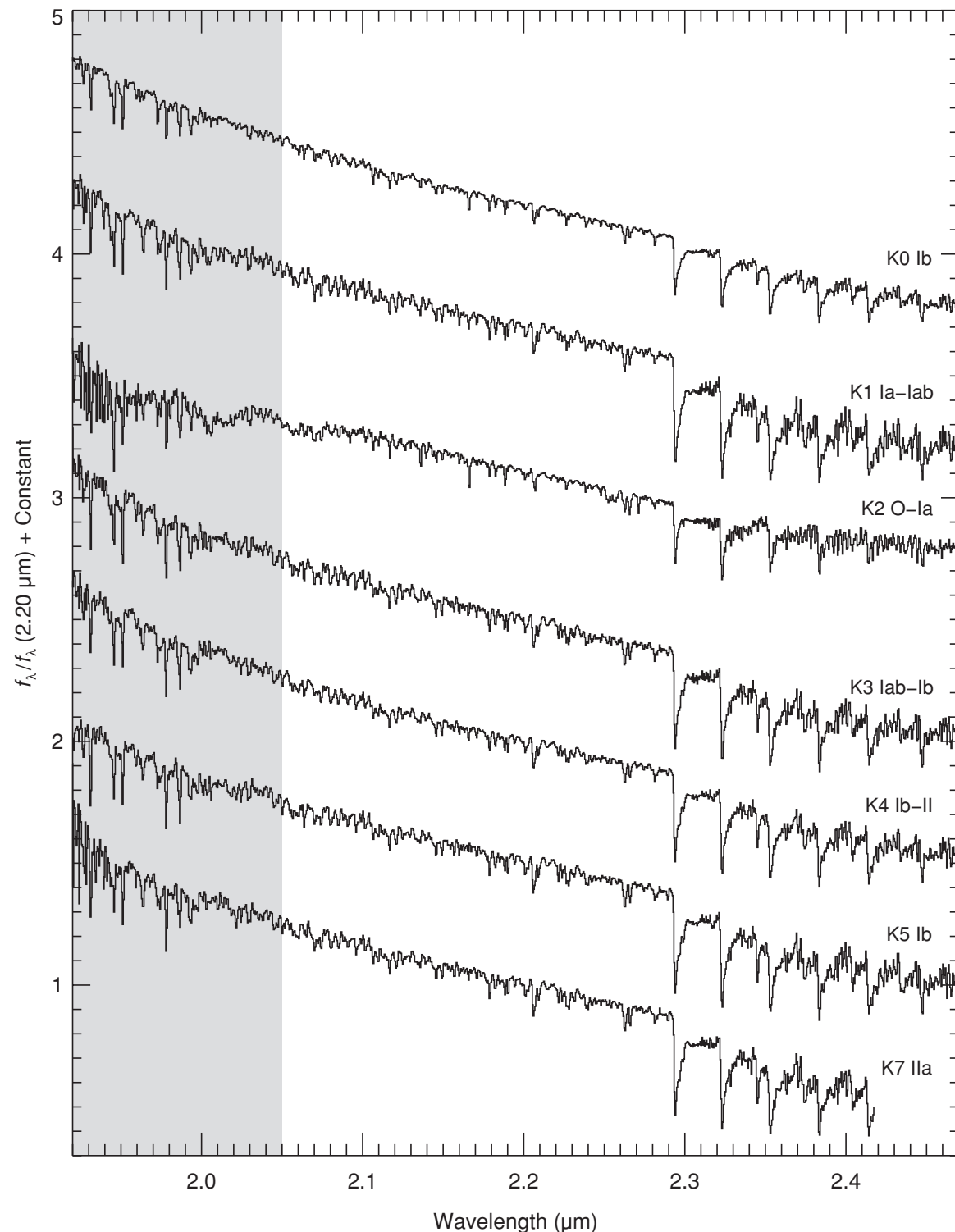


Figure 91. Sequence of K supergiant stars plotted over the K band (1.92– $2.5 \mu\text{m}$). The spectra are of HD 44391 (K0 Ib), HD 63302 (K1 Ia–Iab), HD 212466 (K2 O–Ia), HD 187238 (K3 Iab–Ib), HD 201065 (K4 Ib–II), HD 216946 (K5 Ib), and HD 181475 (K7 IIa). The spectra have been normalized to unity at $2.20 \mu\text{m}$ and offset by constants.

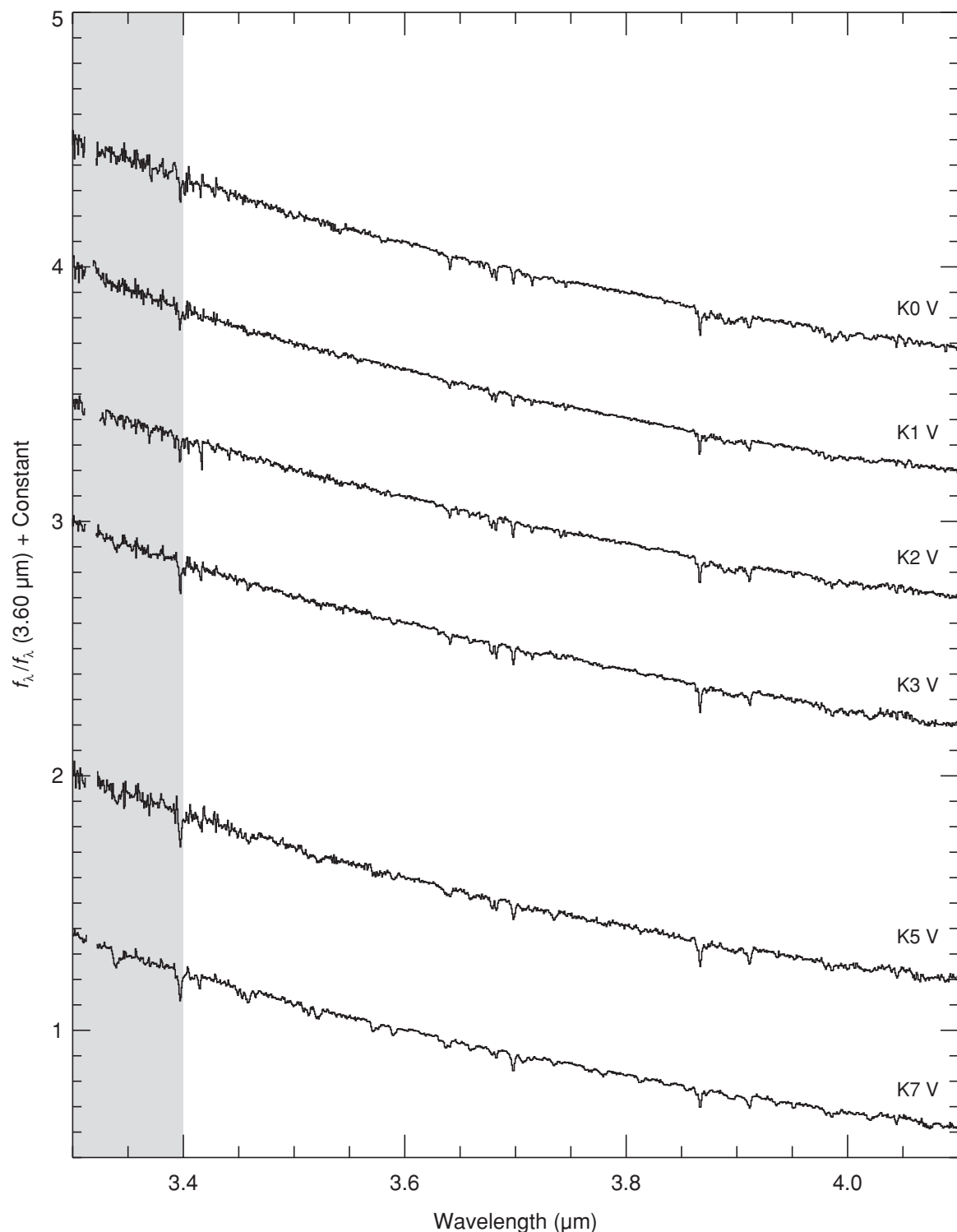


Figure 92. Sequence of K dwarf stars plotted over the L' band ($3.6\text{--}4.1 \mu\text{m}$). The spectra are of HD 145675 (K0 V), HD 10476 (K1 V), HD 3765 (K2 V), HD 219134 (K3 V), HD 36003 (K5 V), and HD 237903 (K7 V). The spectra have been normalized to unity at $2.20 \mu\text{m}$ and offset by constants.

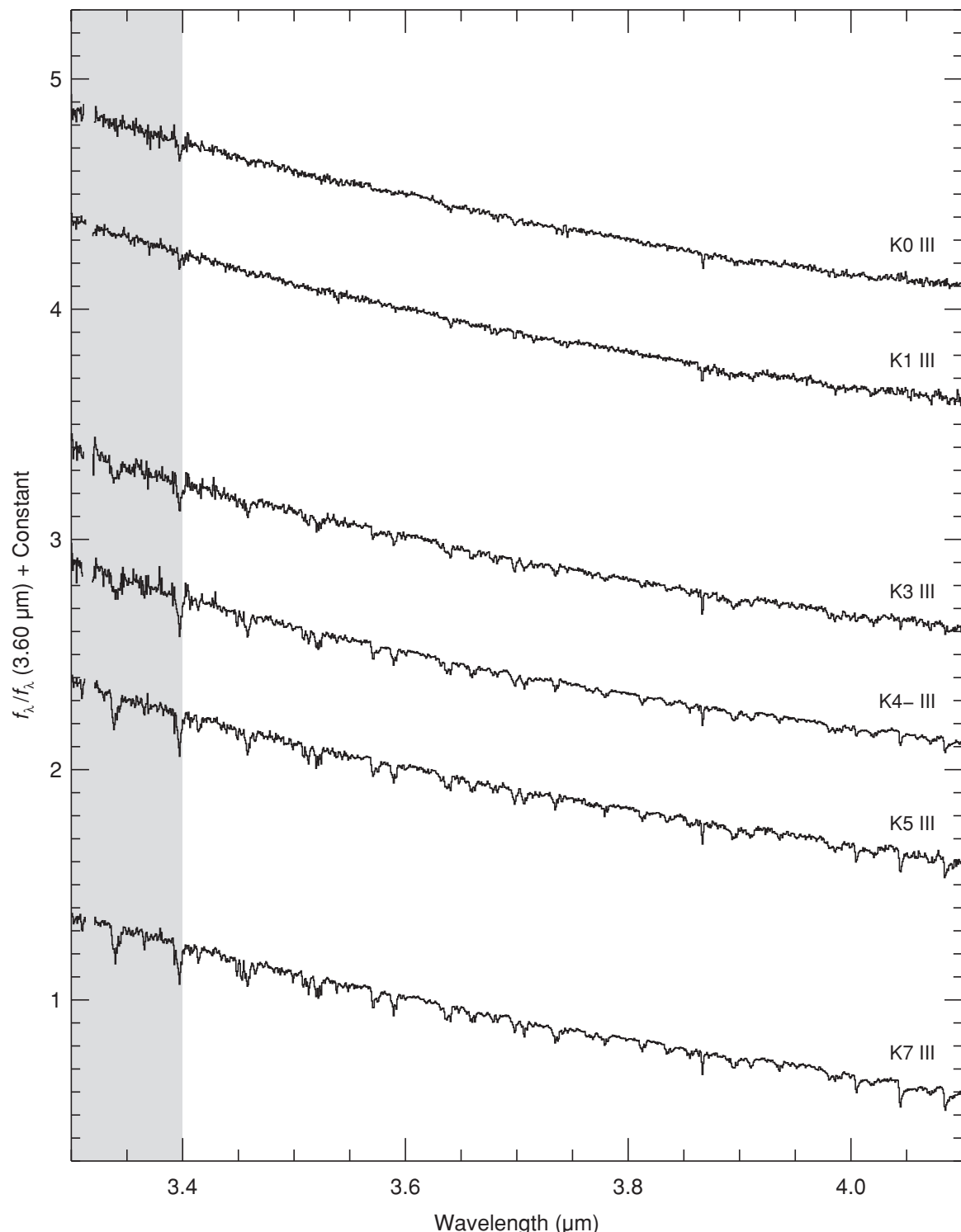


Figure 93. Sequence of K giant stars plotted over the L' band ($3.6\text{--}4.1 \mu\text{m}$). The spectra are of HD 100006 (K0 III), HD 25975 (K1 III), HD 137759 (K2 III), HD 221246 (K3 III), HD 207991 (K4- III), HD 181596 (K5 III), and HD 194193 (K7 III). The spectra have been normalized to unity at $3.6 \mu\text{m}$ and offset by constants.

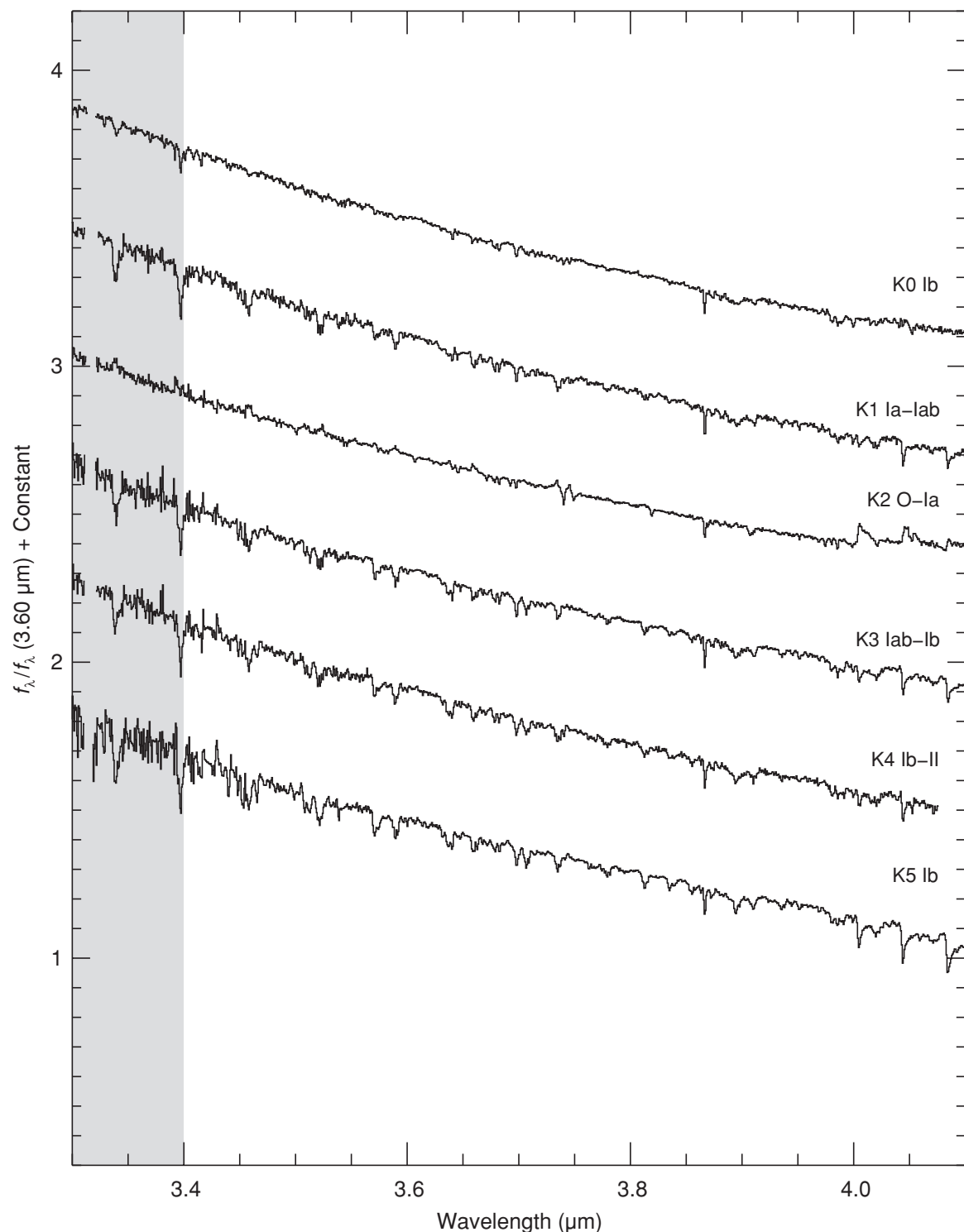


Figure 94. Sequence of K supergiant stars plotted over the L' band ($3.6\text{--}4.1 \mu\text{m}$). The spectra are of HD 44391 (K0 Ib), HD 63302 (K1 Ia-lab), HD 212466 (K2 O-Ia), HD 187238 (K3 Iab-Ib), HD 201065 (K4 Ib-II), and HD 216946 (K5 Ib). The spectra have been normalized to unity at $3.6 \mu\text{m}$ and offset by constants.

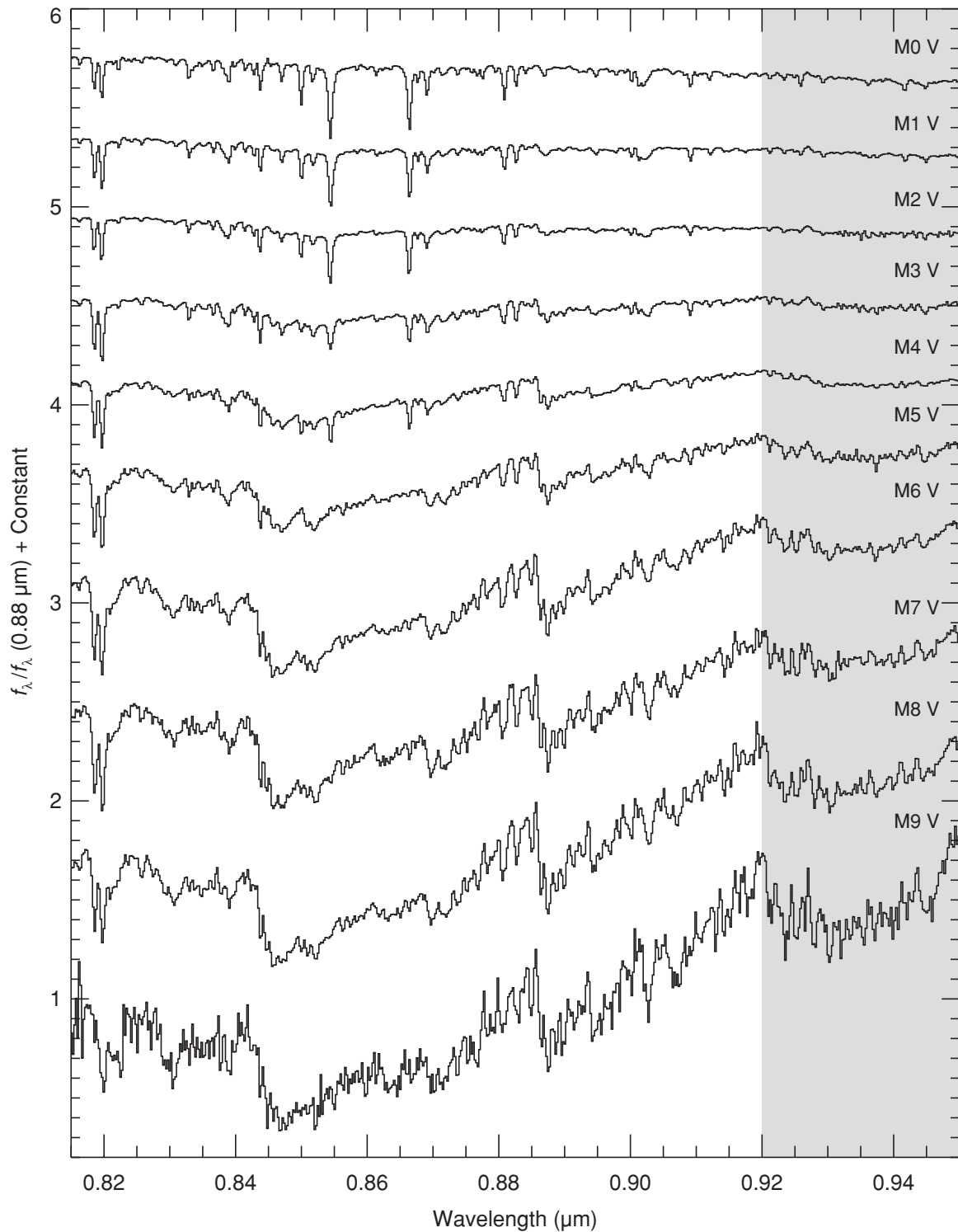


Figure 95. Sequence of M dwarf stars plotted over the *I* band (0.82–0.95 μm). The spectra are of HD 19305 (M0 V), HD 42581 (M1 V), HD 95735 (M2 V), GI 388 (M3 V), GI 213 (M4 V), GI 51 (M5 V), GI 406 (M6 V), GI 644C (M7 V), GI 752B (M8 V), and LP944-20 (M9 V). The spectra have been normalized to unity at 0.88 μm and offset by constants.

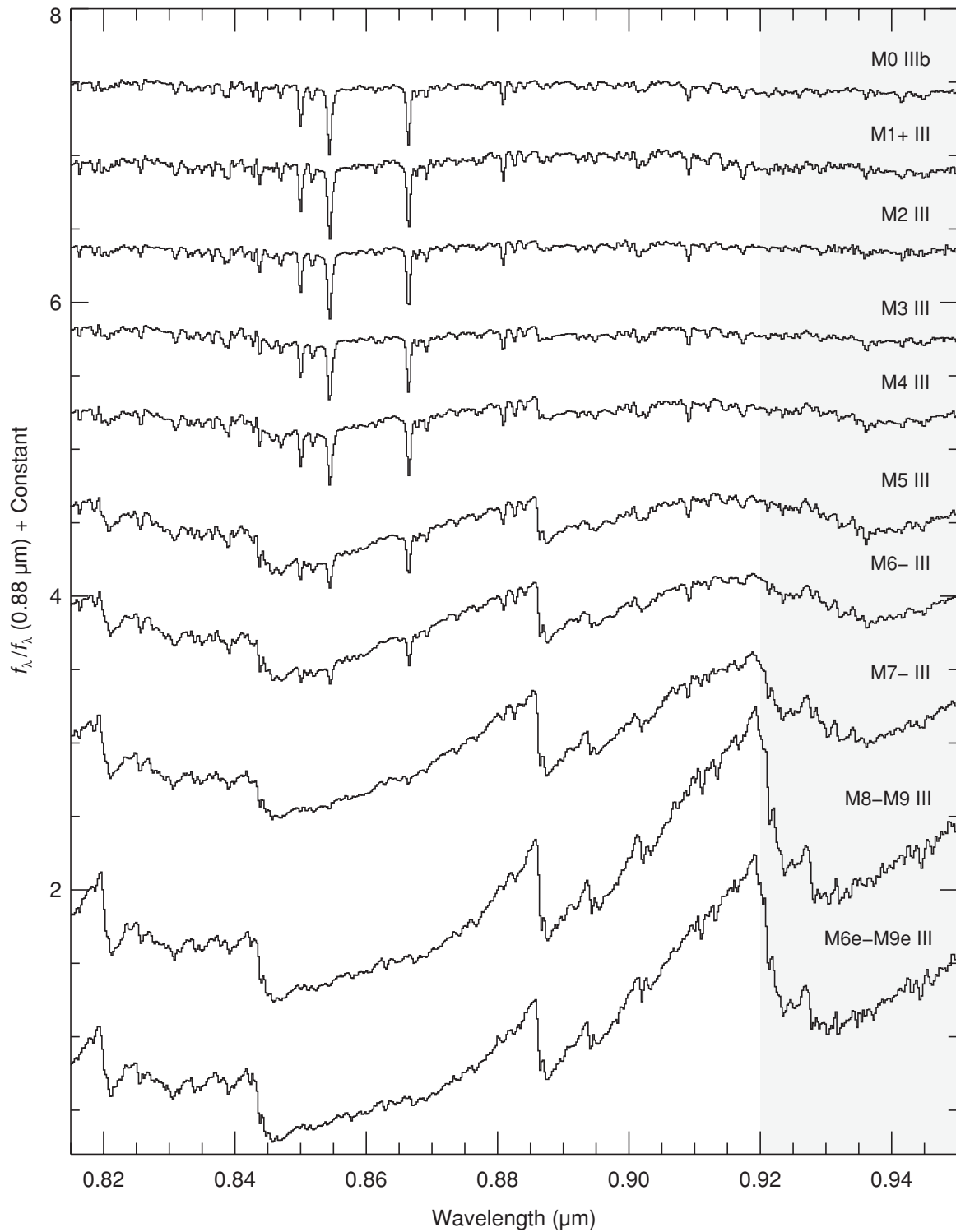


Figure 96. Sequence of M giant stars plotted over the I band (0.82–0.95 μm). The spectra are of HD 213893 (M0 IIIb), HD 204724 (M1+ III), HD 120052 (M2 III), HD 39045 (M3 III), HD 4408 (M4 III), HD 175865 (M5 III), HD 18191 (M6- III), HD 108849 (M7- III), IRAS 21284–0747 (M8–M9 III), and HD 69243 (M6e–M9e III). The spectra have been normalized to unity at 0.88 μm and offset by constants.

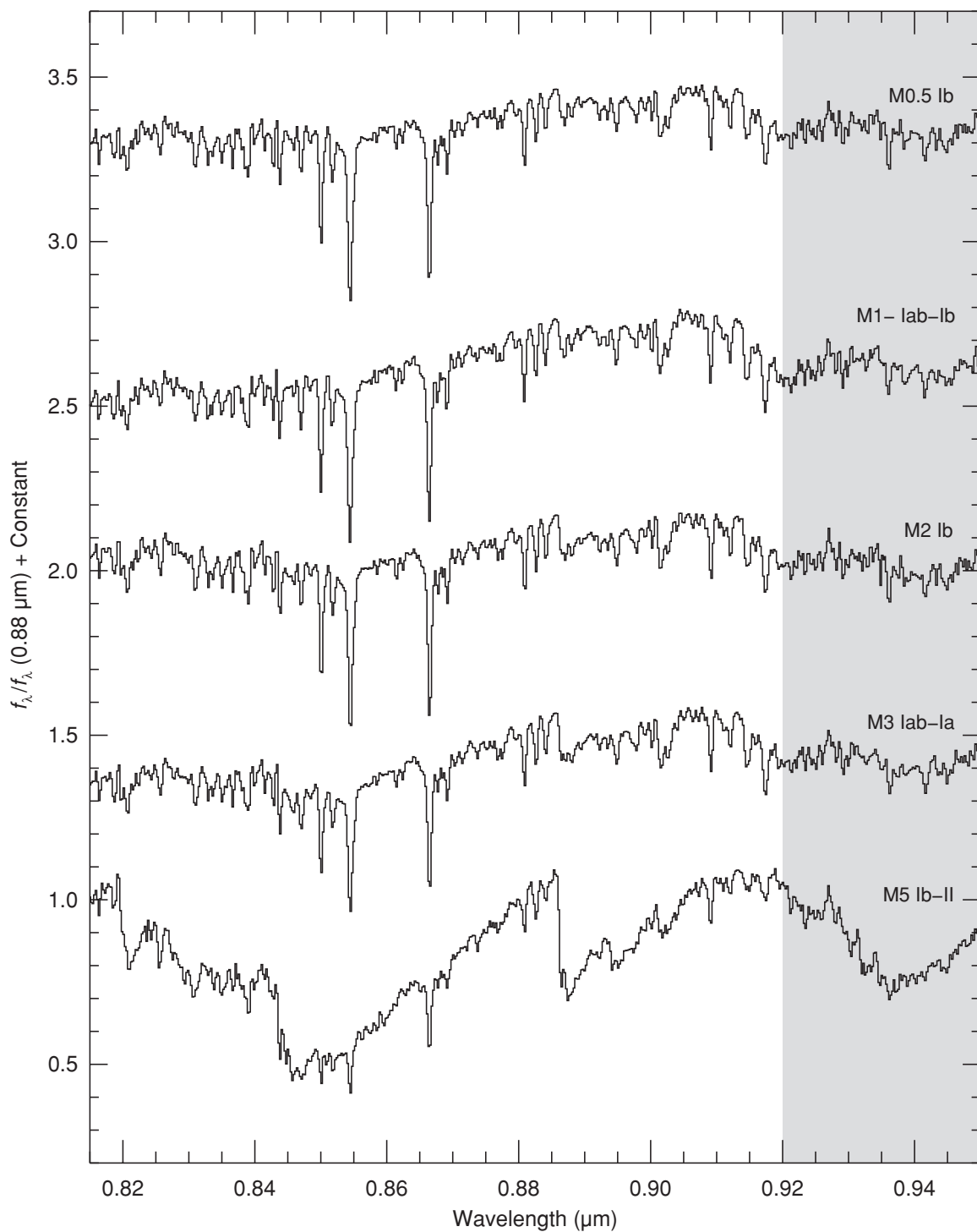


Figure 97. Sequence of M supergiant stars plotted over the I band (0.82–0.95 μm). The spectra are of HD 236697 (M0.5 Ib), HD 14404 (M1– Iab–Ib), HD 10465 (M2 Ib), CD –31 4916 (M3 Iab–Ia), and HD 156014 (M5 Ib–II). The spectra have been normalized to unity at 0.88 μm and offset by constants.

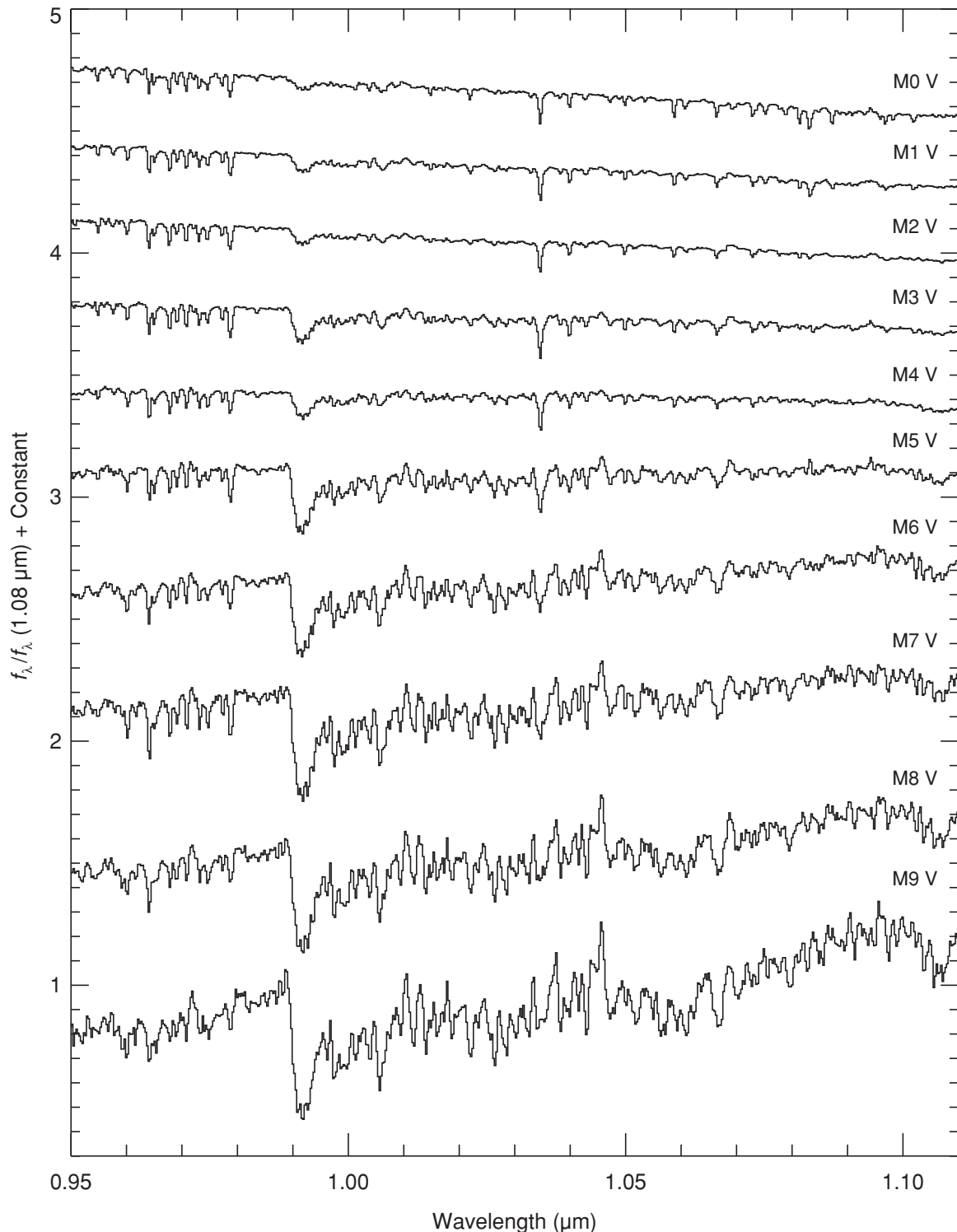


Figure 98. Sequence of M dwarf stars plotted over the Y band (0.95 – $1.10 \mu\text{m}$). The spectra are of HD 19305 (M0 V), HD 42581 (M1 V), HD 95735 (M2 V), Gl 388 (M3 V), Gl 213 (M4 V), Gl 51 (M5 V), Gl 406 (M6 V), Gl 644C (M7 V), Gl 752B (M8 V), and LP944–20 (M9 V). The spectra have been normalized to unity at $1.08 \mu\text{m}$ and offset by constants.

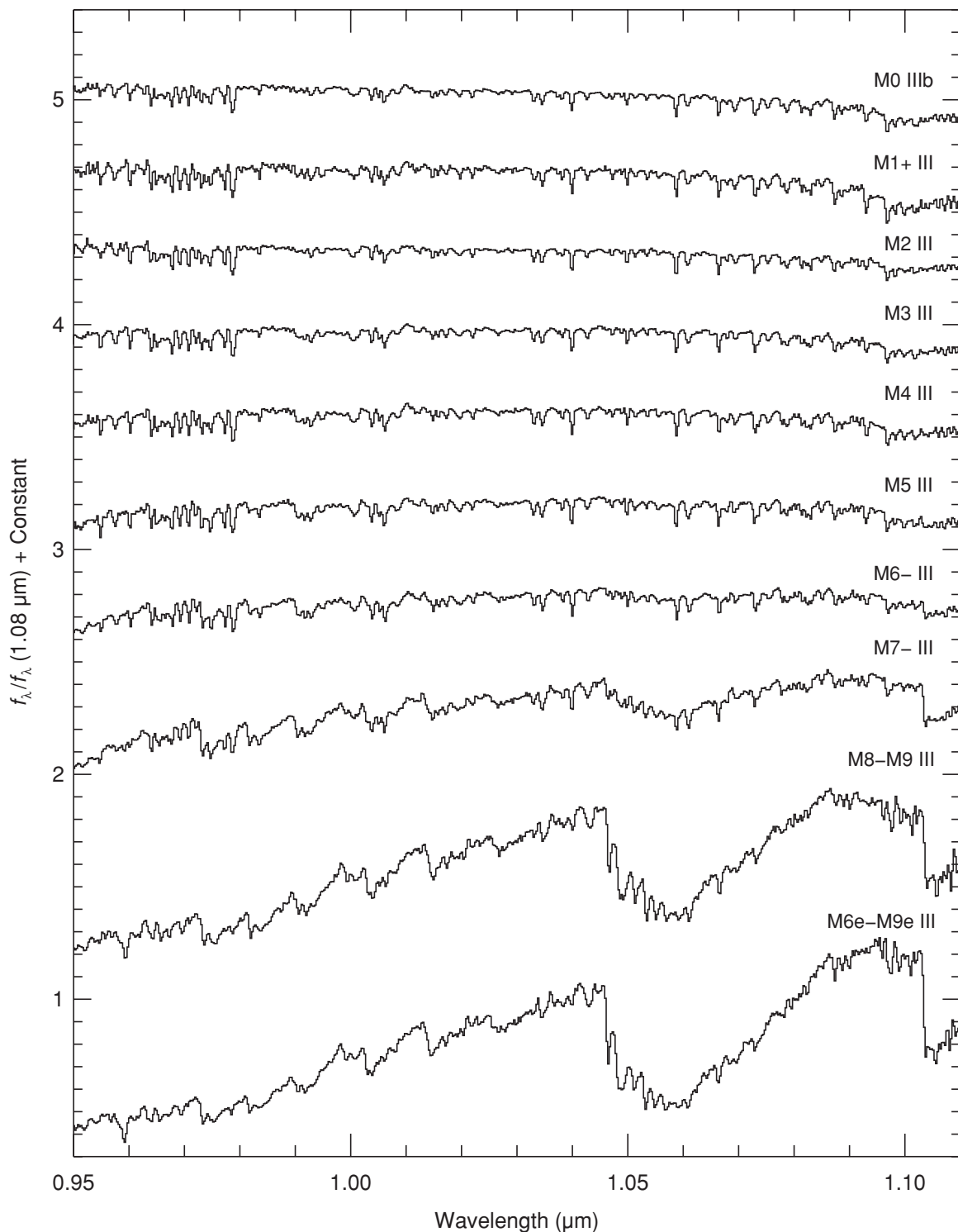


Figure 99. Sequence of M giant stars plotted over the Y band (0.95 – $1.10 \mu\text{m}$). The spectra are of HD 213893 (M0 IIIb), HD 204724 (M1+ III), HD 120052 (M2 III), HD 39045 (M3 III), HD 4408 (M4 III), HD 175865 (M5 III), HD 18191 (M6– III), HD 108849 (M7– III), IRAS 21284–0747 (M8–M9 III), and HD 69243 (M6e–M9e III). The spectra have been normalized to unity at $1.08 \mu\text{m}$ and offset by constants.

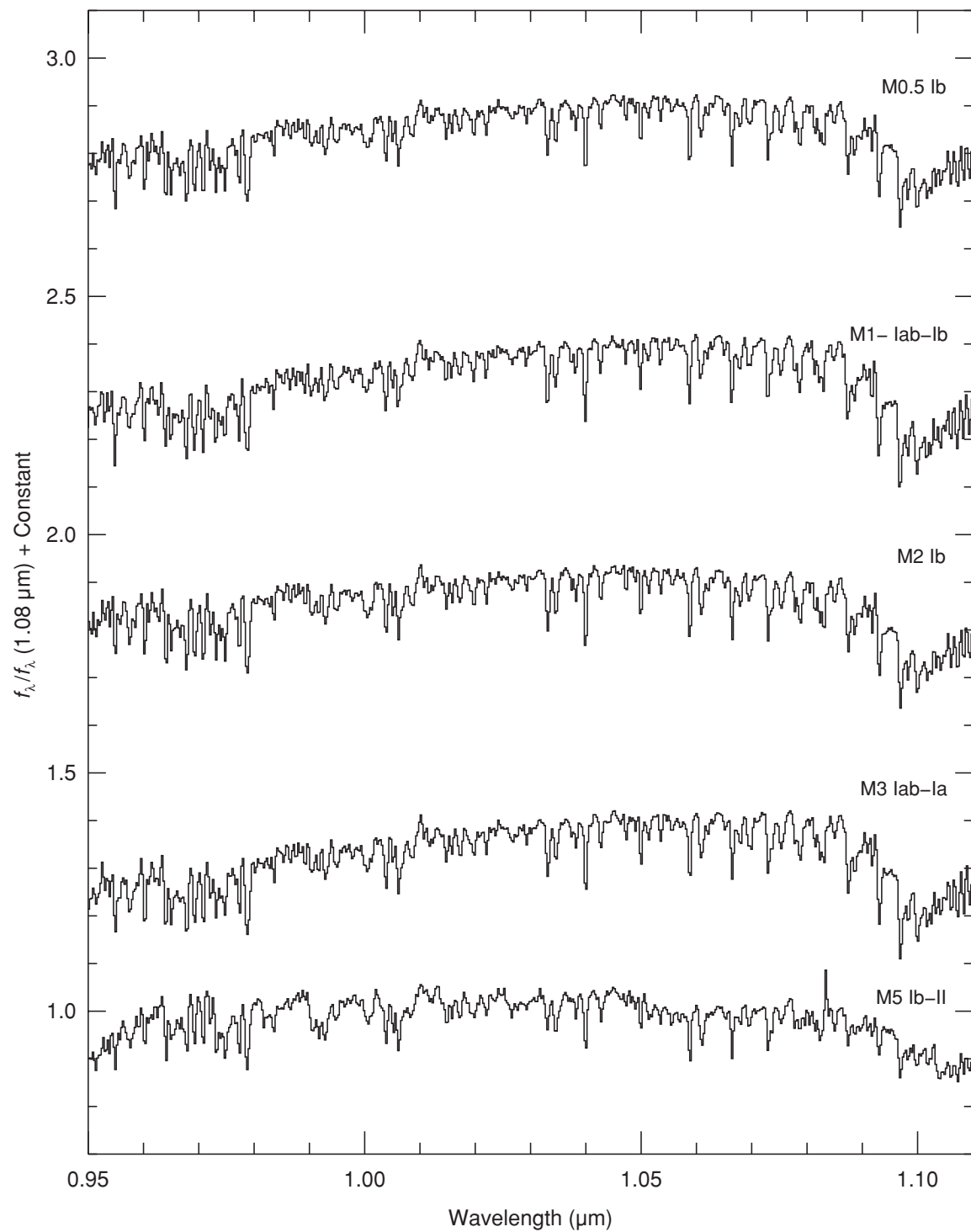


Figure 100. Sequence of M supergiant stars plotted over the Y band (0.95 – $1.10 \mu\text{m}$). The spectra are of HD 236697 (M0.5 Ib), HD 14404 (M1 – Iab–Ib), HD 10465 (M2 Ib), CD –31 4916 (M3 Iab–Ia), and HD 156014 (M5 Ib–II). The spectra have been normalized to unity at $1.08 \mu\text{m}$ and offset by constants.

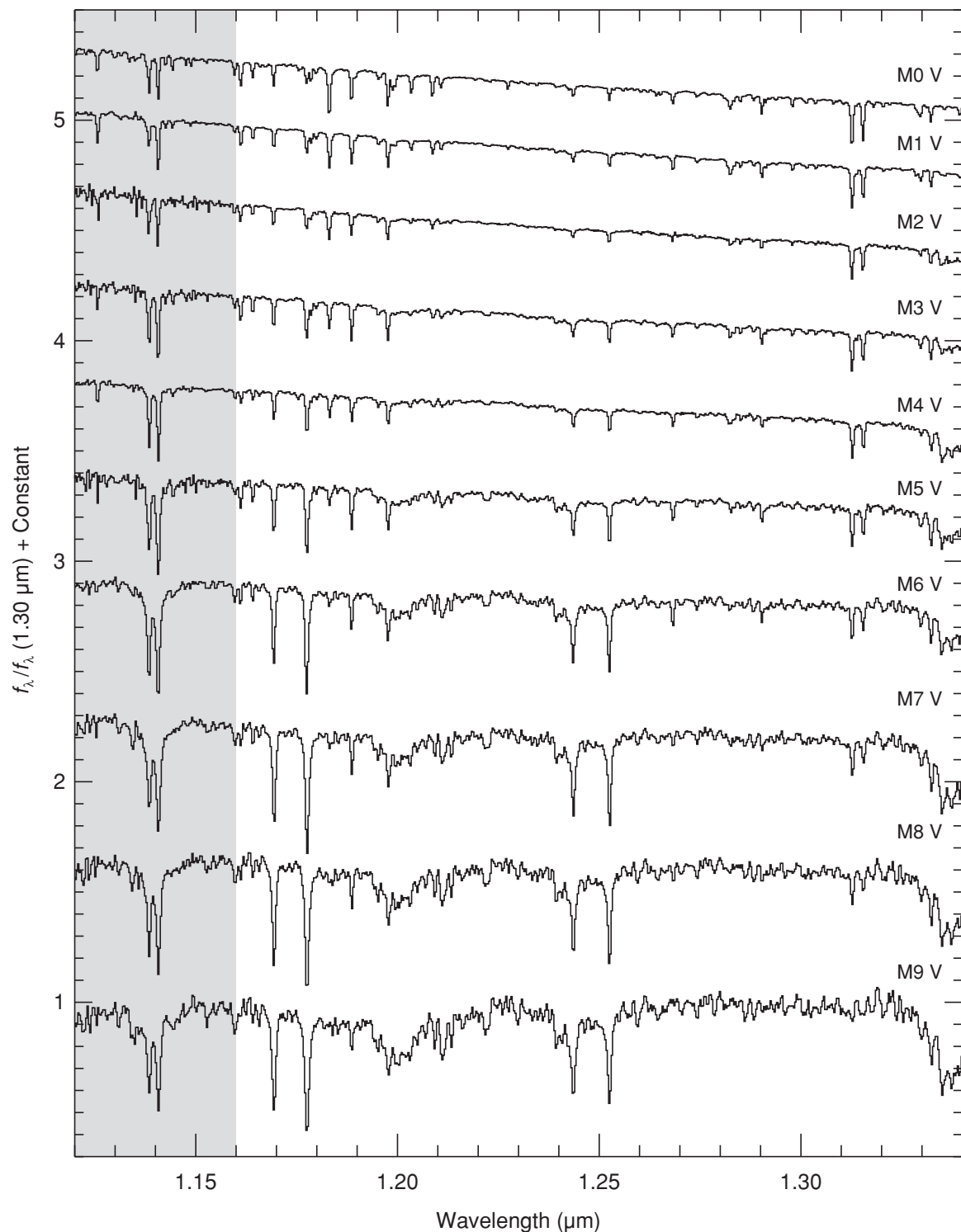


Figure 101. Sequence of M dwarf stars plotted over the *J* band (1.12–1.34 μm). The spectra are of HD 19305 (M0 V), HD 42581 (M1 V), HD 95735 (M2 V), Gl 388 (M3 V), Gl 213 (M4 V), Gl 51 (M5 V), Gl 406 (M6 V), Gl 644C (M7 V), Gl 752B (M8 V), and LP944–20 (M9 V). The spectra have been normalized to unity at 1.30 μm and offset by constants.

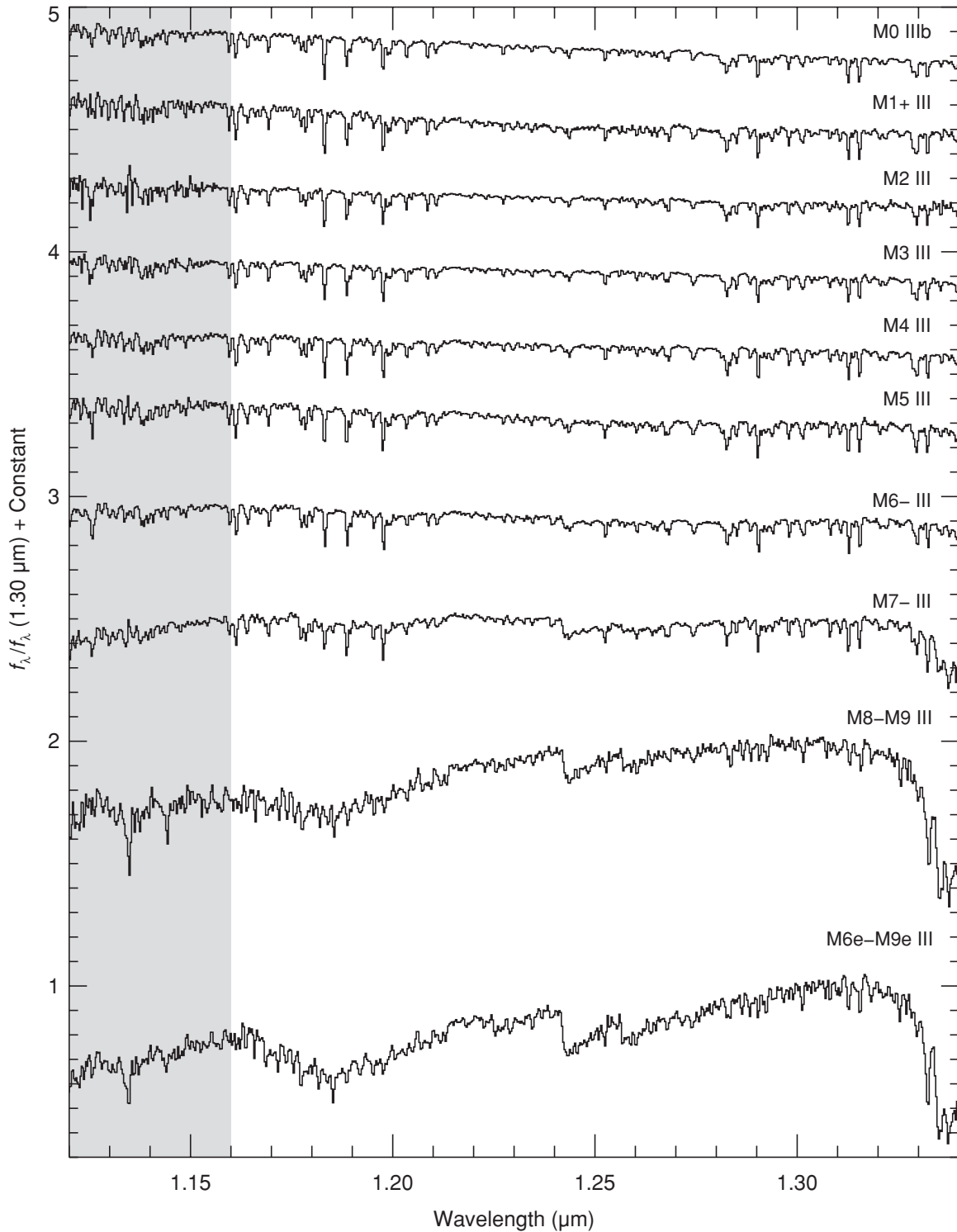


Figure 102. Sequence of M giant stars plotted over the *J* band (1.12–1.34 μm). The spectra are of HD 213893 (M0 IIIb), HD 204724 (M1+ III), HD 120052 (M2 III), HD 39045 (M3 III), HD 4408 (M4 III), HD 175865 (M5 III), HD 18191 (M6– III), HD 108849 (M7– III), IRAS 21284–0747 (M8–M9 III), and HD HD 69243 (M6e–M9e III). The spectra have been normalized to unity at 1.30 μm and offset by constants.

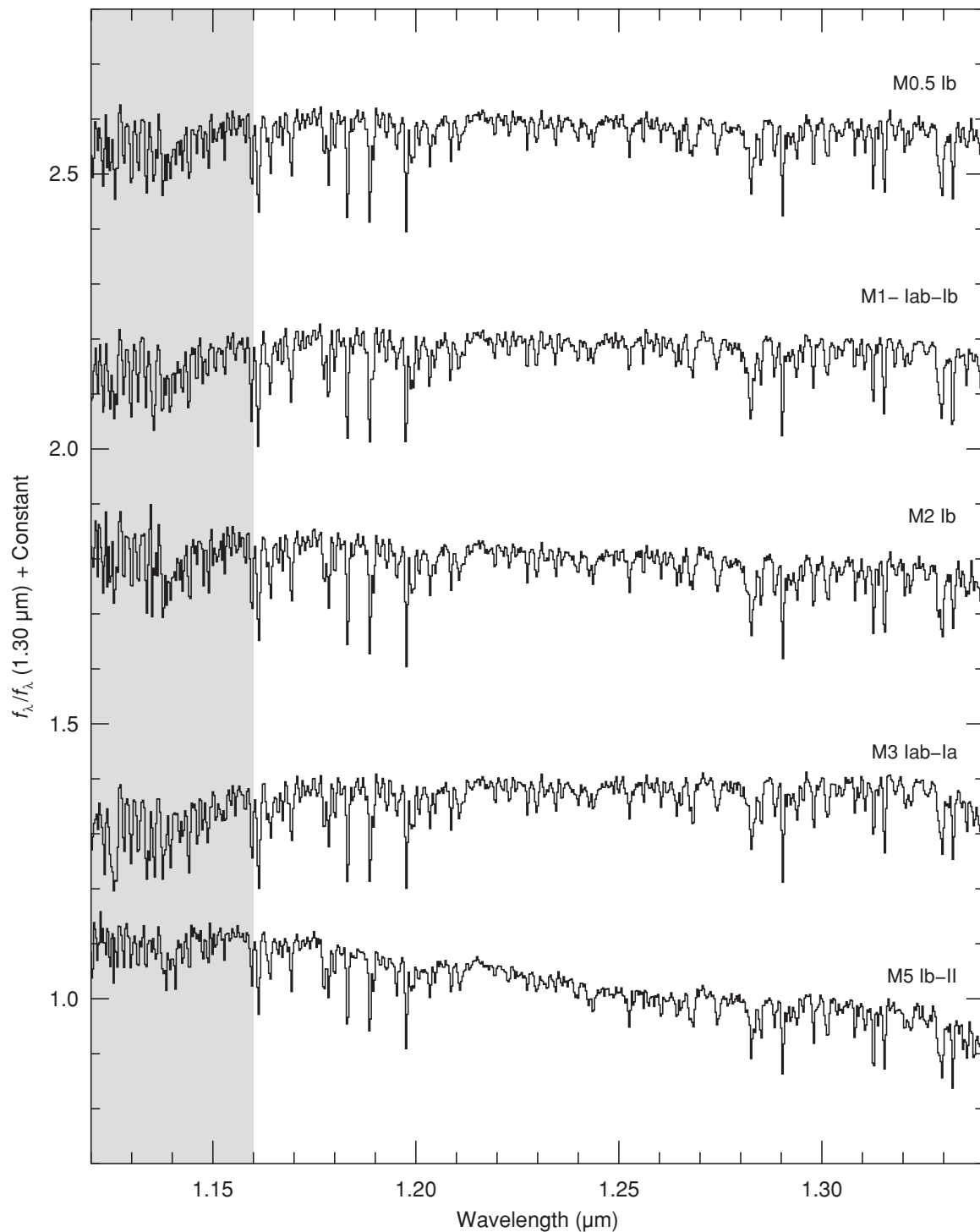


Figure 103. Sequence of M supergiant stars plotted over the *J* band (1.12–1.34 μm). The spectra are of HD 236697 (M0.5 Ib), HD 14404 (M1 – Iab–Ib), HD 10465 (M2 Ib), CD –31 4916 (M3 Iab–Ia), and HD 156014 (M5 Ib–II). The spectra have been normalized to unity at 1.30 μm and offset by constants.

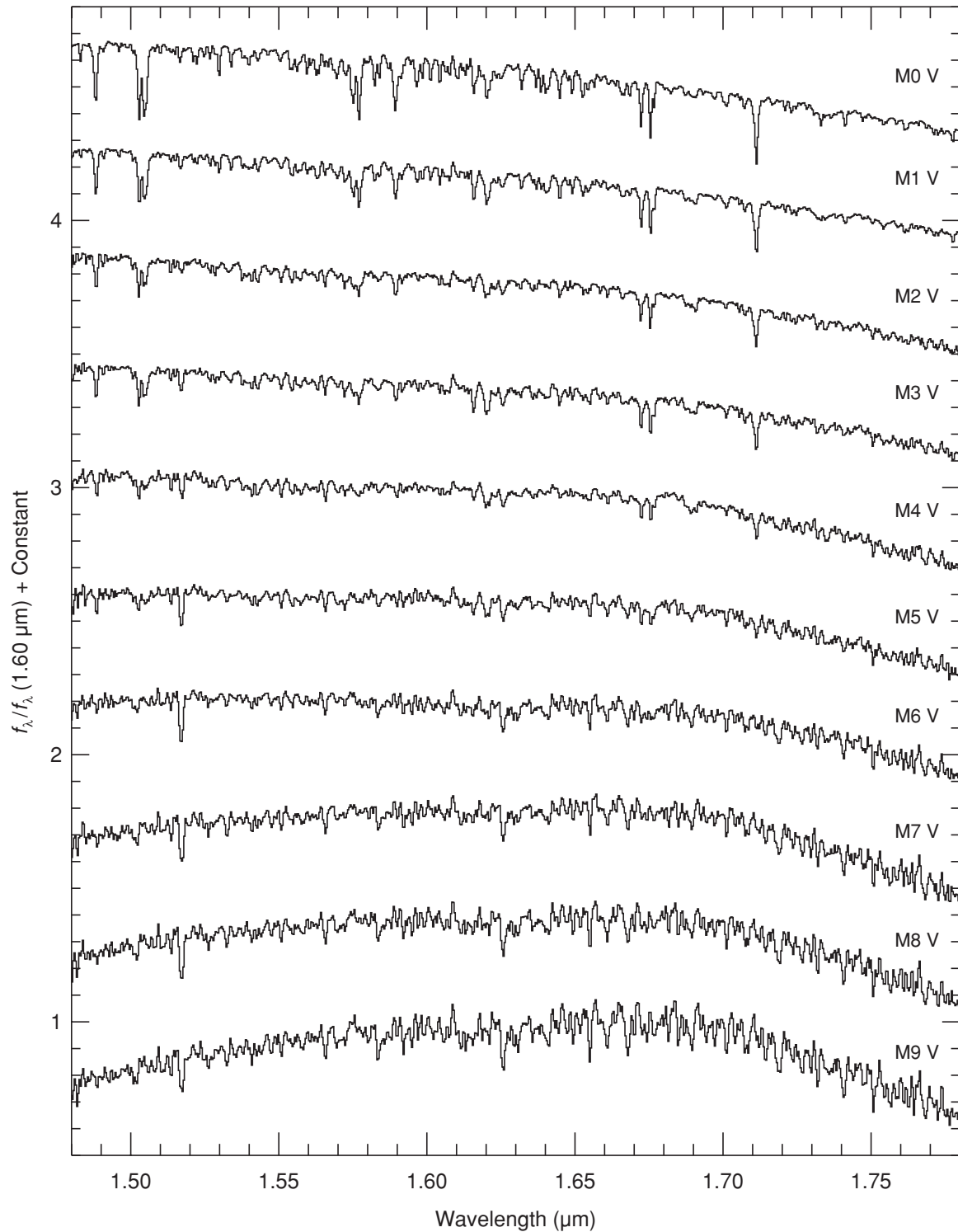


Figure 104. Sequence of M dwarf stars plotted over the *H* band (1.48–1.78 μm). The spectra are of HD 19305 (M0 V), HD 42581 (M1 V), HD 95735 (M2 V), Gl 388 (M3 V), Gl 213 (M4 V), Gl 51 (M5 V), Gl 406 (M6 V), Gl 644C (M7 V), Gl 752B (M8 V), and LP944–20 (M9 V). The spectra have been normalized to unity at $1.60 \mu\text{m}$ and offset by constants.

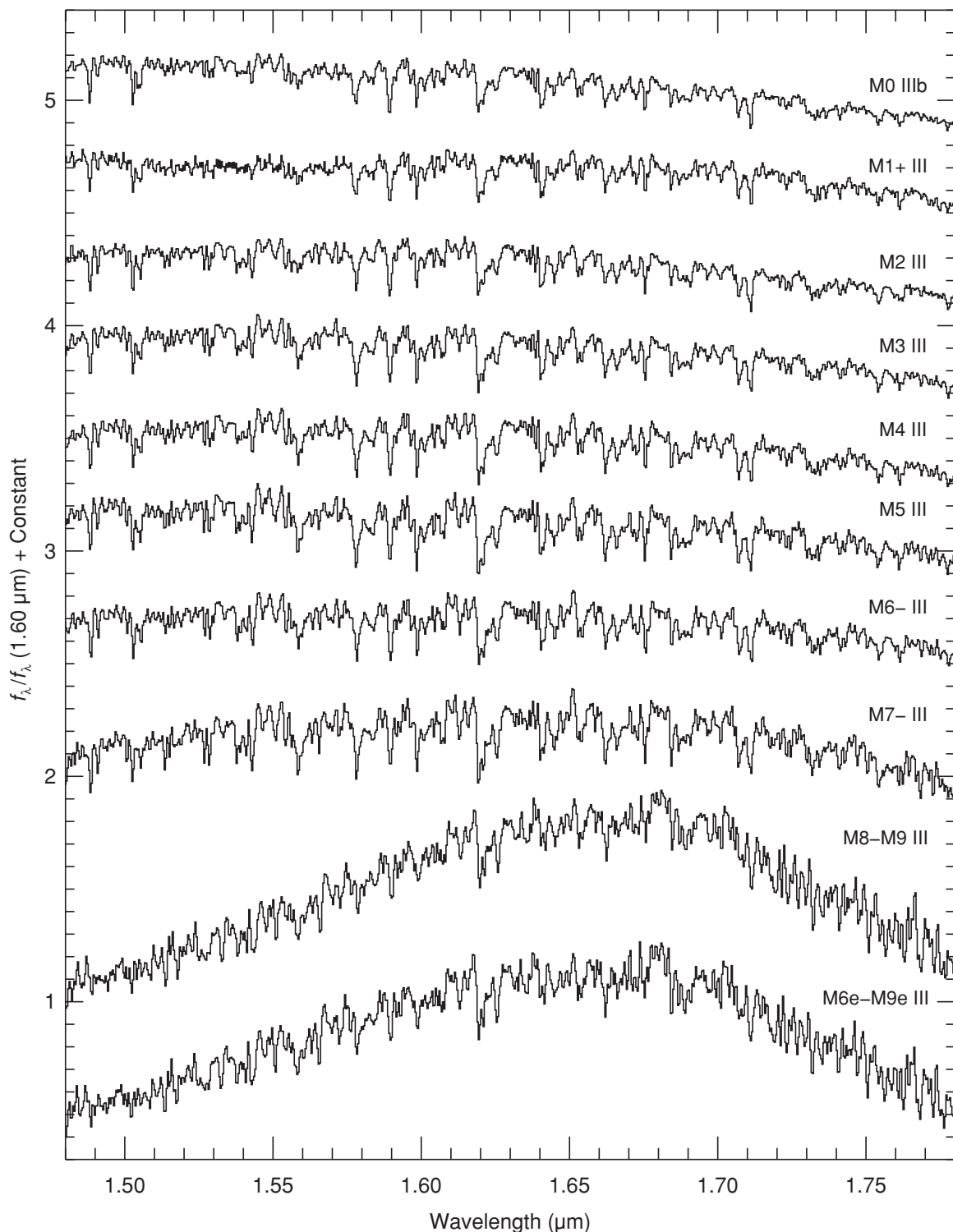


Figure 105. Sequence of M giant stars plotted over the *H* band (1.48–1.78 μm). The spectra are of HD 213893 (M0 IIIb), HD 204724 (M1+ III), HD 120052 (M2 III), HD 39045 (M3 III), HD 4408 (M4 III), HD 175865 (M5 III), HD 18191 (M6- III), HD 108849 (M7- III), IRAS 21284–0747 (M8–M9 III), and HD 69243 (M6e–M9e III). The spectra have been normalized to unity at 1.60 μm and offset by constants.

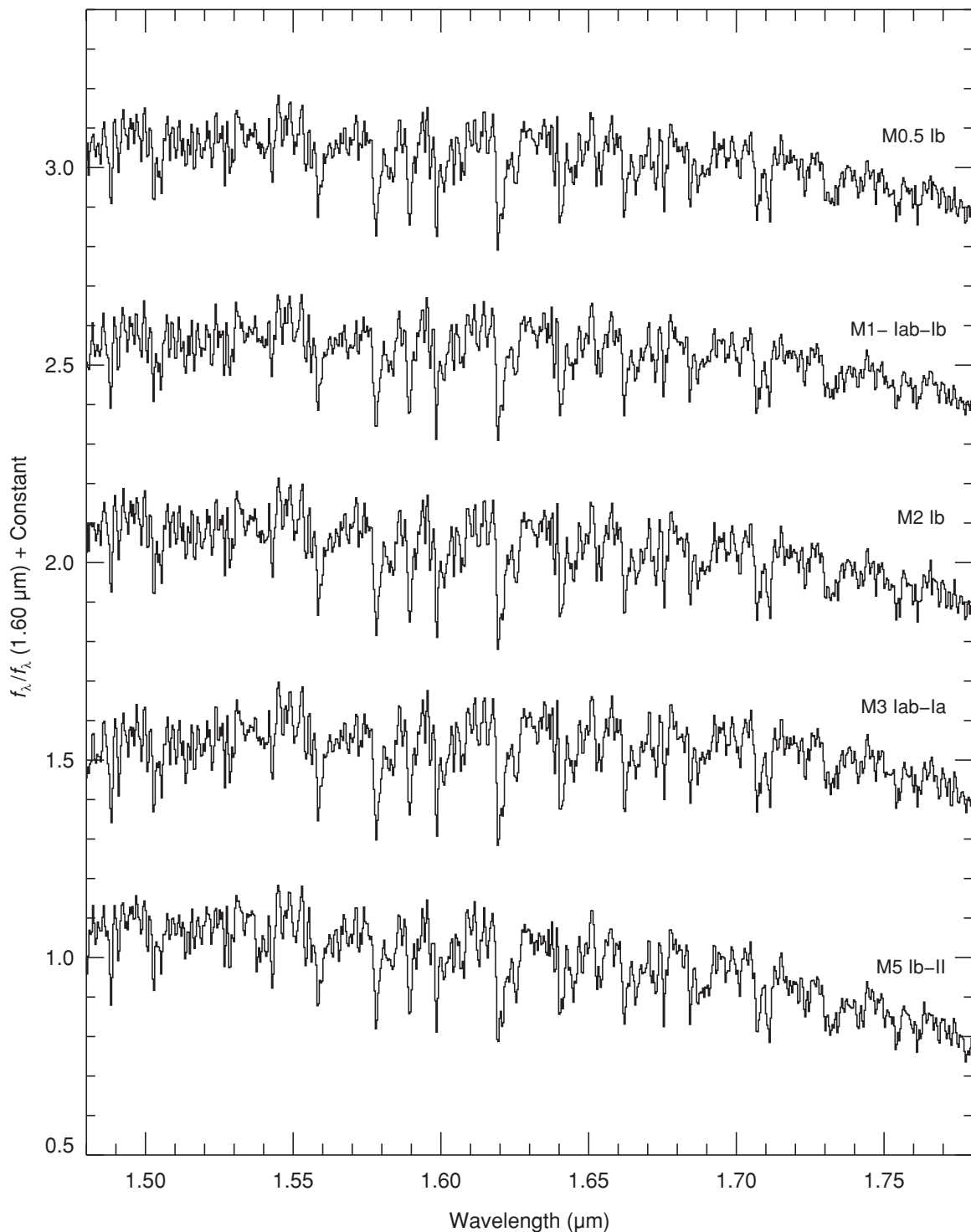


Figure 106. Sequence of M supergiant stars plotted over the H band (1.48–1.78 μm). The spectra are of HD 236697 (M0.5 Ib), HD 14404 (M1 – Iab–Ib), HD 10465 (M2 Ib), CD –31 4916 (M3 Iab–Ia), and HD 156014 (M5 Ib–II). The spectra have been normalized to unity at 1.60 μm and offset by constants.

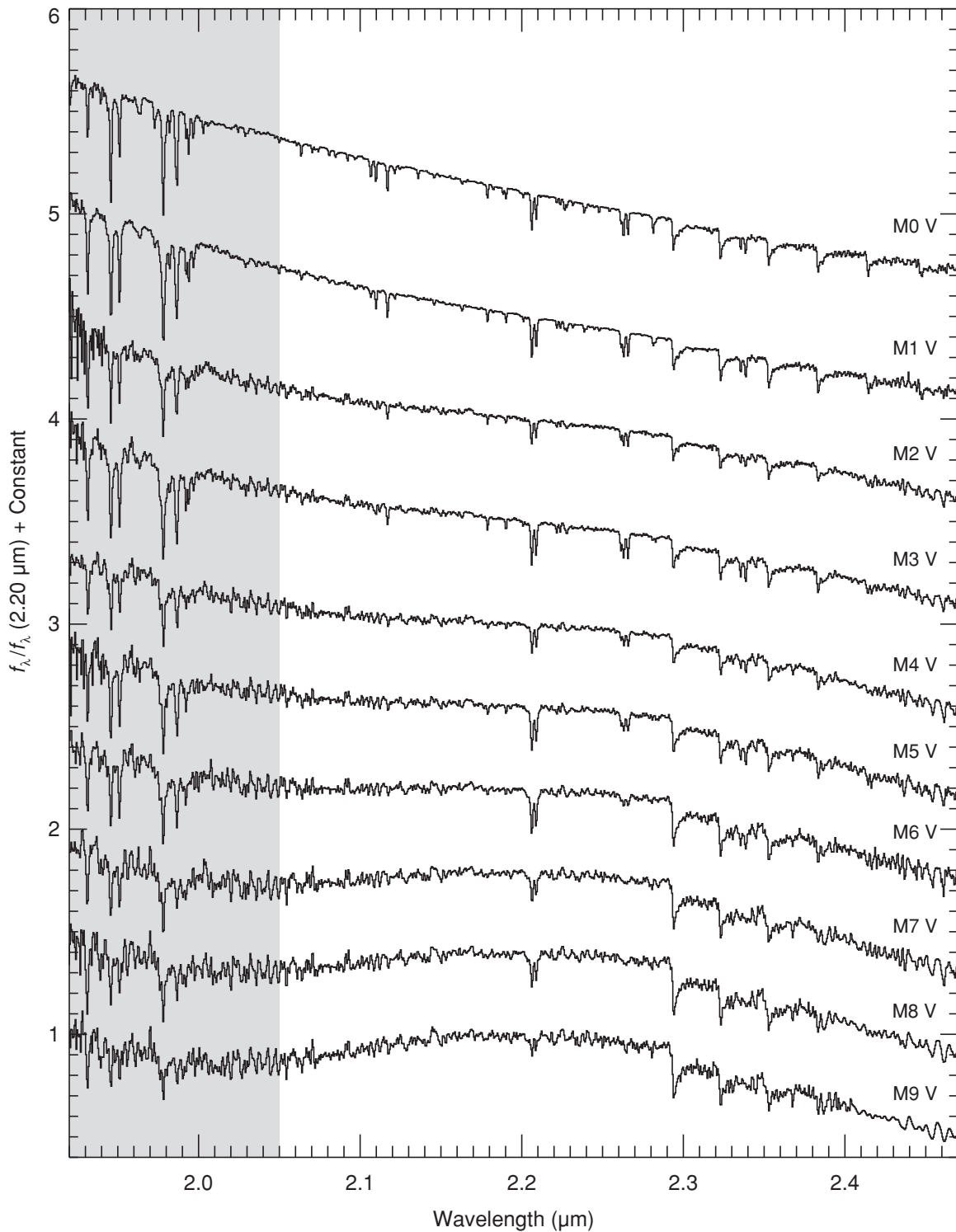


Figure 107. Sequence of M dwarf stars plotted over the K band ($1.92\text{--}2.5 \mu\text{m}$). The spectra are of HD 19305 (M0 V), HD 42581 (M1 V), HD 95735 (M2 V), GI 388 (M3 V), GI 213 (M4 V), GI 51 (M5 V), GI 406 (M6 V), GI 644C (M7 V), GI 752B (M8 V), and LP944–20 (M9 V). The spectra have been normalized to unity at $2.20 \mu\text{m}$ and offset by constants.

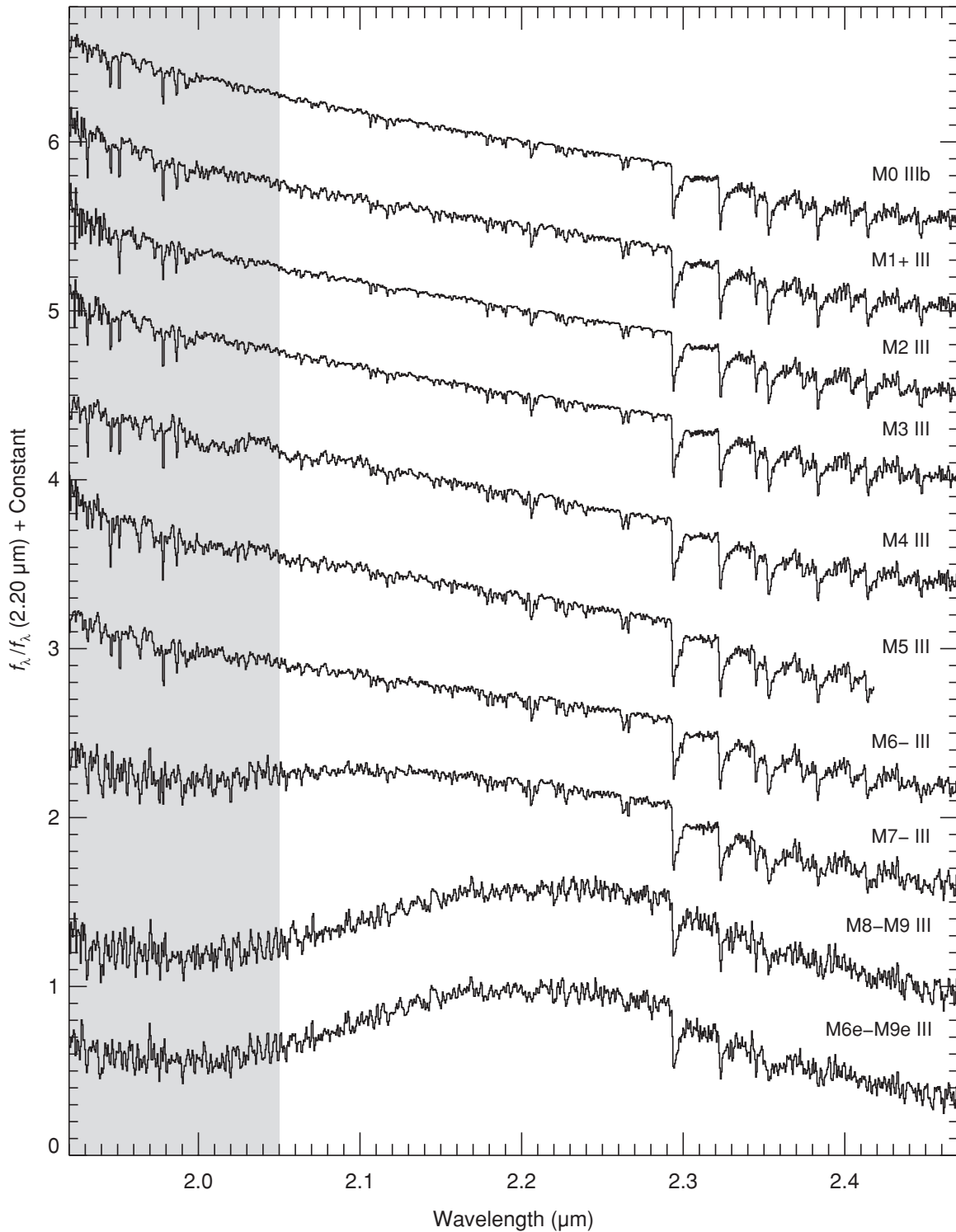


Figure 108. Sequence of M giant stars plotted over the *K* band (1.92–2.5 μm). The spectra are of HD 213893 (M0 IIIb), HD 204724 (M1+ III), HD 120052 (M2 III), HD 39045 (M3 III), HD 4408 (M4 III), HD 175865 (M5 III), HD 18191 (M6- III), HD 108849 (M7- III), IRAS 21284-0747 (M8-M9 III), and HD 69243 (M6e-M9e III). The spectra have been normalized to unity at 2.20 μm and offset by constants.

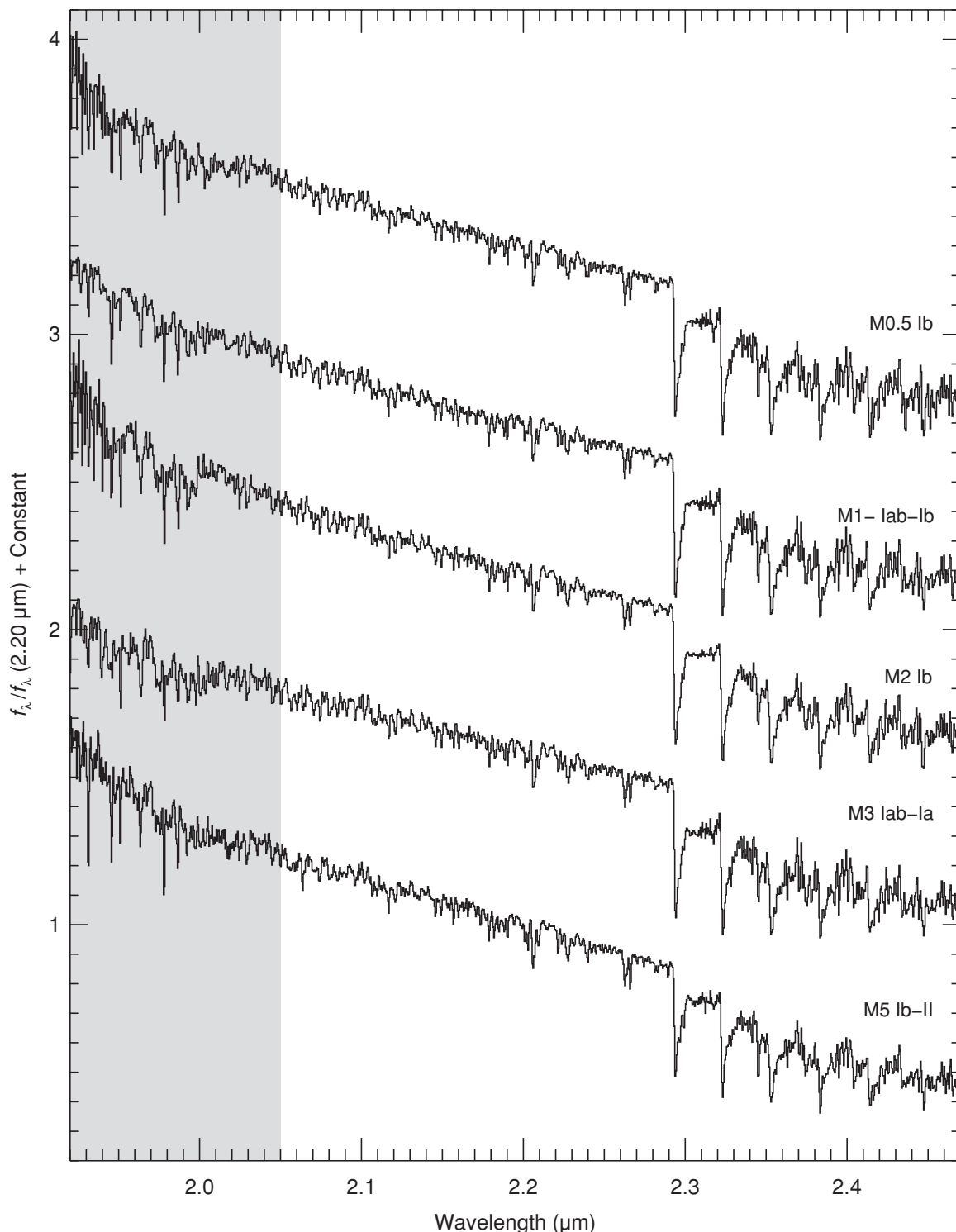


Figure 109. Sequence of M supergiant stars plotted over the *K* band (1.92–2.5 μm). The spectra are of HD 236697 (M0.5 Ib), HD 14404 (M1 – Iab–Ib), HD 10465 (M2 Ib), CD –31 4916 (M3 Iab–Ia), and HD 156014 (M5 Ib–II). The spectra have been normalized to unity at 2.20 μm and offset by constants.

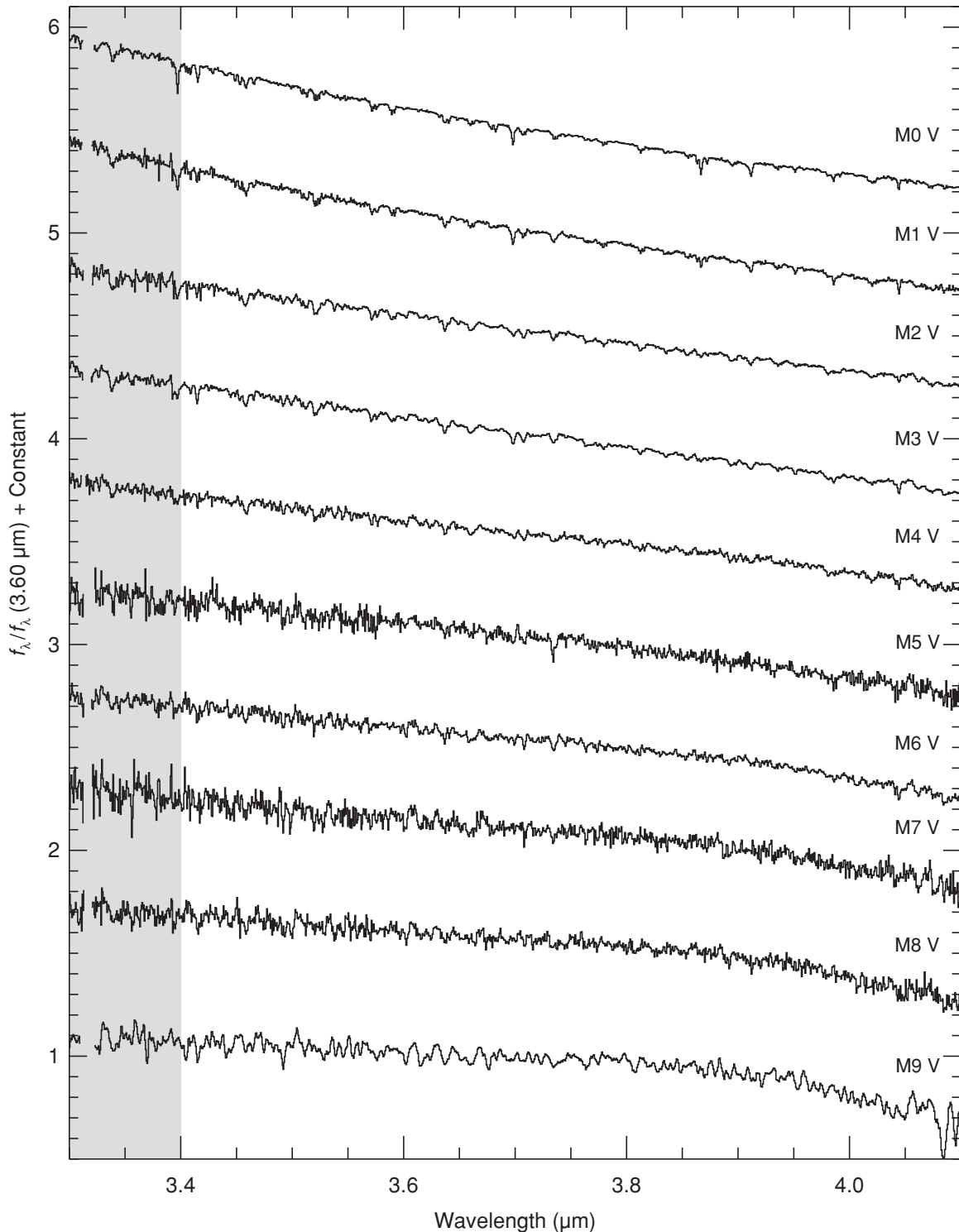


Figure 110. Sequence of M dwarf stars plotted over the L' band (3.6–4.1 μm). The spectra are of HD 19305 (M0 V), HD 42581 (M1 V), HD 95735 (M2 V), GI 388 (M3 V), GI 213 (M4 V), GI 51 (M5 V), GI 406 (M6 V), GI 644C (M7 V), GI 752B (M8 V), and LP944–20 (M9 V). The spectra have been normalized to unity at 3.6 μm and offset by constants.

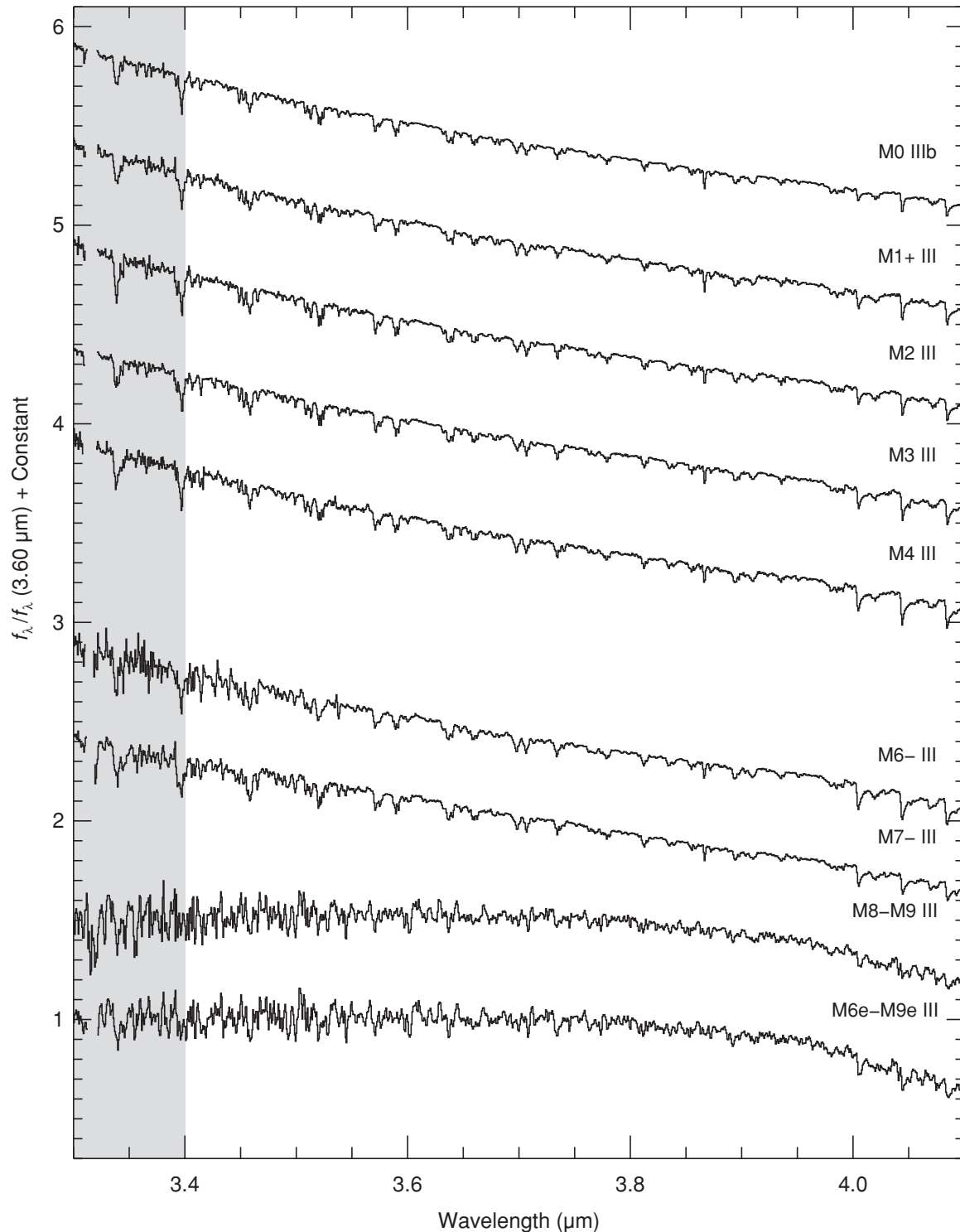


Figure 111. Sequence of M giant stars plotted over the L' band (3.6–4.1 μm). The spectra are of HD 213893 (M0 IIIb), HD 204724 (M1+ III), HD 120052 (M2 III), HD 39045 (M3 III), HD 4408 (M4 III), HD 18191 (M6– III), HD 108849 (M7– III), IRAS 21284–0747 (M8–M9 III), and HD 69243 (M6e–M9e III). The spectra have been normalized to unity at 3.6 μm and offset by constants.

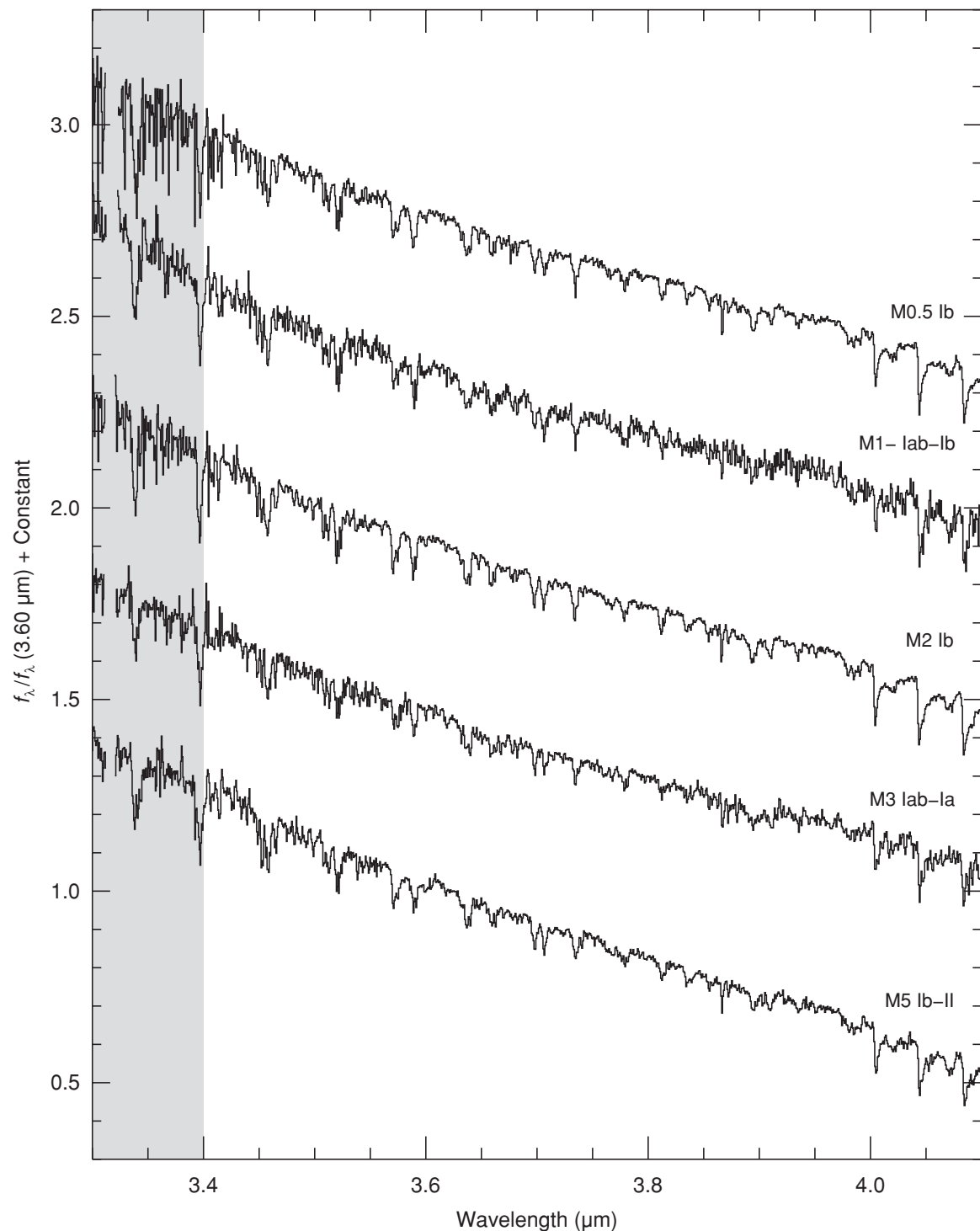


Figure 112. Sequence of M supergiant stars plotted over the L' band (3.6–4.1 μm). The spectra are of HD 236697 (M0.5 Ib), HD 14404 (M1 – Iab–Ib), HD 10465 (M2 Ib), CD –31 4916 (M3 Iab–Ia), and HD 156014 (M5 Ib–II). The spectra have been normalized to unity at 3.6 μm and offset by constants.

REFERENCES

- Abt, H. A. 1981, *ApJS*, **45**, 437
- Abt, H. A., & Morrell, N. I. 1995, *ApJS*, **99**, 135
- Ake, T. B. 1979, *ApJ*, **234**, 538
- Ali, B., Carr, J. S., Depoy, D. L., Frogel, J. A., & Sellgren, K. 1995, *AJ*, **110**, 2415
- Aoki, W., Tsuji, T., & Ohnaka, K. 1998, *A&A*, **340**, 222
- Auman, J. J. 1967, *ApJS*, **14**, 171
- Ballik, E. A., & Ramsay, D. A. 1963, *ApJ*, **137**, 61
- Barnbaum, C., Stone, R. P. S., & Keenan, P. C. 1996, *ApJS*, **105**, 419
- Beauchamp, A., Moffat, A. F. J., & Drissen, L. 1994, *ApJS*, **93**, 187
- Beer, R., Lambert, D. L., & Sneden, C. 1974, *PASP*, **86**, 806
- Bessell, M. S., & Brett, J. M. 1988, *PASP*, **100**, 1134
- Bessell, M. S., Brett, J. M., Wood, P. R., & Scholz, M. 1989, *A&A*, **213**, 209
- Bessell, M. S., Scholz, M., & Wood, P. R. 1996, *A&A*, **307**, 481
- Blum, R. D., Ramond, T. M., Conti, P. S., Figer, D. F., & Sellgren, K. 1997, *AJ*, **113**, 1855
- Brett, J. M. 1989, *MNRAS*, **241**, 247
- Brett, J. M. 1990, *A&A*, **231**, 440
- Brocklehurst, B., Hébert, G., Innanen, S., Sell, R., & Nicholls, R. 1971, The Identification Atlas of Molecular Spectra: The CN $A^2\Pi - X^2\Sigma^+$ Red System, Tech. rep. (Toronto: York University, Centre for Research in Experimental Space Science)
- Bruzual, G. 2007, in ASP Conf. Ser. 374, From Stars to Galaxies: Building the Pieces to Build Up the Universe, ed. A. Vallenari, R. Tantalo, L. Portinari, & A. Moretti (San Francisco, CA: ASP), 303
- Bruzual, G., & Charlot, S. 2003, *MNRAS*, **344**, 1000
- Burgasser, A. J., Geballe, T. R., Leggett, S. K., Kirkpatrick, J. D., & Golimowski, D. A. 2006, *ApJ*, **637**, 1067
- Buser, R., & Kurucz, R. L. 1992, *A&A*, **264**, 557
- Casali, M., et al. 2007, *A&A*, **467**, 777
- Cayrel de Strobel, G., Soubiran, C., Friel, E. D., Ralite, N., & Francois, P. 1997, *A&AS*, **124**, 299
- Cheung, A. S.-C., Taylor, A. W., & Merer, A. J. 1982, *J. Mol. Spectrosc.*, **92**, 391
- Cohen, M., Wheaton, W. A., & Megeath, S. T. 2003, *AJ*, **126**, 1090
- Cowley, A. P. 1976, *PASP*, **88**, 95
- Cowley, A. P., Hiltner, W. A., & Witt, A. N. 1967, *AJ*, **72**, 1334
- Cox, A. N. 2000, Allen's Astrophysical Quantities, ed. A. N. Cox (4th ed.; Berlin: Springer)
- Cushing, M. C., et al. 2008, *ApJ*, **678**, 1372
- Cushing, M. C., Rayner, J. T., Davis, S. P., & Vacca, W. D. 2003, *ApJ*, **582**, 1066
- Cushing, M. C., Rayner, J. T., & Vacca, W. D. 2005, *ApJ*, **623**, 1115
- Cushing, M. C., & Vacca, W. D. 2006, *AJ*, **131**, 1797
- Cushing, M. C., Vacca, W. D., & Rayner, J. T. 2004, *PASP*, **116**, 362
- Dallier, R., Boisson, C., & Joly, M. 1996, *A&AS*, **116**, 239
- Davies, B., Figer, D. F., Kudritzki, R.-P., MacKenty, J., Najarro, F., & Herrero, A. 2007, *ApJ*, **671**, 781
- Delfosse, X., et al. 2001, *A&A*, **366**, L13
- Espaillat, C., Calvet, N., Luhman, K. L., Muzerolle, J., & D'Alessio, P. 2008, *ApJ*, **682**, L125
- Figer, D. F., McLean, I. S., & Morris, M. 1995, *ApJ*, **447**, L29
- Figer, D. F., McLean, I. S., & Najarro, F. 1997, *ApJ*, **486**, 420
- Fioc, M., & Rocca-Volmerange, B. 1997, *A&A*, **326**, 950
- Fitzgerald, M. P. 1970, *A&A*, **4**, 234
- Fitzpatrick, E. L., & Massa, D. 2007, *ApJ*, **663**, 320
- Förster Schreiber, N. M. 2000, *AJ*, **120**, 2089
- Frogel, J. A. 1971, PhD thesis, California Institute of Technology
- Frogel, J. A., Persson, S. E., Matthews, K., & Aaronson, M. 1978, *ApJ*, **220**, 75
- Frogel, J. A., Stephens, A., Ramírez, S., & DePoy, D. L. 2001, *AJ*, **122**, 1896
- Galehouse, D. C., Davis, S. P., & Brault, J. W. 1980, *ApJS*, **42**, 241
- Garcia, B. 1989, Bulletin d'Information du Centre de Donnees Stellaires, **36**, 27
- Garrison, R. F. 1994, in ASP Conf. Ser. 60, The MK Process at 50 Years: A Powerful Tool for Astrophysical Insight, ed. C. J. Corbally, R. O. Gray, & R. F. Garrison (San Francisco, CA: ASP), 3
- Gatterer, A., Junkes, J., & Salpeter, E. W. 1957, Molecular Spectra of Metallic Oxides – Vol. 1: Plates; Vol. 2: Text and Wavelengths (Citta del Vaticano: Specola Vaticana)
- Gautschy-Loidl, R., Höfner, S., Jørgensen, U. G., & Hron, J. 2004, *A&A*, **422**, 289
- Glass, I. S. 1975, *MNRAS*, **171**, 19P
- Gliese, W. 1971, Veroeffentlichungen des Astronomischen Rechen-Instituts Heidelberg, **24**, 1
- Goebel, J. H., et al. 1980, *ApJ*, **235**, 104
- Goorvitch, D. 1994, *ApJS*, **95**, 535
- Gorlova, N. I., Meyer, M. R., Rieke, G. H., & Liebert, J. 2003, *ApJ*, **593**, 1074
- Goto, M., et al. 2003, *Proc. SPIE*, **4839**, 1117
- Gray, R. O., & Garrison, R. F. 1989, *ApJS*, **69**, 301
- Gray, R. O., Napier, M. G., & Winkler, L. I. 2001, *AJ*, **121**, 2148
- Greene, T. P., & Meyer, M. R. 1995, *ApJ*, **450**, 233
- Habing, H. J., & Olofsson, H., ed. 2003, Asymptotic Giant Branch Stars (New York, NY: Springer)
- Hammer, P. D., & Davis, S. P. 1981, *ApJS*, **47**, 201
- Hanson, M. M., Conti, P. S., & Rieke, M. J. 1996, *ApJS*, **107**, 281
- Hanson, M. M., Kudritzki, R.-P., Kenworthy, M. A., Puls, J., & Tokunaga, A. T. 2005, *ApJS*, **161**, 154
- Henry, T. J., Kirkpatrick, J. D., & Simons, D. A. 1994, *AJ*, **108**, 1437
- Herzberg, G., & Phillips, J. G. 1948, *ApJ*, **108**, 163
- Hewett, P. C., Warren, S. J., Leggett, S. K., & Hodgkin, S. T. 2006, *MNRAS*, **367**, 454
- Hillenbrand, L. A., Foster, J. B., Persson, S. E., & Matthews, K. 2002, *PASP*, **114**, 708
- Hinkle, K., Wallace, L., & Livingston, W. C. 1995, Infrared Atlas of the Arcturus Spectrum: 0.9–5.3 μm (San Francisco, CA: ASP)
- Hinkle, K., Wallace, L., Valenti, J., & Harmer, D. 2000, Visible and Near Infrared Atlas of the Arcturus Spectrum: 3727–9300 Å (San Francisco, CA: ASP)
- Horne, K. 1986, *PASP*, **98**, 609
- Hyland, A. R. 1974, in Highlights of Astronomy, Vol. 3, ed. G. Contopoulos (Dordrecht: Reidel), 307
- Ivanov, V. D., Rieke, M. J., Engelbracht, C. W., Alonso-Herrero, A., Rieke, G. H., & Luhman, K. L. 2004, *ApJS*, **151**, 387
- Jaschek, M. 1978, Bulletin d'Information du Centre de Donnees Stellaires, **15**, 121
- Jaschek, C., & Jaschek, M. 1973, in IAU Symp. 50, Spectral Classification and Multicolour Photometry, ed. C. Fehrenbach & B. E. Westerlund (Dordrecht: Reidel), 43
- Johnson, H. J., & Méndez, M. E. 1970, *AJ*, **75**, 785
- Johnson, H. L., & Morgan, W. W. 1953, *ApJ*, **117**, 313
- Jones, H. R. A., Longmore, A. J., Allard, F., & Hauschildt, P. H. 1996, *MNRAS*, **280**, 77
- Joyce, R. R. 1998, *AJ*, **115**, 2059
- Joyce, R. R., Hinkle, K. H., Wallace, L., Dulick, M., & Lambert, D. L. 1998, *AJ*, **116**, 2520
- Keenan, P. C. 1993, *PASP*, **105**, 905
- Keenan, P. C., & McNeil, R. C. 1976, An Atlas of Spectra of the Cooler Stars: Types G, K, M, S, and C. Part 1: Introduction and Tables (Columbus, OH: Ohio State Univ. Press)
- Keenan, P. C., & McNeil, R. C. 1989, *ApJS*, **71**, 245
- Keenan, P. C., & Newsom, G. H. 2000, Revised Catalog of MK Classifications of the Cooler Stars (Columbus, OH: Ohio State Univ.), <http://www.astronomy.ohio-state.edu/MKCool/>
- Keenan, P. C., & Schroeder, L. W. 1952, *ApJ*, **115**, 82
- Kharchenko, N. V. 2001, Kinematika i Fizika Nebesnykh Tel, **17**, 409
- Kholopov, P. N., et al. 1998, in Combined General Catalogue of Variable Stars (4.1 Ed (II)/214A); Moscow: Sternberg Astron. Inst., 0
- Kipper, T. 2008, Baltic Astron., **17**, 87
- Kirkpatrick, J. D., Henry, T. J., & Irwin, M. J. 1997, *AJ*, **113**, 1421
- Kirkpatrick, J. D., Henry, T. J., & McCarthy, D. W. 1991, *ApJS*, **77**, 417
- Kirkpatrick, J. D., Henry, T. J., & Simons, D. A. 1995, *AJ*, **109**, 797
- Kirkpatrick, J. D., et al. 1999, *ApJ*, **519**, 802
- Kleinmann, S. G., & Hall, D. N. B. 1986, *ApJS*, **62**, 501
- Klochkova, V. G., Mishenina, T. V., & Panchuk, V. E. 2000, *Astron. Lett.*, **26**, 398
- Koornneef, J., Bohlin, R., Buser, R., Horne, K., & Turnshek, D. 1986, in Highlights of Astronomy, Vol. 7 (Dordrecht: Reidel), 833
- Kraft, R. P. 1960, *ApJ*, **131**, 330
- Kurtev, R., Borissova, J., Georgiev, L., Ortolani, S., & Ivanov, V. D. 2007, *A&A*, **475**, 209
- Lagerqvist, A., & Selin, L.-E. 1957, Ark. Fys., **11**, 429
- Lambert, D. L., Gustafsson, B., Eriksson, K., & Hinkle, K. H. 1986, *ApJS*, **62**, 373
- Lançon, A. 1999, in IAU Symp. 191, Asymptotic Giant Branch Stars, ed. T. Le Bertre, A. Lebre, & C. Waelkens (Dordrecht: Kluwer), 579
- Lançon, A., Hauschildt, P. H., Ladjal, D., & Mouhcine, M. 2007, *A&A*, **468**, 205
- Lançon, A., Mouhcine, M., Fioc, M., & Silva, D. 1999, *A&A*, **344**, L21
- Lançon, A., & Rocca-Volmerange, B. 1992, *A&AS*, **96**, 593
- Lançon, A., & Wood, P. R. 2000, *A&AS*, **146**, 217
- Lawrence, A., et al. 2007, *MNRAS*, **379**, 1599

- Lazaro, C., Hammersley, P. L., Clegg, R. E. S., Lynas-Gray, A. E., Mountain, C. M., Zadrozny, A., & Selby, M. J. 1994, *MNRAS*, **269**, 365
- Lee, T. A. 1970, *ApJ*, **162**, 217
- Leggett, S. K. 1992, *ApJS*, **82**, 351
- Leitherer, C., et al. 1999, *ApJS*, **123**, 3
- Lenorzer, A., Vandenbussche, B., Morris, P., de Koter, A., Geballe, T. R., Waters, L. B. F. M., Hony, S., & Kaper, L. 2002, *A&A*, **384**, 473
- Lewis, B. M. 2006, *AJ*, **132**, 489
- Linton, C., & Broida, H. P. 1977, *J. Mol. Spectrosc.*, **64**, 382
- Livingston, W., & Wallace, L. 1991, An Atlas of the Solar Spectrum in the Infrared from 1850 to 9000 cm⁻¹ (1.1 to 5.4 μm) (NSO Tech. Rep. 91-001; Tucson, AZ: NSO)
- Lockwood, G. W. 1973, *ApJ*, **180**, 845
- Lodie, N., Scholz, R.-D., McCaughrean, M. J., Ibata, R., Irwin, M., & Zinnecker, H. 2005, *A&A*, **440**, 1061
- Loidl, R., Lançon, A., & Jørgensen, U. G. 2001, *A&A*, **371**, 1065
- Lord, S. D. 1992, A New Software Tool for Computing Earth's Atmospheric Transmission of Near- and Far-Infrared Radiation (NASA Tech. Mem. 103957; Washington, DC: NASA)
- MacConnell, D. J., & Bidelman, W. P. 1976, *AJ*, **81**, 225
- Malkan, M. A., Hicks, E. K., Teplitz, H. I., McLean, I. M., Sugai, H., & Guichard, J. 2002, *ApJS*, **142**, 79
- Maraston, C. 2005, *MNRAS*, **362**, 799
- Mármol-Queraltó, E., Cardiel, N., Cenarro, A. J., Vazdekis, A., Gorgas, J., Pedraz, S., Peletier, R. F., & Sánchez-Blázquez, P. 2008, *A&A*, **489**, 885
- McGregor, P. J., Hyland, A. R., & Hillier, D. J. 1988, *ApJ*, **324**, 1071
- Mégequier, C. 1995, *A&A*, **296**, 771
- Mermilliod, J. C. 2006, VizieR Online Data Catalog, 2168
- Meyer, M. R., Edwards, S., Hinkle, K. H., & Strom, S. E. 1998, *ApJ*, **508**, 397
- Morgan, W. W., & Abt, H. A. 1973, *AJ*, **78**, 386
- Morgan, W. W., Abt, H. A., & Tapscott, J. W. 1978, Revised MK Spectral Atlas for Stars Earlier Than the Sun (Williams Bay, WI: Yerkes Observatory)
- Morgan, W. W., & Keenan, P. C. 1973, *ARA&A*, **11**, 29
- Morgan, W. W., Keenan, P. C., & Kellman, E. 1943, An Atlas of Stellar Spectra, with an Outline of Spectral Classification (Chicago, IL: Univ. Chicago Press)
- Morris, P. W., Eenens, P. R. J., Hanson, M. M., Conti, P. S., & Blum, R. D. 1996, *ApJ*, **470**, 597
- Mould, J. R. 1976, *A&A*, **48**, 443
- Nave, G., Johansson, S., Learner, R. C. M., Thorne, A. P., & Brault, J. W. 1994, *ApJS*, **94**, 221
- Nordström, B., et al. 2004, *A&A*, **418**, 989
- Nyman, L.-A., Hall, P. J., & Olofsson, H. 1998, *A&AS*, **127**, 185
- Omont, A., Loup, C., Forveille, T., Te Lintel Hekkert, P., Habing, H., & Sivagnanam, P. 1993, *A&A*, **267**, 515
- Origlia, L., Moorwood, A. F. M., & Oliva, E. 1993, *A&A*, **280**, 536
- Oudmaijer, R. D., Waters, L. B. F. M., van der Veen, W. E. C. J., & Geballe, T. R. 1995, *A&A*, **299**, 69
- Pearse, R. W. B., & Gaydon, A. G. 1965, The Identification of Molecular Spectra (3rd ed.; London: Chapman and Hall)
- Pearse, R. W. B., & Gaydon, A. G. 1976, The Identification of Molecular Spectra (4th ed.; London: Chapman and Hall)
- Peterson, D. E., et al. 2008, *ApJ*, **685**, 313
- Phillips, J. G. 1950, *ApJ*, **111**, 314
- Phillips, J. G., Davis, S. P., & Galehouse, D. C. 1979, *ApJ*, **234**, 401
- Phillips, J. G., Davis, S. P., Lindgren, B., & Balfour, W. J. 1987, *ApJS*, **65**, 721
- Pickles, A. J. 1998, *PASP*, **110**, 863
- Pinfield, D. J., et al. 2008, *MNRAS*, **390**, 304
- Ramírez, S. V., Depoy, D. L., Frogel, J. A., Sellgren, K., & Blum, R. D. 1997, *AJ*, **113**, 1411
- Ramos Almeida, C., Pérez García, A. M., & Acosta-Pulido, J. A. 2009, *ApJ*, **694**, 1379
- Ranada, A. C., Singh, H. P., Gupta, R., & Ashok, N. M. 2007, *BASI*, **35**, 87
- Ranade, A. C., Ashok, N. M., Singh, H. P., & Gupta, R. 2007, *BASI*, **35**, 359
- Ranade, A., Gupta, R., Ashok, N. M., & Singh, H. P. 2004, *BASI*, **32**, 311
- Rayner, J. T., Onaka, P. M., Cushing, M. C., & Vacca, W. D. 2004, *Proc. SPIE*, **5492**, 1498
- Rayner, J. T., Toomey, D. W., Onaka, P. M., Denault, A. J., Stahlberger, W. E., Vacca, W. D., Cushing, M. C., & Wang, S. 2003, *PASP*, **115**, 362
- Reid, I. N., & Hawley, S. L. 2005, New Light on Dark Stars: Red Dwarfs, Low-Mass Stars, Brown Dwarfs (Chichester: Praxis)
- Reiners, A., Homeier, D., Hauschildt, P. H., & Allard, F. 2007, *A&A*, **473**, 245
- Richter, H., & Wood, P. R. 2001, *A&A*, **369**, 1027
- Riffel, R., Pastoriza, M. G., Rodríguez-Ardila, A., & Maraston, C. 2008, *MNRAS*, **388**, 803
- Roman, N. G. 1955, *ApJS*, **2**, 195
- Rosino, L. 1951, *ApJ*, **113**, 60
- Schmidt-Kaler, T. 1982, Landolt-Börnstein: Numerical Data and Functional Relationships in Science and Technology ed. K. Schaifers & H. Voigt (Berlin: Springer), VI/2b, 14
- Schwenke, D. W. 1998, in Faraday Discussions 109, Chemistry and Physics of Molecules and Grains in Space (London: The Faraday Division of the Royal Society of Chemistry), 321
- Skrutskie, M. F., et al. 2006, *AJ*, **131**, 1163
- Solf, J. 1978, *A&AS*, **34**, 409
- Spinrad, H., & Newburn, R. L., Jr. 1965, *ApJ*, **141**, 965
- Spinrad, H., & Wing, R. F. 1969, *ARA&A*, **7**, 249
- Sylvester, R. J., Skinner, C. J., & Barlow, M. J. 1998, *MNRAS*, **301**, 1083
- Szczerba, R., Siódmiak, N., Stasińska, G., & Borkowski, J. 2007, *A&A*, **469**, 799
- Tanaka, W., Hashimoto, O., Nakada, Y., Onaka, T., & Tanabe, T. 1990, *Publ. Natl. Astron. Obs. Japan*, **1**, 259
- Terndrup, D. M., Frogel, J. A., & Whitford, A. E. 1991, *ApJ*, **378**, 742
- Tinney, C. G., & Reid, I. N. 1998, *MNRAS*, **301**, 1031
- Tokunaga, A. T., Simons, D. A., & Vacca, W. D. 2002, *PASP*, **114**, 180
- Tonry, J., & Davis, M. 1979, *AJ*, **84**, 1511
- Ueta, T., Meixner, M., & Bobrowsky, M. 2000, *ApJ*, **528**, 861
- Upgren, A. R., Grossenbacher, R., Penhallow, W. S., MacConnell, D. J., & Frye, R. L. 1972, *AJ*, **77**, 486
- Vacca, W. D., Cushing, M. C., & Rayner, J. T. 2003, *PASP*, **115**, 389
- Vacca, W. D., Cushing, M. C., & Rayner, J. T. 2004, *PASP*, **116**, 352
- Valenti, J. A., Piskunov, N., & Johns-Krull, C. M. 1998, *ApJ*, **498**, 851
- van Altena, W. F., Lee, J. T., & Hoffleit, E. D. 1995, The Yale Parallax Catalog (4th ed.; New Haven, CT: Yale Univ. Observatory)
- van Loon, J. T., Cohen, M., Oliveira, J. M., Matsuura, M., McDonald, I., Sloan, G. C., Wood, P. R., & Zijlstra, A. A. 2008, *A&A*, **487**, 1055
- Vandenbussche, B., et al. 2002, *A&A*, **390**, 1033
- Venkata Raman, V., & Anandarao, B. G. 2008, *MNRAS*, **385**, 1076
- Wallace, L., & Hinkle, K. 1996, *ApJS*, **107**, 312
- Wallace, L., & Hinkle, K. 1997, *ApJS*, **111**, 445
- Wallace, L., & Hinkle, K. 2001, *ApJ*, **559**, 424
- Wallace, L., & Hinkle, K. 2002, *AJ*, **124**, 3393
- Wallace, L., & Livingston, W. 2003, An Atlas of the Solar Spectrum in the Infrared from 1850 to 9000 cm⁻¹ (1.1 to 5.4 μm), revised (NSO Tech. Rep. 03-001; Tucson, AZ: NSO)
- Wallace, L., Livingston, W. C., & Hinkle, K. 1993, An Atlas of the Solar Photospheric Spectrum in the Region from 8900 to 13600 cm⁻¹ (7350 to 11230 Å): With Decomposition into Solar and Atmospheric Components and Identifications of the Main Solar Features (NSO Tech. Rep. 93-001; Tucson, AZ: NSO)
- Wallace, L., Meyer, M. R., Hinkle, K., & Edwards, S. 2000, *ApJ*, **535**, 325
- Wing, R. F., & Ford, W. K. J. 1969, *PASP*, **81**, 527
- Woolf, N. J., Schwarzschild, M., & Rose, W. K. 1964, *ApJ*, **140**, 833
- Zsoldos, E. 1993, *A&A*, **280**, 177